Titre: Title:	Development of a Dynamic Model to Describe CHO cells Metabolic Network and Regulation
Auteur: Author:	Atefeh Ghorbaniaghdam
Date:	2013
Type:	Mémoire ou thèse / Dissertation or Thesis
Référence: Citation:	Ghorbaniaghdam, A. (2013). Development of a Dynamic Model to Describe CHO cells Metabolic Network and Regulation [Ph.D. thesis, École Polytechnique de Montréal]. PolyPublie. https://publications.polymtl.ca/1228/

UNIVERSITÉ DE MONTRÉAL

DEVELOPMENT OF A DYNAMIC MODEL TO DESCRIBE CHO CELLS METABOLIC NETWORK AND REGULATION

ATEFEH GHORBANIAGHDAM
DÉPARTEMENT DE GÉNIE CHIMIQUE
ÉCOLE POLYTECHNIQUE DE MONTRÉAL

THÈSE PRÉSENTÉE EN VUE DE L'OBTENTION
DU DIPLÔME DEPHILOSOPHIAE DOCTOR
(GÉNIE CHIMIQUE)
AOÛT 2013

UNIVERSITÉ DE MONTRÉAL

ÉCOLE POLYTECHNIQUE DE MONTRÉAL

Cette thèse intitulée:

DEVELOPMENT OF A DYNAMIC MODEL TO DESCRIBE CHO CELLS METABOLIC NETWORK AND REGULATION

présentée par : GHORBANIAGHDAM Atefeh

en vue de l'obtention du diplôme de : Philosophiæ doctor

a été dûment acceptée par le jury d'examen constitué de :

M. PERRIER Michel, Ph. D., président
M. JOLICOEUR Mario, Ph. D., membre et directeur de recherche
M. HENRY Olivier, Ph. D., membre et codirecteur de recherche
M. SRINIVASAN, Bala, Ph. D., membre
M. BUDMAN Hector, Ph. D., membre

- *To my family whom I love the most.*

ACKNOWLEDGMENTS

This study was supported financially by the Natural Sciences and Engineering Research Council of Canada (NSERC) and Monoclonal Antibody Network (MabNet). There are many to thank, and I wish to sincerely acknowledge everybody who has contributed to this work in one way or another. Specially:

I would like to express my most warmly appreciation to my advisor, Professor Mario Jolicoeur, for his valuable guidance, thoughtful advice, continuous support, constant encouragement and for always being there for me throughout the fulfillment of this work.

I also would like to express my appreciation to my co-advisor, Professor Olivier Henry for his valuable guidance, his continuous support, and for sharing knowledge with me.

I warmly thank my colleagues in the lab for their kindness, great help and support throughout the hard times of the work. Special thanks to Zahra Sheikholeslami for sharing her knowledge with me, for helpful discussions and for her generous nature.

Many special thanks to JingkuiChenfor his valuable chemical analyses.

Also, I would like to thank Professor Hector Budman, Professor Bala Srinivasan, and Professor Michel Perrier for accepting to evaluate my PhD thesis.

Last but not least, I would like to thank my friends and my family for their never ending support. Special thanks to my brother who always cheered me up during though times although miles away from me.

Finally, I really don’t know how to thank my parents for all I am or I hope to be is because of them. Enough to say that I so believe they are the main authors of this thesis.

RÉSUMÉ

L'objectif principal de ce travail est de démontrer qu'une approche de modélisation dynamique peut être utile pour comprendre le comportement du métabolisme central du carbone des cellules CHO. La première partie de ce travail se concentre sur le développement d'un modèle dynamique de cellules CHO du métabolisme primaire. Ce travail a été inspiré par un modèle cinétique métabolique auparavant développé dans notre groupe pour décrire le métabolisme cellulaire primaire decellules de plante. Le modèle métabolique a été développé et calibré à l'aide de données obtenues au préalable par notre groupe dans des cultures de cellules CHO produisant un activateur du tissu plasminogène recombinant en bioréacteur. En plus des données de base, telles les concentrations en biomasse, en glucose, en lactate, en glutamine et en ammoniac, les concentrations intracellulaires de plusieurs nucléotides et la consommation d'oxygène par cellule étaient également disponibles.

Le principal résultat de cette partie consiste en un modèle métabolique cinétique qui permet de décrire le comportement des voies métaboliques majeures dans les cellules CHO, c'est-à-dire la glycolyse, la voie des pentoses phosphate, le cycle des acides tricarboxyliques, la glutaminolyse ainsi que la respiration cellulaire. Le modèle possède 30 réactions et plus de 72 paramètres. Les simulations obtenues à l'aide du modèle permettent de décrire les données expérimentales, ce qui suggère que la structure proposée du modèle est en accord avec le fonctionnement biologique des cellules CHO. Le modèle a également été utilisé pour étudier l'effet qu'a l'induction par le butyrate de sodium sur une culture de cellules CHO, celui-ci étant un produit chimique couramment utilisé pour augmenter la production spécifique de protéines recombinantes. En considérant le nombre élevé de paramètres, l'adaptation du modèle a été minime, nécessitant le changement de seulement quelques paramètres, en accord avec les modifications de l'expression des gènes rapportées pour décrire l'effet du butyrate de sodium sur des cellules CHO.

Bien que principalement spéculatifs tout en reposant sur des simulations du modèle, les résultats concordent avec les données ainsi qu'avec les hypothèses issues de la littérature concernant l'effet du butyrate de sodium sur le métabolisme des cellules CHO.

Dans une seconde partie, la capacité descriptive du modèle a également été évaluée à l'aide de données provenant d'une autre lignée cellulaire CHO recombinante cultivée à des conditions de culture différentes. Le modèle a été testé pour simuler des cultures discontinues de différents clones d'une lignée de cellules CHO ayant été génétiquement modifiée pour posséder un système d'expression inductible utilisant le cumate comme agent inducteur et permettant la production d'anticorps monoclonaux anti-CD 20. Une lignée présentant unefaible production spécifique et une lignée possédant une plus haute production ont été comparées à la lignée parentale. De plus, il a été possible d'augmenter le nombre de métabolites extracellulaires et intracellulaires à l'étude. Il a été démontré que la structure du modèle permet à celui-ci de facilement s'adapter à une autre lignée cellulaire CHO et ses clones, en ne nécessitant encore une fois qu'un nombre limité de modifications au modèle, qui ont été interprétés et analysés comme caractéristiques de lignées cellulaires spécifiques. La portée du modèle a été étendue ici de manière à décrire aussi le métabolisme des acides aminés et de la production d'anticorps. Il comprend donc maintenant 35 réactions et 92 paramètres. Toutefois, une modification limitée, c'est-à-dire trois et cinq paramètres pour la lignée à faible production et celle à production élevée respectivement, a permis des simulations qui décrivent avec précision les différences sur le plan métaboliques liées à la variation clonale. En se fiant à nos résultats, il est clair que ce modèle dynamique peut être facilement adapté à l'ensemble des cultures existantes. Enfin, dans la troisième partie de la thèse, le comportement du modèle a été étudié tout en intégrant la régulation métabolique de la glycolyse. Le but de cette étude était d'évaluer dans quelle mesure notre modèle cinétique peut décrire l'effet d'une perturbation soudaine sur le comportement du métabolisme cellulaire, tout en ayant été calibré à l'aide des données de culture montrant une dynamique lente. Les mécanismes de régulation connus de la glycolyse des cellules de mammifères, tels que les mécanismes d'inhibition par rétroaction, par anticipation et les mécanismes d'activation par des métabolites glycolytiques et les variables énergétiques ont été intégrés dans le modèle. Une expérience *in silico* a été réalisée en ajoutant un stress hypoxique soudain, diminuant à 10% de saturation de l'air. Le modèle a ensuite été modifié pour inclure l'effet de sept fonctions de régulation, à savoir l'inhibition par anticipation ou par rétroaction et l'activation de métabolites de la glycolyse et l'activation par rétroaction de l'état

énergétique de la cellule, dans la voie de la glycolyse avec un paramètre pour chaque cas. Fait intéressant, la structure du modèle avec la glycolyse régulée résulte à la simulation du passage d'un métabolisme de phosphorylation oxydative à un métabolisme de la glycolyse anaérobique, un résultat qui est en accord avec la littérature. Le modèle développé a ainsi montré une capacité prédictive. En conclusion, ce travail a abouti à un modèle dynamique décrivant le comportement du métabolisme des cellules CHO, et qui pourrait être utile comme outil *in silico* pour l'optimisation des bioprocédés.

ABSTRACT

The main objective of the work was to demonstrate that a dynamic modelling approach can be useful to elucidate the behaviour of CHO cells' central carbon metabolism. The first part of this work focuses on the development of a dynamic model of CHO cells primary metabolism.This work was inspired by a previously developed kinetic metabolic model in our group to describe plant cell primary metabolism. The metabolic model was developed and calibrated using data previously obtained in our group from bioreactor cultures of CHO cells expressing recombinant t-PA. In addition to routine datasets, including the concentration of cells, glucose, lactate, glutamine and ammonia with time, intracellular concentrations of energetic nucleotides and cell specific oxygen consumption were also available. The main outcome of this part consists in a kinetic metabolic model that allows describing the behaviour of the major metabolic pathways, i.e. glycolysis, pentose phosphate pathway, TCA cycle, glutaminolysis as well as cell respiration,in CHO cells. The model has 30 metabolic reactions and 72 parameters. Model simulations were shown to agree with experimental data, which is suggesting that the proposed model structure copes with CHO cells' biology. The model was also used for studying the effect of inducing CHO cell culture by adding sodium butyrate, a widely used chemical to enhance recombinant protein production. Albeit the high number of parameters, limited model adaptation was required (i.e. the changing of only few parameters values), in agreement with gene expression modifications reported in literature, to describe the effect of sodium butyrate on CHO cells. Results from model simulations further supports our previous findings that butyrate treatment at mid exponential phase may induce a shift in cellular metabolism by increasing the efficiency of glucose utilization, with a greater fraction of this nutrient channeled through TCA cycle. Although mostly speculative while based on model simulations, the results agreed with data as well as common hypothesis found in literature of the effect of sodium butyrate on CHO cell metabolism.

In a second part, the descriptive capacity of the model was further assessed using data from another recombinant CHO cell line under different culture conditions. The model was then challenged to simulate batch cultures for different clones of a CHO cell line genetically modified with an inducible expression system, called the cumate gene-switch,

for the production of anti CD-20 monoclonal antibody. Low- and high-producer cell lines were compared to parental. The extra- and intra-cellular metabolites quantification was also included in the study. The model structure showed to be easily adaptableto another CHO cell line and its clones, by only requiring limited model modifications, which were interpreted and analysed as specific cell line characteristics. The model was extended hereto also describe amino acids metabolism and recombinant monoclonal antibody production kinetics. It thus now includes 35 reactions and 92 parameters. However, limited modification, i.e. changing few parameters in both low-and high-producing clones, allowed simulations that accurately described metabolic variations related to clonal variation. Different patterns of metabolic flux distribution specially in high-producer clone was simulated by the model and the increased efficiency of cell metabolism, i.e. greater portion of glucose incorporated into the TCA as opposed to being converted to lactate, and up regulation of TCA cycle, has shown to be more induced by clonal variation than by recombinant protein induction. From our results, it is clear that such dynamic model can be readily adapted to existing culture datasets. Finally, in a third part of the thesis, model behaviour was studied while integrating metabolic regulation of glycolysis. The aim of that study was to evaluate to what extent our kinetic model can describe the effect of a sudden perturbation on cell metabolic behaviour, while having been calibrated using culture data showing slow dynamics. Regulatory mechanisms known to apply along the glycolysis pathway in mammalian cells, i.e. feedback and feedforward inhibition and activation regulatory mechanisms from glycolytic metabolites and energetic variables, were integrated in the model. An *in silico* experiment was performed adding a sudden hypoxic stress, decreasing oxygen level at 10% of air saturation. The model was then modified to include the effect of seven regulatory functions in glycolysis pathway with one parameter for each case. Interestingly, the model structure with a fully regulated glycolysis results in the simulation of a shift from an oxidative phosphorylation metabolism to an anaerobic glycolysis metabolism, a result that is in agreement with literature. The implemented model thus showed a predictive capacity. In conclusion, this work has led to a dynamic model describing CHO cell metabolic behaviour that could be useful as an *in silico* tool for bioprocess optimization.

TABLE OF CONTENTS

LIST OF TABLES

LIST OF FIGURES

LIST OF ABBREVIATIONS

AA: Amino acids

ACCOA: Acetyl-CoenzymeA

AKG: α-ketoglutarate

ALA: Alanine

ARG: Arginine

ASP: Aspartate

ASX: Extracellular Aspartate and Asparagine

ATP: Adenosine triphosphate

ADP: Adenosine diphosphate

AMP: Adenosine monophosphate

CHO: Chinese Hamster Ovary

CIT: Citrate

C_i : Control coefficients

CoA : CoenzymeA

CO_2: Dioxyde de carbone

Cr:*Creatine*

DO: Dissolved oxygen

DNA: Deoxyribonucleic acid

EALA: Extracellular alanine

EASP: Extracellular aspartate

EGLC: Extracellular glucose

EGLN: Extracellular glutamine

EGLU: Extracellular glutamate

ELAC: Extracellular lactate

ELISA: Enzyme-Linked ImmunoSorbent Assay

ENH_4: Extracellular ammonia

$FADH_2$: Flavine adenine dinucleotide

FUM: fumarate

F6P: Fructose-6- Phosphate

GAP: Glyceraldehyde 3-phosphate

GDP: Guanidine diphosphate

GDP: Guanidine dephosphate

GTP: Guanidine triphosphate

G6P: Glucose-6-phosphate

GC: Gas chromatography

GLC: Glucose concentration

GLN: Glutamine concentration

GLY: Extracellular Glycine

H: Hour

H_2O: Hydrogen dioxide

HEK:Human Embryonic Kidney

HIS: Extracellular histidine

HPLC-MS: High performance liquid chromatography – mass spectroscopy

IgG: Immunoglobulin G

ILE: Extracellular isoLeucine

LUE : Extracellular leucine

LYS : Extracellular lysine

K_m: Affinity constant

Mab: Monoclonal antibody

MAL: Malate

MCA: Metabolic control analysis

MBFA: Metabolic balance flux analysis

MFA: Metabolic flux analysis

NaBu: Sodium butyrate

NAD: Nicotinamide adenine dinucleotide (Oxidized)

NADH: Nicotinamide adenine dinucleotide (reduced)

NADP: nictoniamide adenine dinucleottide phosphate

NADPH: nictoniamide adenine dinucleottide phosphate (reduced)

NMR: nuclear magnetic resonance

OXA: Oxaloacetate

PEP: Phosphoenolpyruvate

PCr:Phosphocreatine

Pi: inorganic phosphate

PYR: Pyruvate

R5P: Ribulose-5-phosphate

RNA:Ribonucleic acid

SER: Extracellular serine

SUC: succinate

SUCCOA: Succinyl coenzyme A

TCA: Tricarboxylic acid

TYR: Extracellular tyrosine

UDP: Uridine dephosphate

UTP: Uracil triphosphate

v: Metabolic flux

v_{max}: Maximum enzymatic reaction rate

Var: Variance

WSSRES: Weighted sum of squared residuals

X5P: Xylulose 5-phosphate

X^{mea}*:* experimental data

X^{sim}*:* Simulated value

LIST OF APPENDICES

CHAPTER 1 INTRODUCTION

1.1 The mammalian cell industrial production platform

Mammalian cells have attracted industrial attention over the last decades because of their unique ability to synthesize human-like high value products that can hardly be made by microorganisms (Aggarwal et al., 2011). These products, often highly glycosylated proteins such as antibodies, are now widely used for diagnostic and therapeutic applications (Leader, Baca, & Golan, 2008). Since the first approval of a therapeutic protein by the USA Food and Drug Administration (FDA) with recombinant insulin in 1982 (Leader et al., 2008) and up to 2011, a total of 96 recombinant protein therapeutics produced from mammalian cells have been approved. The annual revenue for the USA only is now reaching $112.93 billion dollars (www.pipelinereview.com). These numbers continue to increase following biopharmaceutical industry improvements with an average of 15 new drug approvalsper year by the FDA from 2006 to 2011 (Lai, Yang, & Ng, 2013). Nowadays, the majority of biopharmaceutical products are produced at industrial scale in multi-m^3 bioreactors using mammalian cell lines such as Chinese Hamster Ovary (CHO) cells. The CHO platform is used to produce over 40% of monoclonal antibody products currently approved by the FDA (Grillari et al., 2001) while murine myeloma (NS0) account for 25% of monoclonal antibody products (Barnes, Bentley, & Dickson, 2000) and hybridoma cell lines for the production of murine monoclonal antibodies mostly for research and analysis purposes (Davies, Gallo, & Corvalan, 1999). However, there are few other cell lines that are assessed for the production of human-like monoclonal antibody products and human cells are seen as potential alternatives to CHO cells (Jones et al., 2003). Moreover, some other cell lines have a specific niche such as the baby hamster kidney (BHK) cells that are mainly used for virus and vaccine production (Pitti et al., 1994). However, although the industry has now reached high expression titers using mammalian-cell platforms (mg to g L^{-1}), the limited level of understanding on the links between cell behaviour and the physico-chemical environment still affects production reproducibility in quantity and quality (e.g. glycosylation profile), as well as reducing time to market (i.e. cell line and media selection and cell culture management). This thesis thus aims at developing an *in silico* tool that could contribute to minimize the impacts of such limitations.

1.1.1 Mammalian cells versus other cell culture platforms

Glycosylation, which consists in the attachment of a sugar molecule to an amino acid residue of a protein, is a crucial process known to confer multiple specific functional properties to proteins, and thus of protein-based therapeutics (Beck et al., 2008). As a biotherapeutic, a protein glycolytic profile qualifies its *in vivo* efficacy (Durocher & Butler, 2009; Higgins, 2009), and it is highly dependent on the expression cell platform as well as on culture conditions (Ghaderi et al., 2012). It has been shown possible to specifically engineer a biotherapeutic protein glycosylation, in various cell production platforms, to impose human-like characteristics (Higgins, 2009). Fundamentally, bacterial expression systems are not genetically equipped to glycosylate proteins; these prokaryotic cells are lacking the enzymatic machinery required for mammalian-type glycosylation such as N- and O-glycosylations, which are affecting the 3D conformational structure of proteins. Recently, some promising strain/genetic engineering approaches were applied to bacterial platforms with the transfer of mammalian glycosylation machinery (Nothaft & Szymanski, 2011; Schwarz et al., 2010). Although these modifications allowed synthesis of mammalian-like N-glycans and thus markedly enhanced bacterial capacities for recombinant protein production, some issues still need to be addressed. First, strong transcriptional promoters are required to enable high-level gene expression. Promoters thus have to be induced while most inducers can be toxic and are expensive (Samuelson, 2011). Second, recombinant proteins should be released into the medium to ease their harvesting.In bacterial expression systems, however, they are directed to three different locations i.e. the cytoplasm, the periplasm, and to a lesser extent the growth medium (Jana & Deb, 2005). It is generally more preferable that expression of recombinant proteins occurs in cytoplasm since it leads to higher production yields. Low temperature, i.e. the use of cold inducible promoters, has proven to enhance protein folding in cytoplasm. However, that often leads to wrong interactions of amino acids and and not a well-defined three-dimensional structure known as protein misfolding (Khow & Suntrarachun, 2012).

As such, additional improvements are needed in establishing cost-efficient, reliable bacteria-based expression systems. Protein glycosylation can also be performed *a*

posteriori, chemically, on purified proteins, but the costs can be prohibitive and the yields in adequate glycolytic profile are still low (Macmillan et al., 2001).

Yeast, an eukaryotic cell, also provides an attractive expression platform offering considerable advantages, such as ease of culture, ability to maintain high growth rate and to reach high densities using chemically defined media, and finally sharing the same N-glycan core structure with humans (Böer et al., 2007). However, the yeast expression system is also subject to certain drawbacks such as hyper-glycosylation, in which case additional mannose residues are bond to the N-linked carbohydrate chain of the proteins, which is of allergenic potential (Gellissen et al., 2005). Although this issue has been addressed over the past decade with various genetic modifications strategies, any commercialized human-like recombinant N-linked glycoprotein expressed in yeasts has not yet been reported, to the best of our knowledge. Plant-based expression systems also offer some advantages over other recombinant protein production platforms such as lower production costs and ease of scaling up to commercial production (Gomord et al., 2010). Probably the best advantage of plants resides in an unbeatable time-to-market of only few weeks, from product identification to mass production, using the recent agro-infiltration technique based on transient transfection approach (Golemboski, Lomonossoff, & Zaitlin, 1990; Vezina et al., 2013). This transient approach looks promising and many efforts are now placed into the niche of the rapid production of vaccines or virus like particles to face pandemia (Paul & Ma, 2010). However, the first recombinant protein obtained from plant biotech was from transgenic carrot cells cultured in suspension, and homologated by the FDA for the treatment of Gaucher's disease in 2012 (www.protalix.com). Therefore, it has been shown possible to produce proteins in plants that are biosimilar to those in human. Although plant cells can synthesize mammalian type complex N-glycans, glycoproteins expressed in plants have a different glycan structure caused by differences in the plant and human N-glycan processing machinery (Gomord et al., 2010). Therefore, intensive research is directed towards the modification of plant glycosylation pathways for the production of completely humanized proteins (Cox et al., 2006).

Similarly to the plant-based platform, the glycans produced by insect cells also differ significantly from those present in human. Recombinant proteins expressed in insect cells

completely lack some essential parts, such as galactose and sialic acids, both present in human proteins (Ailor et al., 2000). Consequently, more research has to be done on this platform to compete with mammalian cells.

Taking all of the above into consideration, one can understand that the mammalian cell expression platform is still predominant in industry to produce recombinant proteins. However, other platforms may benefit, in a near future, from the coming developments in glycosylation engineering, as well as from the identification of more simple ways to produce drugs' active sub-parts.

1.2 Challenges in the optimization of therapeutic proteins production

The mammalian cell platform is attracting most of the research investments worldwide in order to be continuously improved for recombinant protein production, as well as cell line selection and culture protocols to reduce time-to-market (Ailor et al., 2000). Bioproducts obtained from mammalian cells are highly complex, and because these therapeutics can induce strong and undesired side effects, their production is highly constrained by the regulatory agencies worldwide. The global development process of a new therapeutic product, and its acceptance and homologation by regulation agencies, can require up to 10 years of efforts and significant financial investments; this includes cell line development and the production process, as well as conducting extensive testing of the end-product therapeutic to demonstrate both its medical efficiency and innocuity (DiMasi, Hansen, & Grabowski, 2003). In cases of diseases that are affecting only a small population, in which case the will of pharmaceutical companies could be low to inexistent because of the little size of the market, regulatory agencies allow accelerating the homologation process for these so-called "orphan" drugs. This can thus favor these drugs development whatever their financial context. Although the maximum recombinant protein concentration that is now reported has increased by 1000-fold (mg/L to g/L) in the past decades, there are still important drawbacks limiting product quality and process productivity reproducibility at the industrial scale(Wurm, 2004).Basically, reproducibility of the results is among the most fundamental requirements of mammalian cell culture processes to be acceptable industrially. The clones that are selected should generate cultures reproducing the characteristics of the very first culture, up to the large scale production (Jayapal et al., 2007). Mammalian cells, however, can exhibit a considerable

degree of variability and the sourcesof this variability remain often obscure. This variability in the performance of cell culture processes is mainly related to lot-to-lot inconsistency of production in terms of both quantity and quality. First, one major challenge facing therapeutic protein production in mammalian cells is that the expressionof proteins declinesover time (with cell generation) and is often unstable during the time of development (Anderson & Krummen, 2002a). Since cells are genetically modified (at least for producing a recombinant product), they are even more sensitive to genetic drift and loss of high-producer capacity due to intrinsic genetic repair mechanisms (Palomares, Estrada-Mondaca, & Ramírez, 2013). This implies that the long time required from cell line construction and selection to clinical trials mayface genomic instability of a selected mammalian cell line, and see a high-producer clone becoming a low-producer one.Second, therapeutic product glycosylation profile variations, besides variations in production level, can dramatically lower or even remove any commercial value. Glycosylation pattern has been reported to be extensively affected bycell type, culture process and culture media conditions(Hossler, Khattak, & Li, 2009). Therefore, any mistake in culture protocols or misunderstanding of culture behavior leading to non-reproducible product quality level may dramatically impact the therapeutic safety evaluation by regulatory agencies, thus resulting in the reject of product homologation. So, there is still a need to engineer a well-characterized cell line to expand its capacity so that it can control the glycosylation profile towards optimal pattern in differentculture conditions(Hossler et al., 2009). Third, there are still reports of potential product heterogeneities where a single optimal glycan profile cannot be achieved in mammalian cell culture processes. Glycoform heterogeneity, that highly depends on the manufacturing process, can even occur throughout a batch culture and may decrease the desired therapeutic efficiency. (Abu-Absi et al., 2010). The depletion of nutrients throughout batch cultures has been reported to cause such product heterogeneity (Castro et al., 1995) .So, the status of homogeneous glycoform profiles that can be systematically screened for in mammalian cell culture processes is still too low. Forth, to achievehigh titres of the product, both high cell specificproductivity and cell density should be achieved. Apoptosis, or programmed death, is known to be the major cause of cell death for mammalian cell lines used at industrial scale (Al-Rubeai, 1998; Laken & Leonard,

2001). Engineering of cell lines with anti-apoptotic factors, to be overexpressed during the culture, has been reported to delay the onset of apoptosis (Andersen & Krummen, 2002; Birch, Mainwaring, & Racher, 2005). However, the overexpression of these factors can cause stresses during cell culture that can compromise the productivity (figueroa et al., 2007; Ishaque & Al-Rubeai, 2002). Therefore, enhancement of cellular viability will not necessarily improve the overall productivity.Taken all of the above into account, it is clear that the mammalian cell platform is complex, and the keys allowing reaching an adequate mastering of its output, i.e. a therapeutic product having a high commercial value, require additional fundamental studies linking process conditions and cell physiology. Consequently, the industry has developed impressive high-throughput approaches enabling massive assays for the identification of optimized culture media and cell lines. However, the use of mathematical tools simulating cell and bioprocess behavior may help at defining favorable conditions at a lower cost and more rapidly, thus accelerating high-throughput studies.

1.3 Mathematical modeling of biochemical networks: rationale and objectives

1.3.1 Modeling as a tool for the control of a bioprocess

It is now clear that the development of a bioprocess involving the mammalian cell platform is, indeed, a multi-factorial task implying various disciplines from molecular biology to biochemical engineering (Koutinas, Kiparissides et al., 2011). Molecular biology works are required to generate stable cell lines producing a recombinant product of interest. Although significant breakthrough have been reached enabling the insertion of a new gene expression capacity in cells (Kayser et al., 2006), the challenge is to obtain high titers. As previously explain, cell behavior can be highly affected by its environment (Clark et al., 1990) and the result from an intuitive genetic modifications can be opposite to expectations (Andersen & Krummen, 2002). So, reaching high titers may rely on the combination of various factors such as 1) defining optimal culture media, 2) selecting a parental cell line, 3) identifying the genetic modification protocol, and 4) selecting high-producer stable cell lines (Fox, 2004). Moreover, the final production bioreactor unit may also require a subtle medium management strategy, such as fed-batch or perfusion culture protocols, in order to maximize cell productivity (Chu & Robinson, 2001). Indeed, a

valuable protocol should specifically define optimal feeding time profile, optimizing medium composition at all time. In that context, mathematical models may be expected to play an important role in both bioprocess characterization and control.Classical modelling approaches normally limit bioprocess characterization to mass balances around the bioreactor to determine the concentration time course of nutrients, products and byproducts (Bastin & Dochaln, 1990). These approaches were shown to allow for the control of bioreactor production with the mammalian cell platform (Dhir et al., 2000; Tremblay et al., 1992; Zhou et al., 2006). However, although such modelling approach lead to valuable process information, it may be too partial for enabling a complex control level involving many nutrients that are not necessarily limiting but which respective effects on cell behaviour reside within intracellular flux dynamics. Different compositions of media have been proven to lead to distinct cellular behaviours with regard to metabolic efficiency and reduced formation of by-products (Bonarius et al., 2001; Bonarius et al., 1998; Xie & Wang, 1996). Different medium protein and amino acid concentrations have also been shown to lead to different metabolic states (e.g. higher TCA activity), although the main nutrients, glucose and glutamine, were present in sufficient amounts (Nadeau et al., 2000; Xie & Wang, 1996).Replacement or supplementation of the nutrients with other available sources, e.g. galactose, also showed to modulate cell metabolism with regard to metabolic branch points, e.g. glycolysis and TCA (Altamirano et al., 2006; Altamirano et al., 2000; Wilkens, Altamirano, & Gerdtzen, 2011). An adequate information level ethat permits defining an effective control strategy may thus require a more descriptive model of cell behaviour. Such model could even have predictive properties of cell behaviour. This approach is directly in line with the "Process Analytical Technology" (PAT), an essential quality element of the “Pharmaceutical Current Good Manufacturing Practices (CGMPs)” for the 21st Century (Rathore, Bhambure, & Ghare, 2010), promoted by Food and Drug Administration (FDA) in 2004 (Gnoth et al., 2007).

Moreover, production bioprocesses using a mammalian cell platform normally include defined perturbations from the use of chemical additives (Kumar, Gammell, & Clynes, 2007), inducible promoters (Mullick et al., 2006) or a transient transfection strategy (Durocher, Perret, & Kamen, 2002; Pham, Kamen, & Durocher, 2006). Therefore, the

problem of defining an optimal culture management strategy becomes even more complex when sudden stresses affecting cell metabolism are imposed. Taken all of the above together, it seems obvious that mathematical models able to characterize and describe cell behaviour from various perturbations along bioprocesses are mostly required.

1.3.2 Models to better characterize a living cell

A cell can be considered as an open system which exchange energy and matter with the environment. This, in turn, enables the cell to maintain internal order and to synthesize building blocks for its functions, growth and survival. The material taken up by a cell follows a series of transformations usually referred as cellular metabolism (Alberts et al., 2002a). Cell metabolism is thus a dynamic coordinated ensemble of processes involving biochemical reactions all interrelated within a metabolic network. Metabolites are generally synthesized along metabolic pathways, i.e. the units of a metabolic network (De la Fuente et al., 2013). A living cell has its metabolic activities regulated and controlled by intricateregulatory mechanisms. To efficiently characterize cell physiology, a detailed mathematical representation of the metabolism is required. Depending on the level of detailed information available, different mathematical representations of cell metabolism may be developed. A lumped model, which considered only substrate, product and growth using Monod kinetics, for instance, represents the early attempts at developing metabolic models with a low level of details. A mathematical approach named as metabolic flux analysis (MFA), has then been developed for describing metabolic fluxes rates under steady state condition. In MFA, intracellular fluxes are calculated based on measured exchange rates (Price, Reed, & Palsson, 2004). Metabolic flux balance analysis (MFBA) is a special case of MFA in which a solution for the reaction rates of a network is obtained through the optimization of a particular network function (Edwards et al., 1999). The MFBA approach is not confined to measured reaction rates but it is limited to the assumption of an optimal behaviour of cells. Therefore, living cells are now studied more as a metabolic network with components, i.e. metabolites and biochemical reactions that are highly interconnected. In this regard, mathematical models have proven to provide a framework in which data obtained from high throughput experiments can be analyzed to reveal new insights into the functioning of cellular metabolism. Based on the

concept that cells in culture generally exhibit completely different behaviors depending on the environmental fluctuations, this mathematical framework should get its best use to predict how metabolic network responds dynamically to a changing environmental condition (Chin et al., 2008).

Different concentrations of glucose, glutamine, and amino acids can induce many cultures to shift to different metabolic states, i.e. oxidative metabolism or anaerobic glycolysis, different levels of inhibitory metabolites (Altamirano et al., 2004; chen & Harcum, 2007; Xie & Wang, 2006; Zhang, Shen, & Zhang, 2004). In addition to nutrient concentrations, growth factors, and lipids in culture medium have also shown to effect cellular behaviour, i.e. cell growth. Addition of product enhancers such as sodium butyrate to cell cultures has also proven to effect metabolic efficiency and promote special pathways (De Leon et al., 2007; McMurray-Beaulieu et al., 2009; Yee et al., 2008). More specific conditions include supplementing culture media with intracellular metabolites, i.e. pyruvate, also influencing particular cellular metabolic pathways (Genzel et al., 2005). Therefore, the role of a cell regulatory machinery is crucial to ensure metabolic homeostasis; i.e. maintaining intracellular conditions at defined setpoints (De la Fuente et al., 2013).

Moreover, the mathematical framework should also be able to predict how the introduction of perturbations to a cell, e.g. environmental or genetic, can effect cell metabolism (Cloutier & Wang, 2011). This is encouraged by the fact that cellular pathways are complex and highly interconnected while modulation of metabolic fluxes due to local genetic perturbation should not be studied separately, i.e. increased flux through the overexpression of the corresponding enzyme, but as a network (Morandini, 2009). This lack of systematic analysis is mostly well-known in the field of metabolic engineering. In many studies the overexpression of an enzyme, i.g. phosphofructokinase in glycolysis failed to increase flux rates in glycolysis pathway (Thomas et al., 1997). Therefore, there is a need for a dynamic mathematical framework that can reproduce some of these important observations. Such dynamic model should grasp cellular dynamics and the regulatory mechanisms involved in different conditions and operational systems (Bonarius, Schmid, & Tramper, 1997). MBA and MFBA methods bring valuable

insights into metabolic flux distribution at steady state, however, they lack information on the dynamics of the process.

1.3.1 Modeling cell behaviour: a long term objective of the research group

In 2007, Professor Mario Jolicoeur's research group, at the Ecole Polytechnique de Montréal, developed a kinetic-metabolic model framework adapted to plant cells (Cloutier, Perrier, & Jolicoeur, 2007). It was demonstrated that the model can successfully describe the dynamics of plant cells metabolism. It was also applied to the control of intracellular concentration such as of the cytoplasmic inorganic phosphate at a defined set-point (Cloutier et al., 2009). It was even used as an *in silico* tool to design a culture management strategy to maximize secondary metabolites production in a bioreactor culture (Cloutier et al., 2009). Therefore, we have explored this kinetic-modelling approach for its use on mammalian cells.

1.4 Project objectives and methodology

This work aims to develop a mathematical model capable to describe CHO cell transient behavior in culture. Paying a particular attention to keeping a biologically relevant description of the CHO cell central metabolism, including cell growth and production in a recombinant product such as a protein and a monoclonal antibody (mAb), we have challenged our modelling approach with different CHO cell lines. A first series of data was limited to basic culture datasets (including cell growth, production, respiration, glucose, glutamine, lactate, and ammonia and intracellular concentrations of energetic nucleotides and cell energetics with time) for a cell line producing a recombinant t-PA (transplaminogen activator). This was used to develop the model structure and for the calibration of its parameters. Although mainly extracellular data were used (except for cell energetic), the model was assessed for its capacity to simulate intracellular events such as metabolic fluxes and metabolites concentrations. Then, we tested the adaptability of the model structure by challenging it with another cell line containing an inducible cumate gene switch enabling the production of a monoclonal antibody. We had access to the parental cell line as well as low- and high-producer cell lines. Finally, we assessed for the model predictive capacity while it was challenged to describe an *in silico* perturbation experiment, using a hypoxic stress as a case study.

1.5 Organization of the thesis

The thesis contains nine chapters. Chapter one presents a brief introduction describing the thesis context and objectives. The current status of knowledge on the mammalian cell platform and the challenges at improving bioprocess reproducibility and productivity are discussed. Mathematical modelling of cell behaviour, as a method to study mammalian cell metabolism, is finally introduced. In chapter two we elaborate on the most important characteristics of CHO cells while developing a kinetic metabolic model, putting a particular attention at cell metabolismand regulatory interactions involved in metabolic hemostasis. In the third chapter, the general methodology used in this work is presented, and the general algorithm followed to develop the kinetic metabolic model is shown. In chapter four, a metabolic model is developed on the basis of biochemical information available for CHO cells metabolic network, and assumptions on unknown information are discussed. The model is first calibrated on previously published experimental data obtained in our research group (McMurray-Beaulieu et al., 2009).In chapter five, the capacity of the model to be adapted to another recombinant CHO cell line is presented. Extensive measurements of extra- and intra-cellular metabolites concentrations were obtained for another CHO cell line; a *parental* and its high- and low-producer derived clones producing a recombinant monoclonal antibody under the induction of a cumate gene switch.

In chapter six, the model is implemented with regulation mechanisms of glycolysis pathway and assessed to study the dynamics of metabolic network in response to a hypoxic stress.

In chapter seven, we present the general discussion, in chapter eight, the main conclusions and in chapter nine proposed future works are summarized.

CHAPTER 2 LITERATURE REVIEW

2.1 CHO cells for the production of mAbs

The domestic Chinese hamster originates from Beijing (Peking), and the first report on the use of this animal for the treatment of Pneumococcal infection goes back to 1919 by Hsiehin China (Hsieh, 1919). Much later, subsequent research on Chinese hamster ovary in the mid-20th century suggested that the low chromosome number of this animal made it a good candidate for research. It was at that time that Dr. Theodore T. Puck, a pioneer in mammalian cell culture, established the first Chinese hamster ovary cells (CHO) in plate (Tjio & Puck, 1958).It soon became clear that these cells were readily good candidate in *in vitro* culture. Up to now, CHO cells showed a high adaptive ability and ease of maintenance which make them good candidates for fundamental research in biomedical, pharmacology and cell signaling (Figler et al., 2003; Schulte & Fredholm, 2003). This cell, which naturally grows as adherent cells, can also be adapted to suspension culture showing adequate resistance to shear stress when cultured in bioreactors (Jayapal et al., 2007). Nowadays, over 70% of all recombinant proteins are produced by CHO cell derived platforms (Jayapal et al., 2007). In addition of being predisposed to genetic modification and *in vitro* culture, CHO cells are also being used from the mass effect created after the homologation of various recombinant therapeutics using these cells; i.e. it facilitates homologation of a new product since the cell platform is now well known by the regulatory agencies (Meyer et al., 2008). Among all recombinant proteins, monoclonal antibodies have received special attention during the past decades. Antibodies are large proteins with a Y-shape which are produced by B-cells in response to foreign object and used by the immune system to identify and neutralize it (Riechmann et al., 1988). When antibodies are produced from a population of B cells which is derived from a single parental cell they are homogeneous and named monoclonal antibodies.Monoclonal antibodies have received most of the industrial attention because of the important market share with almost 376 preclinical to market products (Pavlou & Belsey, 2005). For example Vectibix (Anti-EGFR mAb), Avastin (Anti-VEGF mAb), and Herceptin (Anti-HER2 mAb) have been commercialized as therapeutic agents regarding colorectal, lung, and breast cancer respectively. Xolair (Anti-IgE mAb), Raptiva (Anti-CD11a mAb), Campath (Anti-CD52 mAb), and Rituxan

(Anti-CD20 mAb) are also some examples of mAbs commercialized to treat asthma, psoriasis, and lymphoma respectively (Jayapal et al., 2007). From an industrial point of view, CHO cells are highly efficient for the production of antibodies for a couple of reasons. First, they exhibit a stable growth, in terms of cell counts and prolonged cell viability, due to their robust nature (Chu & Robinson, 2001). Second, they can be easily adopted to grow in suspension culture which is favorable for large scale industrial production (Boeger et al., 2005). Third, glycoproteins that are expressed in CHO cells have a glycosylation profile that is more human-like comparing to other cell lines(Ghaderi et al., 2012). Fourth, there is a good record of several genetic amplification systems (e.g. chaperones such as Hsp70 and Hsp27) in CHO cells (Lee et al., 2009). Fifth, host-cell related contaminating impurities are well understood in CHO cells resulting in more efficient downstream processes comparing to other mammalian cell lines (Wurm, 2005). All these factors ultimately results in higher titers of recombinant proteinreaching up to 5 g/L (Kim, Kim, & Lee, 2012) in fedbatch cultures. CHO cells viability has been improved through genetic modifications such as, complementing the cell machinery with growth factor endogenous proteins (e.g. insulin like growth factors) (Galbraith et al., 2006; Sunstrom et al., 2000; Zanghi et al., 2000) or optimizing cell-cycle control genes (e.g. cyclin-dependent kinases) (Fussenegger et al., 1998), or through the enhancement of cellular metabolism (Irani et al., 1996; Wlaschin & Hu, 2006). Various strategies also showed to be successful in enhancing CHO cells productivity at the genomic level, i.g. the use of cytomegalovirus (CMV) and beta-actin and EF-1α as strong promoters, and the insertion of dihydrofolate reductase (DHFR) as an amplification marker (Cacciatore, Chasin, & Leonard, 2010), just to name a few. Above all these, the complete sequencing of CHO Genome has recently been accomplished and can support future breakthroughs in CHO-cell production platform (Xun et al., 2011). However, there is still a risk in terms of performance variability during scaling-up and manufacturing (Li et al., 2010).

2.2 Physiology andmetabolism ofmammalian cells

Thissection presents themain metabolic pathwayspresentin CHO cells, as well as their common behaviour. Mammalian cellsare eukaryoticcells that have a phospholipid membrane composed of proteins and lipids that surround the cytoplasm of the cell

(Figure 2.1). The cytoplasm is filled with dispersed particles and compartments such asnucleus,ribosome, Golgi apparatus, and mitochondria. Thesecompartmentshaveunique properties. The nucleus containsmostof the genetic material. Ribosome is involved in protein synthesis. Golgi apparatus modifies the proteins, specially those for excretion. In mammaliancells, thepower generation mostly takes place inthe mitochondria. Mitochondria, which is the location where theKrebs cycleandoxidative phosphorylationprovidesmost ofthe energy of acellunder aerobic conditions.

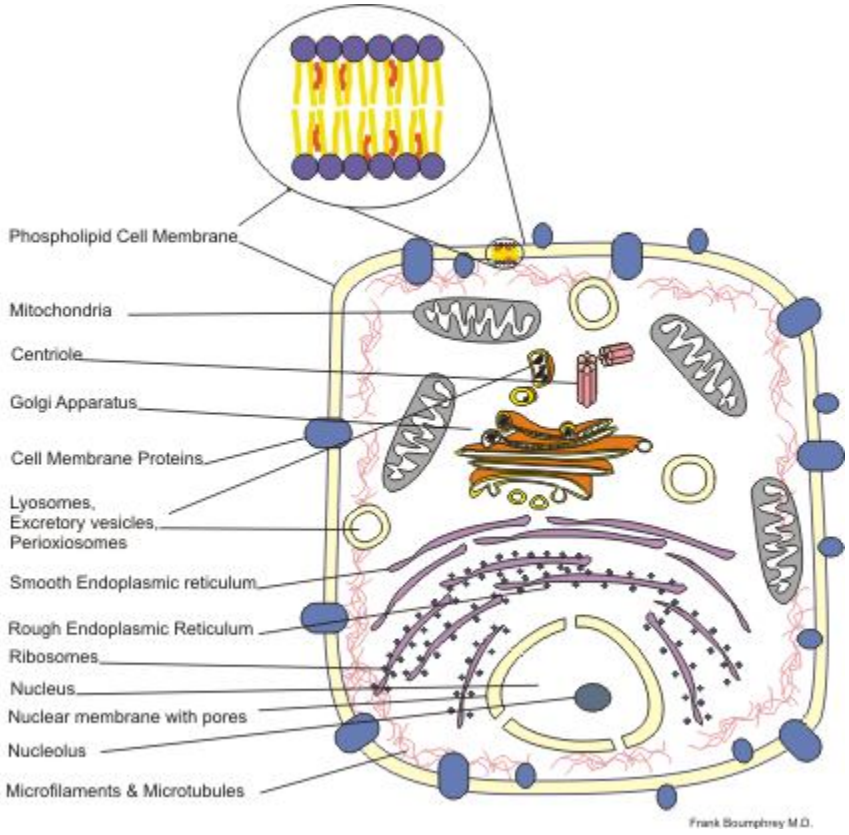

Figure 2.1Schematic diagram ofmammalian cells
(Boumphrey, 2009)

2.2.1 Nutrition management

Mammalian cellsneed various classes ofnutrients: the macronutrients, presents in mM in the culture medium, carbohydrates, amino acids, vitamins, and micronutriments, present

in μM, inorganic ions, each bringingthe cell elementary content in atomssuch ascarbon (C), oxygen (O), hydrogen(H), phosphorus (Pi), sodium, potassium, calcium, magnesium, and nitrogen (N). There are other trace elements (<μM) such as zinc, selenium, copper, manganese oriron (Fe) (to name a few)alsorequired by thecellsbut inmuch smaller amounts plus defined growth factors. Ithas been demonstrated that the nutritional statusof mammalian cellsstronglyinfluencetheir ability for growth and production.In other words, medium composition is known to affect the productivity ofmammalian cells in vitro (Grosvenor, 2008). Furthermore, fed-batch culture protocols are now widely used since these allow for maintaining and controlgrowth condition and is now seen essentialto extend culture durationfor improving final product titers (up to 5 g/L) (Yang & Xiong, 2012). Fed-batch processes are currently highly favorable for industrial scale production because they are reproducible, easy to operate and scale up to as high as 20,000-liter volumes (Whitford, 2006). In order to develop a fed-batch protocol, parameters as optimal feed profile and time should be identified which requires an efficient process monitoring system. Although on-line measurements techniques have been developed during past years, an available tool allowing prediction of cell behaviour in response to culture conditions is still desirable. In that context, kinetic models can be useful as a tool for *a priori* determination of cells requirements for further implementation of control (Pörtner, Schwabe, & Frahm, 2004). Nutrients are then feeding the entry points of the cell metabolism.

2.2.2 Cellular metabolism - The way from genotype to phenotype

Cell functions and operations are accomplished through a series of biochemical reactions usually occurring inside a cell. biochemical reactions involve in the processes of taking up complex molecules (sources of carbon, nitrogen), and further breaking down to produce energy and other intermediate molecules (Alberts et al., 2002). Intermediate molecules finally build up new macromolecules and cellular components (Barnes et al., 2000). Enzymes are protein catalysts that control biochemical reactions and a protein itself consists of a string of amino acids, each one of which is coded by the string of DNA constituting a gene. Recalling that biochemical reactions involve in the conversion of substrates into products, often by transporting chemical groups, giving the function to the

compound, to or from the substrates.Thereare sixmajor classes ofbiochemical reactions involved in cellular metabolism (Berg, Tymoczko, & Stryer, 2002)(Table 2.1).

Table 2.1 Types of reactions involved in metabolism

Classes of reaction	Mechanism	Nomenclature *Enzyme Commission*
Oxidation - Reduction	Electron Transfer	EC 1 : Oxydoreductases
Transfer of a group	Transfer of a functional group from one to another	EC 2 : Transferases
Hydrolysis	Hydrolysis of a biochemical bond	EC 3 : Hydrolases
Addition / Subtractionof functional groups	Additionof a functional groupsto a double bondorsubtractionforma double bond	EC 4 : Lyases
Isomeration	Rearrangementof atoms	EC 5 : Isomerases
“ Ligation “ involving ATP lysis	Formation of covalent bonds	EC 6 : Ligases

Biochemical reactions are thus managed through enzyme-powered pathways in cells. These series of biochemical reactions are collectively known as cellular metabolism. Cell metabolism thus leads to the passage of information between genotype (information held in genome) and phenotype (growth and cell metabolism) (Lewontin, 2011).

2.2.2.1 Catabolism and anabolism – Inputs and outputs of cellular primary metabolism

The cell metabolism consists of two major interdependent parts, with the catabolism and the anabolism (Figure 2.2). Catabolism is responsible for the breakdown of complex organic compounds, nutrients, and macromolecules, while providing positive energy (ATP) and redox potential (NADH, and NADPH) and feeding the rest of the metabolism in precursor molecules. The other part, the anabolism, is responsible for the synthesis of metabolites and macromolecules, from precursors, which are required for cell functions, growth and viability. Anabolism is known to be highly demanding in energy and redox potential (Steuer et al., 2006). Under aerobic condition, oxidative phosphorylation is responsible for massive energy production in support of anabolism (Lunt & Vander Heiden, 2011).

The main metabolic pathwayspresent inCHO cells and integrated in this work, i.e. glycolysis,pentosephosphatepathway, the Krebs cycle, oxidation phosphorylationas well as aminoacids catabolism are described in the following.

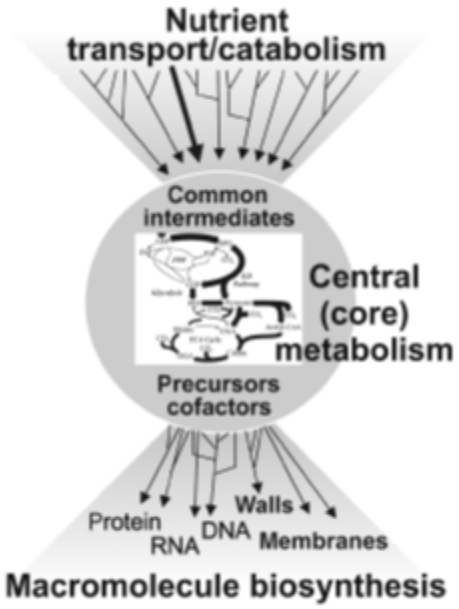

Figure 2.2 The overview of cellular metabolism

Glycolysis

The glycolysis is a fundamental catabolic pathway that is present in almost all living cells, and which role is to provide an entry point for organic carbon source such as glucose and fructose. It also provides metabolic intermediates feeding interrelated pathways such as pentose phosphate pathway and tricarboxylic acid (Kreb's) Cycle (TCA). It is the pathway through which glucose ($C_6H_{12}O_6$) as a carbon source, is first phosphorylated (feeding PPP and other anabolic pathways), then split (or lysed) into two 3 carbon molecules, glyceraldehyde-3-phosphate, which are then partially oxidized to form two molecules of pyruvate ($CH_3COCO_2^-$) (Figure 2.3). The whole pathway has two main functions: it allows the oxidation of glucose with the release of energy in the form of two ATP and two NADH, and the synthesis of pyruvate, which feeds the Krebs cycle (Figure 2.4).

The overall balanceof glycolysisis:

Glucose + 2 NAD^+ + 2 Pi + 2 ADP → 2 pyruvate + 2 NADH + 2 ATP + 2 H^+ + 2 H_2O

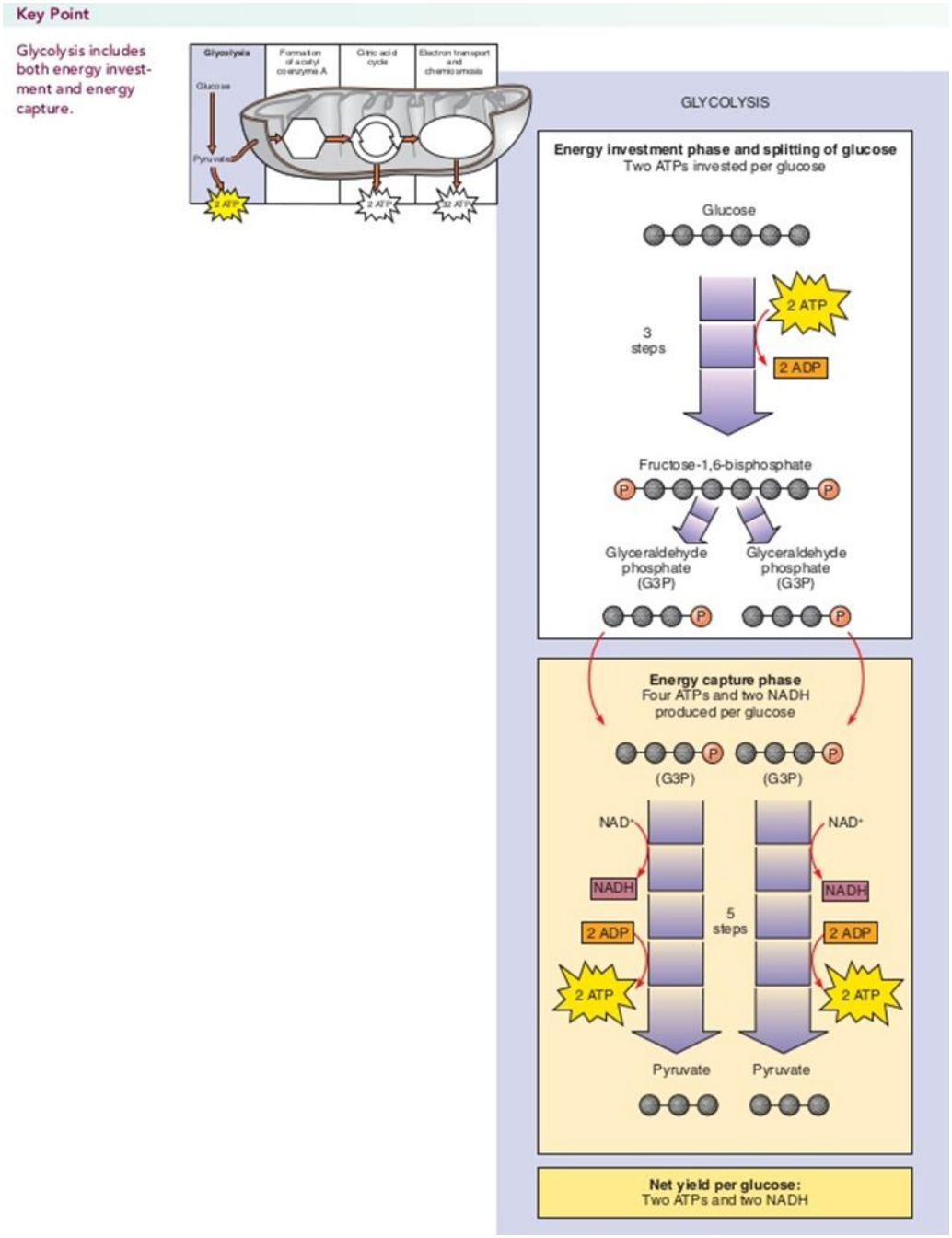

Figure 2.3 An overview of glycolysis
(Solomon, Berg, & Martin, 2005)

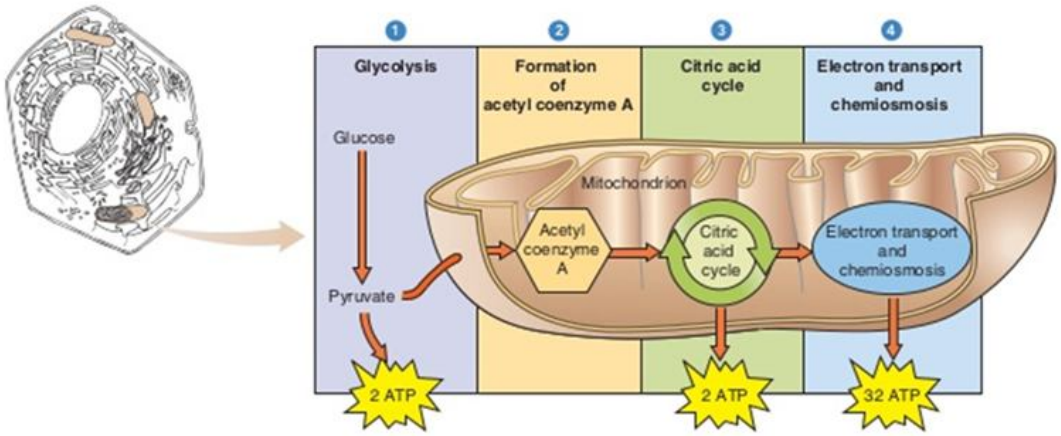

Figure 2.4Summary of glucose utilization through glycolysis
(Solomon et al., 2005)

Tricarboxylic Acid (Kreb's) Cycle (TCA)

The Krebs cycle or tricarboxilic acid cycle (TCA), which occurs in the mitochondria, is another essential pillar of the global cell metabolism. It has a dual role: on the one hand, it is associated with the oxidation of carbon molecules providing reducing power for the oxidative phosphorylation pathway (see next section), and it is also involved in the anabolism providing many precursors of amino acids synthesis, including glutamate (Mackenzie & McIntosh, 1991). There are multiple entry points from glycolysis. Pyruvate (PYR), a 3-carbon molecule, wills subsequently to be decarboxylated (passage 2 carbons) to react with coenzyme A and gives acetyl-coenzyme A, which feeds the Krebs cycle (Figure 2.5).

Reaction summary:

2 pyruvate + 2 NAD + 2 CoA → 2 Acetyl CoA + 2 NADH + 2 CO_2

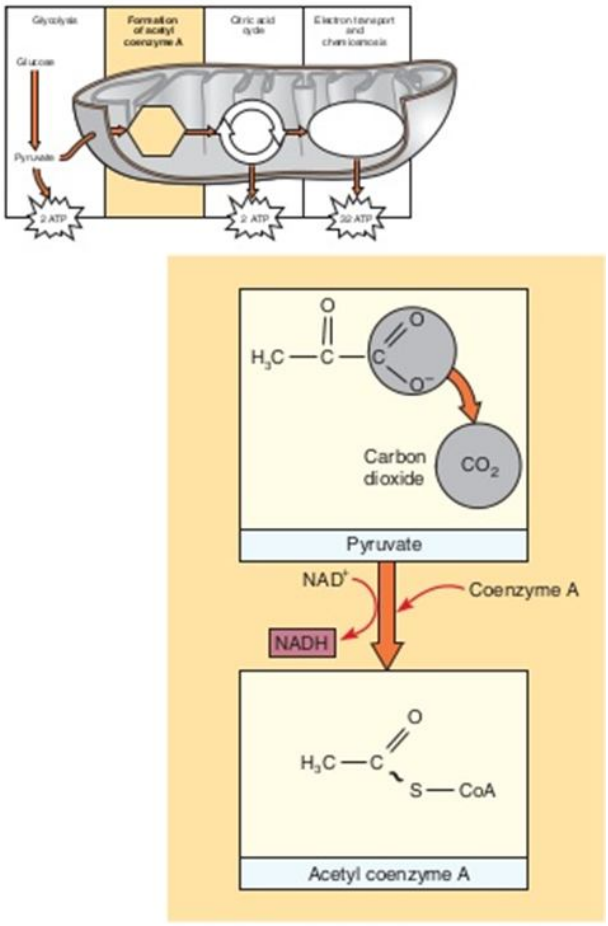

Figure 2.5The formation of acetyl CoA from pyruvate
(Solomon et al., 2005)

As in glycolysis, C-C bonds are cleaved and carbon is oxidized in TCA cycle (Figure 2.6).

Reaction summary:

2 Acetyl CoA + 6 NAD^+ + 2 FAD + 2 ADP + 2 Pi + 2 H2O → 4 CO_2 + 6 NADH + 2 $FADH_2$ + 2 ATP + 2 CoA

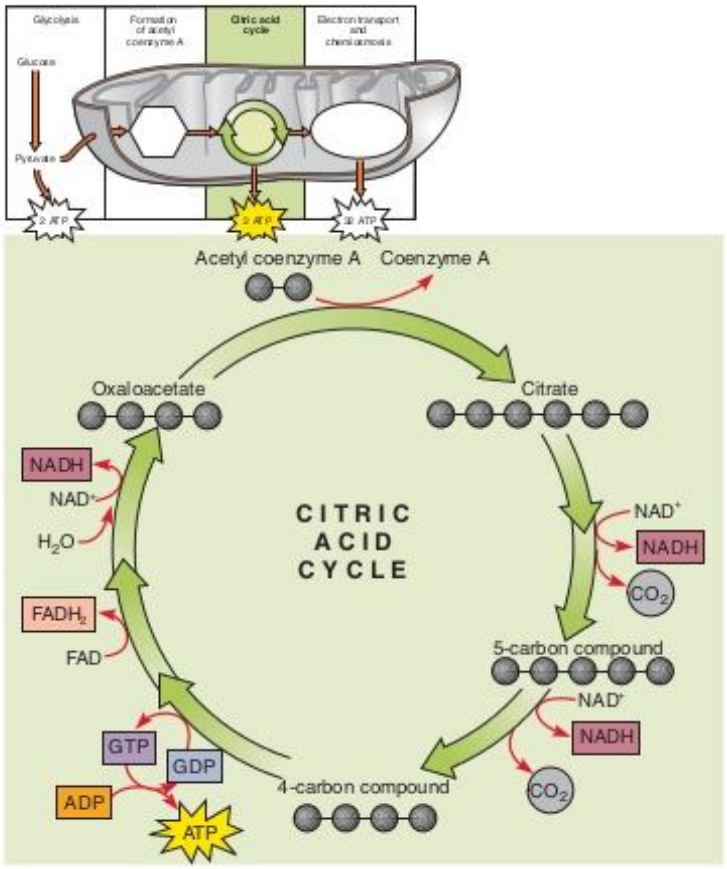

Figure 2.6Overview of the citric acid cycle
(Solomon et al., 2005)

Pentose phosphate pathway

The pentose phosphate pathway (Figure 2.7) can be either feed from Glucose-6-phosphate (G6P) and from Fructose-6-phosphate, all branch points of glycolysis. It aims principally to form a main precursor, ribose-5-phosphate (R5P), used for the biosynthesis of ribose, precursor of cell building blocks. It also allows the production of reducing power in the form of NADPH, which is needed for the synthesis of fatty acids and for the assimilation of inorganic nitrogen (Kruger & von Schaewen, 2003). Pentose phosphate pathway is partly controlled by the concentrations of $NADP^+$-to-NADPH ratio, both redox shuttles assisting various intracellular reactions (Kather, Rivera, & Brand, 1972). In particular, the first reaction catalyzed by glucose-6-phosphate dehydrogenase

(G6PDH) is known as the limiting step of the pentose phosphate pathway, where it controls the flow (Hames & Hooper, 2005; Kruger & von Schaewen, 2003).

$$G6P + 2NADP^{+} + H_2O \rightarrow R5P + 2NADPH + 2H^{+} + CO_2$$

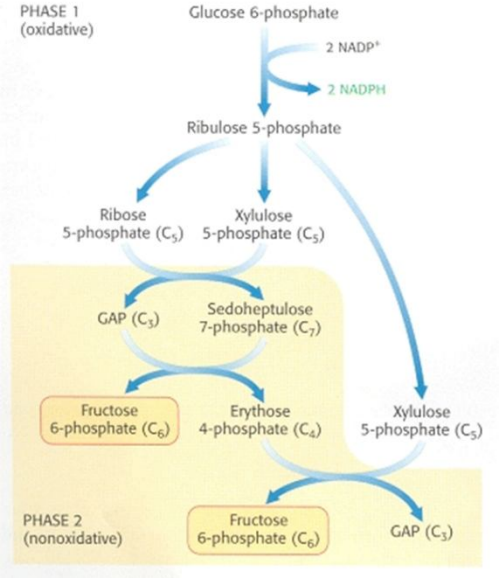

Figure 2.7An overview of pentose phosphate pathway and the formation of five-carbon sugars (Boeger et al., 2005)

Amino acid metabolism

Amino acids contain both an amino ($-NH_2$) and carboxylic acid (-COOH) functional groups, along with a side-chain specific to each amino acid. They are considered as the building blocks for the cell to synthesize proteins. Among eighteen amino acids, some are known as essentials, the ones which cannot be synthesized by the cell, and must be therefore provided in cell culture medium.Another group of amino acids refers to nonessentials that are synthesized by a cell metabolism from metabolic intermediates (Table 2.2). In addition of being used to build proteins, amino acids are involved in the synthesis of other kinds of small molecules with important biological roles such as purines and pyrimidines, which are precursors of DNA and RNA synthesis (Berg et al., 2002).

Table 2.2 Essential and nonessential amino acids for mammalian cells

Essential aminoacids	Nonessential aminoacids
arginine	alanine
isoleucine	aspartate
leucine	cysteine
lysine	glutamate
methionine	glutamine
phenylalanine	glycine
threonine	proline
tryphtophan	serine
valine	tyrosin

Besides their biosynthetic role, individual amino acids can also be catabolized, in a recycling manner, to bring back with nitrogen sources such as NH_4^+, a precursor to amino acid synthesis. In the general overview, the α-amino group is removed and mostly transferred to α-ketoglutarate to form glutamate, and the remaining carbon skeletons are transformed to acetyl CoA, and pyruvate or oxidized by the citric acid cycle and transferred into one of the intermediates of the citric acid cycle such as oxaloacetate, fumarate and succinate. Some amino acids like alanine and aspartate are processed in the citric acid cycle through a transamination reaction, catalyzed by transaminases, with the transfer of an α-amino group from an amino acid to α-ketoglutarate. The amination of α-Ketoglutarate then produces glutamate and other TCA cycle intermediates, i.e. oxaloacetate and pyruvate (Figures 2.8, 2.9).

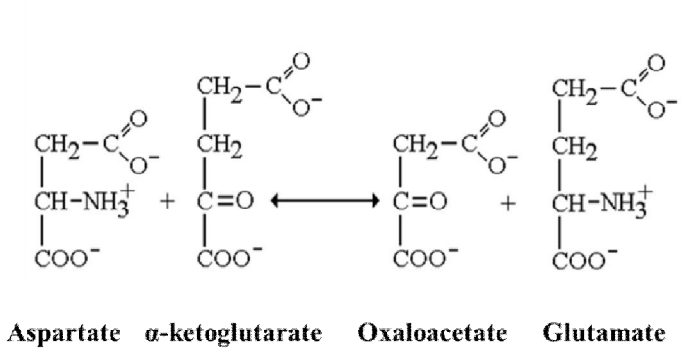

Figure 2.8Aspartate transaminase reaction

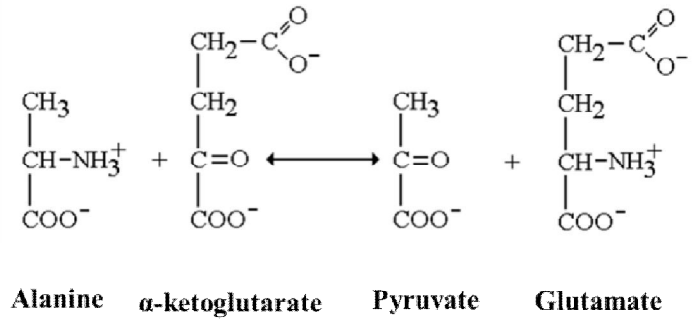

Figure 2.9Alanine transaminase reaction

Produced glutamate can further be de-aminated mostly through the glutamate dehydrogenase reaction (Figure 2.10).

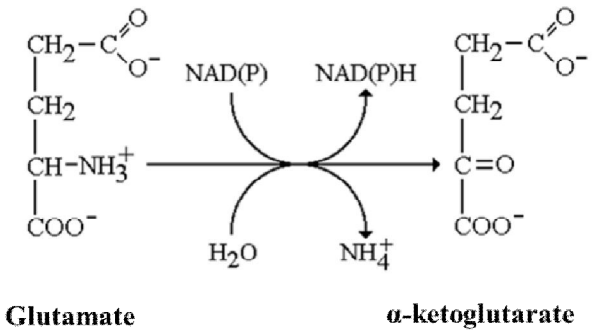

Figure 2.10 Glutamate dehydrogenase reaction

Glutamine metabolism as part of amino acid metabolism

Glutamine, $C_5H_{10}N_2O_3$, is classified as the most important non-essential amino acids. It contains one atom of nitrogen as an amide, which is used in the synthesis of precursor molecules of nucleotides. Glutamine is taken up by cells feeding the glutaminolysis pathway, resulting in glutamate and ammonia. Glutamate is then catabolyzed in the TCA cycle through the processes of transamination or oxidative deamination, as explained in the previous section. These catabolic pathways are reversible and thus contribute, in part, to homeostasis of nitrogenous substrates (Meng et al., 2010).The key steps of glutamine and glutamate metabolism are: (1) Glutamine synthetase (GS), (2) Phosphate-activated glutaminase (PAG), (3) Glutamate dehydrogenase (GDH), (4) Aspartate transaminase, and (5) Alanine transaminase (Figure 2.11).

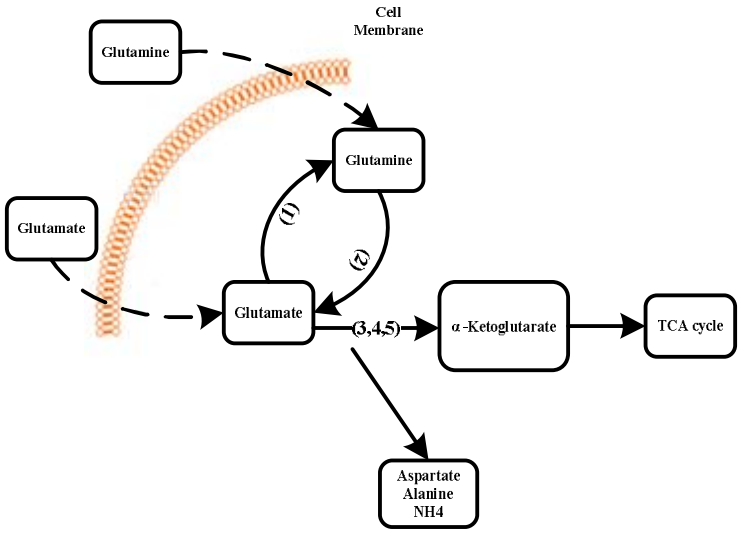

Figure 2.11The key steps of glutamine and glutamate metabolism.
(1) Glutamine synthetase (GS), (2) Phosphate-activated glutaminase (PAG), (3) Glutamate dehydrogenase (GDH), (4) Aspartate transaminase, and (5) Alanine transaminase.
Adopted from McDermott & Butler (1993) (McDermott & Butler, 1993)

Cellular bioenergetics system

The cell bioenergetic system is based on molecular shuttles that are continuously recycled, being coupled to energy demanding and producing biochemical reactions, as

previously discussed. These shuttles are mostly made of nucleotides. Nucleotides, composed of a nucleo-base (nitrogenous base), a five-carbon sugar (either ribose or 2-deoxyribose), coupled to one or more phosphate groups, and di-nucleotides, composed from the assemblage of two nucleotidesjoined through their phosphate groups, are involved in many cellular reactions (Coghill, 2006) (Table 2.3).

Table 2.3Functional and regulatory roles of nucleotides

Nucleotides (ratio)	Function
ATP, ADP, and AMP	ATP as an energy source for metabolic processes convertible to AD(M)P (Knowles, 1980) , ATP and ADP are involved in the kinetic regulation of enzymatic reactions catalysed by either ATP or ADP. AMP is also involved in regulation of glycolytic reaction.
GTP	Essential for many metabolic reactions specially protein synthesis and some polysaccharides of cellular membrane (Berg et al., 2002).
UTP,UDP and UDP	Involved in different anabolic reactions that are mostly growth-related (membrane lipids synthesis, strand break repair and protein glycosylation processes) (Berg et al., 2002).
CTP	Involved in phospholipid synthesis (Berg et al., 2002).
NAD(P)	NAD: the oxidized NAD participates in redox reactions,β-oxidation andkinetic regulation of TCA cycle reactions (Reich & Sel'Kov, 1981). NADP: participates in biosynthetic reactions as reduced form (NADPH). NADP(H): is involved in the regulation of the penthose phosphate pathway (Atkinson, 1977)

Adenylate nucleotides (ATP, ADP, and AMP) act as energy carriers. A healthy cell usually maintains ATP-to-ADP high in the order of 1:10 while keeping the ratio of AMP-to-ATP very low in the order of 1:100 (Hardie & Hawley, 2001). So the ratios of adenylate nucleotides even play more important role in the regulation of cellular processes and pathways (Atkinson, 1968).Given the importance for the cell to maintain appropriate values of ATP-to-ADP and ATP-to-AMP ratios, different stages of cellular bioenergetics system are involved to keep these ratios close to their optimal values (Hardie & Hawley, 2001).

Oxidative phosphorylation

The main site of the bioenergetics system for the cell capacity to generate energy in an aerobic mode is in the oxidative phosphorylation pathway, also called the respiratory chain or cell respiration. Thanks to oxygen, which acts as an electron acceptor, this is where most of cell energy is continuouslyrecycledin cellATPfromADP.Itis therefore necessary togeneratethe energy neededforthe oppositereaction.Reducingintermediaries (electron donor) inthe form ofNADH or$FADH_2$formed viaglycolysis, and the Krebs cyclewill enter the mitochondria and then be used (Figure 2.12). These electronsare transferredthroughseveral stageson aconveyor line(calledrespiratory chain) to finally reachoxygen, the final electron acceptor. Thesereactionsleadtoa strongoxido-reductionelectrochemicalgradient$\Delta\Psi$on eitherside of themitochondrialmembrane.It isthis gradientwhich providesenergy forthe enzymeATPsynthaseto reformATPfromADPandPi, reaction calledoxidative phosphorylation(Siedow & Umbach, 1995).

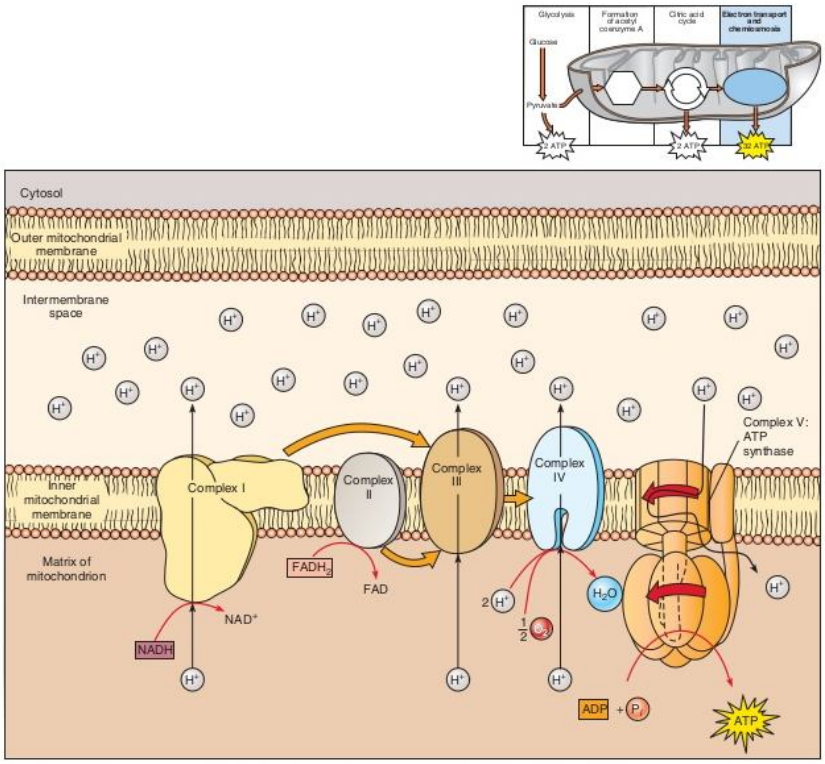

Figure 2.12 Schematic view of the mechanism of oxidative phosphorylation (Solomon et al., 2005)

Reactions summary in the electron transport chain:

$NADH+3ADP+3Pi+1/2O_2 \rightarrow NAD^+ +3ATP+H_2O$

$FADH_2+2ADP+2Pi+1/2O_2 \rightarrow FAD^+ +2ATP+H_2O$

So, ATP can be directly produced from substrate level phosphorylation or indirectly in the oxidative phosphorylation process. In substrate level production a phosphate group is transferred from a molecule to ATP in an enzymatic reaction.The net ATP production from glycolysis is two ATP's and the total number of ATP molecules generated from the oxidation of pyruvate and the Krebs cycle accounts for two other ATP molecules (Figure 2.13). Glycolysis and TCA cycle produce other shuttles compounds besides ATP and GTP (which potentially can be considered as ATP), namely NADH and $FADH_2$. These redox shuttles are molecules that are oxidized (*i.e.*, give up electrons) spontaneously in the oxidative phosphorylation reaction. Although there is a theoretical yield of 36-38 ATP molecules per glucose, such conditions are not generally achieved in cells and the efficiency is lower because pyruvate is not fully metabolized to TCA cycle but is reduced to lactate. In case of oxygen limitation down to levels as low as ~ 20 µM (~10 % air saturation) as reported for CHO cells, (Froncisz, Lai, & Hyde, 1985; Lai et al., 1982) more glucose is consumed by cells an even more pyruvate is converted to lactate. By increasing glycolytic rate, with only 2 ATP molecule produced per molecule of glucose catabolized, compared to 38 ATP produced (maximum) when including the oxidative phosphorylation, a cell tends to maximize the energy production per each molecule of glucose consumed via anaerobic glycolysis (Harper et al., 2002).

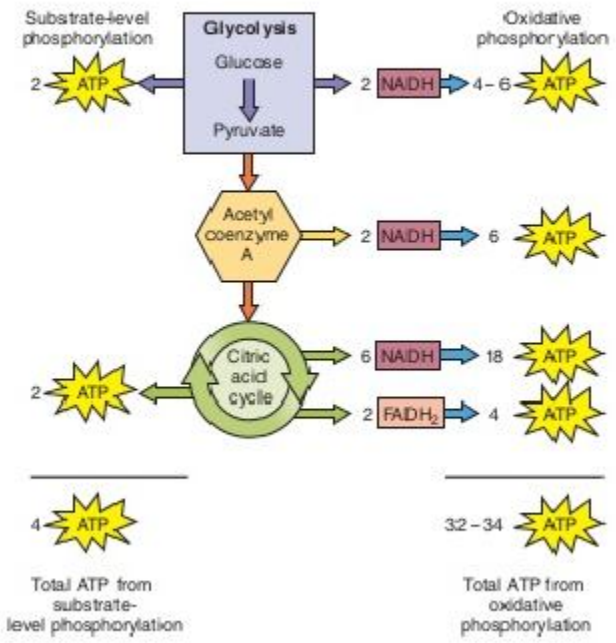

Figure 2.13Summary of ATP generation from one glucose molecule in glycolysis and oxidative phosphorylation
(Solomon et al., 2005)

Energy buffer reactions

Energy buffer reactions are present in mammalian cells mostly for the homeostasis of the ATP-to-ADP ratio. The role of these reactions is thus to adapt the cell energetic state under changing external conditions (Harper et al., 2002). There are many systems and we will cover the most important ones here. Creatine kinase is involved in one of the buffering reactions, as it favors the breakdown of one molecule of *P*Cr (phosphocreatine) to Cr (creatine) coupled to the generation of one molecule of ATP from ADP, without any contribution from other cellular subsystems (see Figure 2.14). Adenylate kinase, a second buffer system, interconverts ATP, ADP and AMP, tending to act in a reciprocal direction. Under ideal conditions, when the rate of ATP consumption matches its generation, adenylate kinase operate from left to right (see Figure 2.15), keeping AMP concentration very low (AMP-to-ATP 1:100).

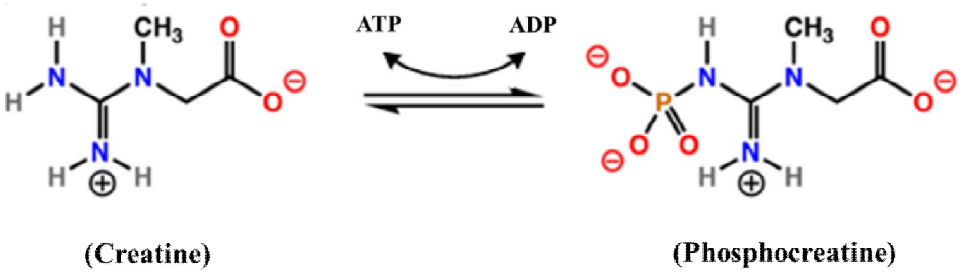

Figure 2.14 Creatine kinase reaction as an energy buffering reaction

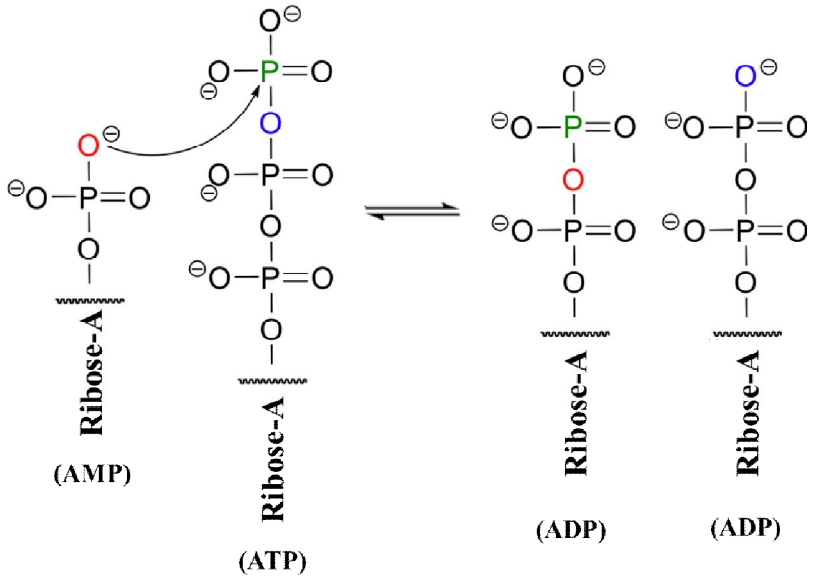

Figure 2.15 Adenylate kinase reaction as an energy buffering reaction

The mass balance on ATP thus includes its production from glycolysis and oxidative phosphorylation, buffering reactions as well as its consumption for biomass synthesis, antibody production, maintenance-related processes, transmembrane transport, and other ATPases-related reactions. There are also reactions that produce intermediate metabolites for pathways, pyruvate to oxaloacetate, known as anaplerotic reactions consuming ATP as well which should be included in its balance.

2.2.3 Mechanisms of metabolic regulation

Homeostasis, originated from two greek words homo (same, like) and stasis (to stand, posture) which means to remain the same, is the property of cells to regulate its internal

environment to keep that in a stable condition. As such, the phenotypic characteristics of mammalian cells are an output of regulatory processes at different functional layers including cellular metabolic system (Cascante et al., 2002). As previously mentioned, a high level of interconnected regulation mechanisms enable cells to grow and stay viable while facing a dynamic environment (Riehl & Segrè, 2008). We thus cover in the following the multiple layers involved in the regulation of a cell metabolism.

2.2.3.1 Enzymatic regulation: The basis of metabolic hemostasis

Enzymes have an intrinsic role on the metabolic homeostasis phenomenon (Koshland, 1968) originating at the genomic level, changes in the induction of a specific gene enables the control of quantitative signals (mRNA) managing a protein expression level (i.e. protein concentration), for finally, but rapidly, modifying the rate of a reaction flux. Then,concentrations in substrate(s), product(s), and enzyme's effector(s) (either activator or inhibitor), in addition to environmental factors such as temperature, also affect an enzyme's activity level. This has been widely studied since early works of Michaelis and Menten in 1913 (Michaelis et al., 2011). Therefore, at any given time (i.e. culture conditions), the flux rate of each enzymatic reaction is controlled by an ensemble of parameters, and as being highly interconnected, the network of biochemical reactions will exhibit a high regulation state at metabolic level.

Regulation of enzymes' activity

Substrate availability

The rate of an enzymatic reaction is primarily affected by its substrate concentration. Mostly, the rate of an enzymatic reaction increases as substrate concentration increases and finally reaches a plateau and does not increase any further at high substrate concentration

(Figure 2.16).

Product inhibition

The rate of an enzymatic reaction can also be responsive to its product concentration. Accumulation of the product can inhibit the activity of some enzymatic reactions. This form of regulation can limit the formation of product when it is produced beyond the use of cells (Figure 2.16).

Allosteric regulation

Allosteric enzymes have a major role in the regulation of cell metabolism. These enzymes have basically two or more binding sites. One active site that recognizes the substrate for processing the biochemical reaction, and a regulatory site that recognizes a regulatory molecule (inhibitor or activator), which can also be the substrate. The activity of the enzyme can be modulated by the binding of the regulatory molecule, causing specific conformational changes that either activate or inhibit enzyme's activity (Figure 2.16).

Covalent modification

Enzyme 3-D conformation, and thus its binding site receptivity, can be modified after covalent type reactions such as phosphorylation, acetylation, methylation, sulfation, glycosylation, amidation and hydroxylation. Among all these, regulation by phosphorylation is the most common. This type of regulation is taking place at the genomic, proteomic and at the enzyme level and kinases and phosphatases are involved in the process (Figure 2.16).

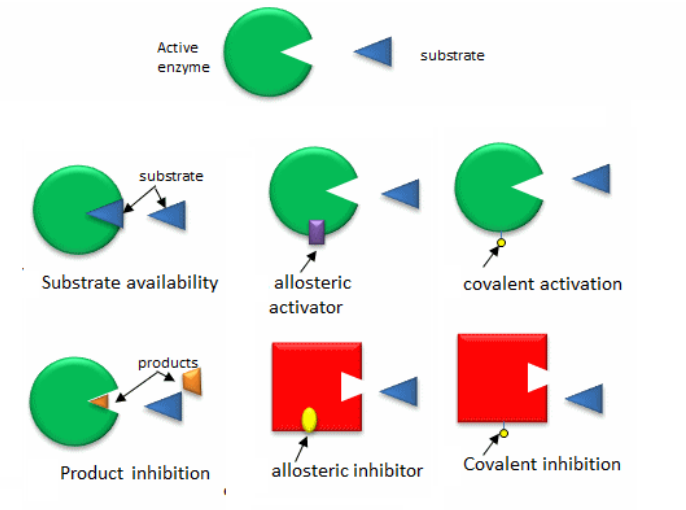

Figure 2.16Regulation of the activity of existing Enzymes
(Jakubowski, 2008)

<u>Types of enzymatic inhibition</u>

Competitive Inhibition

In this case, there is one active site on the enzyme and the inhibitor binds to that and prevents binding of the substrate. In case of competitive inhibition as the concentration

of the inhibitor increases, similar changes in substrate concentration can compensate or even predominate the inhibitory effect. Competitive inhibitors may thus be effective on isolated enzymes but much less effective within a pathway (Sauro, 2011).

Uncompetitive inhibition

In this case, the inhibitor binds to both the enzyme and substrate together so that the product cannot be formed, thus, inhibiting the formation of product.

Noncompetitive Inhibition

In this case the non-competitive inhibitor binds to the enzyme, however, does not compete with the substrate to reach the active site. Therefore, the substrate can also bind to free enzyme or even the enzyme and inhibitor together. However, the enzyme-substrate inhibitor complex cannot form the product.

Types of enzymatic activation

Essential activation

In this case, the reaction does not take place when there is no activator bound to that. Therefore, the enzyme should be activated to be able to bind to substrate to form the product.

Non-essential activation

It this case the activator is not essential: reaction occurs even in absence of the activator, but at a lower speed.

2.2.3.2 Kinetic description of enzyme-catalyzed biochemical reactions

Although biochemical reactions are mostly described in literature with the reaction mechanism, the affinity (K_m) and maximum rate (V_{max}) constants (Sauro, 2011), little to no *a priori* knowledge is available on the kinetics of the reactions as well as regulation interactions. One is often content to write the kinetic expression as the product of individual phenomena such as limitation, activation and inhibition:

$$q(s) = q_{max} \prod \alpha_i(c_i) \quad (1)$$

Where $q(s)$ is the actual reaction rate and q_{max} is the maximum reaction rate with $0 \leq \alpha_i \leq 1, \forall i$. The simplest way to describe an enzyme-catalyzed reaction and also its regulation is referred to Michaelis-Menten kinetics or saturation kinetics. Monod's model

is the most widely used kinetic expression for population behaviour due to its simplicity and its physical and phenomenological reliability (Table 2.4). Other kinetic models have also been developed within specific experimental range or specific description (Heinrich & Papoport, 1977).

Table 2.4General expressions for kinetic description of enzymatic reactions

Rate function	Name of equation
$v = \frac{v_{max} * \frac{S}{K_m}}{1 + \frac{S}{K_m}}$	Michaelis-Menten equation
$v = v_{max} * (1 - e^{\frac{-S}{K_m}})$	Tessier equation
$v = v_{max} * (1 + K_m * S^{-\gamma})^{-1}$	Moser equation

Due to the popularity of the Michaelis-Menten equation, various types of regulation, i.e. inhibition and activation, kinetics have also been reported based to which this equation is modified to also include the effect of an inhibitor/activator (Table 2.5).

Table 2.5Kinetic expressions for most common types of enzymatic regulations

Type of action	Modified Michaelis-Menten rate law for the regulatory enzyme
Inhibition Competitive	$v = v_{max} * \frac{\frac{S}{K_m}}{1 + \frac{S}{K_m} + \frac{I}{K_i}}$
Inhibition- Un-competitive	$v = v_{max} * \frac{\frac{S}{K_m}}{\frac{1}{(1+\frac{I}{K_i})} + \frac{S}{K_m}}$
Inhibition- Non-competitive	$v = v_{max} * \frac{\frac{S}{K_m}}{(1 + \frac{S}{K_m})(1 + \frac{I}{K_i})}$
Inhibition- Allosteric	$v = v_{max} * \frac{\frac{S}{K_m}}{(1 + \frac{S}{K_m})(1 + \frac{L(1+\frac{I}{K_i})^n}{(1+\frac{S}{K_m})^n})}$
Activation Non-essential	$v = v_{max} * \frac{\frac{S}{K_m}}{1 + \frac{K_a}{A} + \frac{S}{K_m}}$

2.2.3.3 Mechanisms of metabolic flux regulation

In addition to regulation within intrinsic enzyme properties, there are regulation mechanisms of enzyme activity that are driven directly from metabolites and other compounds (nutrients, signalling molecules, hormones, peptides, proteins, etc.) concentrations. Mathematical representations of the regulatory mechanisms on the regulated enzymes have been explained in the previous section.

Feedback regulation

There is feedback regulation of a biochemical reaction when its enzyme activity is affected from the concentration of a metabolite (the effector) that is synthetized chronologically after the reaction (Figure 2.17). In that case, the accumulation state of an end product controls the reaction rate of a reaction leading to its production. Feedback regulation is the major regulatory mechanism when rate-controlling enzymes are within the early steps in a pathway. Regulation can either be negative, causing inhibition of a reaction, or positive, with the activation of a reaction. These inhibitory and activation effects obey specific interaction laws that are rarely alike on/off switches, but rather modulated from the effector concentration (Table 2.5).

Feedforward regulation

In feedforward regulation of a biochemical reaction, its enzyme activity is affected from the concentration of a metabolite (the effector) that is synthesized before the reaction.

Like the feedback mechanism, feedforword can either positively or negatively regulate the related enzyme from the effector concentration (Figure 2.17).

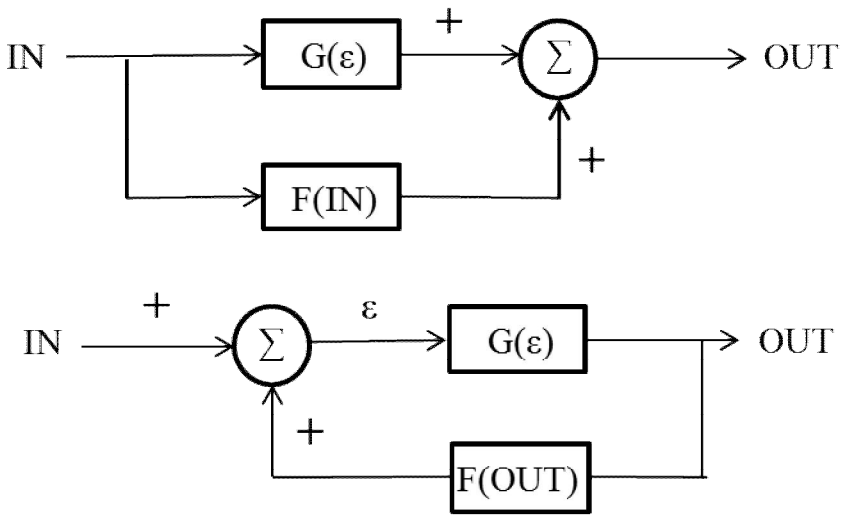

Figure 2.17Feed-forward and feedback configurations.Adopted from Johnson el al. (1998) (Johnson & Prentice-Hall, 1998)

2.2.3.4 Central carbon metabolism: regulation nodes

As previously shown, regulation of enzymes in a cell central metabolism (i.e. glycolysis, TCA, etc.) occurs through both feedback and feedforward mechanisms, although their distribution can differ between cell types. Moreover, a metabolic network circuitry reveals another layer of regulation that is driven by reaction competition for metabolic intermediates at each branch point interconnecting the different pathways. As an example, the major enzymes involved in the regulation of glycolysis as well as the branch points connecting glycolysis to the citric acid cycle, together with their mechanism of action, are listed in Table 2.6. From all these additive non-linear regulation mechanisms, it becomes tedious to study cell behaviour without accounting for their quantitative analysis.

Table 2.6 List of major enzymes involved in the regulation of metabolic reactions

	Effector of a regulation mechanism		
Enzyme	activator	inhibitor	Reference
Hexokinase	AMP/ATP	glucose-6 phosphate	(Berg et al., 2002)
Phosphoglucose isomerase	-	phosphoenolpyruvate	(Berg et al., 2002)
Phosphofructokinase	AMP/ATP	-	(Berg et al., 2002)
Pyruvte kinase	fructose-1,6-bisphosphate	-	(Berg et al., 2002)
Lactate dehydrogenase	AMP/ATP	pyruvate	(Živadinovic & Nikcevic, 2010)
Pyruvate Dehydrogenase	AMP/ATP	-	(Voet & Voet, 2011)
Isocitrate dehydrogenase	AMP/ATP	-	(Berg et al., 2002)

2.3 Characterization of mammalian cells metabolism

2.3.1 Rationale behind the modelling of a cell metabolic network

Acquisition of knowledge on cell platform behaviour is crucial for being able to optimize its culture and productivity for a product of interest at industrial scale. As previously mentioned, our level of knowledge on a biosystem will determine the level of control one can develop on this biosystem, and because of the complexity of its highly regulated metabolic network, the mammalian cell platform has to be characterized at the metabolic level, otherwise one can miss the role of the environment on cell behaviour. Most of the improvements on cell productivity have been accomplished from genetic engineering works, then enhancing cell metabolic capacity towards the product of interest. This field

of research has been called “Metabolic Engineering”. Metabolicengineering, as defined by Stephanopoulos et al. (1998)(Stephanopoulos, Aristodou, & Nielsen, 1998), is "the direct improvement ofproduction levelsof a molecule ofinterest orcellular propertiesthroughthe modification ofspecificbiochemical reactionsor the introduction of newreaction(s),usingtherecombinantDNA technology”. Nowadays, it has become obvious that genetic engineering strategy can accelerate the development of high-producer cell lines but once this is done, one’s capacity to adequately manage culture composition with culture time may be crucial for reaching the expected productivity level of the re-engineered cell line. Therefore, in combination to enhancing cell metabolic capacity playing on internal (genes) factors, there is a need of mastering external (culture management) factors to reach expected enhanced cell catalytic capacity.

There are different modeling approaches that have all proposed: models allowing metabolic flux analysis (MFA) and requiring a quasi steady-state hypothesis specially for CHO cells (Altamirano et al., 2006; Feist & Rosenbloom, 2011; Wilkens et al., 2011; Zamorano, Wouwer, & Bastin, 2010), metabolic flux balance analysis (MFBA) (Martínez et al., 2013; Savinell & Palsson, 1992), and kinetic models capable to describe transient behaviours (i.e. concentrations and metabolic fluxes) based on limiting nutrients of medium (Batt & Kompala, 1989; Bree et al., 1988; Cazzador & Mariani, 1993; Dalili & Ollis, 1989; Dalili, Sayles, & Ollis, 1990; Frame & Hu, 1991; Portner & Schafer, 1996; Provost & Bastin, 2004)and intracellular metabolites (Ghorbaniaghdam, Henry, & Jolicoeur, 2012; Nolan & Lee, 2010).

2.3.1.1 Model structure and segregation

There are several levels of complexity while describing mathematically cell behaviour (Tyson, Chen, & Novak, 2003). One perspective of this categorization is based on how the cell population is represented. Non-segregated models consider a homogeneous cell population while differences between cells within the population are not considered. In a segregated model, however, the cell culture is considered as a heterogeneous population where cells are distinguished from each other according to age, mass, or size. Another perspective is based on the intracellular structure. In structured models, the intracellular state is viewed as a multi-component environment. In unstructured models, however,

cells are viewed as black boxes in which substrates are converted to products (Castilho et al., 2008)(Figure 2.18).

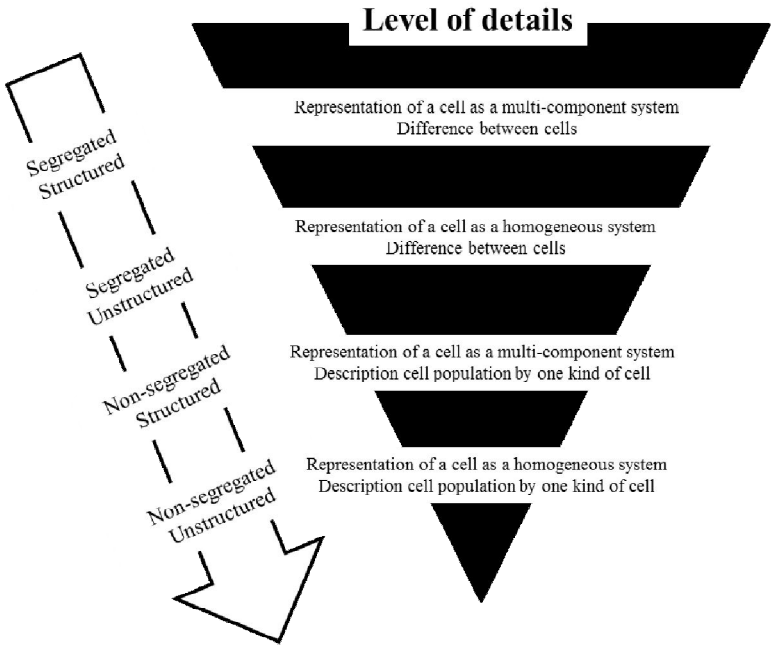

Figure 2.18Different approaches to the modeling of cell metabolism
Based on Tsuchiya et al. (1966) (Tsuchiya, Fredrickson, & Aris, 1966); and Bailey and Ollis (1986) (Bailey & Ollis, 1986)

2.3.2 Current approaches for structured non-segregated mathematical representations of metabolic network

2.3.2.1 Metabolic control analysis

Metabolic control analysis (MCA) is an approach at steady-state used to analyze the effect of a change in the activity level of an enzyme (i.e. change in flux rate) on the other fluxes and intermediate concentrations of a metabolic pathway, after compared to before applying a genetic modification. The two main control coefficients $(C_v^{J,P})$are the flux and concentration control coefficients (Fell, 1997).

Flux control coefficient is defined by:

$$C_v^J = \frac{\left(\frac{dJ}{dp}\frac{p}{J}\right)}{\left(\frac{dv}{dp}\frac{p}{v}\right)} = \frac{dlnJ}{dlnv} \quad (2)$$

And concentration control coefficient is defined by:

$$C_v^S = \frac{\left(\frac{dS}{dp}\frac{p}{S}\right)}{\left(\frac{dv}{dp}\frac{p}{v}\right)} = \frac{dlnS}{dlnv} \quad (3)$$

Where C_v^J and C_v^S are flux and substrate control coefficients, respectively. J is pathway flux and S is the metabolite concentration in response to a relative change in the activity of an enzyme from its initial value at state *v*. In addition, another property which is characterized by MCA is sensitivity coefficient. Sensitivity coefficient $\left(C_i^J\right)$is used to study the effect of a change in substrate concentration or kinetic parameters of a reaction on the reaction rate. Sensitivity coefficient can then be determined as:

$$C_i^J = \frac{dJ}{di} \quad (4)$$

Where J is the pathway flux and i is either the metabolite concentration or kinetic parameter. This approach, based on experimental results from genetically engineered cells is thus used to characterize the control level of a metabolic network in regards to an enzyme (Almaas et al., 2004; Alves & Savageau, 2000; Wang, Birol, & Hatzimanikatis, 2004). Moreover, this method offers quantitative estimations of the responses of reaction rates and metabolite concentrations to the onset of change in the system such as enzymatic activities. Although this method attracts lots of attention specially in basic biology (Berthiaume et al., 2003; Hatzimanikatis & Bailey, 1997)it has no capacity for evaluating flux regulation nor it can predict the adaptive behaviour of cells in response to the engineering modifications.

2.3.2.2 Metabolic flux analysis

The metabolic flux analysis (MFA) approach allows to determine flux rate distribution at steady-state, using extracellular data set (Henry, Perrier, & Kamen, 2005; Klamt & Schuster, 2002; Libourel & Shachar-Hill, 2008; Nadeau et al., 2000; Quek et al., 2010; van der Heijden et al., 1994; Xie & Wang, 1996; Xie & Wang, 1996). From known metabolic network stoichiometry, linearalgebra manipulation enables to transform information of extracellular data set into intracellular flux rate distribution (Steuer & Jenker, 2008).

The first step in MFA is to define metabolic reactions and then mathematically represent them. Metabolic reactions are mathematically represented through a stoichiometric matrix (S) with m rows and n columns. Each row of the stoichiometric matrix belongs to one compound where each column represents a reaction. The values of each column are the stoichiometric coefficients of the corresponding metabolites in a reaction. Negative values represent consumption, positive values represent production, and values equal to zero demonstrate that the metabolite does not participate in the reaction. There are other vectors, v, which represents reaction fluxes and X for metabolites (Figure 2.19 a-c). The general equation for mass balances on metabolites can be written as follow:

$$\frac{dX}{dt} = S.v - \mu.X \qquad (5)$$

Where$\mu$is the cell specific growth rate, accounting for intracellular metabolites dilution from cell division. The equation that represents steady state is thus given as:

$$S.v = 0 \qquad (6)$$

In large-scale metabolic networks, however, there is more than a unique solution to this equation. Introduction of theoretical constrains (Bonarius et al., 1996; Bonarius et al., 2000; Sidorenko et al., 2008; Wahl et al., 2008) or the use of labeling experiments to identify some intracellular fluxes (Antoniewicz, 2006; Bonarius et al., 1998; Goudar et al., 2010; Metallo, Walther, & Stephanopoulos, 2009; Savinell & Palsson, 1992; Sheikholeslami, Jolicoeur, & Henry, 2013; Zupke & Stephanopoulos, 1995) have been suggested and successfully used to overcome this problem. Although MFA is still widely

used for accurately analyzing metabolic pathways by comparing metabolic fluxes intensities, the steady-state hypothesis on metabolite concentrations requires experimental conditions that are rarely encountered in industrial processes. Moreover, because of the steady-state constraint, there are important limitations of this approach; it is highly tedious to study the dynamics ofmetabolism (Rios-Estepa & Lange, 2007). In many cases, a steady state observed in terms of the cell specific growth rate does not necessarily mean a metabolic or nutritional steady state (Cloutier et al., 2007). To study the dynamics of a biosystem metabolism, its regulation and control, transient approaches are required. Therefore, metabolic models that include fluxes kinetics and metabolic regulation functions may enable to describe transient metabolic behaviours.

2.3.2.3 Metabolic flux balance analysis

Similarly to metabolic flux analysis, flux balance analysis (MBFA) is an approach leading to the identification of metabolic fluxes in an assumed metabolic network bordered with finite constrained space of solutions. In MBFA approach, a metabolic network should be developed to identify the stoichiometry coefficient of each metabolite in biochemical reactions. This knowledge is then represented mathematically by constructing a stoichiometric matrix in which every row belongs to one compound and every column represents a reaction. An objective function is then defined to decrease the number of unknowns (Figure 2.19 a-d).

$$Z = c^T * v \qquad (7)$$

The vector c is called the weight vector which demonstrates the contribution of each reaction to the objective. Normally, there is only one reaction desired to be either maximized or minimized. Therefore, the rows of this vector are all zero except for the one at the position representing the reaction of interest. Finally, metabolic flux distribution is defined using linear programming while the constraints regarded to mass balance equations are also taken into account. This method is mostly used to identify the maximum and minimum possible fluxes for a particular reaction in order for an objective function to be close to or equal to its optimal value (Mahadevan & Schilling, 2003).

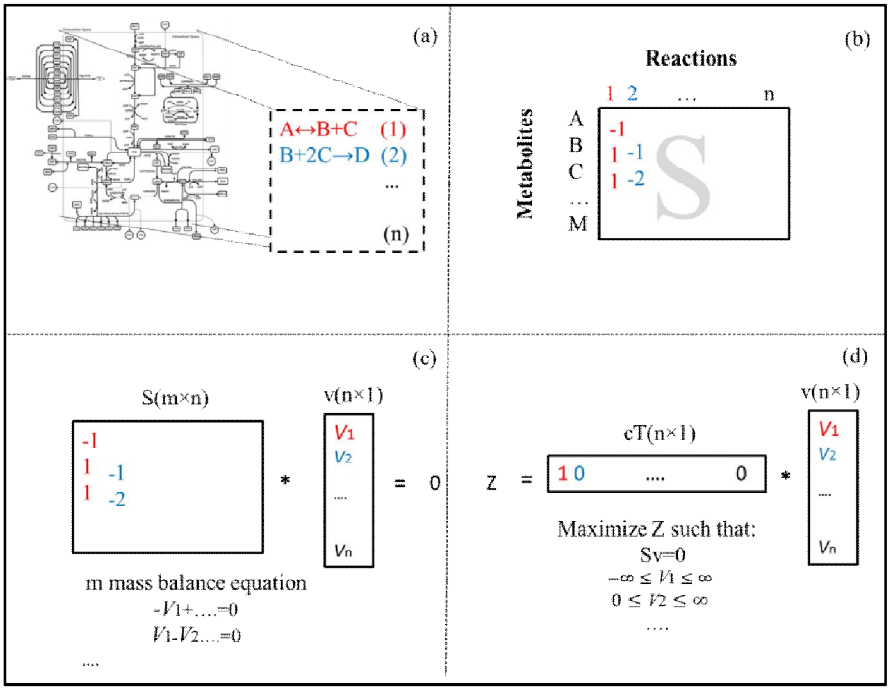

Figure 2.19Different stages for the formulation of MFA and MFBA problems.
Adopted fromOrth, Thiele, & Palsson (2010) (Orth, Thiele, & Palsson, 2010)(a) construction of a metabolic network (b) formation of a stoichiometric matrix (labeled *S*) (c) identification ofmass balance equations at steady state **(**S*v = 0) (d) maximization of an objective function ($Z = c^T v$).

2.3.2.4 Kinetic modeling of metabolic fluxes

As explained in MFA method, mass balances on metabolites can be written as follow:

$$\frac{dX}{dt} = S.v - \mu.X \qquad (8)$$

While some works have been proposed using MFA analyses by deviding the problem into exponential and non-exponential phases to detect important metabolites (Gao et al., 2007), the use of kinetic models including the description of flux kinetics is gaining in interest. Kinetic models cover the dynamic behavior whereas stoichiometric approaches, MFA and MFBA, can only capture a static view of metabolic activity but not time course evolution of the system. Kinetic models allow simulation of the dynamics of the metabolic processes and in case that they also consider regulatory effects, they may have the ability to predict cellular response under different conditions. Therefore, kinetic

mathematical descriptions of the metabolism seem to have a large advantage compared to constraint-based stoichiometric models.Many kinetic formulations have been proposed in literature for simple systems, specially single-substrate, single-biomass, and single-product systems, most of them found heuristically in order to describe a specific phenomenon (Haag et al., 2005). However, there has been growing interest for the development of mathematical descriptions of cellular system, thus including the description of flux kinetics.There are also kinetic models that describe fluxes kinetics of some pathways of cell metabolism. These kinetic models mostly describe glycolysis (Gagneur, Jackson, & Casari, 2003; Hynne, Danø, & Sørensen, 2001; Wolf et al., 2000), TCA cycle (El-Mansi, Dawson, & Bryce, 1994; Wright, Butler, & Albe., 1992; Wu et al., 2007), and to a lesser extent glutamine metabolism (Van den Berg & Garfinkel, 1971) and pentose phosphate pathway (Vaseghi et al., 1990). In that context, a fully dynamic metabolic model describing metabolite mass balances, enzyme kinetics and pathway regulation, can be a useful tool improving our capacity to analyze hypotheses and experimental data on metabolic network behavior.

2.3.3 Current metabolic models for the mammalian cell platform

Over the last decades, our approach towards the understanding of cellular processes has been changed due to increased availabilityof information about cellular processes. Because the biotherapeutics that we are producing are getting more complex, and that we look to lower their side effects by, for instance, a better control of the glycosylation process, we need to develop new tools enabling mastering cell culture processes. Therefore, it becomes clear that our intuitive capacity is no more enough to analyse the massive experimental datasets that are now available (“omics”) and required for adequately characterizing cell behaviour in its complexity(Gerdtzen, 2012). The strategy for building up a model mainly depends on the final objective of the analysis and the type and amount of data which is available. There are different approaches aiming at understanding cellular systems ranging from completely qualitative such as graph theory and topology analysis, which is beyond the scope of this work and a complete review on them can be found in (Ma’ayan, Blitzer, & Iyengar, 2005), to quantitative such as a comprehensive mathematical description of cells including genomic, proteomic and metabolic networks as well as their interactions. These approaches, however, are either

too complex, require too much datasets, or are not enough mature to deliver valuable information. Models aim basically at better understanding of how complex functions and behaviors emerged from the intracellular interactions lead to a specific cells behavior observed during the time course of a culture. This then helps to predict the effects of different conditions on cell behavoiur and to rationally design control strategies to keep cells in desired state. To do this, kinetic models that have predictive power are needed and these models should capture important biochemical and mechanistic details to systematicallydescribe the use ofnutrients, synthesis of primary and secondarymetabolites, the stoichiometry of themetabolic network, and kinetics of metabolic reaction. Such Models, however, require a critical level of knowledge (e.g. about pathway description and regulation), and reliability (e.g. about kinetic representations of reactions, the components and reactions to include, and kineic parameter values). In conclusion,this more elaborate way of representing cells comes with the cost of more complex computations and requires more amounts of experimental data but with the gain of obtaining more complete insight to a bioprocess.

2.3.4 Analytical methods for metabolomic analysis

Chemical analysistechniqueshave improved dramaticallyin recent yearsspeciallyin theirversatility.Indeed,long-termexpertisewith analytical chemistryallowedthemeasurementofspecific familiesof moleculessuch asorganic compounds,lipids, ions, orsugars.The sensitivity (or detection limit), however, nowadays becomes increasinglyimportant. While manytechniques exist, some are particularly prevalent such asnuclear magneticresonance (NMR), liquid/gas chromatography (LC or GC),andmass spectrometry(MS). The choice ofone technique overanotherofteninvolvesa compromise betweenspeed of analysis, selectivity andsensitivity (Table 2.7).For example, NMR is fast andselectivebutisinsensitivewhile theGC/MSorLC/MShavegood sensitivity andselectivity, but arelativelylonganalysis time (Sumner, Mendes, & Dixon, 2003).

Table 2.7Different orders of detection forchemical analysis techniques

Method of analysis	NMR	LC/UV	GC/MS	LC/MS
The order of analyte	10^{-6} mole	10^{-9} mole	10^{-12} mole	10^{-15} mole

2.3.4.1 NMR spectroscopy

NMRspectroscopy is atechnique based onphysicalproperties ofsomenuclei atoms(such as ^{1}H, ^{13}C, and ^{31}P). The basic principle of NMR spectroscopy is that certain nuclei possess intrinsic magnetic moments which are sensitive to magnetic fields. When these nuclei are submitted to strong magnetic fields a net magnetization signal is produced proportional to the number of nuclei present. Therefore, NMR can be used as a quantitative tool (Fernande, 1987). This non-invasive technique has applicationsin chemistry andbiologyallowingdynamic studiesfollowingthe effect of astimulus such aspH change,or dissolved oxygen. However,thedetection threshold isrelativelylow in the order ofmM (orμM), which requiresthequantification ofmolecules with relativelyhigh concentrations,oraccumulation of the spectra for severalminutes orhours toachievea good signal-to-noise ratio. However, few critical metabolites are found in low concentrations (less than 0.1 mM). The most common way to circumvent this problem is by increasing cell density until high quality spectra are achieved. Typically, NMR studies of suspended cells call for high cell densities depending on cell type and size (Fernande, 1987). Therefore, certain process or operating requirements must be met allowing for a viable high cell density which are sometimes not easy to be met (Morris, 1988).

2.3.4.2 Liquid and gas chromatography

Theprincipleis to separatethesample mixture wherethe sampleflowsto the mobile (liquid/gas) phase, due tosequential injections, in order to be separated one by one through specific physical interactions with a detectorcalled stationary phase. A stationaryphase (solid) conventionallymade of a resinwith specific properties, e.g. size, polarity, and branching, which can retainroughly different analytes. Mobile phase (liquid or gas) known as eluentcan transportthemolecules along ofthe separation columnto be analyzed.This phase canbe a mixtureof particular properties, e.g. flow, pH, and Vander Waalsforces, which may be adjustedduring ascan,

andare determinedby the user toimprove the resolution ofpeaks.Thedetection can be donethenbyopticalmeasurement(absorbanceorfluorescence)orby electrical measurementforredox reactionsand even on amass spectrometer oraNMR. This techniqueis widely usedformetabolic measurements, but one or theotheris favoreddepending on the nature of themolecules to be detected(more or less polar) (Figure 2.20). (Theodoridis, Gika, & Wilson, 2008).

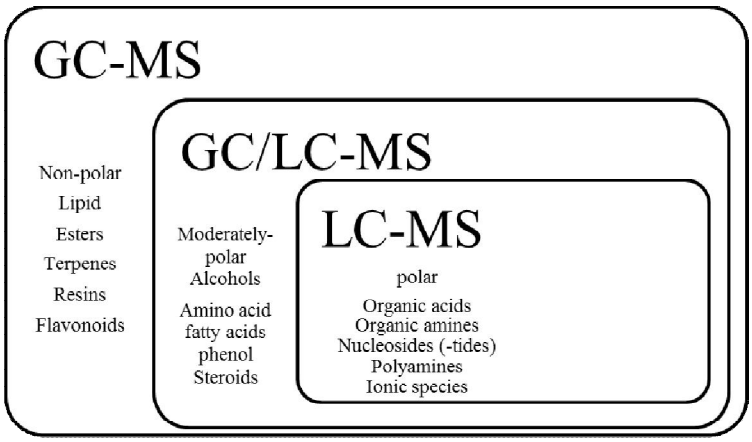

Figure 2.20UsingGCorLCfor metabolicmeasurements

2.3.4.3 Mass spectroscopy

Mass spectrometry(MS) is a technique for the identification of moleculeswith regard to their atomic mass.The device (mass spectrometer) ionizesmoleculeswhich aredetectedbytheir identical mass-to-charge ratio(m/z).The informationis thus primarilyqualitativerather than quantitativebecause itidentifies the molecules present inthe sample. Although the sensitivity of themass spectrometry is high up topicomole, their criterion of "molecular weight" is sometimes not enoughto discernmolecules. This is the caseof proteins thatcome outat the sameratiom/z(Wysocki et al., 2005). To address this usually multiple steps of mass spectrometry is applied to the sample, with some form of fragmentations occurring in between calledMS-MS (Bedair & Sumner, 2008). Traditionally,LCorGCchromatography is coupled to mass spectrometry which enablethe quantification andidentification of awidenumber of metabolitessuch as proteins, lipids,sugars, nucleic acids, amino acids (Kanani, Chrysanthopoulos, & Klapa, 2008).

With the emergence of high through-put analytical methods, it seems that steps are being taken towards a more fundamental approach in a bioprocess

CHAPTER 3 METHODOLOGY

CHO clones that stably produce a recombinant monoclonal human anti-CD20 at different specific productivities (high- and low-producer) were provided by Viropro International Inc. (Montreal, Canada). These cells were derived from CHO-Cum2 cells and stably express the reverse cumate transactivator, as described in details by Mullick et al. (2006) (Mullick et al., 2006). Cells were seeded at 2×10^5 cells/mL in 300 mL of a protein-free medium in 1-L shake flasks, and cultured on a shaker (150 rpm) in a humidified incubator at 37°C and 5% CO_2. The medium used was a customized chemically-defined SFM4CHO medium supplemented with 30 mM glucose, 4 mM glutamine and 0.05 mg/mL dextran sulphate. For the comparative study, the parental clone, together with high- and low-producer clones, were cultured in duplicate. High- and low-producer clones were cultured both in the presence and in absence of cumate, the latter serving as non-induced control. In case of induction, 1 µg/mL of cumate was added after 48 hours of incubation, to trigger the recombinant protein expression. It should be mentioned that no visible effectsonmorphologyorgrowthrates were reported for mammalian cells cultured at a cumate concentration below 200 µg/mL (Mullick et al., 2006). More details of complete cell culture protocols and culture condition are described in Chapter 5 within the Material and Methods section (5.5.1) and in appendices 1-2.

3.1 Metabolomic analysis

Quantification of cell metabolites, i.e. metabolic intermediates and energetic and redox nucleotides,are particularlycritical because of their high instability and their low concentrations. The main steps consist in the sampling of the cell suspension, cell separation from the medium, extraction of metabolites and then the chemicalidentification andquantification of metabolites of interest.The liquid medium composition in nutrients and metabolites also needed to be characterized, and it was obtained after cell separation from the suspension. For more details, the complete method is described in Chapter 5 within the Material and Methods section (5.5.2) and in appendix 3.

3.1.1 Extraction of metabolites

During ametabolicmeasurement, numerous handling stepsof the biological sampleshould beas neutral as possiblewith regards to the analyte moleculesand thusskewthe results the

least possible.In other words,at this stagewe try tostop the metabolism as quickly as possible so that the biochemical process does not change themolecular concentrationsand thus givesan unrepresentativeresult of thecellular stateat the time ofsampling.This stepisparticularly criticalsince itoccurs firstinthe stepsrelatedto a measurement ofmetabolites.The methodsof interruption ofmetabolism (quenching) typically consistin exposingthe sample toconditions of extremepHor temperatureallowingthe rapiddenaturation ofenzymes,without alteringthemetabolites of interest(Álvarez-Sánchez, Priego-Capote, & Castro, 2010). The first methodis byadding sodium hydroxideora strong acidsuch astrichloroaceticacidorperchloric(Mashego et al., 2007). The second is tobring the sample below -20^{o}C throughthe addition of acoldaqueoussolution (lower than -40^{o}C) ofmethanolor withliquid nitrogen at -196^{o}C(Dettmer, Aronov, & Hammock, 2007; Hiller et al., 2007).Methanol hasthe advantage of beingmiscible with waterand has alower freezing temperature thanethanolor glycerol. Moreover, itpreventsthe increase in temperatureas that may leadto the degradation ofthermally labilemolecules. The addition of cold methanol causes cellpermeabilization and a separation step (e.g. by centrifugation) of the biomass from the culture medium at the end is performed torecover endo-metabolome from cell debris. This step is the most difficultstep even forbiotechnological processeswhichseek to followthe metabolic stateof thecellline. An automated way("on-line" measuresor"at-line") thus is supported byindustriallyProcess AnalyticalTechnology. Severalsystems have been developedbased ona samplerconnected to thebioreactorwhich opens upto -50^{o}C and200 mbar which is combined with an aqueous solution of60%methanolusedin bacteria andyeasts cultures (Hiller et al., 2007).For more details of the extraction procedure, the complete method is described in Chapter 5 within the Material and Methods section (5.5.2) and in appendix 4.

3.1.2 Quantification of metabolic concentration

Table3.1 summarizesthe intra- and extracellular moleculesanalyzed in thiswork including the methods of analysis.

Table 3.1 Summary of analytical methods applied to this work

Metabolite	Analytical method	Analytical tool (instrument/assay)
Extracellular glucose, lactate, glutamine and glutamate	Enzyme-based via oxidization of the analyte by the enzyme immobilized on a membrane	Dual-channel immobilized oxidase enzyme biochemistry analyzer (2700 SELECT, YSI Inc. Life Sciences, USA)
Extracellular ammonia	Enzyme-basedvia glutamate dehydrogenaseand absorbanceofNADPHat 340nm	Ammonia Assay Kit (Sigma, Oakville, Canada)
Extracellular amino acids	Chemical-based via separation on a solid phase due to different physiochemical properties	1290 UPLC system coupled to a 6460 triple quadruple mass spectrometer (Agilent Technologies, Canada).
Extracellular monoclonal antibody	Enzyme-based via enzyme-conjugated antibody and the absorbanceof color substrate at 340nm	enzyme-linked immunosorbent assay (ELISA) protocol in appendix 3
NAD(P) and NAD(P)H	Enzyme-based via an enzyme cycling reaction and the absorbance of NAD(P)H at 450 nm	NAD(P)/NAD(P)HQuantification*Kit* (*BioVision, USA*) -Extraction by NADP/NADPH extraction Buffer through freeze/thaw two cycles
Adenylate nucleotides (ATP, ADP, and AMP)	Chemical-based via separation on a solid phase due to different physiochemical properties	1290 UPLC system coupled to a 6460 triple quadruple mass spectrometer (Agilent Technologies, Canada). -Extraction by 80% cold methanol
Organic acids and sugar phosphates	Chemical-based via separation on a solid phase due to different physiochemical properties	1290 UPLC system coupled to a 6460 triple quadruple mass spectrometer (Agilent Technologies, Canada). -Extraction by 80% cold methanol protocol in appendix 4

3.2 A general algorithm as a guide in the development of a metabolic kinetic model

The model developed in this work is presented in details in Chapter 4, with the initial structure and in Chapters 5 and 6, with a fully developed regulated flux kinetics. We also detailed the model structure development as well as parameters calibration procedure in those following chapters. However, in order to expose in a unique section the steps we followed for developing our model, an algorithm is presented in Figures 3.1 and 3.2. As a first step metabolic reactions and metabolites should be defined following by the step of their mathematical representation by stoichiometric matrix. At the next step, a rate equation should be assigned to each reaction. Information on the initial values for kinetic parameters is usually obtained from databases listed in table 3.4.Kinetic parameters determined in vitro may be far from biological ones, giving some latitude on parameter values. Afterwards, the global simulation error should be minimized. Minimization of simulation is then accomplished by non-linear optimization technique, i.e. least-squares fit. Finally, model properties such as adaptability to other conditions, applicability and the reliability of its structure and parameters should be studied (Figure 3.2).

Figure 3.1 A general algorithm for the development of a kinetic metabolic model

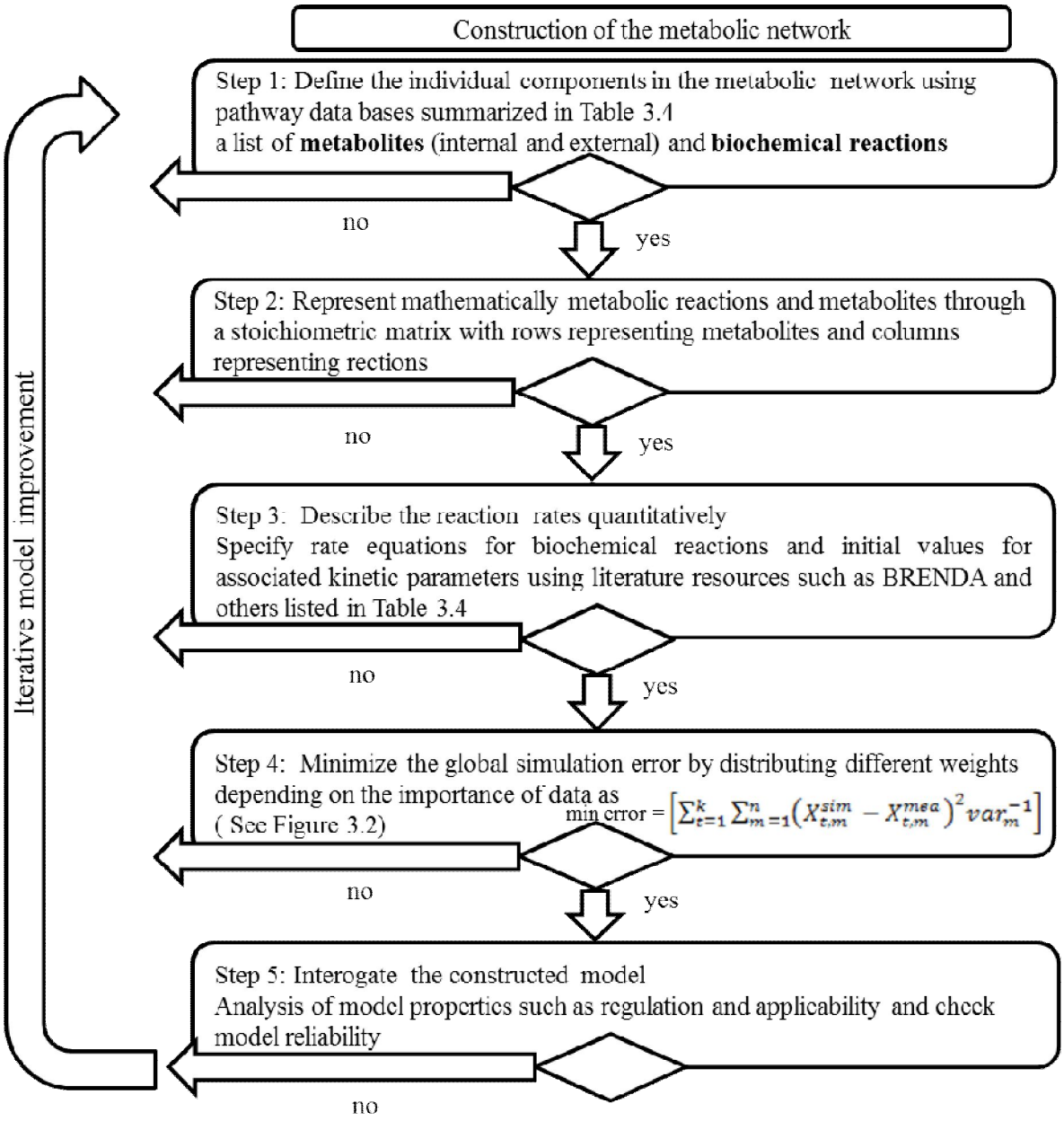

Figure 3.2An algorithm for the estimation of model parameter values

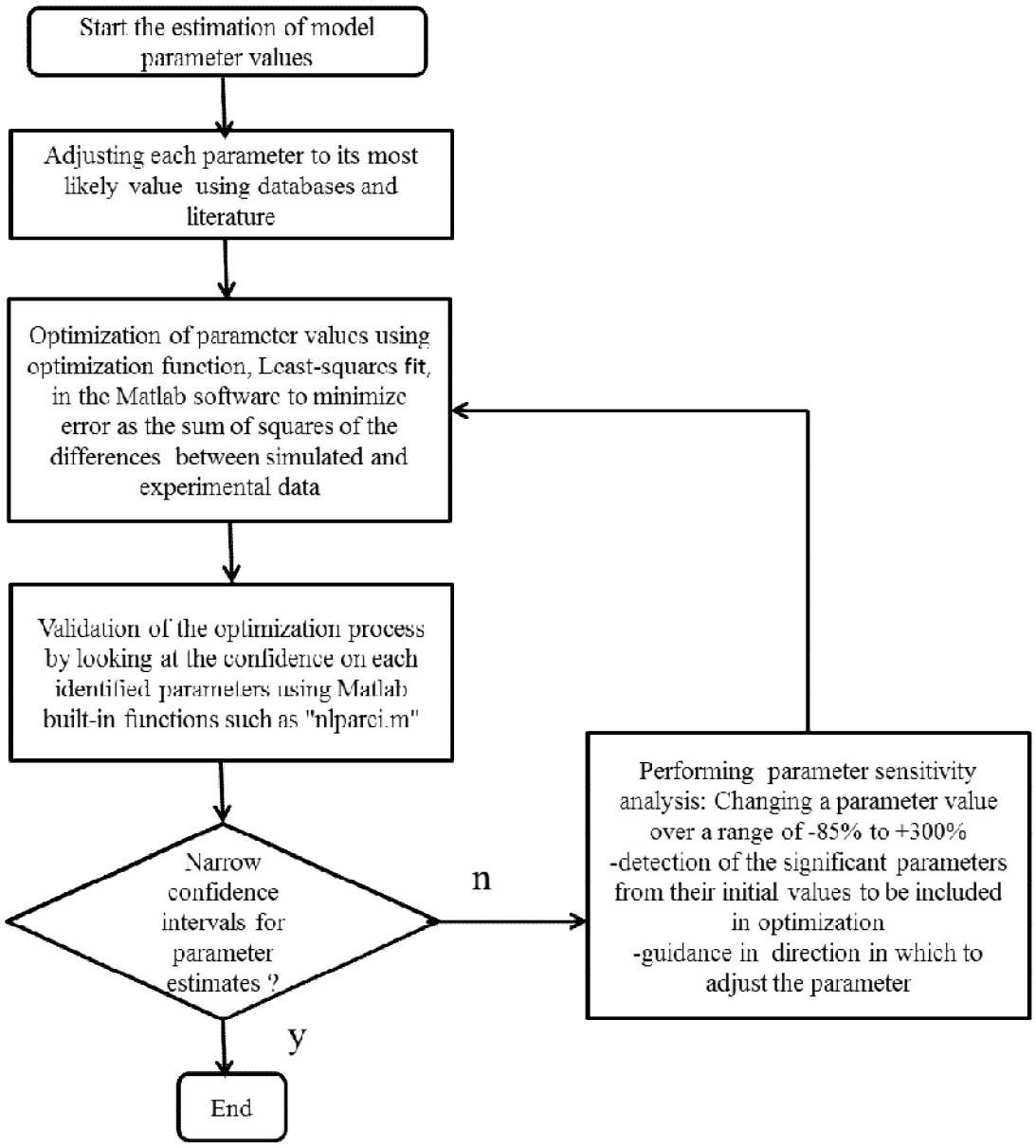

Table 3.2 Web resources and databases for components and pathways for various organisms

Name	Web address and description	Reference
KEGG PATHWAY	http://www.genome.jp/kegg/pathway.html Encyclopedia of pathway maps for various organisms	(Kanehisa et al., 2008)
BRENDA	http://www.brenda-enzymes.org The comprehensive enzyme information system including biochemical, and metabolic knowledge for various organisms	(Chang et al., 2009)
METACYC	http://MetaCyc metacyc.org Database for metabolic pathways and enzymes	(Caspi et al., 2010)
SABIO RK	http://sabio.villabosch.de/SABIORK Database for Biochemical Reactions and their Reaction Kinetics	(Rojas et al., 2007)
BioCyc	http://biocyc.org pathway and genome database for a large number of organisms including mammalian cells	(Karp et al., 2005)
Sigmoid	http://www.sigmoid.org Collection of the models for cellular signaling and metabolic pathways	(Saunders et al., 2008)
Reactome	http://www.reactome.org Curated knowledgebase of biological pathways in humans	(Vastrik et al., 2007)
BioModels	http://www.ebi.ac.uk/biomodels A data resource of Annotated Published Models	(Le NovŁre et al., 2006)
ResNet Mammalian Database	http://www.ariadnegenomics.com/products/databases Commercial database for cellular process and metabolic pathways in human, rat, and mouse	(Szklarczyk et al., 2011)

CHAPTER 4 A KINETIC METABOLIC MODEL BASED ON CELL ENERGETIC STATE: STUDY OF CHO CELLS BEHAVIOUR UNDER Na-BUTYRATE STIMULATION

Atefeh Ghorbaniaghdam[1], Olivier Henry[2], Mario Jolicoeur[1,*]

[1]Canada Research Chair in Applied Metabolic Engineering,

[2]Department of Chemical Engineering, École Polytechnique de Montréal,

P.O. box 6079, Centre-ville Station, Montréal, Québec, H3C 3A7, Canada

*Corresponding author: mario.jolicoeur@polymtl.ca

(Published in Bioprocess and Biosystem Engineering -Vol. 36, No. 4, p: 469-487)

4.1 Presentation of the article

In this article, the kinetic modelling framework is developed describing CHO cell primary metabolism. This framework is adapted from a previous work on the modelling of plant cells metabolism and derived from the metabolic network of CHO cells. The model considers the catabolism of the main nutrients (glucose and glutamine), including glycolysis, pentose phosphate pathway, TCA cycle and respiratory chain. Therefore, more details of model development are presented in this chapter and the ability of the model in describing anabolic pathways, nutrients uptakes and cell growth in different culture conditions is discussed.

4.2 Abstract

A kinetic-metabolic model approach describing and simulating Chinese hamster ovary (CHO) cells behaviour is presented. The model includes glycolysis, pentose phosphate pathway, TCA cycle, respiratory chain, redox state and energetic metabolism. Growth kinetic is defined as a function of the major precursors for the synthesis of cell building blocks. Michaelis-Menten type kinetic is used for metabolic intermediates as well as for regulatory functions from energy shuttles (ATP/ADP) and cofactors (NAD/H and NADP/H). Model structure and parameters were first calibrated using results from bioreactor cultures of CHO cells expressing recombinant t-PA. It is shown that the model can simulate experimental data for all available experimental data, such as extracellular glucose, glutamine, lactate and ammonium concentration time profiles, as well as cell energetic state. A sensitivity analysis allowed identifying the most sensitive parameters. The model was then shown to be readily adaptable for studying the effect of sodium butyrate on CHO cells metabolism, where it was applied to the cases with sodium butyrate addition either at mid-exponential growth phase (48 h) or at the early plateau phase (74 h). In both cases, a global optimisation routine was used for the simultaneous estimation of the most sensitive parameters, while the insensitive parameters were considered as constants. Finally, confidence intervals for the estimated parameters were calculated. Results presented here further substantiate our previous findings that butyrate treatment at mid exponential phase may cause a shift in cellular metabolism toward a sustained and increased efficiency of glucose utilization channeled through TCA cycle.

4.3 Keywords

Metabolic modeling, CHO cells, kinetic model, metabolic regulation, energy regulation, sodium butyrate

4.4 Introduction

In the past decades, high-producer cell lines for recombinant proteins have been developed concomitantly to optimal culture media and bioprocess management strategies. On the cell engineering side, emphasis has been placed at prolonging culture longevity. Genetic modifications were directed mostly toward the increase of Chinese Hamster Ovary (CHO) cells viability such as complementing the cell machinery with growth factor endogenous production (e.g. insulin like growth factors) (Galbraith et al., 2006; Sunstrom et al., 2000) or optimizing cell-cycle control genes (e.g. cyclin-dependent kinases) (Fussenegger et al., 1998). Cell specific productivity has also been increased using various strategies: with the use of strong promoters, such as cytomegalovirus (CMV), beta-actin and EF-1α, through the identification of favorable location of integration on the genome, or by the insertion of amplifiable markers, such asdihydrofolate reductase (DHFR) (Cacciatore et al., 2010). Some studies have also focused on protein synthesis steps and modulation of the glycosylation process, mostly by the incorporation of specific *de novo* glycosylation sites (Elliott, Chang, et al., 2004; Elliott, Egrie, et al., 2004; Elliott et al., 2003). In parallel, bioprocess engineering approaches, such as imposing temperature and pH shifts to prolong productive stationary phase (Quek et al., 2010) , and the addition of chemicals (e.g. sodium butyrate, pentanoic acid, quinidine and thymidine) (Kumar et al., 2007), or development of efficient fed-batch protocols (Birch & Racher, 2006), have allowed to achieve high viable cell densities ($10*10^6$ cells/mL) and cell specific productivities for up to 3 weeks (Wurm, 2004). Interestingly, most optimal culture management protocols have resulted in more efficient nutrient utilization and reduced waste formation.

Today's primary challenge, however, is to increase product quality, i.e. drugs specificity, while maintaining high productivity and reproducibility levels, from lot to lot. This objective refers, among others, to minimizing glycoform diversity of a protein-based therapeutic; variants that are contaminating the final product and are mostly responsible for undesired secondary effects. Various efforts are being explored to this end (Jenkins, 2007), but at the industrial level, such multi-objectives control of a bioprocess (i.e. protein quality and quantity, cell viability, culture longevity and reproducibility) can only be achieved through the fine management of bioreactor culture conditions under fed-

batch or perfusion operation modes. Therefore, the problem of defining an optimal culture management strategy becomes even more complex when sudden stresses affecting cell metabolism are imposed from the use of chemical additives, inducible promoters or a transient transfection strategy. In that context, there is a strong interest at characterizing and describing cell behaviour from the dynamic changes occurring along with bioprocesses. However, classical approaches can hardly bring an adequate information level and a descriptive and predictive metabolic model of cell behaviour is needed. Dynamic models have been developed to describe microbial (Chassagnole et al., 2002), CHO (Nolan & Lee, 2010) as well as plant cells (Cloutier et al., 2007). Particularly in the case of CHO cells, Nolan et al. (2010) (Nolan & Lee, 2010) have describe the transient behaviour of extracellular metabolite concentrations and used metabolic flux analysis (MFA) to calculate intracellular fluxes, assuming that all intermediate metabolites are at pseudo-steady-states. That model also includes parameters related to temperature shift and redox state. To be of general applicability, however, a model must be able to capture the dynamics of the cell metabolic network in a wide range of relevant conditions. In a recent work, we have developed a kinetic-metabolic model framework based on cell energetic and redox states and adapted to plant cells (Cloutier et al., 2007). We have shown that the model can successfully be applied either to control cytoplasmic inorganic phosphate to a defined set-point, or to maximize secondary metabolites productionthrough the in-silico design and real implementation of a bioreactor culture management strategy (Cloutier et al., 2007). We thus propose here to transpose our plant cell model framework, which describes flux kinetics and pathway regulation from cell energetic and redox states, to CHO cells. In order to challenge the model, we have studied its capacity to describe cell behaviour either under standard batch culture conditions or following sodium butyrate addition, a widely used chemical to enhance recombinant protein production (Hendrick et al., 2001; Kim & Lee, 2001; Lee & Lee, 2003; Palermo et al., 1992). The model was first successfully calibrated on previously published experimental data (McMurray-Beaulieu et al., 2009) for a bioreactor culture without the addition of sodium butyrate, where a combination of literature and parameter sensitivity analysis assisted us to manually and mathematically tune the parameters. An *a posteriori* sensitivity analysis was then performed on parameter

estimates to identify which kinetic parameters were to be included or excluded from further estimation processes for bioreactor cultures with sodium butyrate.Confidence intervals for kinetic parameters with relatively high sensitivity were also calculated in order to verify how well the parameters were determined with the available experimental data sets. Finally, model simulations were used to study the effects of sodium butyrate addition on cell metabolism where simulated fluxes and ratios with their confidence intervals were interpreted in relation to statistical significance.

4.5 Material and Methods

4.5.1 Biological material and bioreactor cultures

A detailed description of the cell line, culture conditions and analytical methods can be found in previous work (McMurray-Beaulieu et al., 2009). Briefly, a recombinant t-PA producing CHO cell line (ATCC, CRL9606) was cultured in a 3.5-L stirred tank bioreactor (ChemapAG, Switzerland) equipped with a helical-ribbon impeller (Jolicoeur, Chavarie, Carreau, & Archambault, 1992). One culture was performed as control and two were treated with 1 mM Na-butyrate (Cat. No.B5887, Sigma-Aldrich Canada Ltd., Ontario, Canada); one at mid-exponential phase 48 h post-inoculation (NaBu-48h), and one at the end of exponential phase 74 h post inoculation (NaBu-74h). Dissolved oxygen concentration was measured by a polarographic probe (Cat. No. InPro 6800, Mettler Toledo, Mississauga, Ontario, Canada) connected to a data acquisition and control system (Virgo, Longueuil, Quebec, Canada). Glucose, glutamine, ammonia and lactate concentrations as well as t-PA concentration in the medium were evaluated using enzymatic assays. Intracellular nucleotides were extractedusingperchloric acidas described by Ryll and Wagner (Ryll & Wagner, 1991) and quantified by HPLC-MS (Micromass ZQ, Waters, Milford, MA, USA). Column specification, mobile phase composition and detection method are detailed in McMurray-Beaulieu et al. (2009) (McMurray-Beaulieu et al., 2009).

4.5.2 Model description

4.5.2.1 The model structure

A predictive kinetic-metabolic model previously developed and validated for plant cell culture (Cloutier et al., 2007; Leduc et al., 2006) has been transposed to CHO cells. The

model metabolic network is presented in Figure 4.1.A series of biologically relevant mathematical representations of metabolic flux kinetics are presented in Table 4.1, and the stoichiometry of the reactions is listed in Table 4.2 and the final (calibrated; see below for detailed explanations) model is described in Table 4.3. The major metabolic pathways are considered: glycolysis, pentose phosphate pathway, TCA cycle, glutaminolysis as well as cell respiration. The latter includes phosphorylative oxidation with ATP and H_2O synthesis, and mitochondrial proton leakleading to H_2O synthesis where the P/O ratio is estimated to have a value of 2, which is in agreement with the typical values reported for CHO cells (Nolan & Lee, 2010). In addition, we also considered the reversible reactions involving creatine and adenylate kinases. AMP synthesis from R5P (Table 4.2, reaction 28) is also considered (Zamorano et al., 2010).

The cell specific growth rate (μ) is described (Table 4.2) by considering the precursors of major cell building blocks: G6P (leading to phospholipids and organic phosphate compounds), citrate (to lipids), R5P (to DNA, RNA and nucleotides), glutamate (GLU) and glutamine (GLN) (to proteins); a strategy we previously successfully applied to plant cells (Leduc et al., 2006). t-PA synthesis has not been described in the model because of a flux rate range of ~10^{-7} mmol $(10^6 \text{ cells})^{-1}$ h^{-1} (at a specific productivity of 0.05 μg $(10^6 \text{ cells})^{-1}$ h^{-1}) (Figure 4.9E), which was over 2-3order of magnitude lower than all intracellular fluxes rates and was thus unfortunately mathematically non-significant**.** The consumption of each precursor metabolite is calculated as proposed by Martens (Martens, 2007) and considered in mass balances. The stoichiometric coefficients for biomass synthesis, reaction 30 in Table 4.2, were taken from literature (Ahn & Antoniewicz, 2011), including that 3.78 moles of ATP required to form one mole of biomass (Nolan & Lee, 2010)(Table 4.2, reaction 30). The mass balance onATP thus includes its production from glycolysis and oxidative phosphorylation, as well as its consumption for biomass synthesis, maintenance-related processes, transmembrane transport, and other ATPases-related reactions; the sum of consuming processes being integrated within a unique reaction (Table 4.2, reaction 25).At this stage of model development, and similarly to our previous model for plant cells (Cloutier et al., 2007), CHO cells were taken as a unique compartment with no intracellular sub-compartments

(e.g. mitochondria, nucleus, etc.), and Michaelis-Menten kinetics was used to describe each metabolic reaction flux rate.

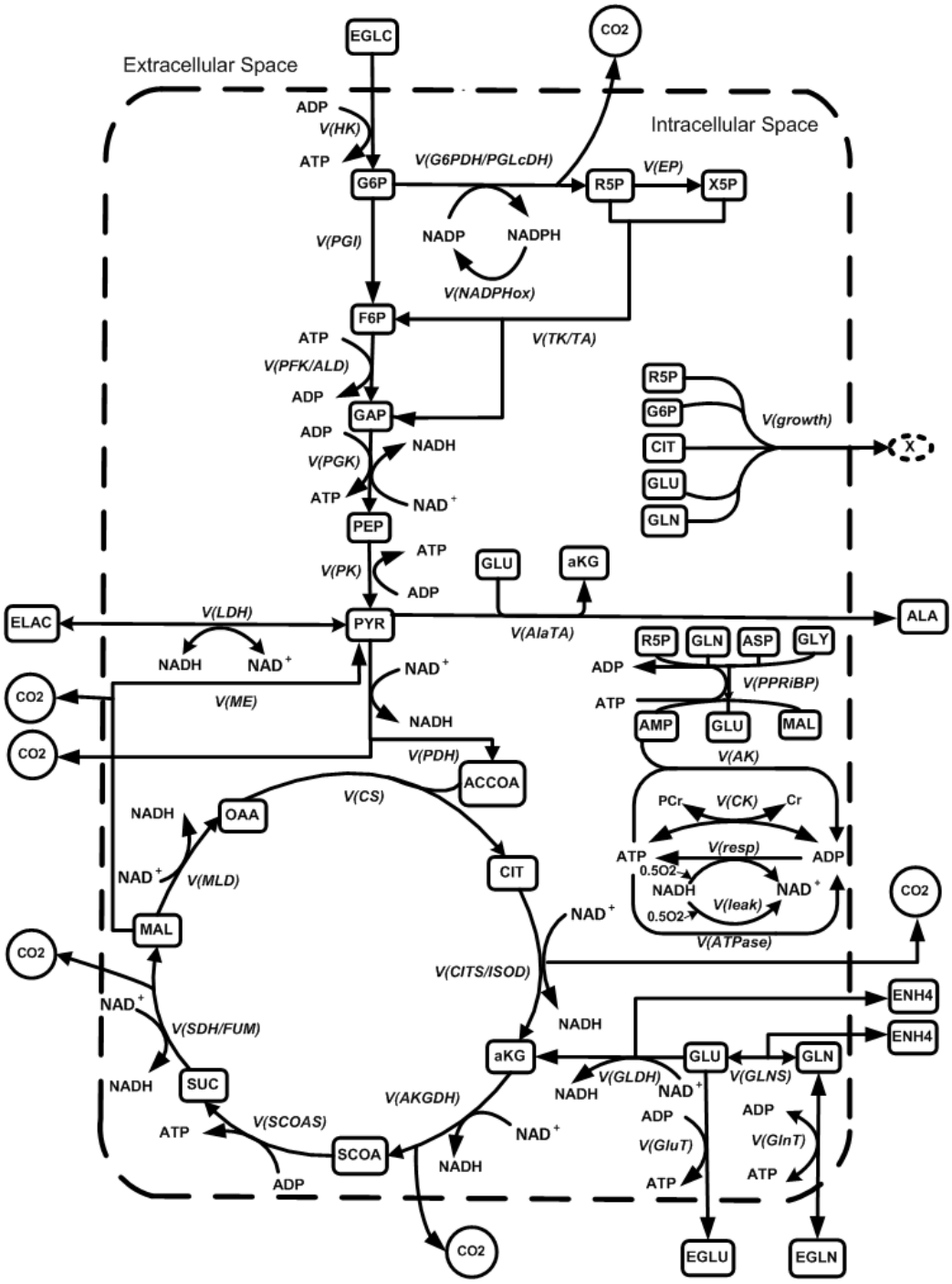

Figure 4.1 The metabolic network described by the model

Table 4.1 Mathematical formulations of metabolic fluxes kinetic

	Regulation	Kinetic Expression $v\left(\sum_{i=1}^{N_S} S_i \overset{P1 \backsim P2}{\underset{R1 \backsim R2}{\rightarrow}} \sum_{i=1}^{N_P} P_i\right)$	Objective Function Value
1	The flux rate is only a function of its substrates concentration with a Michaelis-Menten type kinetic, even when it is coupled to energy and/or electron transfer.	$v_{max}\left[\prod_{i=1}^{N_s}\frac{C_{S_i}}{K_{mS_i}+C_{S_i}}\right]$	181.64
2	The flux rate is a function of its substrates concentration as well as energy (ATP/ADP) and/or electron (NADH/NAD^+, NADPH/ $NADP^+$) transfer nucleotides.	$v_{max}\left[\prod_{i=1}^{N_s}\frac{C_{S_i}}{K_{m_{Si}}+C_{S_i}}\right]\left[\frac{C_{P_1}}{K_{mp_1}+C_{P_1}}\right]\left[\frac{C_{R_1}}{K_{m_{R1}}+C_{R_1}}\right]$	170.1
3	Similar to mathematical formulation #2 but with a Michaelis-Menten type kinetic using substrates and nucleotides ratio.	$v_{max}\left[\prod_{i=1}^{N_s}\frac{C_{S_i}}{K_{m_{Si}}+C_{S_i}}\right]\left[\frac{\frac{C_{P_1}}{C_{P_2}}}{K_{m\frac{C_{P_1}}{C_{P_2}}}+\frac{C_{P_1}}{C_{P_2}}}\right]\left[\frac{\frac{C_{R_1}}{C_{R_2}}}{K_{m\frac{C_{R_1}}{C_{RP_2}}}+\frac{C_{R1}}{C_{R_2}}}\right]$	138.2
4	Combination of mathematical formulations #2 and #3.	$v_{max}\left[\prod_{i=1}^{N_s}\frac{C_{S_i}}{K_{m_{Si}}+C_{S_i}}\right]\left[\frac{\frac{C_{P_1}}{C_{P_2}}}{K_{m\frac{C_{P_1}}{C_{P_2}}}+\frac{C_{P_1}}{C_{P_2}}}\right]\left[\frac{\frac{C_{R_1}}{C_{R_2}}}{K_{m\frac{C_{R_1}}{C_{RP_2}}}+\frac{C_{R1}}{C_{R_2}}}\right]\left[\frac{C_{P_1}}{K_{mp_1}+C_{P_1}}\right]\left[\frac{C_{R_1}}{K_{m_{R1}}+C_{R_1}}\right]$	166.7

*p_1, p_2 are ATP or ADP and R_1, R_2 are either NAD[P]H or NAD[P]$^+$.

Understanding that a model is a simplified representation of a phenomenon, or of a network of biochemical reactions in this case, the kinetic parameters determined in this work have to be seen as global; they also include what is not described, such as metabolic regulation as well as other biochemical reactions that are taking place. The parameters values determined in this work may thus differ from the strict real value for a

biochemical reaction but these are bringing a global view on a group of regulated biochemical reactions occurring around each metabolite described in the model. In that context, a statistical analysis (see below) was performed on model parameters values as well as on the model structure in order to ensure that a unique model structure is able to describe either a control culture than stressed cultures with Na-butyrate. All the reactions related to primary metabolism are considered unidirectional at this stage of model development, except for the pyruvate-lactate and intracellular-extracellular glutamine exchangesas also reported by Nolan et al. (Nolan & Lee, 2010).Finally a sigmoidal function, based on a threshold concentration for extracellular glutamine, was used to manage the change between nitrogenous sources (i.e. glutamate and glutamine) at low extracellular glutamine level.

4.5.2.2 Fluxes kinetic equation

A series of biologically relevant mathematical representations of metabolic flux kinetics (Table 4.1) were evaluated based on the model capacity to fit experimental data. In a first kinetic expression formulation (#1), each metabolic flux rate is simply determined by the concentrations of the substrates (metabolites) using Michaelis-Menten type kinetics; and all of the followings are implementations of #1 formulation. Formulation #2 proposes a Michaelis-Mentenkinetic to account for energetic and redox nucleotides concentrations in the reactions they are involved, as described in other works on mitochondrial energetic metabolism (Bohnensack, 1981; Garfinkel, 1971a; Garfinkel, 1971b; Korzeniewski, 1991; Wu et al., 2007) or on glycolysis (Kauffman et al., 2002). In formulation #3, nucleotide ratios are considered within a Michaelis-Menten kinetic, as proposed in the literature cited in Dash et al. (2007) (Dash, DiBella, & Cabrera, 2007). Finally,in formulation#4, multiplicative Michaelis-Menten kinetics for intracellular concentration of nucleotides and for nucleotide ratios are combined. It thus accounts for both the effect of nucleotide ratios and energetic/redox nucleotides concentrations. The model performance for each of these four kinetic expression formulations was then compared with regard to its ability to describe experimental data.

Table 4.2Reactions of a metabolic network

No.	Reaction
1	EGLC+ATP→G6P+ADP
2	G6P→F6P
3	F6P+ATP→2GAP+ADP
4	GAP+ADP+NAD^++Pi→PEP+ATP+NADH
5	PEP+ADP→PYR+ATP
6	PYR+NADH↔ELAC+NAD^+
7	G6P+2$NADP^+$→R5P+2NADPH+CO_2
8	R5P→X5P
9	R5P+2X5P→2F6P+GAP
10	PYR+COA+NAD^+→ACCOA+NADH+CO_2
11	ACCOA+OXA→CIT+CoA
12	CIT+NAD^+→AKG+NADH+CO_2
13	AKG+CoA+NAD^+→SCOA+NADH+CO_2
14	SCOA+ADP+Pi→SUC+CoA+ATP
15	SUC+2/3NAD^+→MAL+2/3NADH+CO_2
16	MAL+NAD^+→OAA+NADH
17	MAL →PYR+CO_2
18	EGLN+ATP↔GLN+ADP
19	GLN↔GLU+ENH_4
20	GLU+NAD^+→AKG+NADH+ENH_4
21	GLU+PYR→AKG+ALA
22	GLU+ADP+Pi→EGLU+ATP
23	O_2+(P/O ratio)*2ADP+2NADH+(P/O ratio)*2Pi→(P/O ratio)*2ATP+NAD^++2H_2O
24	O_2+2NADH→2NAD^++2H_2O
25	ATP→ADP+Pi
26	ATP+AMP↔2ADP
27	Pcr+ADP↔Cr+ATP
28	2GLN+0.6R5P+2ASP+GLY+2ATP→2GLU+2MAL+AMP+2ADP
29	NADPH→$NADP^+$
30	0.024R5P+0.029G6P+1.86CIT+0.033GLU+0.04GLN+3.78ATP→X

Table 4.3Biokinetic equations of the metabolites fluxes (1-30) of the model

No.	Biokinetic equations
1	$v(HK) = v_{\max HK} * \frac{EGLC}{K_{mEGLC} + EGLC} * \frac{\frac{ATP}{ADP}}{K_{m\frac{ATP}{ADP}} + \frac{ATP}{ADP}}$
2	$v(PGI) = v_{maxf\ PGI} * \frac{G6P}{K_{mG6P} + G6P}$
3	$v(PFK/ALD) = v_{\max PFK/ELD} * \frac{F6P}{K_{mF6P} + F6P} * \frac{\frac{ATP}{ADP}}{K_{m\frac{ATP}{ADP}} + \frac{ATP}{ADP}}$
4	$v(PGK) = v_{maxPGK} * \frac{GAP}{K_{mGAP} + GAP} * \frac{\frac{ADP}{ATP}}{K_{m\frac{ADP}{ATP}} + \frac{ADP}{ATP}} * \frac{Pi}{K_{mPi} + Pi} * \frac{\frac{NAD}{NADH}}{K_{m\frac{NAD}{NADH}} + \frac{NAD}{NADH}}$
5	$v(PK) = v_{\max PK} * \frac{PEP}{K_{mPEP} + PEP} * \frac{\frac{ADP}{ATP}}{K_{m\frac{ADP}{ATP}} + \frac{ADP}{ATP}}$
6	$v(LDH) = v_{maxf\ LDH} * \frac{PYR}{K_{mPYR} + PYR} * \frac{\frac{NADH}{NAD}}{K_{m\frac{NADH}{NAD}} + \frac{NADH}{NAD}} - v_{maxr\ LDH} * \frac{ELAC}{K_{mLAC} + ELAC} * \frac{\frac{NAD}{NADH}}{K_{m\frac{NAD}{NADH}} + \frac{NAD}{NADH}}$
7	$v(G6PDH/PGLcDH) = v_{\max G6PDH/PGLcDH} * \frac{G6P}{K_{mG6P} + G6P} * \frac{\frac{NADP}{NADPH}}{K_{m\frac{NADP}{NADPH}} + \frac{NADP}{NADPH}}$
8	$v(EP) = v_{\max EP} * \frac{R5P}{K_{mR5P} + R5P}$
9	$v(TK/TA) = v_{\max TK/TA} * \frac{R5P}{K_{m2R5P} + R5P} * \frac{X5P}{K_{mX5P} + X5P}$
10	$v(PDH) = v_{max\ PDH} * \frac{PYR}{K_{mPYR} + PYR} * \frac{\frac{NAD}{NADH}}{K_{m\frac{NAD}{NADH}} + \frac{NAD}{NADH}}$

Table 4.3 Biokinetic equations of the metabolites fluxes (1-30) of the model (continued)

11 $$v(CS) = v_{maxCS} * \frac{ACCOA}{K_{mACCOA} + ACCOA} * \frac{OXA}{K_{mOXA} + OXA}$$

12 $$v(CITS/ISOD) = v_{\max CITS/ISOD} * \frac{CIT}{K_{mCIT} + CIT} * \frac{\frac{NAD}{NADH}}{K_{m\frac{NAD}{NADH}} + \frac{NAD}{NADH}}$$

13 $$v(AKGDH) = v_{max\ AKGDH} * \frac{AKG}{K_{mAKG} + AKG} * \frac{\frac{NAD}{NADH}}{K_{m\frac{NAD}{NADH}} + \frac{NAD}{NADH}}$$

14 $$v(SCOAS) = v_{max\ SCOA} * \frac{SCOA}{K_{mSCOA} + GAP} * \frac{\frac{ADP}{ATP}}{K_{m\frac{ADP}{ATP}} + \frac{ADP}{ATP}} * \frac{Pi}{K_{mPi} + Pi}$$

15 $$v(SDH/FUM) = v_{\max SDH/FUM} * \frac{SUC}{K_{mSUC} + SUC} * \frac{\frac{NAD}{NADH}}{K_{m\frac{NAD}{NADH}} + \frac{NAD}{NADH}}$$

16 $$v(MDH) = v_{max\ MDH} * \frac{MAL}{K_{mMAL} + MAL} * \frac{\frac{NAD}{NADH}}{K_{m\frac{NAD}{NADH}} + \frac{NAD}{NADH}}$$

17 $$v(ME) = v_{max\ ME} * \frac{MAL}{K_{mMAL} + MAL}$$

18 $$v(GlnT) = v_{maxfGlnT} * \frac{EGLN}{K_{mEGLN} + EGLN} * \frac{\frac{ATP}{ADP}}{K_{m\frac{ATP}{ADP}} + \frac{ATP}{ADP}} - v_{maxr\ GlnT} * \frac{GLN}{K_{mGLU} + GLN} * \frac{\frac{ADP}{ATP}}{K_{m\frac{ADP}{ATP}} + \frac{ADP}{ATP}}$$

19 $$v(GLNS) = v_{maxf\ GLNS} * \frac{GLN}{K_{mGLU} + GLN} - v_{maxr\ GLNS} * \frac{GLU}{K_{mGLU} + GLU} * \frac{NH_4}{K_{mNH_4} + NH_4} * \left(\frac{1}{1 + e^{(\mathrm{EGLN}-2)}}\right)$$

20 $$v(GLDH) = v_{max\ GLDH} * \frac{GLU}{K_{mGLU} + GLU} * \frac{\frac{NAD}{NADH}}{K_{m\frac{NAD}{NADH}} + \frac{NAD}{NADH}}$$

Table 4.3 Biokinetic equations of the metabolites fluxes (1-30) of the model (continued)

21 $$v(AlaTA) = v_{max\ AlaTA} * \frac{GLU}{K_{mGLU} + GLU} * \frac{PYR}{K_{mPYR} + PYR}$$

22

$$v(GluT) = v_{maxGluT} * \frac{GLU}{K_{mGLU}+GLU} * \frac{\frac{ADP}{ATP}}{K_{m\frac{ADP}{ATP}}+\frac{ADP}{ATP}} * \frac{Pi}{K_{mPi}+Pi}$$

23 $$v(resp) = v_{max\ resp} * \frac{O_2}{K_{mO_2} + O_2} * \frac{\frac{ADP}{ATP}}{K_{m\frac{ADP}{ATP}} + \frac{ADP}{ATP}} * \frac{NADH}{K_{mNADH} + NADH} * \frac{Pi}{K_{mPi} + Pi}$$

24 $$v(leak) = v_{max\ leak} \frac{NADH}{K_{mNADH} + NADH}$$

25 $$v(ATPase) = v_{max\ ATPase} * \frac{ATP}{ATP + ATP}$$

26 $$v(AK) = v_{maxf\ AK} * \frac{ATP}{K_{mATP} + ATP} * \frac{AMP}{K_{mAMP} + AMP} - v_{maxr\ AK} * \frac{ADP}{K_{mADP} + ADP}$$

27 $$v(CK) = v_{maxf\ CK} * \frac{ADP}{K_{mADP} + ADP} * \frac{Pcr}{K_{mPcr} + Pcr} - v_{maxr\ CK} * \frac{ATP}{K_{mATP} + ATP} * \frac{Cr}{K_{mCr} + Cr}$$

28 $$v(PPRiBP) = v_{\max PPRibP} * \frac{R5P}{K_{mR5P} + R5P} * \frac{ASP}{K_{mASP} + ASP} * \frac{GLN}{K_{mGLN} + GLN} * \frac{GLY}{K_{mGLY} + GLY}$$

29 $$v(NADPHox) = v_{\max NADPHox} * \frac{NADPH}{K_{mNADPH} + NADPH}$$

30 $$v(growth) = v_{\max growth} * \frac{R5P}{K_{mR5P} + R5P} * \frac{G6P}{K_{mG6P} + G6P} * \frac{CIT}{K_{mCIT} + CIT} * \frac{GLU}{K_{mGLU} + GLU} * \frac{GLN}{K_{mGLN} + GLN} * \frac{\frac{ATP}{ADP}}{K_{m\frac{ATP}{ADP}} + \frac{ATP}{ADP}}$$

Table 4.4State variables description and initial conditions

Component	Description	Value	Units
ACCoA	Acetyl-CoezymeA	1.39E-7	mmol $(10^6$ cells$)^{-1}$
AKG	α-Ketoglutarate	1.4E-7	‘‘

ADP	Adenosine diphosphate	4.9e-7	‘‘
AMP	Adenosine monophosphate	1.4e-8	‘‘
ATP	Adenosine triphosphate	2.72E-6	‘‘
CIT	Citrate	2E-6	‘‘
CoA	CoenzymeA	2E-8	‘‘
Cr	Creatine	3E-6	‘‘
F6P	Fructose 6-Phosphate	3E-7	‘‘
G6P	Glucose 6-Phosphate	6E-7	‘‘
GAP	Glyceraldehyde 3-Phosphate	1.6E-7	‘‘
GLN	Glutamine	9e-6	‘‘
GLU	Glutamate	8E-6	‘‘
GLY	Glycine	8E-6	‘‘
MAL	Malate	1.5E-7	‘‘
NAD	Nicotinamide adenine dinucleotide	*9E-7*	‘‘
NADH	Nicotinamide adenine dinucleotide (reduced)	3E-8	‘‘
NADP	Nicotinamide adenine dinucleotide phosphate	9E-13	‘‘
NADPH	Nicotinamide adenine dinucleotide phosphate (reduced)	1.4E-11	‘‘
OXA	Oxaloacetate	1E-5	‘‘
O_2	Intracellular oxygen	8E-6	‘‘
PEP	*phosphoenolpyruvate*	3.5E-7	‘‘
PCr	PhosphoCreatine	1E-7	‘‘
Pi	Inorganic phosphate	2E-6	‘‘
PYR	Pyruvate	2E-7	‘‘
R5P	Ribose 5-phosphate	1.5E-7	‘‘
SCoA	Succinyl-CoA	4E-7	‘‘
SUC	Succinate	4E-7	‘‘
X5P	Xylose-5-phosphate	1E-7	‘‘
EALA	Extracellular alanine	0.5	mM
EASP	Extracellular aspartate	0.5	‘‘
EGLC	Extracellular glucose	24	‘‘
EGLN	Extracellular glutamine	3.5	‘‘
EGLU	Extracellular glutamate	0	‘‘
ELAC	Extracellular lactate	1.5	‘‘
ENH_4	Extracellular ammonia	1.1	‘‘

4.5.2.3 Model calibration and sensitivity analysis

The model has 36 differential equations, i.e. mass balances on state variables listed in Table 4.4, which were solved using the Matlab software (The MathWorks Inc., Natick, MA, USA).The model has a high number of parameters with 35 affinity constants (listed in Table 4.5), 35 maximum reaction rates (Table 4.6), and two parameters for each sigmoidal switch functions (Table 4.3). Initial conditions (Table 4.4), at inoculation, and parameters values have been taken from literature, when available, or estimated as

previously described in Leduc et al. (Leduc et al., 2006) and as briefly summarized below. The objective function is *formulated* as the weighted sum of squared residuals (WSSRES) between available experimental data (X^{meq}) and simulated values (X^{sim}) for each state variable *mat time k*, where the weight is the inverse of the variance of the experimental data for each state variable, var_m^{-1}

$$\min WSSRES = \left[\sum_{t=1}^{k}\sum_{m=1}^{n}\left(X_{t,m}^{sim} - X_{t,m}^{mea}\right)^2 var_m^{-1}\right] \quad (9)$$

The objective function was minimized in an iterative process using the Matlab Optimization Toolbox, *Least-squares fit,* and manual tuning of the parameters and initial conditionsto help the convergence. To avoid over parameterization, a parameter sensitivity analysis was first performed using experimental data from CHO cell control batch culture previously described (McMurray-Beaulieu et al., 2009). This step has facilitated the detection of the significant parameters from their initial values, and thus guided us in the following iterative cycle of optimization.In a second step, a sensitivity analysis was performed consisting in changing a parameter value over a range of -85% to +300% around its value, while holding all other parameters constant. The sensitivity of the model on each parameter was then quantified from the objective function. Once no further minimization of the objective function could be obtained, the values of parameters were considered determined. Thereafter, model parameters conferring a high sensitivity to the model were calibrated on the datasets of the two cultures with sodium butyrate, using whole culture data before and after sodium butyrate addition, and changing kinetic parameters at the time of sodium butyrate addition using a sigmoidal switch function to avoid any mathematical discontinuity. In one culture, sodium butyrate has been added at 48 h during mid-exponential growth phase (NaBu-48h) and in the other at 74 h, which corresponded to the early plate growth phase (NaBu-74h) (McMurray-Beaulieu et al., 2009). The process of parameter revision was continued until the simulated profiles closely followed experimental data, and that experimental data -orphans simulation profiles were within ranges found in literature. The parameter values for the final calibrated model are shown in Tables 4.5 and 4.6, those associated to glutamine/glutamate management are shown in Table 4.3. Confidence intervals for highly sensitive parameter estimates (Table 4.6) and simulated fluxes and ratios were then

evaluated using "*nlparci.m"* and"*nlpredci.m",* both Matlab built-in functions, respectively. Moreover, unpaired two-tailed Student's t-test was used and related p-values were calculated to statistically compare parameter values (Table 4.6) and simulated fluxes and ratios for the cultures with and without sodium butyrate (Table 4.7).

4.6 Results

4.6.1 Calibration of model structure and parameters on CHO cells control culture

Model calibration was first performed, as described in the Material and Methods section, on control bioreactor culture data without sodium butyrate (McMurray-Beaulieu et al., 2009). Four kinetic expression formulations (described in Table 4.1) were evaluated in parallel. The use of a Michaelis-Menten type kinetic for the only reaction substrates (formulation #1) led to the highest simulation error compared to experimental data (Table 4.1). Considering the cell energetic (ATP, ADP) and/or redox (NADH, NAD^+, NADPH, $NADP^+$) shuttles concentrations as well (#2) enabled to decrease the simulation error. However, the use of ratios (ATP/ADP, NADH/NAD^+, NADPH/$NADP^+$) in formulations #3 allowed to lower simulation error. Combining formulations #2 and #3 (formulation #4) led to a high and similar error than for formulation #2. Therefore, because of a higher performance level (i.e. lower simulation error) as well as a lower formulation complexity kinetic expression, formulation #3 was used in the remaining of this study. A sensitivity analysis performed on the final calibrated model structure (i.e. kinetic formulation #3), shows that the model is sensitive to 25 of its 72 parameters, where these affected more than 5% the objective function, and thus model appropriateness, when changed from -85 to +300% from their calibrated values. However, based on comparative studies found in literature (Cloutier et al., 2008), we arbitrarily set the criterion to qualify a parameter as a sensitive one when a small variation of its value (±15%) causes an increase on the objective function of more that 10%. The model showed to be more sensitive to rate constants than to affinity constants (Figure 4.2). A series of more precise sensitivity analyses were then performed without enabling to improve (lower) the objective function. As showed in Figure 4.2, the most influential parameters are mostly related to the maximum specific growth rate, ($v_{max,growth}$), and glycolysis (v_{maxHK},$v_{maxPGI,}$ $v_{maxPFK/ALD,}$ $v_{maxPK,}$ $v_{maxfLDH}$ *and* $v_{maxrLDH}$), and

partially to TCA cycle ($v_{maxCIT/ISOD,}$ $v_{maxSCOAS,}$ $and v_{maxMLD}$), and glutaminolysis ($v_{maxfGlnT,}$ $v_{maxfGLNS,}$ and$v_{maxGLDH}$). To a lesser extent, parameters of the pentose phosphate pathway (v_{maxEP}) and of the reaction connecting glycolysis to TCA cycle (v_{maxPDH}) also showed to influence model simulations. Considering the energetic fuelling reactions, the model was highly sensitive to the parameter related to unaccounted ATP consuming reactions, ($v_{maxATPase}$), and NADH consuming reaction, ($v_{maxleak}$). Therefore, a subset of 17 parameters were first challenged to minimize the value of the objective function adapting the model to the cultures with sodium butyrate. All calibrated model parameters values for maximum reaction rates are within the ranges proposed in literature (Tables 4.5 and 4.6). $K_m$values for intracellular metabolites were also withinranges reported in other studies (10^{-7}-10^{-6} (mmol 10^6)$^{-1}$ cells) (skeletal muscle cells: (Dash et al., 2007; Lambeth & Kushmerick, 2002).Finally, *Km* values for extracellular nutrients are within the ranges reported for CHO cells, except for extracellular lactate, which is higher than that found in literature (15 vs 6 mmol L^{-1}) (Nolan & Lee, 2010).

Table 4.5 Affinity (Km) constants

Parameter	**Value**	**Units**

	Control	NaBu-74h	NaBu-48h	
K_{mEGLC}	4.29	4.29	4.29	mM
K_{mEGLN}	1.27	1.27	1.27	"
K_{mELAC}	15	15	15	"
K_{mENH_4}	2	2	2	"
K_{mG6P}	2E-7	2E-7	2E-7	mmol $(10^6$ cells$)^{-1}$
K_{mF6P}	9E-6	9E-6	9E-6	"
K_{mGAP}	8E-7	8E-7	8E-7	"
K_{mPEP}	9.6E-7	9.6E-7	9.6E-7	"
K_{mR5P}	1E-7	1E-7	1E-7	"
K_{mX5P}	3.4E-8	3.4E-8	3.4E-8	"
K_{mPYR}	9E-7	9E-7	9E-7	"
K_{mACCOA}	9.6E-7	9.6E-7	9.6E-7	"
K_{mOXA}	2.4E-7	2.4E-7	2.4E-7	"
K_{mCIT}	1E-7	1E-7	1E-7	"
K_{mAKG}	3E-8	3E-8	3E-8	"
K_{mSCOA}	1.5E-7	1.5E-7	1.5E-7	"
K_{mSUC}	1.6E-7	1.6E-7	1.6E-7	"
K_{mMAL}	2E-7	2E-7	2E-7	"
K_{mGLN}	8.2E-6	8.2E-6	8.2E-6	"
K_{mGLU}	1.25E-5	1.25E-5	1.25E-5	"
K_{mGLY}	3E-8	3E-8	3E-8	"
K_{mATP}	7.6E-6	7.6E-6	7.6E-6	"
K_{mADP}	6.25E-7	6.25E-7	6.25E-7	"
K_{mAMP}	2E-8	2E-8	2E-8	"
K_{mPcr}	7.6E-6	7.6E-6	7.6E-6	"
K_{mCr}	5E-6	5E-6	5E-6	"
K_{mO_2}	4E-6	4E-6	4E-6	"
K_{mPi}	1E-6	1E-6	1E-6	"
K_{mNADH}	1E-7	1E-7	1E-7	"
$K_{m\frac{ATP}{ADP}}$	1	1	1	unitless
$K_{m\frac{ADP}{ATP}}$	9.5E-6	9.5E-6	9.5E-6	"
$K_{m\frac{NADH}{NAD}}$	0.0035	0.0035	0.0035	"
$K_{m\frac{NAD}{NADH}}$	0.061	0.061	0.061	"
K_{mNADPH}	1E-9	1E-9	1E-9	"
$K_{m\frac{NADP}{NADPH}}$	1E-3	1E-3	1E-3	"

Table 4.6 Maximum reaction rates and comparison of highly sensitive parameters with their intervals in control, NaBu-48h and NaBu-74h cultures

Parameter	**Value**			**t-test Results**	**Literature**
	Control	NaBu-74h	NaBu-48h		

v_{maxHK}	2.25E-4 (2.15E-4,2.35E-4)	2.89E-4 (2.59E-4,3.19E-4)	2.25E-4 (1.94E-4,2.56E-4)	p<0.1 +	10^{-4}–10^{-3} (Dash et al., 2007; Goudar et al., 2010; Lambeth & Kushmerick, 2002; Nolan & Lee, 2010; Zamorano et al., 2010)
$v_{maxfPGI}$	2E-4 (5E-5,3.5E-4)	1.8E-4 (2.8E-5,3.32E-4)	2E-4 (3.8E-5,3.62E-4)	—	‘‘
$v_{maxPFK/ALD}$	2.5E-3 (5E-5,3.5E-4)	2.64E-3 (1.91E-3,3.32E-3)	2.5E-3 (1.93E-3,3.35E-3)	—	‘‘
v_{maxPGK}	9E-4	9E-4	9E-4	—	‘‘
v_{maxPK}	1.95E-3 (1.6E-3,2.3E-3)	1.95E-3 (1.25E-4,2.65E-4)	2.19E-3 (1.58E-3,2.8E-3)	—	‘‘
$v_{maxfLDH}$	1.5E-3 (1.03E-3,1.97E-3)	8.5E-4 (5.05E-4,1.2E-3)	6.04E-4 (2.73E-4,7.29E-3)	p<0.1 *	‘‘
$v_{maxrLDH}$	7.25E-4 (1.86E-3,1.26E-3)	8.9E-4 (4.25E-4,1.53E-3)	6.04E-4 (1.03E-4,1.1E-3)	—	‘‘
$v_{\max G6PDH/PGLcDH}$	9E-4	9E-4	9E-4	—	10^{-5}-10^{-4}(Holzhutter, 2004; Lambeth & Kushmerick, 2002; Zamorano et al., 2010)
v_{maxEP}	5E-4 (4.3E-4,5.6E-4)	5E-4 (4.4E-4,5.55E-4)	5E-4 (4.5E-4,5.4E-4)	—	‘‘
$v_{\max TK/TA}$	3E-5	3E-5	3E-5	—	‘‘
v_{maxPDH}	1.6E-4 (3.42E-5,2.85E-4)	2E-4 (8.75E-5,3.1E-4)	1.12E-4 (3.04E-5,1.94E-4)	—	10^{-5}-10^{-4} (Dash et al., 2007; Nolan & Lee, 2010; Wu et al., 2007)
v_{maxCS}	2.65E-4	2.65E-4	2.65E-4	—	‘‘
$v_{\max CITS/ISOD}$	1.16E-4 (1.34E-5,2.18E-4)	2.5E-4 (1.1E-4,3.9E-4)	2.5E-4 (7E-5,4.3E-4)	—	‘‘
$v_{maxAKGDH}$	9.5E-5	9.5E-5	9.5E-5	—	‘‘
$v_{maxSCOAS}$	1.4E-4 (4.02E-5,2.4E-4)	2.75E-4 (1.3E-4,4.1E-4)	3E-4 (1E-5,5E-4)	—	‘‘
$v_{\max SDH/FUM}$	2.5E-4	2.5E-4	2.5E-4	—	‘‘
v_{maxMDH}	1.5E-4 (3.97E-5,2.58E-4)	2.5E-4 (6E-5,4E-4)	2.5E-4 (4.9E-4,4.5-4)	—	‘‘
$v_{\max SDH/FUM}$	2.5E-4	2.5E-4	2.5E-4	—	‘‘
v_{maxMDH}	1.5E-4	2.5E-4	2.5E-4	—	‘‘

Table 4.6 Maximum reaction rates and comparison of highly sensitive parameters with their intervals in control, NaBu-48h and NaBu-74h cultures (Continued)

v_{maxME}	2.5E-6	2.5E-6	2.5E-6	—	N/A
$v_{maxfGlnT}$	8.7E-5 (7.65E-5,9.75E-5)	6E-5 (4.4E-5,7.53E-5)	4E-5 (1.1E-5,6.9E-5)	p<0.1 *[+]	10^{-6}-10^{-4} (Nolan & Lee, 2010)
$v_{maxrGlnT}$	2.5E-5	2.5E-5	2.5E-5	—	‘‘
$v_{maxfGLNS}$	9.5E-5 (4.51E-5,1.36E-4)	9.5E-5 (6.01E-5,1.3E-4)	9.5E-5 (7.2E-5,1.18E-4)	—	‘‘
$v_{maxrGLNS}$	1E-4	1E-4	1E-4	—	‘‘
$v_{maxGluT}$	5E-5	5E-5	5E-5	—	‘‘
$v_{maxGLDH}$	1.8E-5 (0,2.34E-5)	1.8E-5 (0,3.36E-5)	1.8E-5 (0,4.14E-5)	—	‘‘
$v_{maxresp}$	8E-4	8E-4	8E-4		10^{-3}-10^{-5} (Dash et al., 2007)
$v_{maxATPase}$	4E-3 (3.7E-3,4.3E-3)	6E-3 (5.3E-3,6.7E-3)	6E-3 (5.4E-3,6.6E-3)	p<0.1 *[+]	‘‘
$v_{maxleak}$	4.7E-5 (5E-6,8.9E-5)	4.7E-5 (5E-6,8.9E-5)	4.7E-5 [3E-6,9.1E-5)	—	‘‘
v_{maxfCK}	2.3E-4	2.3E-4	2.3E-4	—	‘‘
v_{maxrCK}	9E-5	9E-5	9E-5	—	‘‘
v_{maxfAK}	2E-5	2E-5	2E-5	—	‘‘
v_{maxrAK}	3E-5	3E-5	3E-5	—	‘‘
$v_{maxPPRibP}$	2E-8	2E-8	2E-8	—	N/A
$v_{maxNADPHox}$	4E-5	4E-5	4E-5	—	N/A
$v_{maxgrowth}$	0.215 (0.21,0.22)	0.043 (0.35,0.56)	0.04 (0.03,0.05)	p<0.1 *[+]	N/A

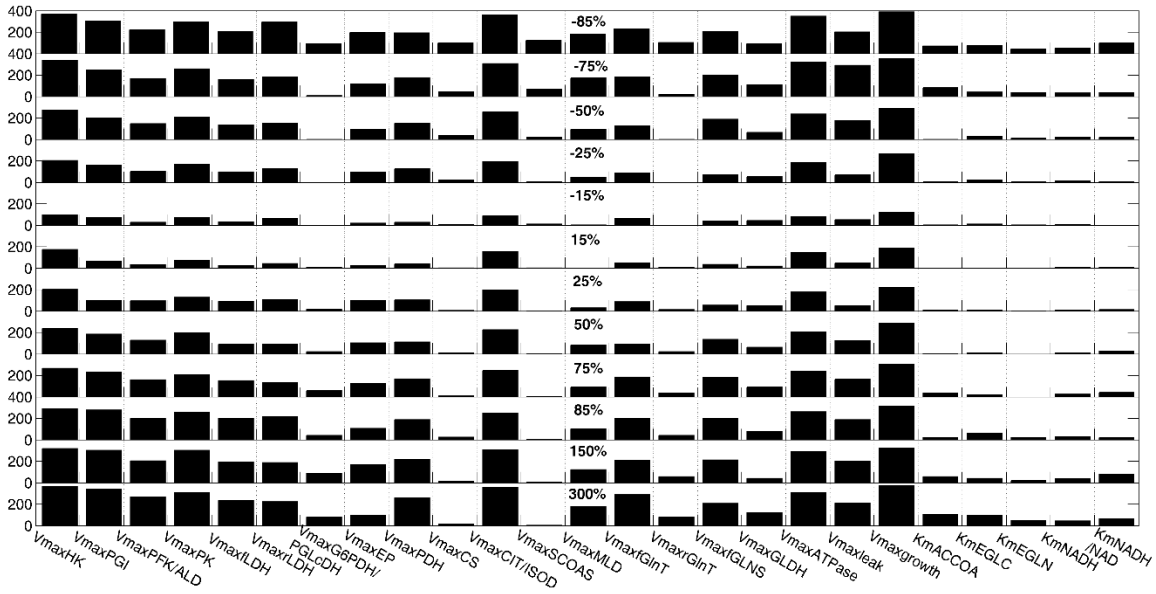

Figure 4.2Sensitivity analysis on model parameters for sodium butyrate control culture. Each column represents percentage change in the objective function (solid bars) for parameter adjustment of -85% to +300%. Parameters not shown have percentage changes that are below 5%.

4.6.2 The model simulates CHO cells behaviour in sodium butyrate stimulated cultures

Interestingly, the model simulates experimental data for CHO cells bioreactor control culture as well as for both NaBu-48h and NaBu-74h cultures (Figure 4.5). *C*ell growth is well simulated in all cultures. More importantly, the cell energetic state represented by intracellular ATP, ADP, and AMP levels, and the cell specific oxygen consumption rate (qO_2) were also all well simulated, except for the data point of qO_2 at 48h, for which we have no explanation. Model simulations for intracellular metabolites, for which no experimental data were available, are shown in supplementary material (Figure 4.11) for clarity purposes. However, we paid a rigorous attention at simulations of these non-measured intracellular metabolites, defining constraints ensuring they all agree with the very few available data in literature. Using an average cell volume of 1000 μm^3, as proposed by Li et al. (2006) (Li, Sun, & Zhang, 2006a) for CHO cells, simulated concentrations of intracellular intermediates were compared to literature (Figure 4.11). These results confirm that the model can provide a satisfactory description of cell behavior over the course of a culture, including at the metabolic level.Parameter

estimates together with their intervals (for highly sensitive ones), priorand posterior to sodium butyrate addition, are presented in Table 4.6. Weighted residuals were also verified to be both independent and normally distributed since all the points fell along a straight line as shown in the normal probability plot of the weighted residuals for the three cultures (Figure 4.4).

4.6.3 Statistical analysis on estimated parameters

In Figure 4.3, we show 95% confidence intervals for the highly sensitive parameter estimates for the three cultures, i.e. with and without sodium butyrate. In all cases, parameter estimates and model calculated 95-percent linear confidence intervals are within the reported ranges for these parameters. As clearly showed in Figure 4.3 and considering the p-values reported in Table 4.6, the effect of sodium butyrate can be described through 4 distinct parameters only, on a total of 72 considering 95% confidence interval, with some differences for a sodium butyrate addition at mid-exponential or the early plateau phases. More specifically, in the case of the NaBu-48h culture the $v_{maxfLDH}$needed to be reduced by 66% from that determined for the control culture.In the case of the NaBu-74h culture, however, v_{maxHK}required a 28% increase of the maximal rate.Butyratehas been reported to affect Lactate dehydrogenaseactivity level (De Leon et al., 2007; Yee et al., 2008). Moreover, $v_{maxfGlnT}$needed to decrease by 54 % in the NaBu-48h culture and by 31% in the NaBu-74h culture. The inhibitory effect of butyrate on glutamine transport has been previously reported (Bode & Souba, 1994). In addition, our model parameters calibration strategy resulted in a 81 % reduction of the cell $v_{maxgrowth}$from sodium butyrate addition. However, only the parameter related to ATP consumption, ($v_{maxATPase}$), lumped as ATPase pumps requirements, needed to be increased by 48 % for both NaBu-48h and the NaBu-74h cultures. Interestingly, sodium butyrate, a four-carbon short chain fatty acid, has been reported of being transported across CHO cells membrane due to the presence of monocarboxylate transporters family (Rizhaupt et al., 1998). The transport process itself may then signal transcriptional and translational events, which are accompanied by higher energy requirements which is in agreement with an increase of $v_{maxATPase}$ in this work. A similar result has been previously reported by Beauvieux et al. (1986) (Beauvieux et al., 1986) for CHO cells.

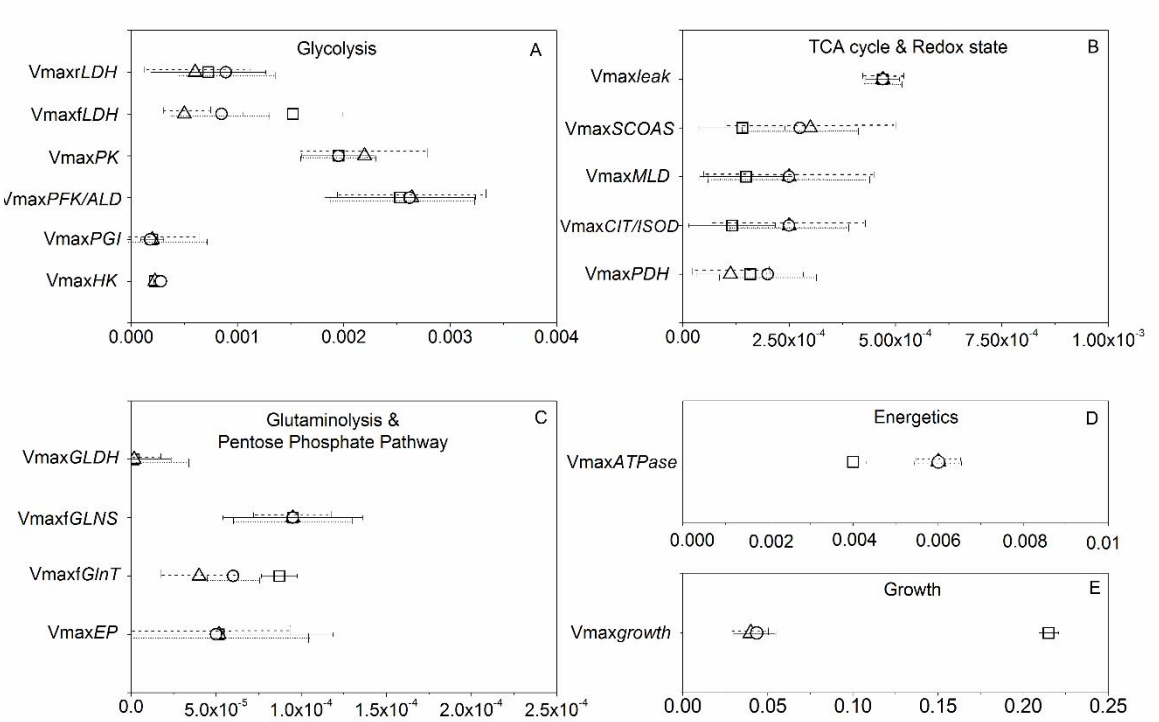

Figure 4.3Parameter estimates with their error bars for highly sensitive parameters of glycolysis (A), TCA cycle and redox state (B), glutaminolysis and pentose phosphate pathway (C), and energetic and growth (D).

Horizontal lines are 1.96 standard error bars and represent parameter estimate ±1.96 standard error. Sodium butyrate was added at 48 h (NaBu-48h : open triangles for parameter estimates and dashed line for error bars) or 74 h (NaBu-74h : open circles and dotted line for error bars). Control culture (open squares and solid line for error bars) without sodium butyrate.A parameter is considered highly sensitive if a small variation in its value (± 15%) causes more than a 10 % increase of in the objective function.

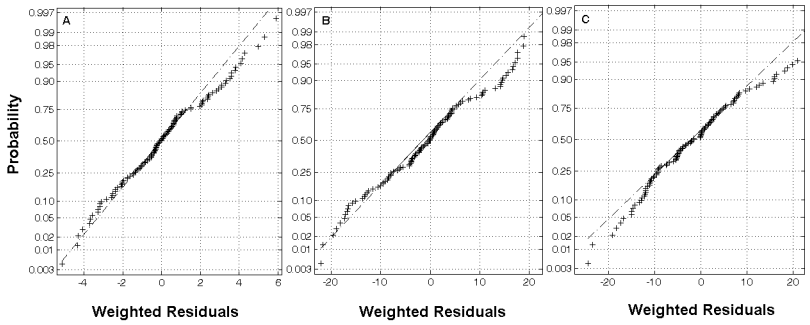

Figure 4.4Normal probability plot of the weighted residuals for Control (A), (NaBu-48h) (B) and (NaBu-74h) (C) cultures.

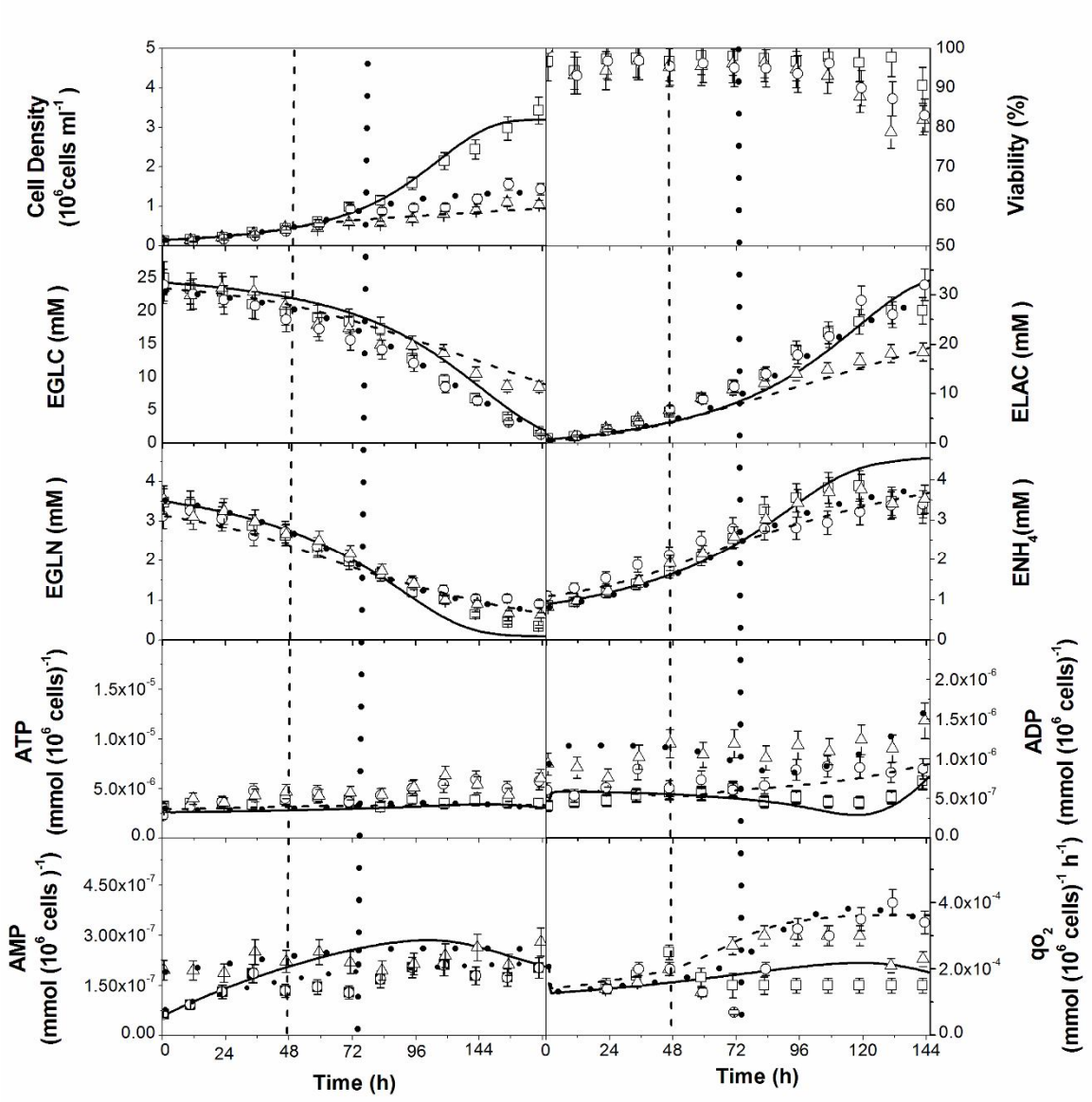

Figure 4.5Simulated and experimental data for Control and cultures with sodium butyrate addition.

Control: experimental data: open squares, simulated data: solid line. Cultures with sodium butyrate addition at 48 h (NaBu-48h): experimental data: open triangles, simulated data: dashed line) and at 74 h (NaBu-74h): experimental data: open circles, simulated data: dotted line. Experimental data are taken from a previous work(McMurray-Beaulieu et al., 2009)

4.7 Discussion

Taking all of the above, it is clear that the model structure, which is based on the cell energetic state, allows simulating CHO cells culture behaviour. Therefore, in the following, the calibrated model is used as an *in silico* platform to analyse the effect of butyrate on CHO cells metabolic network behaviour. It is important to note that all results shown in Figures 4.6 to 4.10, and discussed in this section, were obtained from model simulations. In order to statistically interpret model simulations, confidence intervals are shown together with simulations at each 24 hours and a t-statistic associated significance value was calculated in case of statistical comparison (Table 4.7).

4.7.1 Effect of sodium butyrate on CHO cells nutritional behaviour

To further study the dynamic effects of sodium butyrate on CHO cell metabolism, simulated fluxes for CHO cells nutritional state were first analysed (Figure 4.6). The culture with butyrate addition at mid-exponential growth phase (NaBu-48h) exhibits a high and stable specific glucose uptake rate, with a slight decrease from 72 h. This decrease was more pronounced in the control culture where specific glucose uptake rate was 73% less at 144 h (Figure 4.6A). Interestingly, however, the cells seem to become more efficient when butyrate is added at mid-exponential phase since the ratio of lactate production rate-to-glucose consumption rate decreases by 18% after 72 h (Figure 4.6C). The values for the ratio of lactate production rate-to-glucose consumption rate showed to be in the range previously reported in the literature (1.4 – 2.2 to 0.05 – 0.5) (Wlaschin & Hu, 2006). In contrast, butyrate addition at the early plateau phase (NaBu-74h) causes an increase of the specific glucose uptake rate from 96 h; the NaBu-74h culture shows a 22% increase of the specific glucose uptake rate at 120 h compared to control culture, which then decreases 44% below the value for 120 h. In parallel, the ratio of lactate production rate-to-glucose consumption rate stays initially constant and increases by 20% at 120 h when compared to the value for control culture. In cases of the specific glutamine uptake rate (Figure 4.6B) and the ratio of ammonia production rate-to-glutamine consumption rate (Figure 4.6D), no statistical difference can be determined among the three cultures. The ratios of ammonia production rate-to-glutamine consumption rate were also within ranges reported in literature (0.5 – 1.3 to 0.1 – 0.3) (Wlaschin & Hu, 2006). The culture with butyrate addition at mid-exponential phase thus

shows a sustained and higher metabolic activity.

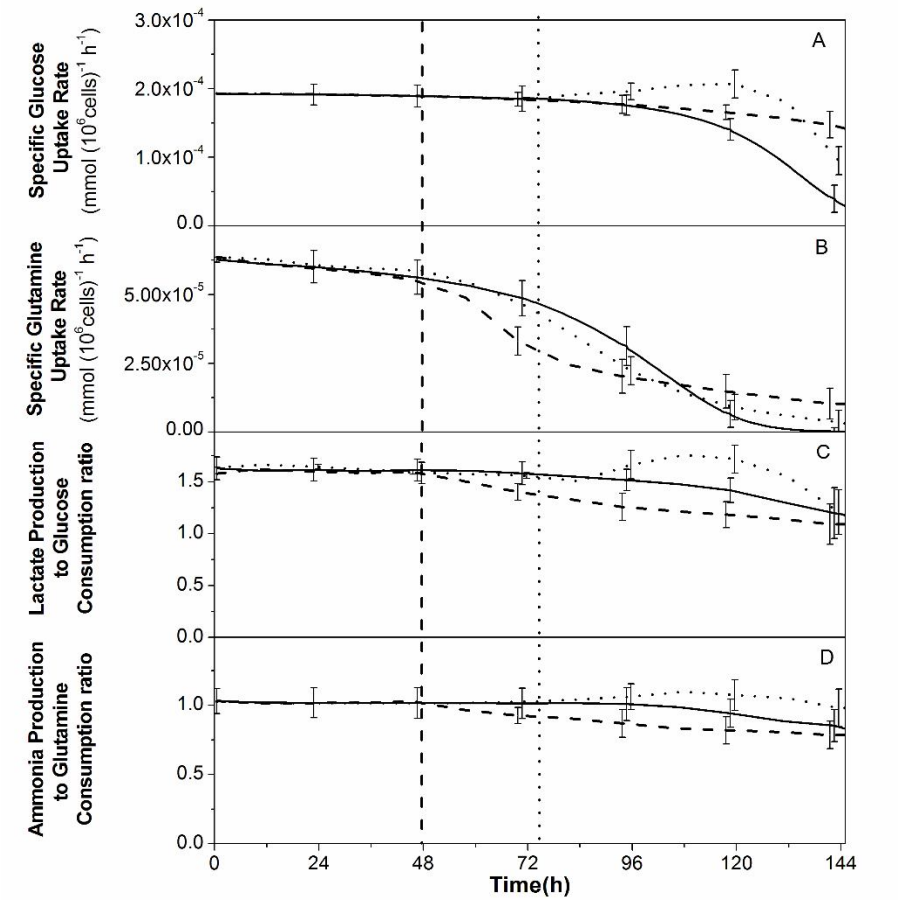

Figure 4.6Simulated time profiles of specific glucose uptake rate (A), specific glutamine uptake rate (B), lactate production-to-glucose consumption ratio (C), and ammonia production-to-glutamine consumption ratio (D), over time.
specific glucose uptake rate: *v(HK*), specific glutamine uptake rate: *vf(GlnT)-vr(GlnT*)), lactate production-to-glucose consumption ratio: *(vf(LDH)-vr(LDH))/v(HK)*, ammonia production-to-glutamine consumption ratio: (*vf(GLNS)-vr(GLNS)+v(GLDH))*/(*vf(GlnT)-vr(GlnT*)). Vertical lines indicate the time of sodium butyrate addition. 95% confidence intervals for model simulations are shown. Same conditions as Figure 4.5 applied.

4.7.2 Effect of sodium butyrate on CHO cells metabolism and energetic behaviour

4.7.2.1 G6P branch point

The glycolytic flux (Figure 4.7A) follows closely the evolution of the specific glucose uptake rate for all three cultures, where in the case of an addition at mid-exponential

phase, the model simulates a final value that is 22 % higher at 120 h compared to that for the control culture. We then looked at the major branch points within glycolysis. First, we evaluated the portion of glucose that goes to cell mass. The glucose used for the synthesis of DNA/RNA (via R5P pool) and carbohydrates (via G6P pool), and taken as going to biomass synthesis, rapidly decreases by 69 % and 64% for the NaBu-48h and the NaBu-74h at 120 h, respectively (Figure 4.7B) . The value identified for the percentage of glucose derived to biomass is consistent with the reported value in literature (hybridoma cells: 3.9 %) (Follstand et al., 2000). The percentage of glucose flowing through the pentose phosphate pathway, defined as the ratio of pentose phosphate oxidative flux to glucose uptake rate, does not show an increase when butyrate was added at mid exponential phase with a 34.5% lower value at 144 h (Figure 4.7C). Around 23.1±4 % of the glucose uptake flux enters the pentose phosphate pathway at mid-exponential phase for all cultures while a value of 41% has been reported for CHO cells (Goudar et al., 2010). The ratio of pentose phosphate reflux to glycolysis (non-oxidative) (*v(TK/TA)*) to the pentose phosphate oxidative flux (*v(G6PDH/PGLcDH)*) shows stable values in all cultures (Figure 4.7D).A simulated average ratio of 0.32±0.2 is in agreement with literature for CHO cells (0.33±0.056) (Goudar et al., 2010), hybridoma cells (0.37) (Bonarius et al., 1996) and hepatic cells (~0.3) (Maier et al., 2008) where the first and last results are based on independent measurement of intracellular fluxed using tracers. Consequently, the addition of butyrate has not modified the pentose phosphate pathway fluxes distribution, except for the NaBu-48h culture at the end of exponential phase. Therefore, since less glucose is used for biomass synthesis (Figure 4.7B), and that less lactate is produced per glucose consumed (Figure 4.6C), one can expect the glycolytic flux to pyruvate to be increased.

4.7.2.2 Pyruvate branchpoint ratio

The pyruvate branch point ratio shows a 44 % increase in the NaBu-48h culture at 120 h compared to the control culture. (Figure 4.8A) and, however, a decreasing trend when butyrate was only added at the early plateau phase. Simulation results are thus in agreement with that for the lactate-to-glucose ratio (Figure 4.6C). Although butyrate addition leads to lower values of pyruvate branch point ratio in the NaBu-74h culture, the increased glucose consumption rate simulated by the model can compensate as seen by

elevated values for the TCA flux (Figure 4.8B). Moreover, Altamirano et al. (2001) (Altamirano et al., 2001) have also reported, in CHO cell cultures, a higher metabolic efficiency in terms of higher pyruvate branch point ratios. Albeit experimental data for NADH/NAD were not available, simulated values are in agreement with a reported value of 0.05 for CHO cells in a recent study (Zhang et al., 2006). Therefore, taken together, model simulations coupled to experimental data clearly suggest that adding butyrate at mid-exponential growth phase sustains a high cell metabolic activity level favouring energy production.

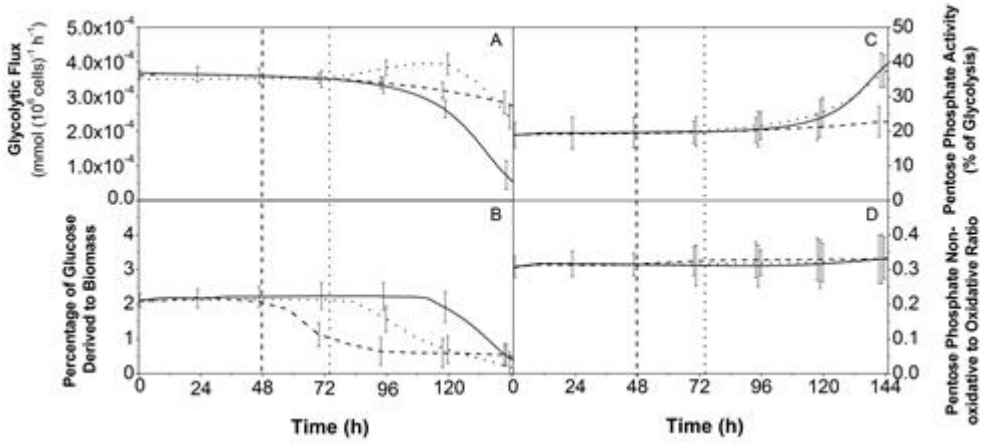

Figure 4.7Simulated time profiles of glycolytic flux (A), the percentage of glucose derived to biomass (B), pentose phosphate activity (C), and pentose phosphate non-oxidative branch activity (D).
The percentage of glucose derived to biomass is determined as the glucose contribution to biomass synthesis and calculated as the percentage of glycolytic flux toward the synthesis of biomass precursors. The pentose phosphate activity is defined as the percentage of the glycolytic flux channeled through pentose phosphate pathway, i.e. the ratio of pentose cycle oxidative flux to the glucose uptake (*v(G6PDH/PGLcDH)/v(HK)*). Pentose phosphate non-oxidative branch activity is identified as the ratio of the pentose phosphate reflux to glycolysis to the pentose phosphate oxidative flux (*v(TK/TA)/*(*v(G6PDH/PGLcDH)*). Same conditions as Figure 4.6 applied.

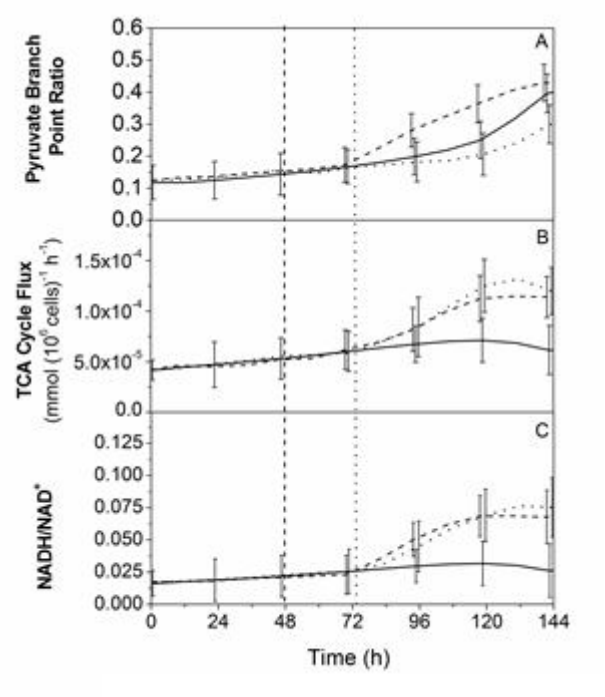

Figure 4.8Simulated values of metabolic flux distribution around pyruvate branch point, defined as the ratio of the pyruvate influx through TCA cycle to the glycolytic flux (A), TCA cycle flux (B), and cellular redox state (NADH/NAD) (C).
The ratio of the pyruvate influx through TCA cycle to the glycolytic flux: *v(PDH/v(PK)*, TCA cycle flux: *v(SCOAS)*. Same conditions as Figure 4.6 applied.

4.7.2.3 ATP production

The addition of sodium butyrate caused an increase of the specific ATP production rate, with more stable high values for the NaBu-48h culture, compared to the control and the NaBu-74h cultures (Figure 4.9A). However, the contribution of the oxidative phosphorylative respiration to ATP production is estimated to be similar for all cultures and of 59±7%, at mid exponential phase (Figure 4.9B), which is in agreement with reported values for CHO cells (Van der Valk et al., 1998). Model simulations also show a similar tendency for the ATP generation yield from glucose to increase, with time, among all cultures, with, however, higher average values (but not statistically different) in the NaBu-48h culture between 96 h and 120 h (Figure 4.9D). This may suggest a more efficient utilization of glucose (i.e. for ATP and biosynthesis reactions) induced by the addition of sodium butyrate at mid-exponential phase. As summarized in Figure 4.10, our results, both from model simulations and experimental data (McMurray-Beaulieu et al., 2009), suggest that the addition of butyrate at mid-exponential phase enhances the

stability of specific glucose (higher) (Figures 4.6A and 4.10A) and glutamine (lower) (Figures 4.6B and 4.10A) uptake rates. It also shows a lower lactate production-to-glucose consumption rate, with both forward and backward fluxes of lactate dehydrogenase decreased (Figures 4.6C and 4.10A). Higher fluxes for protonleak and oxidative phosphorylation are also simulated (Figure 4.10A),suggesting an increased specific O_2 consumption rate compared to the control culture (Figures 4.5). The increased oxidative phosphorylative respiration (i.e. qO_2) is supported by the increased pyruvate branch point ratio (Figure 4.8A), TCA cycle activity (Figures 4.8B and 4.10A) and NADH-to-NAD ratio (Figure 4.8C). In the case of pyruvate branch point ratio, the glycolytic flux to pyruvate, as well as the pyruvate influx to TCA cycle, were also increased (Figure 4.10A). This was not the case for Na-Bu 74h asboth forward and backward fluxes of lactate dehydrogenase increased simultaneously (Figure 4.10B).The model simulated higher pentose phosphate pathway fluxes (Figure 4.10A) although related ratios remained the same (Figure 4.7C and 4.7D). The cells that are stimulated by sodium butyrate at mid-exponential phase may thus stabilize their glucose uptake per cell per unit of time. ATP is then being produced at a higher rate per cell as supported by qO_2 experimental data (Figure 4.5). Finally, although a high energetic state is thought to coincide to a higher global metabolic activity, it was not possible, in this work, to establish a statistically significant correlation between the cell energetic state and its productivity level in recombinant t-PA, probably due to the low productivity level of the cell line under study.

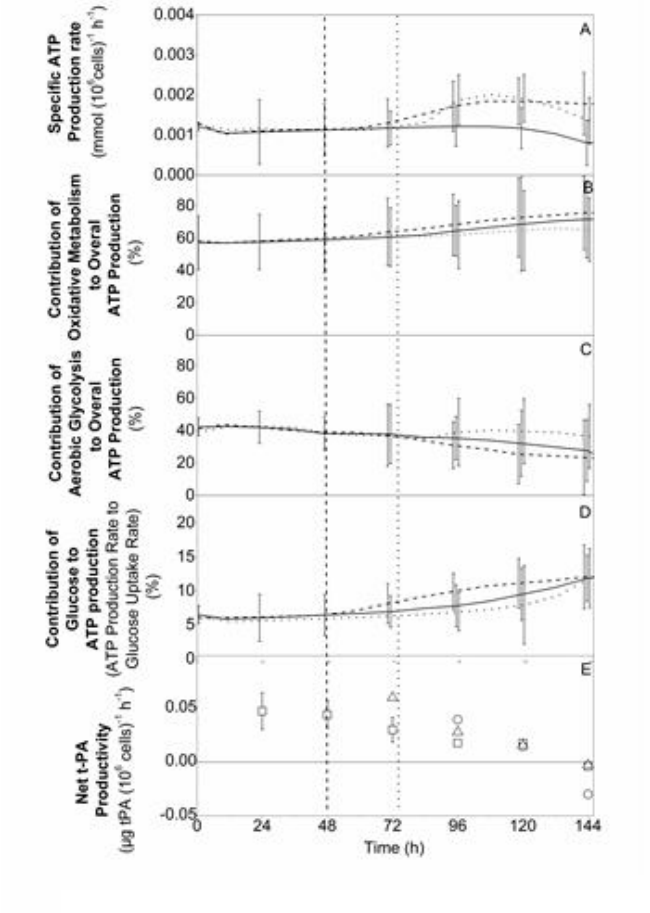

Figure 4.9Simulation of CHO cell energetic state. ATP turnover rate (A), contribution of oxidative metabolism to overall ATP production (B), contribution of aerobic glycolysis to overall ATP production (C), contribution of glucose to total ATP production (D), and the net specific productivity in recombinant t-PA observed experimentally (E), over time. ATP turnover rate is defined as $v(PGK)+v(PK)+v(SCOAS)+vr(GlnT)+vf(CK)+vr(AK)+2P/O\ ratio*v(resp)$. The contribution of oxidative metabolism to overall ATP production is defined as the portion of ATP generated from oxidative metabolism divided by the total ATP production rate ($2P/O\ ratio\ *v(resp)/(v(PGK)+v(PK)+v(SCOAS)+\ vr(GlnT)+\ vf(CK)+vr(AK)+2P/O\ ratio*v(resp)$). The contribution of glucose to ATP production is defined as the molar ratio of ATP production rate ($v(HK)/(v(PGK)+v(PK)+v(SCOAS)+vr(GlnT)+vf(CK)+vr(AK)+2P/O\ ratio*v(resp)$) over glucose uptake rate. The contribution of glycolysis was determined as the sum of glycolytic fluxes producing ATP over the total ATP production rate ($(v(PGK)+v(PK))/(\ v(PGK)+v(PK)+v(SCOAS)+\ vr(GlnT)+\ vf(CK)+vr(AK)+2P/O\ ratio*v(resp)$).Values for net specific t-PA productivity were obtained from experimental data published in a previous work (McMurray-Beaulieu et al., 2009). Control (opensquares), NaBu-48h (open triangles), and NaBu-74h (open circles). Same conditions as Figure 4.6 applied for (A-D).

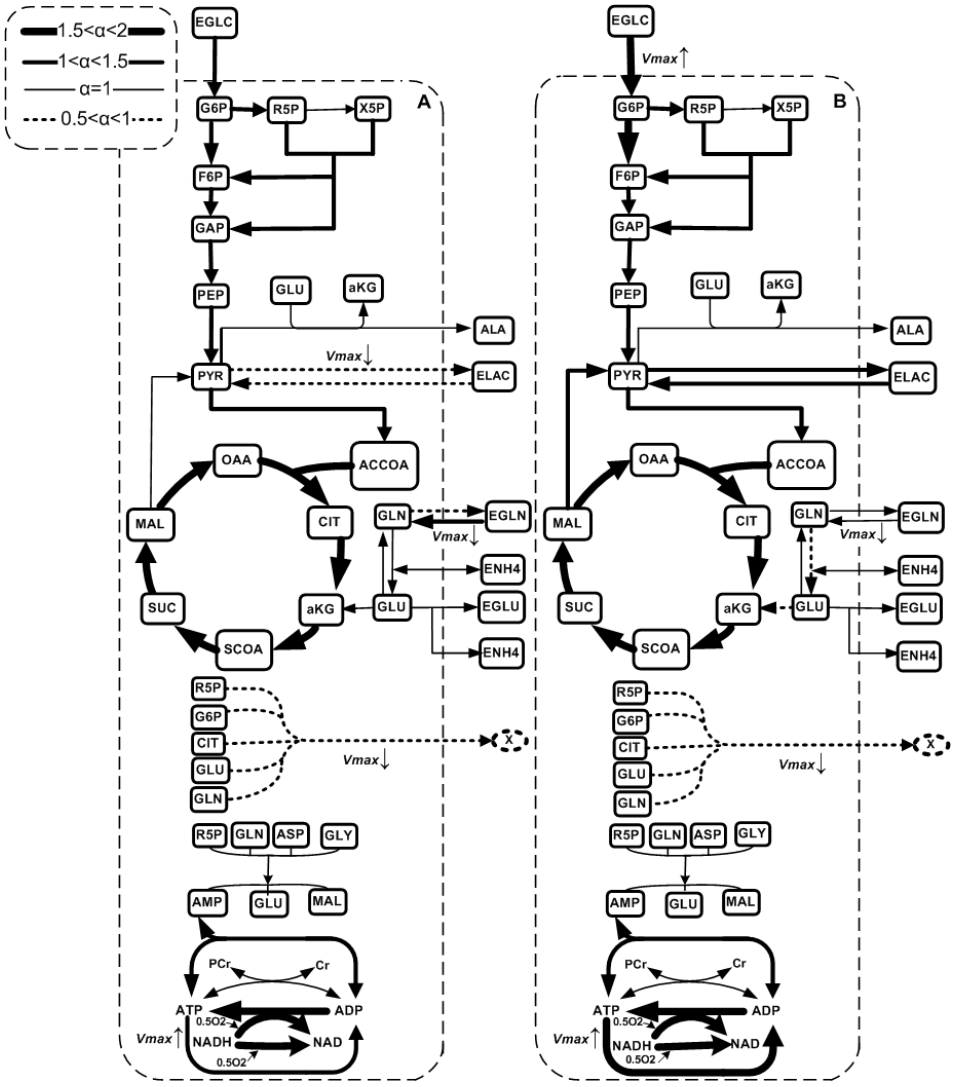

Figure 4.10Comparison of metabolic flux maps for CHO cells NaBu-48h culture (A) and NaBu-74h culture (B) from model simulations at 120 h.
α is defined as the ratio of specific flux (mmol $(10^6 cells)^{-1}$ h^{-1}) in either NaBu-48h or NaBu-74h cultures to that in the control culture. α is considered statistically different when $p<0.05$.

4.8 Conclusion

A model simulating CHO cells metabolic behaviour and describing metabolic network fluxes kinetics, as well as the cell redox and energetic states, has been proposed and calibrated. Simulation results were shown to satisfactorily describe experimental data and to agree with literature data.Moreover, the proposed model proved to be useful to describe the effect of sodium butyrate on CHO cells, with limited model adaptation requirements (i.e. the changing of only few parameters values) that are in agreement with gene expression modifications reported in literature. The model was also used to analyse the effect of butyrate at the metabolic network level, and the previous observations by McMurray et al. (2009) of a sustained high metabolic activity following butyrate addition was further confirmed from model simulations with higher glucose flux and TCA activity, and high cell redox (NADH-to-NAD^+ ratio), while energetic states (specific ATP turnover rate) did not significantly change. Finally, albeit the model structure includes a high number of parameters, it showed to describe not only all in-line and off-line experimental data, but most of the metabolic changes simulated following sodium butyrate addition showed statistical significance. Finally, most of the sensitive parameters were also estimated with relatively narrow confidence intervals. However, in a future work, it would be of interest to have access to extended experimental datasets of intracellular metabolites for a high producer cell line, conditions enhancing model parameters identification. From our results, it thus seems conceivable that our model can be readily calibrated on different industrial CHO cell lines. It can then be used as an *in silico* platform for characterizing the cell lines as well as to search for "optimal" culture management by rational adjustment of the main nutrient concentrations playing on glucose and/or glutamine concentration with time. However, much work remains to be done, anchoring the model onto larger datasets including both extra- and intracellular experimental data in order to test and validate the platform as a predictive tool.

4.9 Acknowledgements

This project was funded by the MabNet Research Network of the Natural Sciences and Engineering Research Council of Canada (NSERC) (MJ), and by an NSERC Discovery grants to MJ and OH.

4.10 References

Ahn, W. S., & Antoniewicz, M. R. (2011). Metabolic flux analysis of CHO cells at growth and non-growth phases using isotopic tracers and mass spectrometry. *Metabolic Engineering*, 13(5), 598-609.

Altamirano, C., Illanes, A., Casablancas, A., Gamez, X., Cairo, J. J., & Godia, C. (2001). Analysis of CHO cells metabolic redistribution in a glutamate-based defined medium in continuous culture. *Biotechnology Progress*, 17(6), 1032-1041.

Beauvieux, M. C., Tissier, P., Gin, H., Canioni, P., & Gallis, J. L. (1986). Butyrate impairs energy metabolism in isolated perfused liver of fed rats. *Journal of nutrition*, 131(7), 1986-1992.

Birch, J. R., & Racher, A. J. (2006). Antibody production. *Advanced Drug Delivery Reviews*, 58(5-6), 671–685.

Bode, B. P., & Souba, W. W. (1994). Modulation of cellular proliferation alters glutamine transport and metabolism in human hepatoma cells. *Annals of Surgery* 220(4), 411-424.

Bohnensack, R. (1981). Control of energy transformation of mitochondria: Analysis by aquantitative model. *Biochimica et Biophysica Acta (BBA) -Bioenergetics*, 634, 203-218.

Bonarius, H. P., Hatzimanikatis, V., Meesters, K. P., de Gooijer, C. D., Schmid, G., & Tramper, J. (1996). Metabolic flux analysis of hybridoma cells in different culture media using mass balances. *Biotechnology and Bioengineering*, 50(3), 299-318.

Cacciatore, J. J., Chasin, L. A., & Leonard, E. F. (2010). Gene amplification and vector engineering to achieve rapid and high-level therapeutic protein production using the Dhfr-based CHO cell selection system. *Biotechnology Advances*, 28(6), 673–681.

Chassagnole, C., Noisommit-Rizzi, N., Schmid, J., Mauch, K., & Reuss, M. (2002). Dynamic modeling of the central carbon metabolism of Escherichia coli. *Biotechnology and Bioengineering*, 79(1), 53-73.

Cloutier, M., Bouchard-Marchand, E., Perrier, M., & Jolicoeur, M. (2008). A predictive nutritional model for plant cells and hairy roots. *Biotechnology and Bioengineering*, 99(1), 189-200.

Cloutier, M., Perrier, M., & Jolicoeur, M. (2007). Dynamic flux cartography of hairy roots primary metabolism. *Phytochemistry*, 68(16-18), 2393-2404.

Dash, R. K., DiBella, J. A., & Cabrera, M. E. (2007). A computational model of skeletal muscle metabolism linking cellular adaptations induced by altered loading states to metabolic responses during exercise. *BioMedical Engineering OnLine*, 6, 14.

De Leon, G. M., Wlaschin, K. F., Nissom, P. M., Yap, M., & Hu, W. S. (2007). Comparative transcriptional analysis of mouse hybridoma and recombinant Chinese hamster ovary cells undergoing butyrate treatment. *Journal of Bioscience and Bioengineering*, 103(1), 82–91.

Elliott, S., Chang, D., Delorme, E., Dunn, C., Egrie, J., Giffin, J., . Hesterberg, L. (2004). Structural requirements for additional N-linked carbohydrate on recombinant human erythropoietin. *Journal of Biological Chemistry*, 279(16), 16854–16862.

Elliott, S., Egrie, J., Browne, J., Lorenzini, T., Busse, L., Rogers, N., & Ponting, I. (2004). Control of rHuEPO biological activity: The role of carbohydrate. *Experimental Hematology*, 32(12), 1146–1155.

Elliott, S., Lorenzini, T., Asher, S., Aoki, K., Brankow, D., Buck, L., . . . Egrie, J. (2003). Enhancement of therapeutic protein in vivo activities through glycoengineering. *Nature Biotechnology*, 21(4), 414–421.

Follstand, B. D., Balcarcel, R. R., Stephanopoulos, G., & Wang, D. I. (2000). Metabolic flux analysis of hybridoma continuous culture steady state mutiplicity. *Biotechnology and Bioengineering*, 63(6), 675-683.

Fussenegger, M., Schlatter, S., Datwyler, D., Mazur, X., & Bailey, J. E. (1998). Controlled proliferation by multigene metabolic engineering enhances the productivity of Chinese hamster ovary cells. *Nature Biotechnology*, 16(5), 468–472.

Galbraith, D. J., Tait, A. S., Racher, A. J., Birch, J. R., & James, D. C. (2006). Control of Culture Environment for Improved Polyethylenimine-Mediated Transient Production of Recombinant Monoclonal Antibodies by CHO Cells. *Biotechnology Progress*, 22(3), 753–762.

Garfinkel, D. (1971a). Simulation of the Krebs cycle and closely related metabolism in perfused rat liver.I.Construction of a model. *Computers and Biomedical Research*, 4(1), 1-17.

Garfinkel, D. (1971B). Simulation of the Krebs cycle and closely related metabolism in perfused rat liver. II. Properties of the model. *Computers and Biomedical Research*, 4(1), 18-42.

Goudar, C., Biener, R., Boisart, C., Heidemann, R., Piret, J., de Graaf, A., & Konstantinov, K. (2010). Metabolic flux analysis of CHO cells inperfusion culture by metabolite balancing and 2D [13C,1H] Cosy NMR spectroscopy. *Metabolic Engineering*, 12(2), 138-149.

Hendrick, V., Winnepenninckx, P., Abdelkafi, C., Vandeputte, O., Cherlet, M., Marique, T., Werenne, J. (2001). Increased productivity of recombinant tissular plasminogen activator (t-PA) by butyrate and shift of temperature: a cell cycle phases analysis. *Cytotechnology*, 36(1), 71-83.

Holzhutter, H. G. (2004). The principle of flux minimization and its application to estimate stationary fluxes in metabolic networks. *Europian Journal of Biochemistry*, 271(14), 2905–2922.

Jenkins, N. (2007). Modifications of therapeutic proteins: challenges and prospects. *Cytotechnology*, 53(1-3), 121-125.

Jolicoeur, M., Chavarie, C., Carreau, P. J., & Archambault, J. (1992). Development of a helical-ribbon impeller bioreactor for high-density plant cell suspension culture. *Biotechnology and Bioengineering*, 39(5), 511-521.

Kauffman, L. G., Pajerowski, J. D., Jamshidi, N., Palsson, B. O., & Edwards, J. S. (2002). Description and Analysis of Metabolic Connectivity and Dynamics in the Human Red Blood Cell. *Biophysical Journal*, 83(2), 646–662.

Kim, N. S., & Lee, G. M. (2001). Overexpression of bcl-2 inhibits sodium butyrate-induced apoptosis in Chinese hamster ovary cells resulting in enhanced humanized antibody production. *Biotechnology and Bioengineering*, 71(3), 184–193

Korzeniewski, B. (1991). An extended dynamic model of oxidative phosphorylation. *Biochimica et Biophysica Acta*, 1060(2), 210-223.

Kumar, N., Gammell, P., & Clynes, M. (2007). Proliferation control strategies to improve productivity and survival during CHO based production culture. *Cytotechnology,* 53(1-3), 33-46.

Lambeth, M. J., & Kushmerick, M. J. (2002). A computational model for glycogenolysis in skeletal muscle. *Annals of Biomedical Engineering*, 30(6), 808–827.

Leduc, M., Tikhomiroff, C., Cloutier, M., Perrier, M., & Jolicoeur, M. (2006). Development of a kinetic metabolic model: application to Catharanthus roseus hairy root. *Bioprocess and Biosystems Engineering*, 28(5), 295-313.

Lee, S. K., & Lee, G. M. (2003). Development of apoptosis resistant dihydrofolate reductase-deficient Chinese hamster ovary cell line. *Biotechnology and Bioengineering*, 82(7), 872–876.

Li, J. H., Sun, X. M., & Zhang, Y. X. (2006a). Improvement of hepatitis B surface antigen expression by dimethyl sulfoxide in the culture of recombinant Chinese hamster ovary cells. *Process Biochemistry*, 41(2), 317–322.

Maier, K., Hofmann, U., Reuss, M., & Mauch, K. (2008). Identification of metabolic fluxes in hepatic cells from transient 13C-labeling experiments: Part II. Flux estimation. *Biotechnology and Bioengineering*, 100(2), 355-370.

Martens, D. E. (2007). Metabolic Flux Analysis of Mammalian Cells. In M. Al-Rubeai & M. Fussenegger (Eds.), *Systems Biology*, 5, 275-299.

McMurray-Beaulieu, V., Hisiger, S., Durand, C., Perrier, M., & Jolicoeur, M. (2009). Na-butyrate sustains energetic states of metabolism and t-PA productivity of CHO cells. *Journal of Bioscience and Bioengineering*, 108(2), 160-167.

Nolan, R. P., & Lee, K. (2010). Dynamic model of CHO cell metabolism. *Metabolic Engineering,* 13(1), 108-124.

Palermo, D. P., DeGruf, M. E., Marotti, K. R., Rehberg, E., & Post, L. E. (1992). Production of analytical quantities of recombinant proteins in Chinese hamster ovary cells using sodium butyrate to elevate gene expression. *Journal of Biotechnology*, 19(1), 35-48.

Quek, L. E., Dietmair, S., Kromer, J. O., & Nielsen, J. (2010). Metabolic flux analysis in mammalian cell culture. *Metabolic Engineering*, 12(2), 161-171.

Rizhaupt, A., Ellis, A., Hosie, K. B., & P Shirazi-Beechey, S. (1998). The characterization of butyrate transport across pig and human colonic luminal membrane. *Journal of Physiology*, 507(Pt 3), 819-830.

Ryll, T., & Wagner, R. (1991). Improved ion-pair high-performance liquid chromatographic method for the quantification of a wide variety of nucleotides and sugar nucleotides in animal cells. *Journal of Chromatography*, 570(1), 77–88.

Sunstrom, N. S., Gay, R. D., Wong, D. C., Kitchen, N. A., Deboer, L., & Gray, P. P. (2000). Insulin-Like Growth Factor-I and Transferrin Mediate Growth and Survival of Chinese Hamster Ovary Cells. *Biotechnology Progress*, 16, 698-702.

Van der Valk, P., Gille, J. J. P., van der Plas, L. H. W., Jongkind, J. F., Verkerk, A., Konings, A. W. T., & Joenje, H. (1998). Characterization of oxygen-tolerant Chinese hamster ovary cells: II. Energy metabolism and antioxidant status. *Free Radical Biology and Medicine*, 4(6), 345-356.

Wlaschin, K., & Hu, W.-S. (2006). Fedbatch Culture and Dynamic Nutrient Feeding. In W.-S. Hu (Ed.), *Cell Culture Engineering*, 101 (43-74

Wu, F., Yang, F., Vinnakota, K. C., & Beard, D. A. (2007). Computer Modeling of Mitochondrial Tricarboxylic Acid Cycle, Oxidative Phosphorylation, Metabolite Transport, and Electrophysiology. *Journal of Biological Chemistry*, 282(34), 24525–24537.

Wurm, F. M. (2004). Production of recombinant protein therapeutics in cultivated mammalian cells. *Nature Biotechnology*, 22(11), 1393-1398.

Yee, J. C., De Leon, G. M., Philp, R. J., Yap, M., & Hu, W. S. (2008). Genomic and proteome exploration of CHO and hybridoma cells under sodium butyrate treatment. *Biotechnology and Bioengineering*, 99(5), 1186-1204.

Zamorano, F., Wouwer, A. V., & Bastin, G. (2010). A detailed metabolic flux analysis of an underdetermined network of CHO cells. *Journal of Biotechnology*, 150(4), 497-508.

Zhang, F., Sun, X., Yi, X., & Zhang, Y. (2006). Metabolic characteristics of recombinant Chinese hamster ovary cells expressing glutamine synthetase in presence and absence of glutamine. *Cytotechnology*, 51(1), 21-28.

Table 4.7(Supplementary) Metabolic fluxes and ratios with their intervals in Control, NaBu-48h and NaBu-74h cultures at 120 h. Same conditions as Table 4.6 applied.

Metabolic Flux/Ratio	Control	NaBu-48h	NaBu-74h	t- test Result
	Value Interval	Value Interval	Value Interval	
Glucose uptake rate ***mmol (10^6 cells)$^{-1}h^{-1}$***	1.4E-4 (1.26E-4,1.57E-4)	1.66E-4 (1.59E-4,1.72E-4)	2.07E-4 (1.87E-4,2.27E-4)	p<0.1 * +
Lactate production - to -glucose Consumption	1.44 (1.3,1.54)	1.18 (1.06,1.31)	1.72 (1.58,1.86)	p<0.1 * +
Glutamine uptake rate ***mmol (10^6 cells)$^{-1}h^{-1}$***	6.6E-6 (1.76E-6,1.05E-5)	1.48E-5 (8.7E-6,2.09E-5)	9.03E-6 (4.33E-6,1.75E-5)	—
Ammonia production - to - glutamine consumption	0.94 (0.84,1.04)	0.81 (0.72,0.91)	1.07 (0.96,1.19)	—
Glycolytic flux ***mmol (106 cells)-1h-1***	2.6E-4 (2.4E-4,2.95E-4)	3.18E-4 (2.97E-4,3.41E-4)	3.94E-4 (3.65E-4,4.24E-4)	p<0.1 * +
Percentage of glucose derived to biomass	1.93 (1.55,2.31)	0.59 (0.19,1)	0.68 (0.3,1.08)	p<0.1 * +
Pentose phosphate activity ***(% of glycolysis)***	23.14 (19.2,27.1)	21.2 (17.4,25)	25.39 (21.1,29.7)	—
Pentose phosphate non oxidatie - to - oxidative ratio	0.31 (0.24,0.38)	0.31 (0.26,0.39)]	0.32 (0.27,0.37)	—
Pyruvate branch point ratio	0.25 (0.19,0.3)	0.36 (0.31,0.42)	0.2 (0.14,0.27)	p<0.1 *
TCA flux ***mmol (10^6 cells)$^{-1}h^{-1}$***	7.1E-5 (4.9E-5,9.3E-5)	1.12E-4 (8.9E-5,1.3E-4)	1.25E-4 (0.943E-5,1.5E-4)	p<0.1 +
NADH/NAD	0.031 (0.014,0.049)	0.068 (0.052,0.084)	0.069 (0.048,0.089)	p<0.1 * +
Specific ATP production rate ***mmol (10^6 cells)$^{-1}h^{-1}$***	1.1E-3 (6.6E-4,1.7E-3)	1.8E-3 (1.2E-3,2.4E-3)	1.9E-3 (1.3E-3,2.5E-3)	—

Table 4.7 (Supplementary) Metabolic fluxes and ratios in Control, NaBu-48h and NaBu-74h cultures at 144 h (Continued).

Metabolic Flux/Ratio	Control	NaBu-48h	NaBu-74h	t- test Result
	Value Interval	Value Interval	Value Interval	
Glucose uptake rate ***mmol (10^6 cells)$^{-1}h^{-1}$***	3.97E-5 (2E-5,5.94E-5)	1.48E-4 (1.28E-4,1.67E-4)	9.51E-5 (7.46E-5,1.16E-4)	p<0.1 * $^{+}$
Lactate production - to -glucose consumption	1.19 (0.95,1.44)	1.09 (0.89,1.29)	1.2 (0.99,1.42)	p<0.1 * $^{+}$
Glutamine uptake rate ***mmol (10^6 cells)$^{-1}h^{-1}$***	2.8E-7 (0,1.62E-6)	1.03E-5 (4.67E-6,1.59E-5)	3.64E-6 (0,7.92E-6)	—
Ammonia production - to - glutamine consumption	0.853 (0.73,0.96)	0.785 (0.68,0.88)	0.98 (0.84,1.12)	—
Glycolytic flux ***mmol (106 cells)-1h-1***	1.09E-4 (5.78E-5,1.6E-4)	2.83E-4 (2.5E-4,3.15E-4)	2.4E-4 (2.09E-4,2.71E-4)	p<0.1 * $^{+}$
Percentage of glucose derived to biomass	0.47 (0.16,0.78)	0.54 (0.23,0.85)	0.2 (0.07,0.61)	p<0.1 * $^{+}$
Pentose phosphate activity ***(% of glycolysis)***	34.74 (30.7,38.8)	22.76 (18.4,27.2)	37.38 (32.7,42)	—
Pentose phosphate ***non oxidatie - to - oxidative ratio***	0.33 (0.26,0.4)	0.33 (0.26,0.4)	0.33 (0.27,0.39)	—
Pyruvate branch point ratio	0.39 (0.33,0.45)	0.42 (0.37,0.48)	0.42 (0.24,0.4)	p<0.1 *
TCA flux ***mmol (10^6 cells)$^{-1}h^{-1}$***	6.16E-5 (3.7E-5,8.5E-5)	1.14E-4 (9.3E-5,1.3E-4)	1.2E-4 (9.6E-5,1.4E-4)	p<0.1 $^{+}$
NADH/NAD	0.026 (0.06,0.046)	0.067 (0.047,0.088)	0.075 (0.052,0.098)	p<0.1 * $^{+}$
Specific ATP production rate ***mmol (10^6 cells)$^{-1}h^{-1}$***	8.8E-4 (2.4E-4,1.3E-4)	1.78E-3 (1E-3,2.5E-3)	1.36E-3 (7.8E-4,1.9E-3)	—

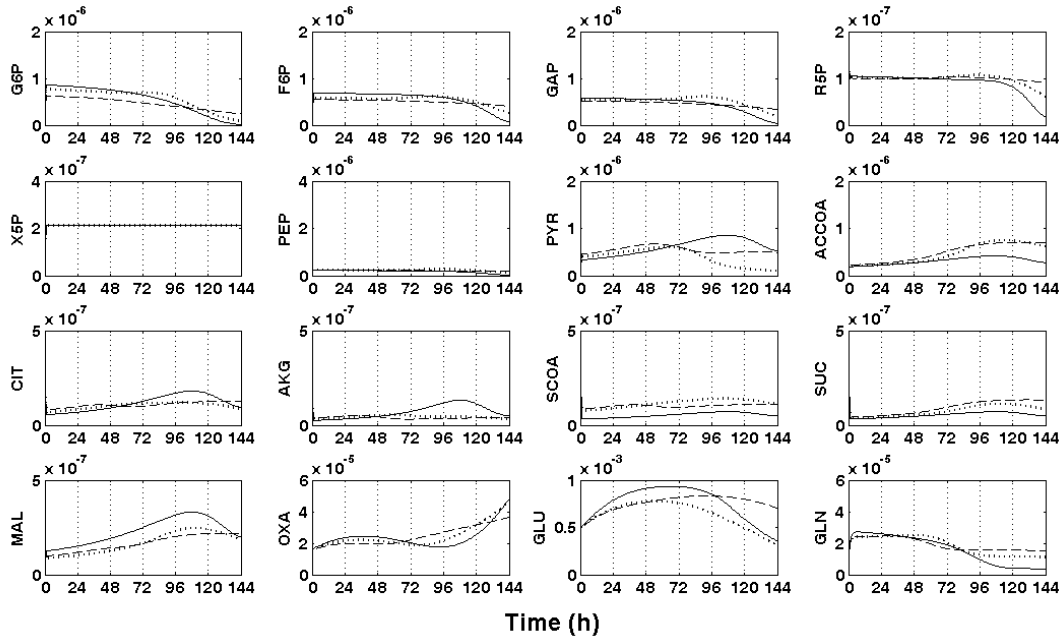

Figure 4.11 (Supplementary)Simulated data of intracellular metabolites for Control, and cultures with sodium butyrate addition at 48 h (NaBu-48h) and at 74 h (NaBu-74h). Control: solid line, NaBu-48 h: dashed line, NaBu-74h: dotted line.
Axis units are mmol $(10^6$ cells$)^{-1}$. Simulated values of intracellular concentrations showed to be within the range found in literature for TCA cycle intermediates (10^{-7}-10^{-6} mmol $(10^6$ cells$)^{-1}$) (Lu et al., 2003; F. Zhang et al., 2006), intracellular sugar phosphates (10^{-7}-10^{-6} mmol $(10^6$cells$)^{-1}$) (CHO cells: (Sellick et al., 2009); Hepatic cells: (Maier et al., 2007); MDCK cells: (Ritter, Wahl, S., Genzel, & Reichl, 2010), intracellular glutamine (10^{-7}-10^{-6} mmol $(10^6$ cells$)^{-1}$) and glutamate (10^{-6}-10^{-5} mmol $(10^6$ cells$)^{-1}$) (CHO cells: (Kontoravdi et al., 2007; Lu, Sun, & Zhang, 2005); HEK-293 cells: (Kontoravdi et al., 2007).

CHAPTER 5 METABOLOMICS AND IN-SILICO ANALYSIS OF MONOCLONAL ANTIBODY- PRODUCING CHO CELL CLONES

Atefeh Ghorbaniaghdam[1,], Jingkui Chen[1,2], Olivier Henry[2], Mario Jolicoeur[1,2*]

[1]Canada Research Chair in Applied Metabolic Engineering,

[2]Department of Chemical Engineering, École Polytechnique de Montréal,

P.O. box 6079, Centre-ville Station, Montréal, Québec, H3C 3A7, Canada

*Corresponding author: mario.jolicoeur@polymtl.ca

(Submittend to the PLOS Computational Biology Journal)

5.1 Presentation of the article

The kinetic modelling approach for cell metabolism has proven efficient to study CHO cell cultures.Due to the rather high number of parameters it was of great interest to challenge model adaptability to other CHO cell lines and its engineered clones. Towards this end, the model was further developed to describe another CHO cell line. Previous estimates for most of the parameter values were remained unchanged using results from our previous work. Model simulations were then used to quantify the main intracellular fluxes and ratios in clonal derivatives. Comparison of experimental data completed by model simulations then shed light to metabolic changes associated with clonal variations and onset of protein expression.

5.2 Abstract

Monoclonal antibodyproducingChinese hamster ovarycells have been shown to undergo metabolic changes whenengineered to produce high titers of recombinant proteins. Inthis work, we have studied the distinct metabolism of Chinese hamster ovary cell clones harboring an efficient inducible expression system, based on the cumate gene switch, and displaying different expression levels, high and low productivities, compared to that of the parental cells from which they were derived. A kinetic model for Chinese hamster ovary cell metabolismwas further developed*to* includemetabolic regulation. Model calibration was performed using intracellular and extracellular metabolite profiles obtained from shake flask batch cultures. Model simulations of intracellular fluxes and ratios known as biomarkers revealed significant changes correlated with clonal variation but not to the recombinant protein expression level. Metabolic flux distribution mostly differs in the reactions involving pyruvate metabolism, with an increased net flux of pyruvate into the tricarboxylic acid cycle in the high-producer clone, either being induced or non-induced with cumate. More specifically, Chinese hamster ovary cell metabolism in this clone was characterized by an efficient utilization of glucose and a high pyruvate dehydrogenase flux. Moreover, the high-producer clone shows a high rate of anaplerosis from pyruvate to oxaloacetate, through pyruvate carboxylase and from glutamate to α-ketoglutarate, through glutamate dehydrogenase, and a reduced rate of cataplerosis from malate to pyruvate, through malic enzyme. Indeed, the increase of flux through pyruvate carboxylase was not driven by an increased anabolic demand. It is in fact linked to an increase of the TCA cycle global flux, which allows better regulation of higher redox and more efficient metabolic states.

5.3 Author Summary

Therapeutics of the future are now mostly produced by animal cells, such as from the Chinese Hamster Ovary cell (CHO) platform, cultured in bioreactors. Although this mammalian cell platform can produce recombinant proteins at the gram-per-liter level, there are still significant pitfalls in the generation and selection processes of stable high-producing cell lines. In this work, we specifically address these problems by the development of an *in-silico* simulation plarform enabling to deeply characterize the effect of recombinant protein productionon a cell line metabolic behaviour. Thus, in order to

establish the in-silico platform reliability, we first performed cultures for two different clones of a parental CHO cell line and the experimental data accounting for a wide diversity of metaboliteswere used to further develop and challenge a metabolic model that is mathematically describing cell metabolism with time. Using our model, we were then able to identify changes in the metabolic fingerprint associated with clonal variation and the onset of recombinant protein production. In particular, we were able to predict the up-regulation in the tricarboxylic acid cycle. Importantly, changes observed were not directly linked to recombinant protein production. This kind of *in-silico* platform thus tends to show being useful to the cell line selection process as well as ultimately as to identify target for cell engineering works.

5.4 Introduction

Monoclonal antibodies (mAbs) are among the largest segment of today's therapeuticproteinsmarket, with a 21% annual increase rate in launching into clinical trial (Pavlou & Belsey, 2005). However, a low FDA approval success rate has been reported for mAbs.Indeed, although CHO cells is now the major cell line used industrially with culture and production protocols that have been largely optimized (Durocher & Butler, 2009), mAbs production at high quantities and of high quality, e.g. with defined glycosylation profile, still has to be achieved. Among many factors affecting mAbs quality, the stability with time of high producing level CHO cell clones with enhanced endogenous pathways (e.gendogenous *CHO* GS gene) (Bebbington et al., 1992), and presenting a prolonged cell viability level due to the over-expression of some cytoplasmic proteins(e.g. chaperones such as Hsp70 and Hsp27)is highly critical(Lee et al., 2009). Moreover, media composition and culture conditions, as well as their management along with culture duration, have to be optimized to achieve not only the objective of desired cell productivity and viability but also mAbs quality specifications (Bi, Shuttleworth, & Al-Rubeai, 2004). Ultimately and within this context, efficient process control strategies, fed through on-line and off-line analyses, may allow seeking and maintaining desired optimal conditions with time. However, due to the large number of variables and decision steps associated with the development and the identification of a stable high-producer cell line, it is a highly challengingand time consuming process (Eppink et al., 2009; Shukla et al., 2007). Indeed, high-throughput

screening approaches are normally used for clone selection, but there is a risk of performance discrepancy during scaled-up and manufacturing (Li et al., 2010). Therefore, only a knowledge-based strategy capable to detect at each step desired and undesired cell traits, as well as to extrapolate its behavior at the process scale, can efficiently guide and accelerate cell line screening works. Indeed, such level of knowledge has thus to be based on an adequate description of cell behaviour in a managed environment.In that context, various "omic" approaches have been applied to cell linecharacterization. Clonal variations in rat fibroblasts (Clarke, 1965) and hepatoma cells (Peterson, 1976) were first reported and revealed differences in growth characteristics under both oxygen deficient and aerobic culture conditions. Proteomic and genomic studies on various NS0 (Alete et al., 2005; Seth et al., 2007; Smales et al., 2004) and murine cell lines (Oh et al., 2003), and of their recombinant derivative clones, allowed to clearly demonstrate that clones differing in their mAb productivities also differ in the abundance of proteins involved in cellular functions such as energetic metabolism, mAb folding/assembly, and cytoskeletal organization. The issue of clonal variation in recombinant CHO cell cloneshas also been largely addressed. Early works compared clones for their growth and morphological aspects, and showed altered cell morphology and different sub-population spatial organization types between clones when grown on agar (Konrad et al., 1977; Zdzienicka, Cupido, & Simons, 1985). Clone-specific variations at the functional genetic level were also extensively described. It has been reported that high- and low-producer CHO-mAb subclones differ mainly in their DNA fragment sizes where high numbers of differentially expressed genes were identified (Kim, Byun, & Lee, 2001). Analyses at the proteomic level also revealed that different clones show different behaviours at different culture phases, mid-exponential and stationary phases (Chusainow et al., 2009; Davies et al., 2012; Hayduk, Choe, & Lee, 2004; Hayduk & Lee, 2005; Nissom et al., 2006). The effect of culture conditions on different CHO cell clones, with respect to cell growth and productivity, was also investigated at reduced temperature (Yoon, Hwang, & Lee, 2004). Regarding specific productivity, different enhancing effects of low culture temperature were observed in different clones. Recently, a metabolomic study focusing on clonal variations in response to culture condition variation has been conducted (Dahodwala et al., 2012). Comparing clone-*to*-clone changes, beside specific productivity, strong

variations in cell density, nutrient uptake and metabolic generation patterns were also detected. Indeed, *v*arious *f*luxomic approaches (Mo, Palsson, & Herrgård, 2009)have been developed to estimate metabolic fluxes rates, such as using labeling techniques (Ahn & Antoniewicz, 2011; Dean & Reddy, 2013; Metallo et al., 2009; Sheikholeslami, Jolicoeur, & Henry, 2013; Templeton et al., 2013) and metabolic mathematical models (Dorka et al., 2009; Ghorbaniaghdam, Henry, & Jolicoeur, 2012; Naderi et al., 2011; Nolan & Lee, 2010; Zamorano et al., 2012; Zomorrodi et al., 2012).Using isotope labeling experiments, MFA techniques, and mathematical models different metabolic patterns in CHO cells were demonstrated, mostly higher metabolic efficiency as a result of lower production of by-products, to be highly associated with different states of growth and productivity either over the course of one culture or in different clones.Taken together, these works have significantly improved our knowledge on CHO cell behaviour, as well as our conviction on the need for developing tools allowing a more in-depth capacity to describe cell metabolic behaviour. In that context, kinetic models, when they describe transient behaviours, can serve as *in silico* platform enabling either intuitive or counter-intuitive metabolic flux exploration.In this work, we have further developed a kinetic-metabolic model for CHO cells. The model, which is based on cell energetic and redox states (Ghorbaniaghdam, Henry, & Jolicoeur, 2012), was implemented with metabolic regulation aspects and then applied as an *in silico* platform to the characterization of clonal variation comparing *a* parental CHO cell line to its high- and low-producer derived clones. High- and low-producer clones, engineered with the inducible cumate gene-switch expression system (Gaillet et al., 2010; Mullick et al., 2006) were cultured in shake flask cultures, under both induced and non-induced conditions. The model was calibrated on experimental data of extra- and intracellular metabolites**.** In the present work, the descriptive precision as well as the predictive capacity of the model were thus improved.

5.5 Materials and methods

Ethics statement

All cell culture experiments were approved by the ethics committee of the Ecole Polytechnique.

5.5.1 CHO clones and culture

CHO clones that stably produce a recombinant monoclonal human anti-CD20 at different specific productivities (high- and low-producer) were provided by Viropro International Inc. (Montreal, Canada). These cells were derived from CHO-Cum2 cells and stably express the reverse cumate transactivator, as described in details by Mullick et al. (2006) (Mullick et al., 2006). Cells were seeded at 2×10^5 cells/mL in 300 mL of a protein-free medium in 1-L shake flasks, and cultured on a shaker (150 rpm) in a humidified incubator at 37°C and 5% CO_2. The medium used was a customized chemically-defined SFM4CHO medium (Hyclone, Utah, USA) supplemented with 4 mM glutamine (Hyclone, Utah, USA, cat. # SH30034), 30 mM glucose (Sigma, Oakville, Canada, cat. # G8270), and 0.05 mg/mL dextran sulphate (MW: 500000, Sigma, Oakville, Canada, cat. # D7037). For the comparative study, the parental clone, together with high- and low-producer clones, were cultured in duplicate. High- and low-producer clones were cultured both in the presence and in absence of cumate, the latter serving as non-induced control. In case of induction, 1 µg/mL of cumate was added after 48 hours of incubation, to trigger the recombinant protein expression. It should be mentioned that no visible effects*on*morphology*or*growthrates were reported for mammalian cells cultured at a cumate concentration below *200 µg/mL*(Mullick et al., 2006). Cell culture samples were taken every 24 h for cell counts, biochemical assays, and quantification of amino acids and human IgG, the recombinant mAb. Samples were centrifuged at 300 *g* for 5 min to remove cells, and supernatant samples were stored at -20°C for further analysis. Cultures were monitored for a total of 6 days.

5.5.2 Analytical methods

Cell density was determined by cell counting using a hemocytometer,and cell viability was estimated using the trypan blue (sigma, Oakville, Canada cat. # T8154) exclusion method. The concentration of glucose, lactate, glutamine and glutamate in the culture supernatant were determined using a dual-channel immobilized oxidase enzyme biochemistry analyzer (2700 SELECT, YSI Inc. Life Sciences, Yellow Springs, OH, USA), using calibration buffers provided by the manufacturer. Ammonia concentration in supernatants was assayed by an enzymatic kit with respect to manufacturer technical instructions: Ammonia Assay Kit (Sigma, Oakville, Canada cat. # AA0100). NAD(P) and NAD(P)H were also extracted and assayed by an enzymatic kit with respect to manufacturer technical instructions: NAD(P)/NAD(P)H QuantitationKit (BioVision,CA,USA, *cat. #* K337-100*)*.Monoclonal antibody concentration was quantified using an enzyme-linked immunosorbent assay (ELISA). First, 96-well plates (Costar) *(*Fisher Scientific,Burlington, Canada, *cat*. # 3795)were coated with a goat anti-human IgG1 (H+L) solution (Jackson ImmunoResearch, PA, USA, cat. # 109-165-003) diluted to 2.5 µg/mL in 50 mM sodium carbonate (Fischer Scientific, Burlington, Canada, cat. # S263-1), and incubated at 4°C overnight. Then, the blocking of non-specific sites was carried out by adding PBS solution containing 1% casein. After incubation for 1 h at 37°C, either samples or standards diluted in PBS-casein were added in triplicate to each well and incubated for 1 h at 37°C. After the plates were incubated 1 h at 37°C, peroxidise-conjugated affinipure fragment Goat anti-human IgG (Jackson Immuno Research, PA, USA, cat. # 109-035-003) (1:10,000 dilution) was added to each well, and the plates were incubated for 1 h at 37°C. After each of the previous steps, the wells were washed three times (PBS with 1% w/v Tween 20). Finally, the reaction was revealed by 3,3,5,5′-Tetramethylbenzidine (TMB) (Sigma, Oakville, Canada, cat. # T0440) and stopped after 15-20 min by adding1 N hydrochloric acid and the plates were read by an automatic plate reader at 450 nm usinga Victor^{3}V microplate reader (Perkin-Elmer, Vaudreuil-Dorion, Canada). The analysis of amino acid concentrations was performed on an Agilent 1290 UPLC system (Agilent technologies, Montreal, Canada) coupled to an Agilent 6460 triple quadruple mass spectrometer (Agilent technologies, Montreal, Canada). The underivatized amino acids were separated by a 2.1×150 mm

ZICTM-Hilic column (3.5 µm, 200 A, PEEK) (Merck SeQuant,Peterborough, Canada) and 2.1×20 mm ZICTM-Hilic guard column (5 µm, 200 A, PEEK) (Merck SeQuant, Peterborough, Canada) at a column temperature of 35^{o}C and injection volume of 5 µL. The mobile phase buffer contained 20 mM $HCOONH_4$ (Sigma, Oakville, Canada, cat. # 74314) at pH 4. The mobile phase A was 10% of the mobile phase buffer in water, and the mobile phase B was 10% of the mobile phase buffer in acetonitrile (ACN) (Sigma, Oakville, Canada, cat. # A3396). The mobile phase B was linearly decreased from 90% to 35% in 19 min, then was increased to 90% in one minute and hold at 90% for 15 min at a flow rate of 0.1 mL/min.

5.5.2.1 Respirometry test

Respirometry assays were performed as described by Lamboursain et al. (2002) (Lamboursain, St-Onge, & Jolicoeur, 2002). Briefly, 3 mL of cell suspension containing at least 5×10^6 cells were inoculated in a 10-mL borosilicate glass syringe (Sigma, Oakville, Canada), in which the plunger was substituted by an In-gold pO_2 probe (Mettler Toledo, Canada). At low cell densities, a volume of cell suspension containing5×10^6 cells was collected and centrifuged, and the pellet was re-suspended in a total of 3 mL of spent media. The respirometer was kept at 37°C and magnetically agitated (60 RPM) to ensure the homogeneity of cell suspension. Dissolved oxygen was recorded by an acquisition system (Virgo, Longueuil, Canada).

5.5.2.2 Extraction of intracellular metabolites

For intracellular metabolomic analysis, 5×10^6 cells were obtained daily, washed twice with cold PBS and extracted with 400 µL of 80% cold methanol in the presence of 0.2 g of Sand (Sigma, Oakville, Canada, cat. # 274739). After 10 min on dry ice, the mixture was vortexed and then sonicated in ice and water for 5 min. Suspensions were then centrifuged at 4°C for 7 min at 21,000 *g*. The supernatants were then transferred to a clean tube as extracts. Pellets were re-extracted as mentioned above with 200 µL of 50% cold methanol and 200 µL of cold water. At each extraction, supernatants were combined with the first extract and stored in −80 °C prior to analysis.

5.5.2.3 Energetic nucleotide concentrations

Extracts were filtered through 0.2 µm filters (Millipore, Etobicoke, Canada) before analysis. Nucleotides in CHO cells extracts were analyzed using a 1290 UPLC system

coupled to a 6460 triple quadruple mass spectrometer (both from Agilent Technologies, Montreal, Canada). Nucleotides were separated by a Symmetry C18 column (150×2.1mm, 3.5μm) (Waters, Milford, USA) equipped with a Security C18 guard-column (Waters, Milford, USA 10×2.1mm, 3.5μm) by the ion-pair method. DMHA (N,N-dimethylhexylanine, Sigma, Oakville, Canada, cat. # 308102) was used as an ion-pair reagent to improve the signal-to-noise ratio with positive ionization mode. The mobile phase consisted of Buffer A: 10mM ammonium acetate, 15mM DMHA at pH 7.0, and Buffer B: 50/50% (v/v) acetonitrile, 20mM NH_4OAc at pH 7.0. Mobile phase flow rate was set at 0.3mL/min with the following gradient: 0–10min at 10% B, 10–20min at linear gradient from 10 to 30% B, 20–21min at linear gradient from 30 to 60% B, 21–26min at 60% B, 26–27min at linear gradient from 60 to 10% B and 27–35min at 10% B.

5.5.2.4 Organic acid and sugar phosphate concentrations

Extracts were filtered through 0.2 μm filters (Millipore, Etobicoke, Canada) before UPLC–MS/MS (Agilent, Montreal, Canada) analysis equipped with a Hypercarb column (100×2.1 mm, 5 μm) and a Hypercarb pre-column (2.1×10, 5 μm) (Thermo Fisher, Burlington, Canada). Mobile phase consisted in Buffer A: 20 mM ammonium acetate at pH 7.5, and Buffer B: 10% (v/v) methanol in water. Flow rate was set at 0.3 mL/min using the following gradient: 0–5 min at 10% A, 5–10 min at linear gradient from 10% to 20% A, 10–20 min at linear gradient from 20% to 100% A, 20–30 min at 100% A, 30–32 min at linear gradient from 100% to 10% A and 32–40 min at 10% A.

5.5.3 Model development

The mathematical model developed and presented here is based on a previous model describing CHO cells central metabolism (Ghorbaniaghdam, Henry, & Jolicoeur, 2012). In the present work, the descriptive precision as well as the predictive capacity of the model were improved, by including catabolic pathways of amino acids metabolism along with other biochemical pathways (glycolysis, pentose phosphate pathway, TCA cycle, glutaminolysis as well as cell respiration) providing carbon skeletons to the central metabolism. Amino acids are pooled into 3 groups channeled through TCA intermediates such as succinate, oxaloacetate and α-ketoglutarate (Figure 5.1). The other entry points for amino acid carbon skeletons are lumped to pyruvate. A special care was taken to preserve all stoichiometric relationships while lumping and/or combining reactions. We

also further described the cell specific growth rate from its precursor's building blocks by considering G6P (leading to phospholipids and organic phosphate compounds), R5P (to DNA, RNA and nucleotides), and extracellular glutamine together with other amino acids (to proteins) (reaction 34, Table 5.2). Cell growth is described from the main cell building blocks for which experimental data were available; thus excluding precursors of lipids. This approach, although simplistic, allowed describing cell growth, as well as identifying the major anabolic pathways that are logically expected to affect growth behavior. Furthermore, a description of the cell-specific recombinant protein production rate is incorporated into the model. Extracellular amino acid concentrations are included individually in the kinetic expression for both the cell specific growth rate and mAb productivity. For simplification purposes and because of a lack of available data in literature, a single affinity constant value is used for each amino acid, either as a substrate for biomass formation or antibody production, except for glutamine. Indeed, experimental data show that cell growth stopped specifically upon depletion of glutamine, while it has not limited antibody production.Consumption rate of each precursor for the synthesis of biomass or recombinantprotein is calculated as proposed by Martens (2007) (Martens, 2007), considering the stoichiometry of precursor metabolites (Table 5.1, reactions 34-35). The stoichiometric coefficients of the respective biosynthetic equations were taken from literature (Ahn & Antoniewicz, 2011).The global metabolic network is presented in Figure 5.1, and a detailed summary of each flux reactions is given in Table 5.1.

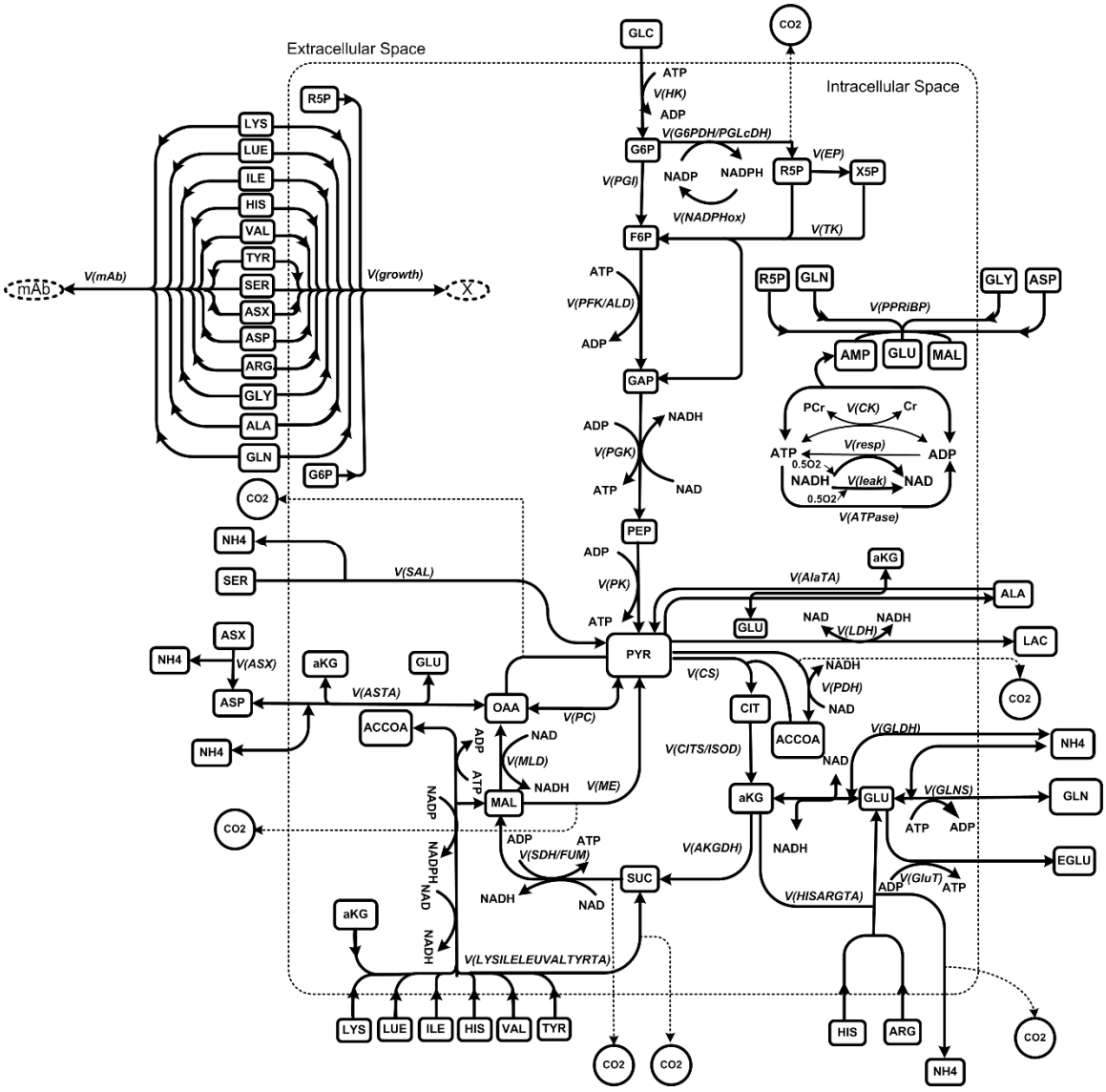

Figure 5.1 The metabolic network considered in the model

Table 5.1 Reactions of a metabolic network

No.	Reaction
1	GLC+ATP→G6P+ADP
2	G6P→F6P
3	F6P+ATP→2GAP+ADP
4	GAP+ADP+NAD^++Pi→PEP+ATP+NADH
5	PEP+ADP→PYR+ATP
6	PYR+NADH↔LAC+NAD^+
7	G6P+2$NADP^+$→R5P+2NADPH+CO_2
8	R5P→X5P
9	R5P+2X5P→2F6P+GAP
10	PYR+COA+NAD^+→ACCOA+NADH+CO_2
11	ACCOA+OXA→CIT+CoA
12	CIT+NAD^+→AKG+NADH+CO_2
13	AKG+CoA+NAD^++ADP+Pi →SUC+NADH+CO_2+CoA+ATP
14	SUC+2/3NAD^+→MAL+2/3NADH+CO_2
15	MAL+NAD^+→OAA+NADH
16	MAL+NADP →PYR+NADPH+CO_2
17	PYR →OAA+CO_2
18	GLN+ATP↔GLU+ADP+NH_4
19	GLU+NAD^+↔AKG+NADH+NH_4
20	GLU+PYR↔AKG+ALA
21	GLU+ADP+Pi→EGLU+ATP
22	O_2+(P/O ratio)*2ADP+2NADH+(P/O ratio)*2Pi→(P/O ratio)*2ATP+NAD^++2H_2O
23	O_2+2NADH→2NAD^++2H_2O
24	ATP→ADP+Pi
25	ATP+AMP↔2ADP
26	Pcr+ADP↔Cr+ATP
27	2GLN+0.6R5P+2ASP+GLY+2ATP→2GLU+2MAL+AMP+2ADP
28	NADPH→$NADP^+$
29	SER→PYR+ NH_4
30	ASX→ASP+ NH_4
31	ASP+AKG↔GLU+OAA+NH_4
32	HIS+ARG+AKG→GLU+NH_4+CO_2
33	LYS+ILE+LEU+HIS+VAL+TYR+7AKG+ATP+9NAD+2NADP→4GLU+3SUC+MAL+8ACCOA+ADP+9NADH+2NADPH+4CO_2
34	0.024R5P+0.029G6P+0.04GLN+0.013ALA+0.007ARG+0.0261ASP+0.003HIS+0.0084ILE+0.013LEU+0.01LYS+0.099SER+0.004TYR+0.0096VAL+0.016GLY+3.78ATP→X
35	0.01GLU+0.01GLN+0.01ALA+0.005ARG+0.007ASN+0.008ASP+0.003HIS+0.005ILE+0.014LEU+0.014LYS+0.026SER+0.008TYR+0.018VAL+0.0145GLY+4ATP→mAb

Only amino acids measured in this work are considered in the model. For amino acids, only extracellular pools were considered except for glutamate; extracellular glutamine is directly converted to intracellular glutamate, and intracellular glutamate exchange*f*or extracellular glutamine is also considered to account for the management of nitrogenous sources as the culture enters the plateau phase. Intracellular glutamate is channeled through TCA cycle via a bidirectional exchange for α-ketoglutarate, as reported by Nolan et al. (2010) (Nolan & Lee, 2010).From experimental data obtained in this work, extracellular aspartate concentration showed low constant values as the culture reaches the plateau phase, which suggests a possible exchangeof intracellular oxaloacetatefor extracellular aspartate, a phenomenon that has thus been described in the model. Finally, it is assumed that at low extracellular glutamine level, the cells take up extracellular alanine; an activation term based on a threshold concentration for extracellular glutamine was thus included in the model.

5.5.3.1 Description of flux kinetic regulation

Mathematical formulations of metabolic flux kinetics have been determined in a previous work (Ghorbaniaghdam, Henry, & Jolicoeur, 2012),based on the model capacity to simulate experimental data for another CHO cell line in bioreactor cultures. In this work, additional regulatory functions, mainly in glycolysis (Figure 5.2), were introduced and evaluated, one by one, to either describe activation or inhibition of enzyme kinetics, as documented in literature (Chang et al., 2009). Indeed, hexokinase feedback-inhibition by its product (term I), G6P, phosphoglucose isomerase (term II) and phosphofructokinase inhibition (term III) by PEP and G6P, thefeed-forward activation of pyruvate kinaseby F6P (term IV), as well as the substrate inhibition of lactate dehydrogenase forward reaction (term V) were integrated in the model and simulations compared were to experimental data, as described in the next section.

Table 5.2 Biokinetic equations of the metabolites fluxes (1-35) of the model

No.	Biokinetic equations
1	$v(HK) = v_{\max HK} * \frac{GLC}{K_{mGLC} + GLC} * \frac{\frac{ATP}{ADP}}{K_{m\frac{ATP}{ADP}} + \frac{ATP}{ADP}} * \frac{K_{dG6P}}{K_{dG6P} + G6P}$
2	$v(PGI) = v_{maxf\ PGI} * \frac{G6P}{K_{mG6P} + G6P} * \frac{K_{dPEP}}{K_{dPEP} + PEP}$
3	$v(PFK/ALD) = v_{\max PFK/ELD} * \frac{F6P}{K_{mF6P} + F6P} * \frac{\frac{ATP}{ADP}}{K_{m\frac{ATP}{ADP}} + \frac{ATP}{ADP}}$
4	$v(PGK) = v_{maxPGK} * \frac{GAP}{K_{mGAP}+GAP} * \frac{\frac{ADP}{ATP}}{K_{m\frac{ADP}{ATP}}+\frac{ADP}{ATP}} * \frac{Pi}{K_{mPi}+Pi} * \frac{\frac{NAD}{NADH}}{K_{m\frac{NAD}{NADH}} + \frac{NAD}{NADH}}$
5	$v(PK) = v_{\max PK} * \frac{PEP}{K_{mPEP} + PEP} * \frac{\frac{ADP}{ATP}}{K_{m\frac{ADP}{ATP}} + \frac{ADP}{ATP}}$
6	$v(LDH) = v_{maxf\ LDH} * \frac{PYR}{K_{mPYR} + PYR} * \frac{\frac{NADH}{NAD}}{K_{m\frac{NADH}{NAD}} + \frac{NADH}{NAD}} - v_{maxr\ LDH} * \frac{LAC}{K_{mLAC} + LAC} * \frac{\frac{NAD}{NADH}}{K_{m\frac{NAD}{NADH}} + \frac{NAD}{NADH}}$
7	$v(G6PDH/PGLcDH) = v_{\max G6PDH/PGLcDH} * \frac{G6P}{K_{mG6P} + G6P} * \frac{\frac{NADP}{NADPH}}{K_{m\frac{NADP}{NADPH}} + \frac{NADP}{NADPH}}$
8	$v(EP) = v_{\max EP} * \frac{R5P}{K_{mR5P} + R5P}$
9	$v(TK/TA) = v_{\max TK/TA} * \frac{R5P}{K_{m2R5P} + R5P} * \frac{X5P}{K_{mX5P} + X5P}$
10	$v(PDH) = v_{max\ PDH} * \frac{PYR}{K_{mPYR} + PYR} * \frac{\frac{NAD}{NADH}}{K_{m\frac{NAD}{NADH}} + \frac{NAD}{NADH}}$
11	$v(CS) = v_{max\ CS} * \frac{ACCOA}{K_{mACCOA} + ACCOA} * \frac{OAA}{K_{mOXA} + OAA}$
12	$v(CITS/ISOD) = v_{\max CITS/ISOD} * \frac{CIT}{K_{mCIT} + CIT} * \frac{\frac{NAD}{NADH}}{K_{m\frac{NAD}{NADH}} + \frac{NAD}{NADH}}$

Table 5.2 Biokinetic equations of the metabolites fluxes (1-35) of the model (Continued)

13	$\boldsymbol{v(AKGDH) = v_{max\ AKGDH} * \frac{AKG}{K_{mAKG} + AKG} * \frac{\frac{NAD}{NADH}}{K_{m\frac{NAD}{NADH}} + \frac{NAD}{NADH}} * \frac{\frac{ADP}{ATP}}{K_{m\frac{ADP}{ATP}} + \frac{ADP}{ATP}} * \frac{Pi}{K_{mPi} + Pi}}$

14 $$v(SDH/FUM) = v_{\max SDH/FUM} * \frac{SUC}{K_{mSUC} + SUC} * \frac{\frac{NAD}{NADH}}{K_{m\frac{NAD}{NADH}} + \frac{NAD}{NADH}}$$

15 $$v(MDH) = v_{max\ MDH} * \frac{MAL}{K_{mMAL} + MAL} * \frac{\frac{NAD}{NADH}}{K_{m\frac{NAD}{NADH}} + \frac{NAD}{NADH}}$$

16 $$v(ME) = v_{max\ ME} * \frac{MAL}{K_{mMAL} + MAL} * \frac{\frac{NAPD}{NADPH}}{K_{m\frac{NADP}{NADPH}} + \frac{NADP}{NADPH}}$$

17 $$v(PC) = v_{max\ ME} * \frac{PYR}{K_{mPYR} + PYR}$$

18 $$v(GLNS) = v_{maxfGLNS} * \frac{GLN}{K_{mGLN} + GLN} * \frac{\frac{ATP}{ADP}}{K_{m\frac{ATP}{ADP}} + \frac{ATP}{ADP}} - v_{maxr\ GLNS} * \frac{GLU}{K_{mGLU} + GLU} * \frac{\frac{ADP}{ATP}}{K_{m\frac{ADP}{ATP}} + \frac{ADP}{ATP}} * \frac{NH_4}{K_{mNH_4} + NH_4}$$

19 $$v(GLDH) = v_{maxf\ GLDH} * \frac{GLU}{K_{mGLU} + GLU} * \frac{\frac{NAD}{NADH}}{K_{m\frac{NAD}{NADH}} + \frac{NAD}{NADH}} - v_{maxr\ GLDH} * \frac{AKG}{K_{mAKG} + AKG} * \frac{\frac{NADH}{NAD}}{K_{m\frac{NADH}{NAD}} + \frac{NADH}{NAD}} * \frac{NH_4}{K_{mNH_4} + NH_4}$$

20 $$v(AlaTA) = v_{maxf\ AlaTA} * \frac{GLU}{K_{mGLU} + GLU} * \frac{PYR}{K_{mPYR} + PYR} - v_{maxr\ AlaTA} * \frac{ALA}{K_{mALA} + ALA} * \frac{AKG}{K_{mPYR} + AKG} * (1 + \frac{K_{aGLN}}{GLN})$$

21 $$v(GluT) = v_{max\ GluT} * \frac{GLU}{K_{mGLU} + GLU} * \frac{\frac{ADP}{ATP}}{K_{m\frac{ADP}{ATP}} + \frac{ADP}{ATP}} * \frac{Pi}{K_{mPi} + Pi}$$

22 $$v(resp) = v_{max\ resp} * \frac{O_2}{K_{mO_2} + O_2} * \frac{\frac{ADP}{ATP}}{K_{m\frac{ADP}{ATP}} + \frac{ADP}{ATP}} * \frac{NADH}{K_{mNADH} + NADH} * \frac{Pi}{K_{mPi} + Pi}$$

23 $$v(leak) = v_{max\ leak} \frac{NADH}{K_{mNADH} + NADH}$$

24 $$v(ATPase) = v_{max\ ATPase} * \frac{ATP}{ATP + ATP}$$

Table 5.2 Biokinetic equations of the metabolites fluxes (1-35) of the model (Continued)

25 $$\boldsymbol{v(AK) = v_{maxf\ AK} * \frac{ATP}{K_{mATP} + ATP} * \frac{AMP}{K_{mAMP} + AMP} - v_{maxr\ AK} * \frac{ADP}{K_{mADP} + ADP}}$$

26 $$v(CK) = v_{maxf\ CK} * \frac{ADP}{K_{mADP} + ADP} * \frac{Pcr}{K_{mPcr} + Pcr} - v_{maxr\ CK} * \frac{ATP}{K_{mATP} + ATP} * \frac{Cr}{K_{mCr} + Cr}$$

27 $$v(PPRiBP) = v_{\max PPRibP} * \frac{R5P}{K_{mR5P} + R5P} * \frac{ASP}{K_{mASP} + ASP} * \frac{GLN}{K_{mGLN} + GLN} * \frac{GLY}{K_{mGLY} + GLY}$$

28 $$v(NADPHox) = v_{\max NADPHox} * \frac{NADPH}{K_{mNADPH} + NADPH}$$

29 $$v(SAL) = v_{max\ SAL} * \frac{SER}{K_{mSER} + SER}$$

30 $$v(ASX) = v_{max\ ASX} * \frac{ASX}{K_{mASX} + ASX}$$

31 $$v(ASTA) = v_{maxf\ ASTA} * \frac{ASP}{K_{mASP} + ASP} * \frac{AKG}{K_{mAKG} + AKG} - v_{maxr\ ASTA} * \frac{GLU}{K_{mGLU} + GLU} * \frac{OAA}{K_{mOXA} + OAA} * \frac{NH_4}{K_{mNH_4} + NH_4}$$

32 $$v(HISARGTA) = v_{\max HISARGTA} * \frac{HIS}{K_{mHIS} + HIS} * \frac{ARG}{K_{mARG} + ARG} * \frac{AKG}{K_{mAKG} + AKG}$$

33 $$v(LYSILELEUHISVALTYRTA) = v_{\max LYSILELEUVALTYRTAwth} * \frac{LYS}{K_{mLYS} + LYS} * \frac{ILE}{K_{mILE} + ILE} * \frac{LEU}{K_{mLEU} + LEU} * \frac{VAL}{K_{mVAL} + VAL} * \frac{HIS}{K_{mHIS} + HIS} * \frac{TYR}{K_{mTYR} + TYR} ** \frac{AKG}{K_{mAKG} + AKG} * \frac{\frac{ATP}{ADP}}{K_{m\frac{ATP}{ADP}} + \frac{ATP}{ADP}} * \frac{\frac{NAD}{NADH}}{K_{m\frac{NAD}{NADH}} + \frac{NAD}{NADH}} * \frac{\frac{NADP}{NADPH}}{K_{m\frac{NADP}{NADPH}} + \frac{NADP}{NADPH}}$$

34 $$v(growth) = v_{\max growth} * \frac{R5P}{K_{mR5P} + R5P} * \frac{G6P}{K_{mG6P} + G6P} * \frac{GLN}{K_{mGLN} + GLN} * \frac{ALA}{K_{mALA} + ALA} * \frac{ARG}{K_{mARG} + ARG} ** \frac{ASP}{K_{mASP} + ASP} * \frac{HIS}{K_{mHIS} + HIS} * \frac{ILE}{K_{mILE} + ILE} * \frac{LEU}{K_{mLEU} + LEU} * \frac{LYS}{K_{mLYS} + LYS} * \frac{SER}{K_{mSER} + SER} * \frac{TYR}{K_{mTYR} + TYR} * \frac{VAL}{K_{mVAL} + VAL} * \frac{GLY}{K_{mGLY} + GLY} \frac{\frac{ATP}{ADP}}{K_{m\frac{ATP}{ADP}} + \frac{ATP}{ADP}}$$

Table 5.3State variables description and initial conditions

Component	Description	Value	Units
ACCoA	Acetyl-CoezymeA	1.4E-7	mmol.$(10^6$ cells$)^{-1}$
AKG	α-Ketoglutarate	4E-7	‘‘
ADP	Adenosine Diphosphate	1.4E-7	‘‘
AMP	Adenosine Monophosphate	2E-8	‘‘
ATP	Adenosine Triphosphate	1.5E-6	‘‘
CIT	Citrate	2E-7	‘‘

CoA	CoenzymeA	2E-8	‘‘
Cr	Creatine	4E-6	‘‘
F6P	Fructose 6-Phosphate	3E-7	‘‘
G6P	Glucose 6-Phosphate	5E-8	‘‘
GAP	Glyceraldehyde 3-Phosphate	4E-7	‘‘
GLU	Glutamate	7E-4	‘‘
GLY	Glycine	8E-6	‘‘
MAL	Malate	1 E-6	‘‘
NAD	Nicotinamide Adenine Dinucleotide	*9E-7*	‘‘
NADH	Nicotinamide adenine dinucleotide(reduced)	2E-8	‘‘
NADP	Nicotinamide Adenine Dinucleotide Phosphate	9E-13	‘‘
NADPH	Nicotinamide Adenine Dinucleotide Phosphate(reduced)	5.3E-12	‘‘
OXA	Oxaloacetate	5E-5	‘‘
O_2	Intracellular Oxygen	8E-6	‘‘
PEP	*Phosphoenolpyruvate*	4E-8	‘‘
PCr	PhosphoCreatine	2E-6	‘‘
Pi	Phosphate	2E-6	‘‘
PYR	Pyruvate	5E-7	‘‘
R5P	Ribose 5-Phosphate	1.5E-7	‘‘
SUC	Succinate	5.3E-7	‘‘
X5P	Xylose-5-Phosphate	9.2E-8	‘‘
ALA	Extracellular Alanine	0.75	mM
ARG	Extracellular Arginine	2.8	‘‘
ASP	Extracellular Aspartate	1	‘‘
ASX	Extracellular Aspartate and Asparagine	2.8	‘‘
GLY	Extracellular Glycine	1	‘‘
HIS	Extracellular Histidine	0.95	‘‘
ILE	Extracellular IsoLeucine	1	‘‘
LUE	Extracellular Leucine	0.8	‘‘
LYS	Extracellular Lysine	1.2	‘‘
SER	Extracellular Serine	2.1	‘‘
TYR	Extracellular Tyrosine	0.55	‘‘

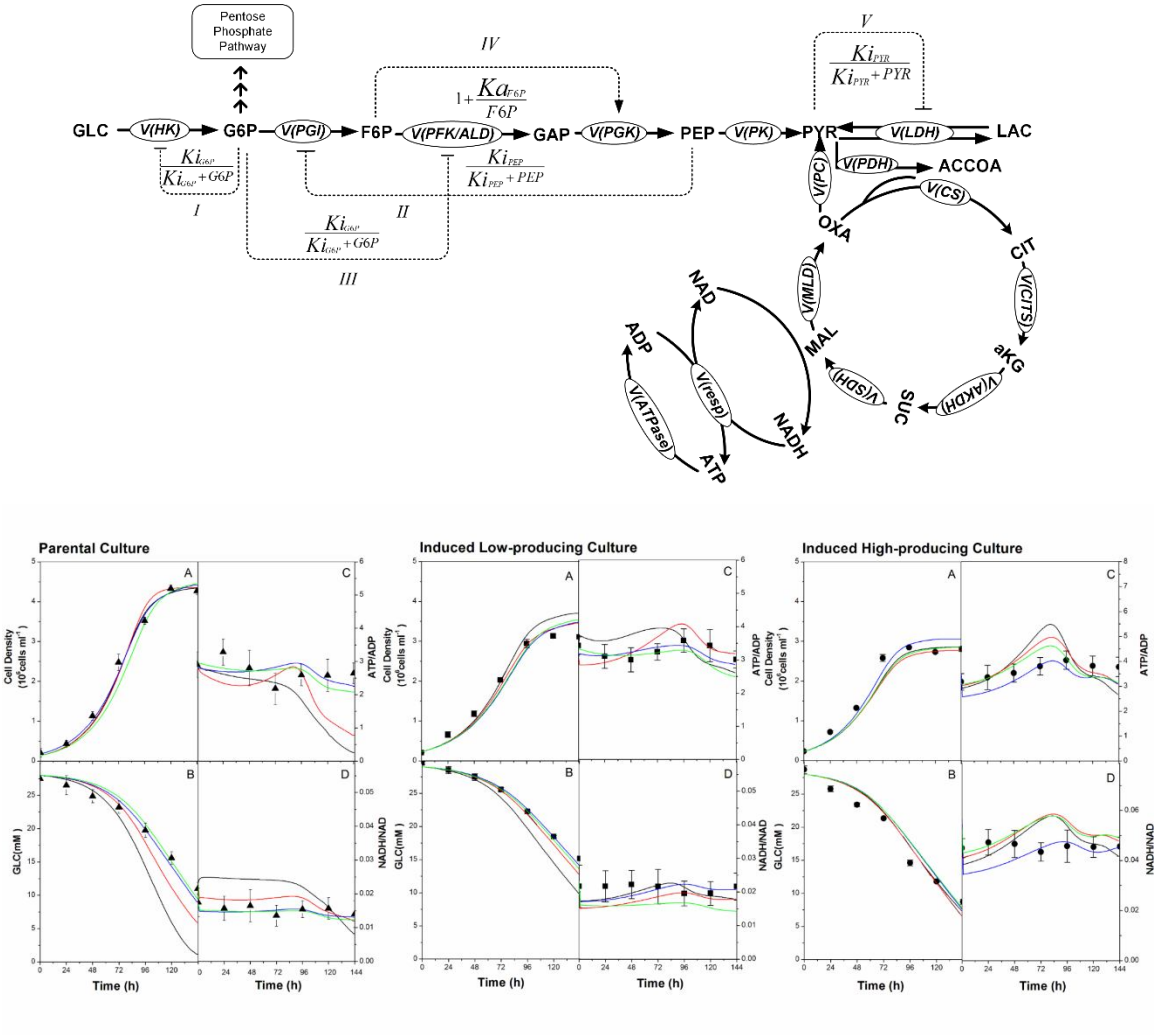

Figure 5.2Regulation scheme of the model through the activation or inhibition of the enzymes.

Symbol "↓" indicates activation and "⊥" inhibition. Glycolytic enzymes are either inhibited ($\frac{Ki_{\alpha}}{Ki_{\alpha}+\alpha}$) or activated($\mathbf{1}+\frac{Ka_{\alpha}}{\alpha}$)by an effecter "$\alpha$" where "$\alpha$" is mainly one of the glycolytic metabolites. The corresponding activation/inhibition terms labeled as I, II, III, IV, and V. The bottom diagram represents model simulations for parental, induced low- and induced high-producer cell lines with no regulation (solid black line), with the addition of term I (solid red line), with the addition of terms I and II (solid blue line), and the addition of all terms (solid green line). Experimental data are represented by triangles (parental culture), squares (induced low-producing culture), and circles (induced high-producing culture) for cell density (A), glucose (B), ATP-to-ADP ratio (C), and NADH-to-NAD ratio (D). Error bars are standard deviations from duplicate flasks. Error bars are standard deviations for duplicate cultures.

5.5.3.2 Model calibration

The final fully dynamic model includes 35 reactions and 46 variables. The kinetic equations for the flux regulation are presented in Table 5.2. The model has 95 kinetic parameters, 48 affinity constants (listed in Table 5.4), 42 maximum reaction rates (Table 5.5) and one parameter for each regulatory function (Table 5.4). Initial conditions for most of the variables were available from culture data (Table 5.3), while those remaining were taken from literature for similar conditions. The set of kinetic parameters previously determined for another CHO cell line in bioreactor cultures (Ghorbaniaghdam, Henry, & Jolicoeur, 2012) was used as initial estimates, and the new parameters were taken from literature for similar biological systems. The parameter estimation approach used *i*sextensively discussed in a previous study (Ghorbaniaghdam, Henry, & Jolicoeur, 2012). Briefly, foreach of the five cultures under investigation, a sensitivity analysis was performed for evaluating the influence of each parameter on the model output. In order to define their influence, parameters were systematically varied from their initial value comparing respective model output, defined as the weighted sum of squared residuals (WSSRES) between available experimental data (X^{mea}) and simulated values (X^{sim}) for each state variable *m*at time *k*, where the weight is the inverse of the variance of the experimental data for each state variable, var_m^{-1}.

$$\min WSSRES = \left[\sum_{t=1}^{k}\sum_{m=1}^{n}\left(X_{t,m}^{sim} - X_{t,m}^{mea}\right)^2 var_m^{-1}\right] \quad (10)$$

The sensitivity analysis procedure allowed to rank the parameters by their decreasing influence, and to remove parameters that were not contributing to model sensitivity from further optimization cycle, keeping them at their initial value. Optimal parameter values (for the sensitive ones) were then obtained by minimizing the normalized sum-squared errors using a *Least-squares* minimization function in MATLAB's Optimization Toolbox for non-linear regression. Finally, 95% confidence intervals for both model sensitive parameters and model predictions were calculated using built-in MATLAB functions

5.6 Results

5.6.1 Model structure fine-tuning and characterization

The model was first applied to parental cell line culture data obtained in shake flasks. Model performance assessment with cumate-induced and non-induced cultures of low-producer and high-producer clones is presented thereafter.

5.6.1.1 Describing the regulation of glycolysis ameliorates model simulations of experimental data

Biologically relevant scenarios (Figure 5.2) of enzyme regulation mechanisms, known to play a role in glycolysis robustness, were successively evaluated from model performance to simulate experimental data. For clarity reasons, only simulations for four significant model variables, such as cell density, glucose, ATP-to-ADP and NADH-to-NAD ratios, are shown here (Figure 5.2) for parental, induced low- and high-producer cultures and the remaining results can be found as supplementary materials (Figures 5.10-5.15). The last two model variables are markers of cell energetic and redox states, respectively (Reich & Sel'Kov, 1981). Interestingly, one can observe that model simulations of cell growth agreed with experimental data in all regulation scenarios. However, the errorbetween model simulation and experimental datafor extracellular glucose and energetic nucleotides ratio shows to be high, when no regulation term are included in kinetic flux expressions. Hexokinase inhibition by G6P (term I) decreases the simulation error for extracellular glucose and redox nucleotides ratio, and to a lesser extent for energetic nucleotides ratio. Adding a term (II) to account for PGI inhibition by PEP further reduces the error between model simulations and experimental data, and this is particularly obvious for energetic nucleotide ratios. This suggests that variations in sugar phosphate cell concentrations, although of low magnitudes, may trigger the first two regulatory mechanisms to control glycolytic fluxes.To verify whether incorporating other regulatory terms into rate expressions significantly influences simulation results, a formulation with all main regulatory steps was also tested. The last formulation also shows to allow simulating experimental data almost similarly to the case when the first two terms are considered. This may suggest that not all the regulatory terms are solicited within experimental conditions in this study. Therefore, because of a higher performance level as well as a lower formulation complexity, a kinetic formulation including the first and the second regulatory terms was used in the remaining of this study. Considering

extracellular metabolites, presented in supplementary material, (Figures 5.10, 5.12, 5.14) the model is far from predicting experimental data when no regulatory terms are considered. However, model simulations are closer to experimental data when only adding the first (I) and the second (II) regulatory terms, respectively hexokinase feedback-inhibition by its product, G6P, and phosphoglucose isomerase inhibition by PEP. Interestingly, our experimental data set accounts for a wide diversity of metabolites such as by-products (lactate, NH_4^+, glutamate), amino acids (alanine, glutamine, serine, aspartate, and amino acid pools to TCA cycle), sugar phosphates of glycolysis (G6P and PEP) as well as glucose, cell density and energetic nucleotides, which are all well simulated by the model implemented with I and II regulation terms. Similar observations can be drawn for scenarios of intracellular organic acids such as PYR and SUC. In addition, model simulations corresponded more closely to experimental data for organic acids such as AKG and MAL in induced low- and high-producer cultures, but to a lesser extent to no clear effect for other amino acids and AMP, presented in supplementary material, (Figures 5.11, 5.13, 5.15). Finally,the same behaviour can be observed for the cell specific oxygen consumption rate (qO_2), for which simulations were closer to experimental data comparing to the case with no regulation (Figures 5.10, 5.12, 5.14).

5.6.1.2 A limited subset of model parameters drives the in silico cell behaviour

A sensitivity analysis was performed on the resulting model, aiming to identify the most critical parameters. Values of model parameters were changed from -85 to +300%, one at a time, from their optimal value, and the normalized sum-squared differences **(**WSSRES)were calculated as previously described. Resulting WSSRESvalues were then further normalized to that obtained for original optimal parameter values (i.e. 0% change). Parameters showing a deviation of ±15% and higher were considered sensitive; a colormap (Figure 5.3) was drawn to illustrate the extent to which normalized WSSRESvalues vary from that of the optimal value (i.e. minimal simulation error). The model reveals to be primarily sensitive to parameters of glycolysis, TCA cycle and energetic reactions, amino acid catabolism pathways, partially to glutaminolysis, and to a lesser extent to the pentose phosphate pathway. The specific glucose uptake rate (v_{maxHK}) and other parameters of glycolysis ($v_{maxPGI,}$ $v_{maxPK,}$ $v_{maxf\ LDH}$ *and* $v_{maxr\ LDH}$) show to strongly affect simulation error. Moreover, maximum reaction rates for three enzymes in TCA

cycle ($v_{maxAKGDH}$, v_{maxCS}, andv_{maxMLD}), and for the reaction connecting glycolysis to TCA cycle ($v_{maxPDH,}v_{maxME,}$ andv_{maxPC}),also reveal to be significant. The model is also highly sensitive to three reactions related to glutaminolysis ($v_{maxfGLNS,}$ $v_{maxrGLNS,}$ $v_{maxfGLDH,}$ $v_{maxrGLDH,}$ $v_{maxfAlaTA,}$ andv_{maxASX}), and to a lesse extent to two parameters related to the pentose phosphate pathway oxidative branch ($v_{maxG6PDH,}$ and v_{maxEP}). The model shows a high sensitivity to energetic reactions, represented here by parameters related to non-specifically described ATP ($v_{maxATPase}$) and NADH consuming reaction ($v_{maxresp}$). Furthermore, the maximum specific growth rate ($v_{maxgrowth}$) also strongly influences the simulation error. Finally, parameters related to amino acid catabolism ($v_{maxrAlaTA,}$ $v_{maxSAL,}$ $v_{maxfASTA,}v_{maxHISARGTA,}$ and$v_{maxLYSILELEUHISVALTYRTA}$) also demonstrate to be influential. There are therefore a high number of non-influential parameters with 65 out of 95. This lack of sensitivity may partially come from the experimental space in hand that was used to calibrate and to challenge the model. Although these non-sensitive parameters are biologically relevant describing existing active pathways and enzymatic reactions, they may require more varying experimental culture conditions to be solicited (Mailier et al., 2011). For space limitation only sensitivity results for parental culture are shown while the other cultures exhibited almost the same results. Therefore, the model was kept as is at this point because actual non-sensitive parameters may become sensitive and thus be useful in a future study exploring outside the actual experimental space.

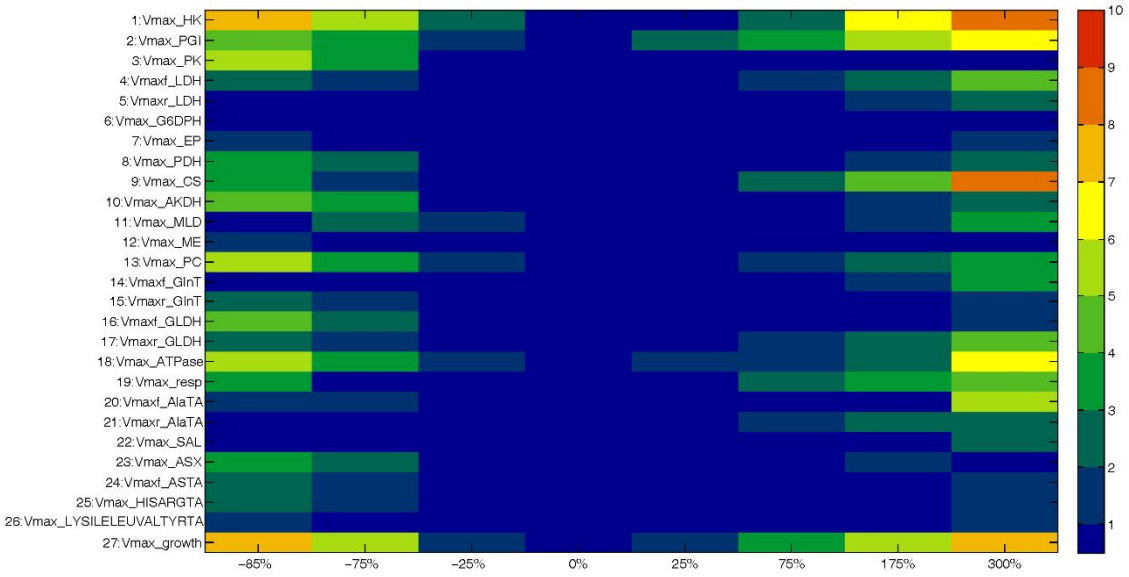

Figure 5.3Sensitivity analysis on model parameters for parental cell line culture**.**
The colormap represents the normalized sum of squared difference between model simulations and experimental data, when the parameter (row) is changed from -85% to +300% (column) of the optimal value. The values for sum of squared difference are normalized by the value corresponding to optimal values for parameters.

5.6.1.3 A limited subset of measured variables contribute to the overall model sensitivity

The specific contribution of each measured variable to the overall model sensitivity was also investigated. Among measured variables, cell density, extracellular glucose, glutamine, lactate, ammonia, ASX (ASN+ASP), amino acids pool to glutamate and nucleotide ratios showed a high sensitivity level compared to pyruvate and succinate (Figure 5.4). Not surprisingly, energetic nucleotide ratios exhibited the highest sensitivity as it is affected by multiple reactions in various parts of the metabolic network, through their regulatory role. Interestingly, parameters with a relatively high global sensitivity on model overall output may not systematically impact on all variables simulated. Here again, results are conditioned by the experimental space studied. It may thus suggest that experimental intracellular concentrations have never reached threshold levels, above or below which a higher impact could have been observed. The whole procedure of model parameters calibration has then been performed on the cumate-inducible cell lines, induced and non-induced. For space limitation and clarity reasons, only final calibrated

results are shown and discussed in the following sections (see Tables 5.4 and 5.5 for parameters values)

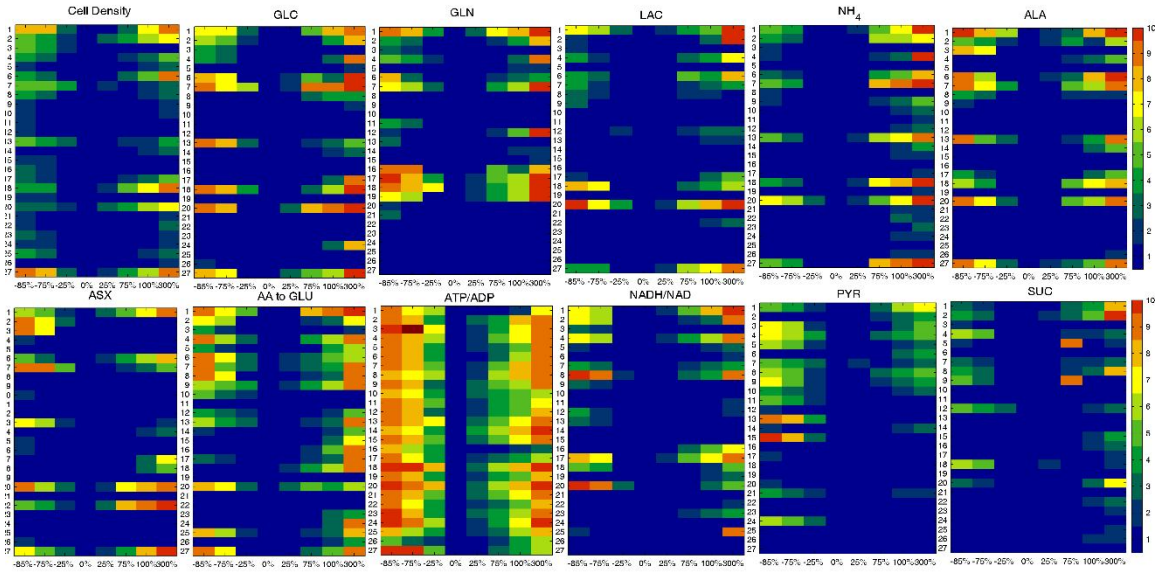

Figure 5.4 Partial Sensitivity analysis on model parameters for parental cell line culture. Each colormap represents the normalized sum of squared difference between the simulated and measured extracellular metabolite concentration over time, when the parameter (row) is changed from -85% to +300% (column) of the optimal value. The values for sum of squared difference are normalized by the value corresponding to optimal values for parameters. The number for each row corresponds to the parameter presented next to the same row in figure 5.3.

5.6.2 Assessment of the *in silico* platform performance

5.6.2.1 *The model describes intra- and extracellular* metabolites *concentration profiles and growth* kinetics

The model assumed for cell specific growth rate, as multiplicative Michaelis-Menten kinetics for precursors of cell building blocks, was able to simulate the viable cell concentration profile in all CHO cells cultures under study (Figure 5.6). High- and low-producing clones exhibit almost similar growth profiles, reaching maximum viable cell densities of ~3.5×10^{6}cells mL^{-1}, while parental cell line reached slightly higher maximum viable cell density (~4.5×10^{6} cells mL^{-1}). The model also simulates extracellular metabolites profile with time althoughsignificant differences in behaviour are observed between the parental, low- and especially high- producer clones(Figure 5.6).

Interestingly,differences between induced and non-induced cultures of the same cloneare non-significant. Irrespective of the clone or induction state, all cultures were not glucose-limited (> 5-15 mM at culture harvest), with the higher consumption in high-producer clone cultures. Parental and low-producer cultures exhibit similar glutamine profiles, and a faster depletion is again observed for the high-producer clone. Growth cessation coincided with the depletion of glutamine. Interestingly, unlike glucose, lactate concentration profile differs among clones but the modelstructure is able to simulate each case. Lactate is produced all along cultures but, however, the high-producer clone seems to start consuming lactate at glutamine depletion, suggesting the coupling of these phenomena as suggested by Zagari et al. (2013) (Zagari et al., 2013). Ammonia production was almost similar in parental and low-producer cultures reaching a final concentration of approximately ~4 mM, whereas it was ~5 mM in the case of the high-producer clone. Similarly to lactate, the high-producer clone seems to start consuming ammonia following glutamine depletion. Differences in extracellular metabolites profiles are significantly related to amino acids metabolism (see table 5.6 for statistical analysis).Globally,all amino acids exceptalanine andglutamate were consumed and the consumption/production rates were greater in the case of high-producer clone (Figure 5.6). Glutamate concentration constantly increases in all culture media, and alanine is also constantly produced during exponential phase but consumed thereafter (from ~96 h), with a more pronounced decrease inthe high-producer clone. In that culture, alanine may have compensated for the lack of glutamine, once the later was depleted. Beside alanine, extracellular concentrations in (ASN+ASP) and SER in the high-producer reached depletion. These amino acids are expected to contribute to pyruvate synthesis. Although a higher consumption of grouped amino acids channeled through succinate and glutamate can be identified in the high-producer culture, there is no depletion observed. Interestingly, most intracellular metabolites show constant and similar levels between cultures except for G6P and PEP with an increasing trend after exponential phase (Figure 5.16).

Table 5.4 Affinity (*Km*), activation (*Ka*), and inhibition (*Kd*) constants

Parameter	Value			units
	Parental	Low-producing	High-producing	
K_{mGLC}	4.19	4.19	4.199	mM
K_{mGLN}	1.58	1.5893	1.5893	‘‘
K_{mLAC}	5	5	3.5	‘‘
K_{mNH_4}	0.5	0.5	0.5	‘‘
K_{mALA}	1	1	1	‘‘
K_{mARG}	0.05	0.05	0.05	‘‘
K_{mASP}	0.015	0.015	0.015	‘‘
K_{mASX}	0.15	0.15	0.15	‘‘
K_{mGLY}	0.05	0.05	0.05	‘‘
K_{mHIS}	0.5	0.5	0.5	‘‘
K_{mILE}	0.025	0.025	0.025	‘‘
K_{mLUE}	0.025	0.025	0.025	‘‘
K_{mLYS}	0.05	0.05	0.05	‘‘
K_{mSER}	0.015	0.015	0.015	‘‘
K_{mTYR}	0.05	0.05	0.05	‘‘
K_{mVAL}	0.05	0.05	0.05	‘‘
K_{aGLN}	10	10	10	‘‘
$K_{mGLNmAb}$	0.01	0.01	0.01	
K_{mG6P}	8.20E-08	8.20E-08	8.20E-08	mmol.$(10^6$ cells$)^{-1}$
K_{mF6P}	4.00E-07	4.00E-07	3.22E-07	‘‘
K_{mGAP}	8.00E-07	8.00E-07	8.00E-07	‘‘
K_{mPEP}	1.70E-07	1.73E-07	1.70E-07	‘‘
K_{mR5P}	1.30E-08	1.35E-08	1.35E-08	‘‘
K_{mX5P}	3.40E-08	3.40E-08	3.40E-08	‘‘
K_{mPYR}	9.80E-07	7.98E-07	9.80E-08	‘‘
K_{mACCOA}	9.60E-07	9.60E-07	9.80E-07	‘‘
K_{mOXA}	2.40E-07	2.40E-07	2.46E-07	‘‘
K_{mCIT}	1.00E-07	8.51E-08	9.00E-08	‘‘
K_{mAKG}	8.60E-07	9.40E-07	7.11E-07	‘‘
K_{mSUC}	2.80E-08	2.03E-07	1.62E-07	‘‘
K_{mMAL}	8.50E-07	8.54E-07	6.21E-07	‘‘
K_{mGLU}	1.28E-04	1.28E-04	1.28E-04	‘‘
K_{mATP}	4.20E-06	5.00E-06	4.61E-06	‘‘
K_{mADP}	3.65E-07	3.65E-07	3.65E-07	‘‘
K_{mAMP}	2.52E-08	2.52E-08	2.52E-08	‘‘
K_{mPcr}	7.70E-6	7.70E-06	7.70E-06	‘‘
K_{mCr}	6.00E-7	6.00E-07	6.00E-07	‘‘
K_{mO_2}	4.00E-6	4.00E-6	4.00E-6	‘‘
K_{mPi}	1.00E-6	1.00E-6	1.00E-6	‘‘

Table 5.5 Maximum reaction rates (v_{max}) and Comparison of highly sensitive parameters in parental, low-producing and high-producing clones.
Asterisks (*) and (+) denote statistically significant difference between parental and either induced low-producing or induced high-producing cell lines considering shown confidence intervals. All units are in mmol. $(10^6 cells)^{-1}.h^{-1}$except for $v_{max\ growth}$ which is in h^{-1}.

Parameter	**Value**			**t-test Results**
	Parental	**Low-producing**	**High-producing**	
v_{maxHK}	2.65E-4 [2.35E-4,2.98E-4]	2.73E-4 [2.54E-4,2.93E-4]	2.98E-4 [2.76E-4,3.21E-4]	—
$v_{maxfPGI}$	2E-4 [3.75E-5,3.05E-4]	1.76E-4 [3.42E-5,3.14E-4]	1.47E-4 [1.08E-5,2.62E-4]	—
$v_{maxPFK/ALD}$	2.40E-3	2.40E-3	2.40E-3	—
v_{maxPGK}	9.00E-4	9.00E-4	9.00E-4	—
v_{maxPK}	5.78E-4 [2.21E-4,9.32E-4]	6.00E-4 [3.48E-4,8.75E-4]	6.00E-4 [3.44E-4,8.67E-4]	—
$v_{maxfLDH}$	3.62E-4 [1.65E-4,5.65E-4]	3.50E-4 [8.15E-5,6.2E-4]	5E-4 [2.13E-4,7.87E-4]	—
$v_{maxrLDH}$	2.75E-5 [1.95E-5,3.51E-5]	1.20E-4 [6.78E-5,1.73E-4]	2.10E-4 [1.23E-4,3.01E-4]	$p<0.1$ $*^{+}$
$v_{max\,G6PDH/PGLcDH}$	1.00E-4 [7.85E-5,1.25E-4]	9.93E-5 [5.46E-5,1.46E-4]	6.80E-5 [5.48E-5,8.29E-5]	—
v_{maxEP}	9.50E-6 [1.53E-6,1.75E-5]	9.91E-6 [1.63E-6,1.82E-5]	9.61E-6 [3.9E-6,1.54E-5]	—
$v_{max\,TK/TA}$	2.00E-5	2.00E-5	2.00E-5	—
v_{maxPDH}	1.40E-4 [1.01E-4,1.79E-4]	1.47E-4 [1.25E-4,1.61E-4]	2.60E-4 [2.1E-4,3.04E-4]	$p<0.1$ $^{+}$
v_{maxCS}	6.30E-5 [4.34E-5,8.23E-5]	9.67E-5 [2.19E-5,1.7E-4]	1.52E-4 [6.57E-5,2.39E-4]	—
$v_{max\,CITS/ISOD}$	8.20E-5	8.20E-5	8.20E-4	—
$v_{maxAKGDH}$	1.50E-4 [4.57E-5,2.51E-4]	1.44E-4 [4.34E-5,2.4E-4]	1.95E-4 [1.11E-4,2.8E-4]	—
$v_{max\,SDH/FUM}$	8.51E-5	8.51E-5	8.51E-5	—
v_{maxMLD}	6.40E-5 [8.76E-6,1.21E-4]	6.61E-5 [8.45E-6,1.31E-4]	1.85E-4 [1.2E-4,2.35-4]	—
v_{maxME}	7.14E-5 [3E-5,2.58E-4]	4.56E-5 [1.55E-5,7.58E-4]	1.05E-4 [6.07E-5,1.58E-4]	—

Table 5.5 Maximum reaction rates (vmax) and Comparison of highly sensitive parameters in parental, low-producing and high-producing clones (Continued).

v_{maxfPC}	8.00E-5 [4.44E-6,1.58E-4]	8.11E-5 [3.51E-5,1.28E-4]	9.95E-5 [4.39E-5,1.58E-4]	— —
$v_{maxfGLNS}$	6.40E-5 [3.86E-5,9.11E-5]	7.65E-5 [5.91E-5,9.36E-5]	9.00E-5 [7.57E-5,1.18E-4]	
$v_{maxrGLNS}$	3.25E-6 [2.49E-6,3.95E-6]	3.25E-6 [2.71E-6,3.82E-6]	3.65E-5 [2.42E-5,4.88E-4]	—
$v_{maxfGLDH}$	1.06E-5 [2.97E-7, 2.15E-5]	1.31E-5 [6.33E-7,2.56E-5]	2.05E-5 [7.00E-7,3.14E-5]	—
$v_{maxrGLDH}$	5.35E-5 [2.00E-6, 4.50E-5]	3.61E-5 [2.42E-5,4.80E-5]	3.10E-6 [2.33E-5,4.00E-5]	—
$v_{maxfAlaTA}$	6.00E-5 [3.55E-5,8.50E-5]	6.00E-5 [3.71E-5,8.36E-5]	1.15E-4 [6.29E-5,1.66E-4]	—
$v_{maxrAlaTA}$	1.07E-6 [0,12.53E-6]	1.22E-6 [0,2.56E-6]	5.50E-6 [3.81E-6,7.16E-6]	—
$v_{maxGluT}$	1.28E-6	1.65E-6	2.5E-6	—
$v_{maxresp}$	7.00E-4 [5.61E-4,8.70E-4]	8.13E-4 [5.53E-4,1.00E-3]	8.70E-4 [7.67E-4,9.98E-4]	—
$v_{maxATPase}$	5.451E-3 [4.12E-3,6.84E-3]	9.16E-3 [8.13E-3,1.02E-2]	9.30E-3 [8.04E-3,1.06E-2]	p<0.1 *+
$v_{maxleak}$	9.70E-5	9.70E-5	9.70E-5	—
	2.30E-4	2.30E-4	2.30E-4	—
$v_{maxfCK}v_{maxrCK}$	9.00E-5	9.00E-5	9.00E-5	—
v_{maxfAK}	2.00E-5	2.00E-5	2.00E-5	—
v_{maxrAK}	3.00E-5	3.00E-5	3.00E-5	—
$v_{maxPPRibP}$	2.00E-8	1.00E-8	1.00E-8	—
$v_{maxNADPHox}$	4.00E-3	4.00E-3	4.00E-3	—
v_{maxSAL}	6.65E-6 [5.18E-6,8.13E-6]	8.54E-6 [4.70E-6,1.23E-5]	1.00E-5 [4.22E-6,1.58E-5]	—
v_{maxASX}	8.05E-6 [4.19E-6,1.20E-5]	9.91E-6 [3.7E-6,1.63E-5]	1.29E-5 [5.07E-6,2.08E-5]	—
$v_{maxfASTA}$	5.41E-6 [4.32E-6,6.55E-6]	5.65E-6 [5.00E-6,6.3E-6]	3.50E-5 [2.97E-6,4.03E-5]	p<0.1 +
$v_{maxrASTA}$	3.25E-6	2.16E-6	3.2E-6	—
$v_{maxHISARGTA}$	1.50E-5 [5.4E-6,2.46E-5]	1.85E-5 [8.10E-6,2.89E-5]	2.05E-5 [1.07E-5,3.3E-5]	—
$v_{maxLYSILELEUHISVALTYRTA}$	2.61E-5 [1.81E-5,3.43E-5]	2.80E-5 [1.85E-5,3.75E-5]	3.45E-5 [2.27E-5,4.65E-5]	—
$v_{maxgrowth}$	0.34 [0.25,0.43]	0.42 [0.38,0.54]	0.49 [0.45,0.54]	—
v_{maxmAb}	0	1.60E-6 [1.05E-6,2.15E-6]	1.00E-5 [5.55E-6,1.5E-5]	p<0.1 *+

5.6.2.2 Model simulates CHO cells clonal variations in energetic state

As previously mentioned for the parental cell line, the cell energetic state represented by ATP-to-ADP, NADH-to-NAD ratios, and the cell specific oxygen consumption rate

(qO_2) are well simulated for all cultures (Figure 5.6). Although the cell specific oxygen consumption rate is generally greater for the high-producer clone, the ATP-to-ADP ratio, a marker of respiration and energy consumption, showed relatively stable and similar values in all cultures. NADPH-to-NAPD was also substantially similar and stable in exponential phase in all cell lines, with a slight decrease after exponential phase suggesting the down-regulation of NADPH production.Finally, the NADH-to-NAD ratio, which is a marker of TCA cycle activity, was considerably higher in high-producer clone than in parental and low-producer cell lines, indicating a sustained up-regulated TCA activity, as discussed in the next sections.

Clonal variation in physiology can be inferred from a limited set of model kinetic parameters

In order to further evaluate parameters adjustment attributed to clonal variation, the associated p-values for each pair of estimates (control vs. either induced low-producer or high- producer cultures) were calculated (Table 5.5). In low- and high- producer clones, only two and four parameters, respectively, were statistically different from those for parental to allow the model to simulate the effect of cumate induction. Briefly, in the case of the induced low-producer clone, main differences can be observed for parameters related to glycolysis ($v_{maxrLDH}$), and ATP consumption reactions, which are lumped as ATPase pumps requirements ($v_{maxATPase}$). However, in the case of the induced high-producer clone, $v_{maxr\ LDH}$ and $v_{maxATPase}$ are both significantly changed in addition to one parameter related to glutaminolysis ($v_{maxfASTA}$) and one related to the reactions connecting glycolysis to TCA cycle (v_{maxPDH}). The high-producer clone thus resulted in a significantly different *in silico* behaviour compared to the parental cell line and, to a lesser extent, to the low-producer clone (Figure 5.5 and Table 5.5) regarding the simulations that are however in agreement with experimental data. Interestingly, the high-producer clone only requires the adjustment of four parameters values from those of the parental for the simulations to cope with experimental data.

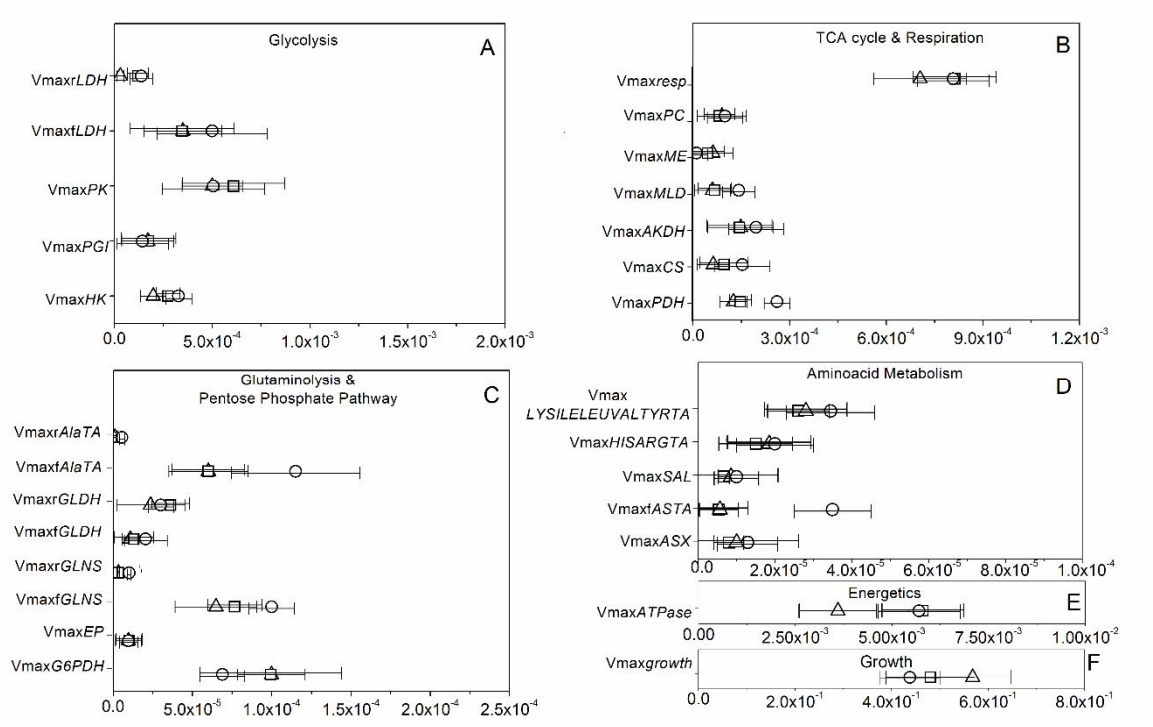

Figure 5.5 Parameter estimates with their error bars for sensitive parameters.
Glycolysis (A), TCA cycle and Redox state (B), glutaminolysis and pentose phosphate pathway (C), amino acid metabolism (D) and energetic and growth (E). Horizontal solid lines are 1.96 standard error bars and represent parameter estimate ±1.96 standard error. Parental cell line: open triangles for parameter estimates, induced low-producer cell line: open squares for parameter estimates, andinduced high-producer cell line: open circles for parameter estimates. A parameter is considered highly sensitive if a small variation in its value (± 25%) causes more than a 15 % increase of in the objective function.

5.6.2.3 The model simulates mAb production

The dynamics of mAb production, modeled as multiplicative Michaelis-Menten kinetics of amino acids, resulted in the simulation of mAb titers (Figure 5.6) in low- and high-producer clones. The model fits to experimental data in induced cultures while it simulates the production resulting from the leaky expression of the inducible system.

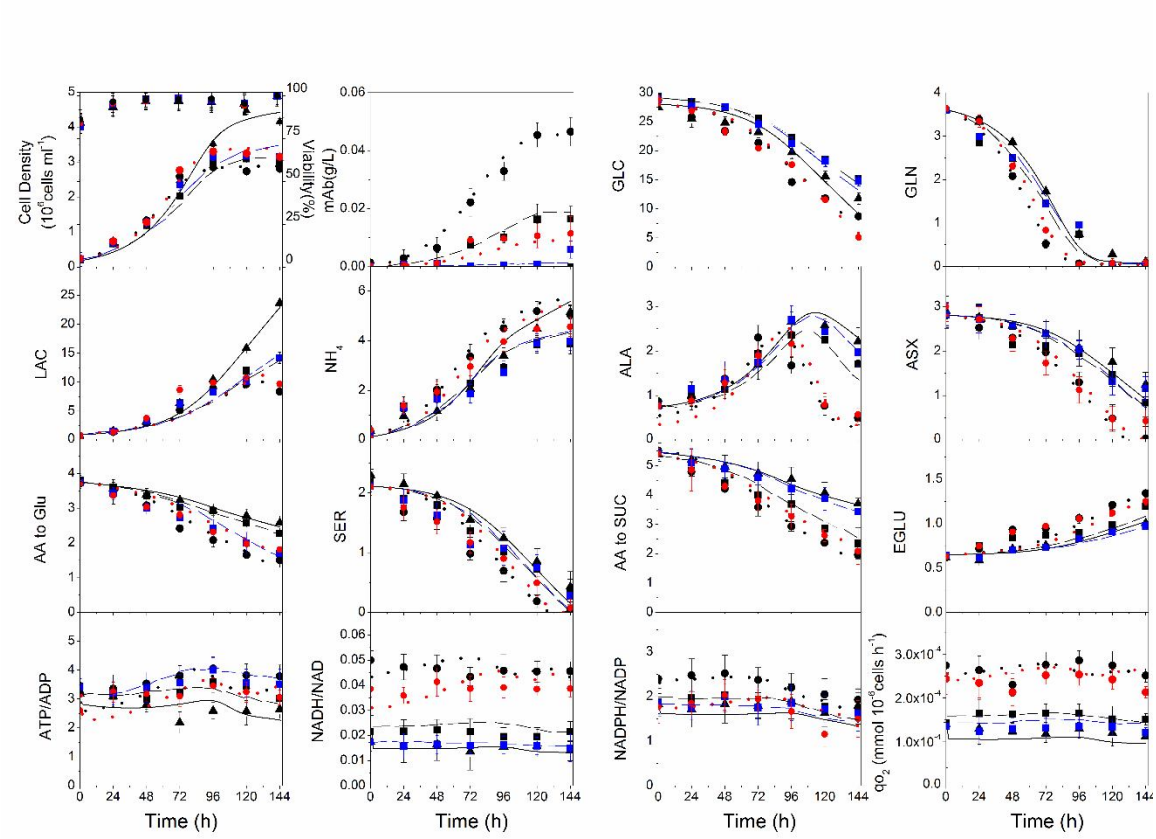

Figure 5.6Simulated and experimental data for parental and induced/non-induced cell lines.

Parental (experimental data: black triangles, simulated data: solid black line), induced low-producer (experimental data: black squares, simulated data: dashed black line), non-induced low producer (experimental data: blue squares, simulated data: dashed blue line), induced high-producer (experimental data: black circles, simulated data: dotted black line), and non-induced high-producer (experimental data: red circles, simulated data: dotted red line).

5.7 Discussion

5.7.1 The kinetic-metabolic model is a reliable *in silico* tool to assess CHO cells clonal variations

Induction of recombinant proteins in microbial cell platforms has been shown to cause an increased energy demand in support to a metabolic burden (Heyland, Blank, & Schmid, 2011a; Heyland et al., 2011b). Unlike microbial cells, the links between cell metabolic load and protein productivity in engineered mammalian cells has yet to be tackled, although some progress has been accomplished with the help of ^{13}C-labeling (Sheikholeslami, Jolicoeur, & Henry, 2013). In this work, an inducible system with a high-producer clone has been selected in order to study an induction effect on CHO cell

metabolic behaviour and load. Towards this goal, the use of an *in silico* platform, made of a kinetic-metabolic model, confers a unique capacity to explore mAbCHO producing cells beyond experimental observations onto which the model has been anchored *a priori*. Therefore, the remaining discussion will be based on the results derived from the developed *in silico* platform.

5.7.2 Clone to clone variations yield more significant metabolic changes than recombinant protein expression

In the previous sections, we reported large differences in behaviour between the low- and the high- producer clones, comparing non-induced and induced cells (Figure 5.6). However, it is of interest to evaluate the source of these differences. The contribution of mAb production is estimated to account for atmost 5% of total carbon uptake by the cells, even for the high-producer clone, and one can expect the *de novo* metabolic load associated to the recombinant proteins to be low compared to the intrinsic one related to endogeneous protein synthesis. This estimate is calculated taking the carbon mass in 1 mol of mAb to the augmentation of the total mass of carbon from cellular growth, considering a specific productivity of ~ 1×10^{-6} mmol 10^{-6} cells h^{-1} and growth rate of ~ 0.04 h^{-1},and assuming a dry cell weight of 350 pg $cell^{-1}$, a cellular molecular weight of 150 g mol^{-1} and the reported elemental formulas for both biomass and mAb (Nolan & Lee, 2010).Therefore, the production capacity is thought not to be limited at the anabolic level, but rather at the protein processing stage (assembly and the folding) (Dinnis et al., 2006). We then used the model to evaluate the effect of cumate induction on the metabolic load, and similar intracellular flux distribution, metabolic fluxes and ratios were found when normalized to their time-corresponding values in non-induced controls (Figure 5.7). Only metabolic fluxes and ratios of major metabolic networks such as glycolysis and TCAare shown.Interestingly, most normalized values of metabolic fluxes and ratios are close to 1 for the high-producer clone, while the low-producer clone exhibits deviations from 0 to 10% for a series of fluxes with +10% for V_{HK}, V_{PGK}, V_{GLNS}, TCA flux and ATP turnover rate. In the case of the high-producer clone, the contribution of glutamine to TCA cycle is lower in the induced culture. Indeed, the higher deviation between the induced and non-induced cells is observed comparing the mAb specific production rates with time, with production rates that are 13 to 8 times higher in the low-

producer clone and 5 to 1 times higher in the high-producer clone. This higher deviation level in the low-producer clone looks surprising but it can be attributed to a higher leakage level of the cumate gene switch in the high-producer clone in the absence of cumate induction (Figure 5.6). Our results, both experimental and from simulations, thus suggest that within our experimental conditions, differences in metabolic pattern caused by clonal variation (Dahodwala et al., 2012) exceeded that induced by recombinant protein expression (Heyland et al., 2011a; Heyland et al., 2011b).

5.7.3 High producer clone selection favors metabolically efficient cell population subsets

5.7.3.1 *The high-producer clone shows a more efficient lactate metabolism*

Model simulations (Figure 5.7) suggest that distinct metabolism of the high-producer clone is simply somehow more favorable for production irrespective of cumate induction. Induced and non-induced high-producer show similar glycolytic rates (V_{HK}, V_{PGK}), glutamine metabolism (V_{GLNS}) and ATP turnover rate for the whole culture duration. However, interestingly, although hexokinase and phosphoglucose isomerase activities are both not affected by cumate induction, lactate dehydrogenase activity shows the lowest values for the high-producer clone, and to a lesser extent for the low-producer clone (Figure 5.8). Lactate production rate for the high-producer clone is lower (-46% at mid exponential phase and -56% at the end of exponential phase)than that for parental (Figure 5.8, Table 5.6). Therefore, although an overflow of glycolytic flux to lactate has been extensively reported under non-limiting glucose conditions (Europa et al., 2006), irrespective to recombinant protein expression, the high-producer CHO cell clone seems to maintain a more efficient metabolic state; a result that is also supported form simulated lower values of lactate production rate-to-glucose consumption rate ratio (Figure 5.9). While a quasi-constant ratio value is maintained for the parental clone, the low-producer also exhibits a decreasing trend, but to a lower extent than for the high-producer. With ratios lower than 1, while literature usually reports a 1-2 range, one can clearly conclude of a respiratory metabolism, coupled to a high feeding rate of intermediates to anabolic reactions.

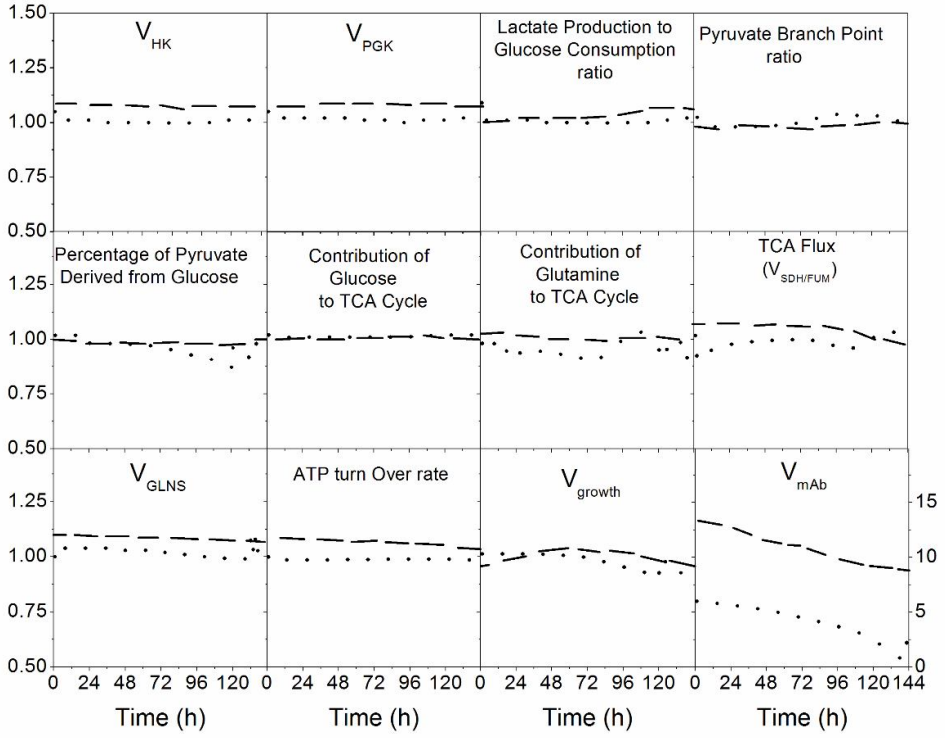

Figure 5.7 Comparison of metabolic fluxes and ratios.
Specific glucose uptake rate (*v(HK*)), glycolytic flux*(v(PK))*, lactate production-to-glucose consumption ratio (*((vf(LDH)-vr(LDH))/v(HK))*, pyruvate branch point as the ratio of the pyruvate influx through TCA cycle divided by the total flux into pyruvate pool ((*v(PDH)+ v(PC)/(v(PK)+v(SDH)+v(ME)+v(AlaTA*)), when the last two fluxes positively fed pyruvare, percentage of pyruvate derived from glucose (*v(PK/(v(PK)+v(SAL)+v(ML-PC)+v(AlaTA*)), Contribution of glucose to TCA cycle as the ratio of pyruvate influx to TCA cycle via *v(PDH)* , considering most of the *v(PDH)* has beenoriginated from*v(PK)*, to the total flux channeled through TCA cycle via its intermediates (*v(PDH)/(v(PDH)+ v(ASTA)+ v(GLDH)+ v(LYSILELEUVALTYRTA)+v(PC))*, Contribution of glutamine to TCA cycle as the ratio of glutamate influx to TCA cycle via *v(GLDH)* to the total flux channeled through TCA cycle via its intermediates (*v(GLDH)/(v(PDH)+v(ASTA)+v(GLDH)+v(LYSILELEUVALTYRTA)+v(PC)))*, Contribution of other amino acids to TCA cycle((*v(LYSILELEUVALTYRTA)+v(ASTA))/(v(PDH)+v(ASTA)+v(GLDH)+v(LYSILEL EUVALTYRTA)+v(PC)))*, TCA cycle flux (*v(SDH/FUM)*), specific glutamine uptake rate (*vf(GLNS)-vr(GLNS*)), ATP turnover rate (*v(PGK)+v(PK)+v(SCOAS)+vr(GlnT)+ vf(CK)+vr(AK)+2P/O ratio*v(resp)), Specific* growth rate *v(growth)*, and specific production rate *v(mAb)*,between induced and non-induced low-producer (dashed line) and high-producer (dotted line) cell lines. The values are defined as the ratio of specific metabolic fluxes (mmol $(10^{6}\text{cells})^{-1}\ h^{-1}$) or ratio in induced cultures to that in the non-induced control cultures at each time point.

Table 5.6Comparison of metabolic fluxes and ratios in parental, induced low-producing and induced high-producing cell lines at 48 h. Same conditions as table 5.5 applied.

Metabolic Flux/Ratio	Parental		Low-producing		High-producing		Significance Level (t- test Result)
	Value	Interval	Value	Interval	Value	Interval	
v_{HK}	7.67E-5	[6.33E-5,9.03E-5]	7.32E-5	[6.11E-5,8.52E-5]	7.66E-5	[6.14E-5,9.18E-5]	—
v_{PGK}	1.35E-4	[8.19E-5,1.88E-4]	1.31E-4	[8.78E-5,1.74E-4]	1.38E-4	[1.08E-4,3E-4]	—
v_{LDH}	8.74E-5	[7.13E-5,1.04E-4]	7.36E-5	[5.68E-5,9.09E-5]	4.49E-5	[2.68E-5,6.30E-5]	$p<0.1^{+}$
v_{PDH}	4.04E-5	[2.64E-5,5.45E-5]	4.86E-5	[3.65E-5,6.08E-5]	7.06E-5	[5.60E-5,8.52E-5]	$p<0.1^{+}$
$v_{SDH/FUM}$	4.90E-5	[3.23E-5,6.57E-5]	6.16E-5	[4.68E-5,7.63E-5]	9.35E-5	[7.65E-5,1.11E-4]	$p<0.1^{+}$
$v_{ME} - v_{PC}$	3.70E-6	[1.73E-6,5.67E-6]	4.72E-6	[2.75E-6,6.69E-6]	-3.57E-6	[-1.86E-6,-5.27E-6]	$p<0.1^{+}$
v_{GLNS}	2.91E-5	[2.05E-5,3.80E-5]	3.89E-5	[2.69E-5,3.89E-5]	3.81E-5	[2.74E-5,4.87E-5]	—
v_{GLDH}	5.27E-7	[2.43E-7,8.11E-7]	3.23E-7	[1.19E-7,5.27E-7]	6.73E-6	[3.29E-6,1.02E-5]	$p<0.1^{+}$
v_{AlaTA}	1.36E-5	[9.46E-6,1.77E-5]	1.61E-5	[1.20E-5,2.02E-5]	2.02E-5	[1.52E-5,2.53E-5]	—
$v_{HISARGTA}$	3.16E-6	[2.14E-6,4.25E-6]	4.38E-6	[3.14E-6,5.62E-6]	4.99E-6	[3.45E-6,6.53E-6]	—
v_{SAL}	5.95E-6	[5.67E-6,6.23E-6]	7.95E-6	[4.37E-6,1.15E-5]	9.71E-6	[6.12E-6,1.33E-5]	—
v_{ATPase}	4.78E-4	[2.13E-4,7.43E-4]	5.51E-4	[2.86E-4,8.16E-4]	9.93E-4	[4.27E-4,1.56E-3]	—
v_{resp}	9.32E-5	[4.99E-5,1.36E-4]	1,44E-4	[1.09E-4,1.79E-4]	2.10E-4	[1.68E-4,2.53E-4]	—
v_{leak}	1.52E-5	[9.06E-6,2.13E-5]	1.75E-5	[8.16E-6,2.68E-5]	2.47E-5	[1.16E-5,3.77E-5]	—
v_{growth}	0.035	[0.031,0.038]	0.028	[0.025,0.031]	0.031	[0.026,0.035]	—
v_{mAb}	-	-	6.43E-7	[5.43E-7,7.43E-7]	3.11E-6	[2.21E-6,9.00E-7]	—
Lactate Production - to - Glucose Consumption	1.07	[0.75,1.39]	0.97	[0.69,1.25]	0.58	[0.43,0.73]	$p<0.1^{+}$
Pyruvate Branch point Ratio	0.26	[0.15,0.36]	0.33	[0.14,0.51]	0.54	[0.37,0.70]	$p<0.1^{+}$
Percentage of Pyruvate Derived from Glucose	84.9	[71,98]	85.42	[68,101]	76.75	[62,91]	—
Contribution of Glucose to TCA Cycle	65.03	[50,79]	61.95	[47,76]	57.05	[41,72]	—

Table 5.6Comparison of metabolic fluxes and ratios in parental, induced low-producing and induced high-producing cell lines at 48 h (Continued)

Metabolic Flux/Ratio	Parental		Low-producing		High-producing		Significance Level (t- test Result)
	Value	Interval	Value	Interval	Value	Interval	
Contribution of Glutamine to TCA Cycle	1.21	[0.83,1.58]	-	-	7	[5.23,8.76]	$p<0.1^{+}$
Contribution of Aminoacids to TCA Cycle	4.89	[2.80,6.97]	14.35	[10.52,18.17]	12.54	[9.45,15.62]	—
Specific ATP Production Rate mmol $(10^6$ cells$)^{-1}h^{-1}$	7.20E-4	[3.69E-4,1.07E-3]	9.36E-4	[4.85E-4,1.38E-3]	1.24E-3	[7.28E-4,1.75E-3]	—
Percentage of ATP Consumption for Biomass Synthesis	7.95	[5.57,10.33]	4.91	[3.03,6.79]	3.91	[2.53,13.81]	—
Percentage of ATP Consumption for mAb Synthesis	-	-	0.28	[0.26,0.31]	1.02	[0.82,1.22]	$p<0.1^{*\ +}$

Table 5.6B Comparison of metabolic fluxes and ratios in parental, induced low-producing and induced high-producing cell lines at 74 h. Same conditions as table 5.5 applied.

Metabolic Flux/Ratio	Parental		Low-producing		High-producing		Significance Level (t- test Result)
	Value	Interval	Value	Interval	Value	Interval	
v_{HK}	7.61E-5	[6.51E-5,8.71E-5]	7.33E-5	[6.42E-5,8.25E-5]	7.73E-5	[6.70E-5,8.75E-5]	—
v_{PGK}	1.35E-4	[9.03E-5,1.80E-4]	1.33E-4	[7.81E-5,1.88E-4]	1.41E-4	[9.16E-5,1.91E-4]	—
v_{LDH}	8.53E-5	[7.20E-5,9.86E-5]	6.85E-5	[5.22E-5,8.48E-5]	3.64E-5	[2.12E-5,5.18E-5]	$p<0.1^{+}$
v_{PDH}	4.15E-5	[2.63E-5,5.67E-5]	5.29E-5	[3.26E-5,7.31E-5]	7.84E-5	[6.62E-5,9.06E-5]	$p<0.1^{+}$
$v_{SDH/FUM}$	5.06E-5	[2.63E-5,5.67E-5]	6.51E-5	[4.79E-5,8.21E-5]	1.01E-4	[8.54E-5,1.17E-4]	$p<0.1^{+}$
$v_{ME} - v_{PC}$	2.51E-6	[1.03E-6,3.99E-6]	3.37E-6	[1.9E-6,4.85E-6]	-4.53E-6	[-2.48E-6,-6.58E-6]	$p<0.1^{+}$
v_{GLNS}	2.48E-5	[1.87E-5,3.09E-5]	3.21E-5	[2.43E-5,3.20E-5]	3.01E-5	[2.33E-5,3.68E-5]	—
v_{GLDH}	-1.41E-6	[-3.4E-7,-2.45E-6]	-1.44E-6	[-1.18E-6,-2.9E-6]	4.75E-6	[3.29E-6,6.20E-6]	$p<0.1^{+}$
v_{AlaTA}	1.38E-5	[1.07E-5,1.68E-5]	1.69E-5	[1.29E-5,2.09E-5]	1.80E-5	[1.50E-5,2.11E-5]	—
$v_{HISARGTA}$	3.01E-6	[1.53E-6,4.49E-6]	4.25E-6	[2.23E-6,6.26E-6]	4.76E-6	[2.61E-6,6.91E-6]	—
v_{SAL}	5.94E-6	[3.38E-6,8.50E-6]	7.92E-6	[5.36E-6,1.05E-5]	9.56E-6	[6.69E-6,1.26E-5]	—
v_{ATPase}	4.89E-4	[2.12E-4,7.64E-4]	5.91E-4	[3.13E-4,8.68E-4]	1.06E-3	[4.62E-4,1.68E-3]	—
v_{resp}	9.53E-5	[5.35E-5,1.37E-4]	1.54E-5	[1.30E-4,1.78E-4]	2.94E-4	[2.15E-4,2.43E-4]	—
v_{leak}	1.52E-5	[1.01E-5,2.04E-5]	1.86E-5	[7.92E-6,2.92E-5]	2.66E-5	[1.03E-5,4.30E-5]	—
v_{growth}	0.03	[0.027,0.032]	0.025	[0.022,0.027]	0.023	[0.021,0.025]	—
v_{mAb}	-	-	5.71E-7	[4.51E-7,6.91E-7]	2.59E-6	[1.79E-6,3.39E-6]	—
Lactate Production - to -Glucose Consumption	1.06	[0.65,1.46]	0.88	[0.56,1.20]	0.47	[0.29,0.65]	$p<0.1^{+}$
Pyruvate Branch pointRatio	0.29	[0.16,0.41]	0.35	[0.14,0.55]	0.55	[0.33,0.76]	$p<0.1^{+}$
Percentage of Pyruvate Derived from Glucose	84.55	[70,98]	84.68	[71,98]	75.44	[62,88]	—
Contribution of Glucose to TCA Cycle	66.02	[50,81]	63.02	[47,78]	59.36	[41,76]	—

Table 5.6B Comparison of metabolic fluxes and ratios in parental, induced low-producing and induced high-producing cell lines at 48 h (Continued)

Metabolic Flux/Ratio	Parental		Low-producing		High-producing		Significance Level (t- test Result)
	Value	Interval	Value	Interval	Value	Interval	
Contribution of Glutamine to TCA Cycle	-	-	-	-	4.47	[2.97,5.96]	$p<0.1^{+}$
Contribution of Aminoacids to TCA Cycle	4.15	[1.92,6.37]	13.44	[10.82,16.05]	11.47	[9.40,13.53]	—
Specific ATP Production Rate mmol $(10^6$ cells$)^{-1}h^{-1}$	7.19E-4	[4.00E-4,1.00E-3]	9.72E-4	[5.21E-4,1.41E-3]	1.32E-3	[7.43E-4,1.89E-3]	—
Percentage of ATP Consumption for Biomass Synthesis	6.86	[3.95,9.77]	4.19	[2.28,6.11]	2.72	[1.81,3.63]	—
Percentage of ATP Consumption for mAb Synthesis	-	-	0.24	[0.14,0.33]	0.81	[0.69,0.91]	$p<0.1^{*\ +}$

5.7.3.2 Anaplerosis/cataplerosis requirements allows for different flux distribution around pyruvate node in the high-producer clone

Lower values for the lactate production rate-to-glucose consumption rate ratio were concomitant to higher fluxes through pyruvate dehydrogenase in high-producer clone. Pyruvate dehydrogenase activity remains almost constant in parental, while it increases of 75% in high-producer and of 45% in low-producer at mid exponential phase (Figure 5.8, Table 5.6). In addition, both pyruvate carboxylase and malic enzyme show non-zero fluxes in all clones (Figure 5.8). Our values agree in the order of magnitude with non-zero values that has been recently obtained for CHO cells using tracer technique (Ahn & Antoniewicz, 2011). These anaplerotic/cataplerotic reactions are known to be important for the replenishment of TCA-cycle intermediates (Lehninger, 1977). Unlike parental and low-producer, the balance *between* these two fluxes favors the formation of oxaloacetate from the beginning of the culture, which implies a higher activity of pyruvate carboxylase and a lower activity of malic enzymes in high-producer clone. Higher efflux of malate out of TCA cycle implies a higher rate for its conversion to pyruvate, and finally to

lactate in parental clone. The latter agrees with higher values of lactate production rate, both observed experimentally and from simulations (Figure 5.8, Table 5.6). In addition, slightly higher values of the NADPH-to-NADP ratio suggest a greater contribution of malic enzyme in both lactate and NADPH production in parental cell line.Moreover,a higher pyruvate carboxylase activity in the high-producer may decrease the available pyruvate pool, which could in fine reduce lactate formation rate. The anaplerotic flux through glutamate dehydrogenase stay moderate in all three cultures, suggesting that acetyl coenzyme A derived from pyruvate is by far the most important intermediate fuelling the TCA cycle. This result is supported by a high glucose contribution to TCA cycle (50-60%) (Figure 5.9, Table 5.6). A higher portion of pyruvate directed to TCA leads to higher values of the pyruvate branch point ratio (+75%) estimated in high-producer, and in low-producer to a lesser extent (Figure 5.9, Table 5.6). While a large fraction of pyruvate enters the TCA cycle (55 to 75%), only 15-35% is converted into lactate in the high-producer clone. A lower value of lactate production-to-glucose consumption rate has been associated to the over-expression of pyruvate dehydrogenase in other animal cells (Fogolín et al., 2004; Irani, Beccaria, & Wagner, 2002). The fraction of pyruvate entering the TCA is noticeably higher compared to values previously reported for other CHO cell lines (Altamirano et al., 2001; Goudar et al., 2010), but they are in agreement with recent reports on low values of lactate production (Sengupta, Rose, & Morgan, 2011) or even showing a net lactate consumption (Ahn & Antoniewicz, 2011). The pyruvate branch point ratio shows an increasing trend in the high-producer clone, with a more active TCA cycle along culture time. Independently of the clone, the flux distribution around the pyruvate branch point suggests that a high proportion of pyruvate is derived directly from glycolysis (~80%) (Figure 5.9, Table 5.6), while the remaining 20% may mainly originate from malic enzyme activity, through the efflux of malate from TCA cycle, and amino acids catabolism. The estimated flux from malate to pyruvate is high at the beginning but this flux drops and stays at a low value as culture progressed (Figure 5.8); a behavior that has also reported recently (Niklas et al., 2011).

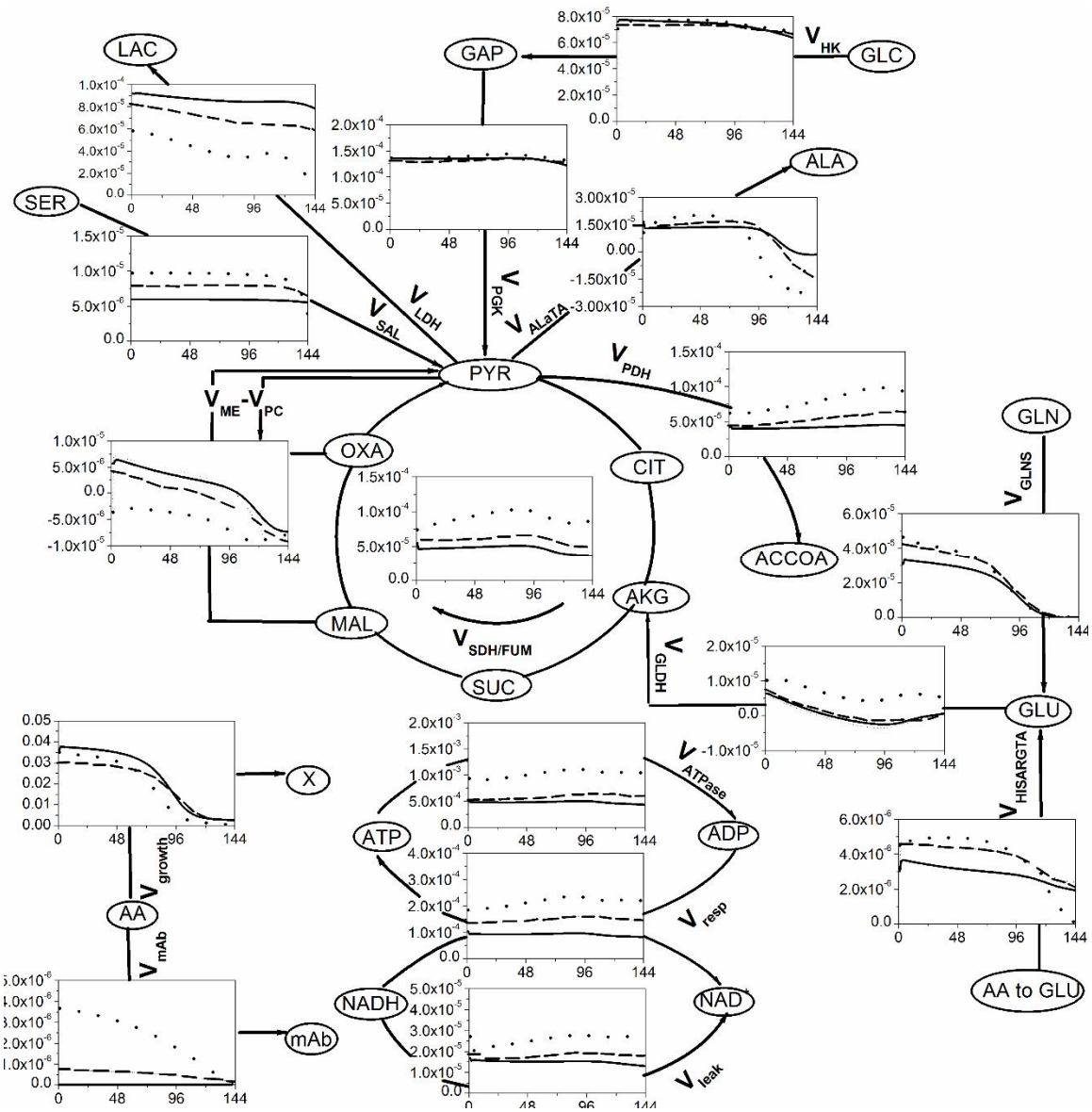

Figure 5.8Selected metabolic fluxes of parental (solid line), induced low-producer (dashed line), and induced high-producer cell lines.
The fluxes (*y*-axis) are given in mmol $(10^6 \text{ cells})^{-1}\ h^{-1}$ and the time (*x*-axis) in days. Negative values indicate fluxes in the opposite direction of the arrow.

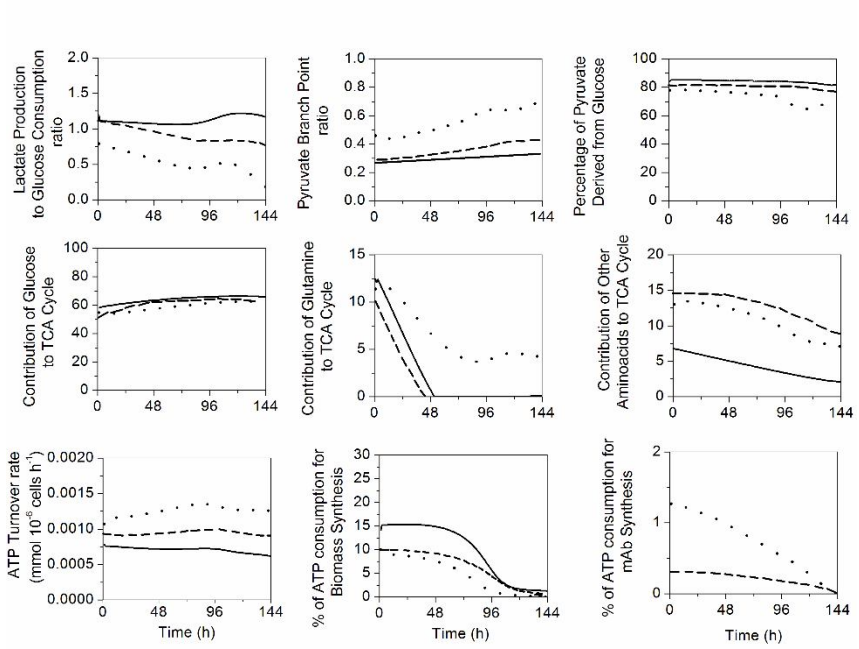

Figure 5.9Comparison of metabolic ratios.
Lactate production-to-glucose consumption ratio (*(vf(LDH)-vr(LDH))/v(HK))*, pyruvate branch point as the ratio of the pyruvate influx through TCA cycle divided by the total flux into pyruvate pool (*v(PDH/(v(PK)+v(SAL)+v(ML-PC)+v(AlaTA*)), when the last two fluxes positively fed pyruvare, percentage of pyruvate derived from glucose ((*v(PK)+ v(PC))/(v(PK)+v(SAL)+v(ML)+v(AlaTA*)), Contribution of glucose to TCA cycle as the ratio of pyruvate influx to TCA cycle via *v(PDH)* , considering most of the *v(PDH)* has beenoriginated from*v(PK),* to the total flux channeled through TCA cycle via its intermediates (*v(PDH)/(v(PDH)+ v(ASTA)+ v(GLDH)+ v(LYSILELEUVALTYRTA)+v(PC))*, Contribution of glutamine to TCA cycle as the ratio of glutamate influx to TCA cycle either via *v(GLDH)* to the total flux channeled through TCA cycle via its intermediates (*v(GLDH) /(v(PDH)+v(ASTA)+v(GLDH)+v(LYSILELEUVALTYRTA)+v(PC)))*, Contribution of other aminoacids to TCA cycle ((*v(LYSILELEUVALTYRTA)+v(ASTA))/(v(PDH)+v(ASTA)+v(GLDH)+ v(LYSILELEUVALTYRTA)+v(PC)))*, ATP turnover rate (*v(PGK)+v(PK*)+*v(SCOAS)+vr(GlnT)+ vf(CK)+vr(AK)+2P/O ratio*v(resp)),* percentage of ATP consumption for biomasssynethesis(*0.00043*3.78*v(growth)/*(*v(LYSILELEUVALTYRTA)+v(ASTA))/(v(PDH)+v(ASTA)+v(GLDH)+v(LYSILELEUVALTYRTA)+v(PC)*),and percentage of ATP consumption for antibody synthesis (*4*v(mAb)/(v(LYSILELEUVALTYRTA)+v(ASTA))/(v(PDH)+v(ASTA)+v(GLDH)+v(LYSILELEUVALTYRTA)+v(PC)*),between parental (solid line), induced low-producer (dashed line) and induced high-producer (dotted line) clones.

5.7.3.3 Ammonia accumulation impaires the contribution of glutamine-metabolism to TCA cycle activity in all clones except in high-producer

Although glutamine has been shown to be the major amino acid catabolized in the TCA cycle (Martens, 2007; Sheikholeslami, Jolicoeur, & Henry, 2013), its contribution to TCA decreases with respect to time to values close to zero at ~48 h for the parental and the low-producer clones only, while it reduces to ~4.5% for the high-producer clone at 72 h for then remaining quasi-constant until the end of the culture (Figures 5.8, 5.9). It even appears that the direction of the glutamate dehydrogenase flux is reversing from an α-ketoglutarate-producing (positive flux) to a glutamate-producing (negative flux) reaction in parental and low-producing cultures. This result suggests that the CHO cell lines under study may redirect the flux through glutamate dehydrogenase when the ammonia concentration increases, since glutamate dehydrogenase provides an alternative for the uptake (i.e. detoxification) of NH_4^+. It was reported in the literature that at 10 Mm NH_4^+ in the medium, the flux was reversed (Bonarius et al., 1998). However, it seems from our experimental data for extracellular ammonia even below that value that the reverse direction of the glutamate dehydrogenase flux is favored. NH_4^+ concentrations staying in the order of magnitude of the Michaelis affinity constant of glutamate dehydrogenase for NH_4^+ (Km_{NH4}) (0.5 to 3.2 mM) may partially explain the low level for the direct contribution of glutamine to TCA cycle, via glutamate dehydrogenase. Interestingly, alanine, which is constantly produced during cell growth, is then consumed after glutamine depletion, and at higher rates for the high-producer, and to a lower extent for the low-producer. The alanine aminotransferase flux even shows to turn negative (Figure 5.8). This also suggests that under low glutamine concentration, a-ketoglutarate is re-channeled to the TCA cycle through aminotransferase, thus maintaining TCA cycle activity. The combined catabolism of all other amino acids represents ~7% (parental) to ~15% (low- and high-producers) of the total carbon metabolized through the TCA cycle (Figure 5.9), entering as either succinate or oxaloacetate. However, this contribution decreases of ~5% with time in the three cultures. The slow increasing contribution of glycolysis (expressed as glucose contribution) to TCA cycle suggests that extracellular glutamine and other amino acids may contribute less with time as they are getting depleted from the culture medium. Further analyzing of both lactate and glutamine profiles reveals that the high-producer clone switches to lactate consumption toward the

end of the culture from glutamine depletion (Figure 5.8). Once glutamine was depleted, lactate was readily consumed presumably to compensate for the reduced glutamine entry to TCA cycle. This also shows that generally, a low contribution of glutamine to TCA cycle may result in a lower net lactate production rate, resulting from a metabolic switch while glucose is still non-limiting, as observed in the high-producer clone and to a lesser extent in the low-producer clone.

5.7.3.4 The high-producer clone showed enhanced TCA cycle activity and ATP turnover rate

Greater pyruvate dehydrogenase and pyruvate carboxylase fluxes provide higher TCA cycle activity in the high-producer compared to the low-producer clone, and to the parental. Concurrently, the high-producer clone exhibits high values of NADH-to-NAD (Figure 5.6). In agreement with this result, high-producer CHO cells were reported to have higher levels of intracellular NADH when compared to low-level producers (Mo et al., 2009). Hence, a higher NADH-to-NAD combined to higher TCA cycle fluxes in the high-producer suggests both active glycolysis and oxidative phosphorylation, meaning an intense production of intermediates as well as of energy. This result is in agreement with a higher ATP turnover rate and as reported in literature that experimental values for that energetic phosphate concentrations remain constant over a range of ATP turnover rates (Beard, 2006). Indeed, cell respiration determined experimentally is well simulated by the model. Interestingly, the analysis of cell respiration rate and oxidative phosphorylation activity (Figure 5.6) reveals that ~15 % of the total oxygen uptake rate is not devoted to ATP-producing purposesbut may be consumed through theproton leak phenomenon in the mitochondria. However, this is still speculative given the large confidence intervals associated with the flux representing ATP production, but it is in agreement with values found in literature (10%-13%) (Harper et al., 2002). Although high-producer cultures undergo metabolism with a high energy yield, the specific cell concentration in ATP stays constant (data not shown) whereas the ATP-to-ADP is similar to that observed in the parental and low-producer cultures (Figure 5.6). This may be due to a higher mitochondrial proton leak in addition to a higher ATP consumption rate by the maintenance processes, which are lumped as ATPas flux in the model. Overall, simulations suggest that biomass synthesis only requires a minor part of ATP production with ~15% (parental), ~10% (low-producer) and ~7% (high-producer) (Figure 5.9, Table

5.6). Recombinant protein synthesis is simulated to consume below 2% of the ATP production rate, respectively for the high- and the low-producer, regularly decreasing until the end of the culture(Figure 5.9, Table 5.6). The major portion of ATP production goes into maintaining catabolic and anabolic reactions, such as endogenous protein synthesis (80%-90%). Thus, as also suggested by Link et al.(2004) (Link et al., 2004) the rate of oxidative phosphorylation, and consequently ATP production rate, may positively affect cell specific productivity but unlike bacterial cells (Heyland et al., 2011b), no direct correlation has been established yet linking the ATP turnover rate and the recombinant protein productivity in CHO cells. A higher ATP production rate may thus favor a better coordination of cellular functions, including enabling a better processing of endogenous proteins as well as of a recombinant protein, *in extensio*. This result correlates with our observation that ATP production rate is similarly elevated in both induced and non-induced high-producer cultures, i.e. independently of the recombinant mAb production rate. Taken together, it is clear both from our experimental data and model simulations, that the higher productivity level of the high-producer clone in recombinant mAb may be a consequence of its higher global metabolic activity. This up-regulation of central carbon metabolism was not a cause or a consequence of protein production but clonal variation since the same result was observed in non-induced cultures. Therefore, one may think the major criterion for a successful clonal selection relies on the identification of clones showing a high metabolic efficiency and activity. In conclusion, this work on the characterization of different CHO mAb cell clones and their parental cell line, brings a wide set of experimental data for extra- and intracellular metabolites concentrations that were used to develop a descriptive and predictive kinetic-metabolic model. An *in silico* platform then enabled to better describe and quantify the metabolic differences resulting from CHO cells clonal variability. Such platform represents a valuable tool for cell line selection, as well as bioprocess development, but it may have also interesting applications in biomedical and medical applications.

5.8 Acknowledgements

The authors wish to thank Dr. Patrick Benoist and Dr. Patrick Daoust of Viropro International Inc. (Montreal, Quebec, Canada) for providing the cell lines employed in this study.

5.9 References

Ahn, W. S., & Antoniewicz, M. R. (2011). Metabolic flux analysis of CHO cells at growth and non-growth phases using isotopic tracers and mass spectrometry. *Metabolic Engineering, 13*(5), 598-609.

Alete, D. E., Racher, A. J., Birch, J. R., Stansfield, S. H., James, D. C., & Smales, C. M. (2005). Proteomic analysis of enriched microsomal fractions from GS-NS0 murine myeloma cells with varying secreted recombinant monoclonal antibody productivities. *Proteomics 5*(18), 4689-4704.

Altamirano, C., Illanes, A., Casablancas, A., Gamez, X., Cairo, J. J., & Godia, C. (2001). Analysis of CHO cells metabolic redistribution in a glutamate-based defined medium in continuous culture. *Biotechnology Progress, 17*(6), 1032-1041.

Beard, D. A. (2006). Modeling of oxygen transport and cellular energetics explains observations on in vivo cardiac energy metabolism. *PLoS Computational Biology, 2*(9), 1093-1097.

Bebbington, C. R., Renner, G., Thomson, S., King, D., Abrams, D., & Yarranton, G. T. (1992). High-level expression of a recombinant antibody from myeloma cells using a glutamine synthetase gene as an amplifiable selectable marker. *Biotechnology (NY), 10*(2), 169-175.

Bi, J. X., Shuttleworth, J., & Al-Rubeai, M. (2004). Uncoupling of cell growth and proliferation results in enhancement of productivity in p21CIP1-arrested CHO cells. *Biotechnology and Bioengineering 85*(7), 741-749.

Bonarius, H. P., Houtman, J. H., de Gooijer, C. D., Tramper, J., & Schmid, G. (1998). Activity of glutamate dehydrogenase is increased in ammonia-stressed hybridoma cells. *Biotechnology and Bioengineering, 57*(4), 447-453.

Chang, A., Scheer, M., Grote, A., Schomburg, I., & Schomburg, D. (2009). BRENDA, AMENDA and FRENDA the enzyme information system: new content and tools in 2009. *Nucleic Acids Research 37(Database issue):D588–D592*.

Chusainow, J., Yang, Y. S., Yeo, J. H., Toh, P. C., Asvadi, P., Wong, N. S., & Yap, M. G. (2009). A study of monoclonal antibody-producing CHO cell lines: what makes a stable high producer? . *Biotechnology and Bioengineering, 102*(4), 1182-1196.

Clarke, G. D. (1965). Variations in the tumour-forming capacity of a line of rat fibroblasts (16C) following selection in vitro. *British Journal of Cance,r 19*(4), 840-854.

Dahodwala, H., Nowey, M., Mitina, T., & Sharfstein, S. T. (2012). Effect of clonal variation in growth, metabolism, and productivity in response to trophic factor stimulation: a study of Chinese hamster ovary cells. *Cytotechnology, 64*(1), 27-41.

Davies, S. L., Lovelady, C. S., Grainger, R. K., Racher, A. J., Young, R. J., & James, D. C. (2012). Functional heterogeneity and heritability in CHO cell populations. *Biotechnology and Bioengineering, 110*(1), 260-274.

Dean, J., & Reddy, P. (2013). Metabolic analysis of antibody producing CHO cells in fed-batch production. *Biotechnology and Bioengineering, 110*(6), 1735-1747. doi: 10.1002/bit.24826

Dinnis, D. M., Stansfield, S. H., Schlatter, S., Smales, C. M., Alete, D., Birch, J. R., . . . James, D. C. (2006). Functional proteomic analysis of GS-NS0 murine myeloma cell lines with varying recombinant monoclonal antibody production rate. *Biotechnology and Bioengineering, 94*(5), 830-841.

Dorka, P., Fischer, C., Budman, H., & Scharer, J. M. (2009). Metabolic flux-based modeling of MAb production during batch and fed-batch operations. *Bioprocess and Biosystems Engineering, 32*(2), 183-196.

Durocher, Y., & Butler, M. (2009). Expression systems for therapeutic glycoprotein production. *Current Opinion in Biotechnology, 20*(6), 700–707.

Eppink, M. H. M., Schreurs, R., Gusen, A., & Verhoeven, K. (2009). Platform technology for developing purification processes. *Biopharm International, 20*, 44.

Europa, A. F., Gambhir, A., Fu, P. C., & Hu, W. S. (2006). Multiple steady states with distinct cellular metabolism in continuous culture of mammalian cells. *Biotechnology and Bioengineering, 67*(1), 25-34.

Fogolín, M. B., Wagner, R., Etcheverrigaray, M., & Kratje, R. (2004). Impact of temperature reduction and expression of yeast pyruvate carboxylase on hGM-CSF-producing CHO cells. *Journal of Biotechnolology, 109*(1-2), 179-191.

Gaillet, B., Gilbert, R., Broussau, S., Pilotte, A., Malenfant, F., Mullick, A., . . . Massie, B. (2010). High-level recombinant protein production in CHO cells using lentiviral vectors and the cumate gene-switch. *Biotechnology and Bioengineering ,106*(2), 203-215.

Ghorbaniaghdam, A., Henry, O., & Jolicoeur, M. (2012). A kinetic-metabolic model based on cell energetic state: study of CHO cell behavior under Na-butyrate stimulation. *Bioprocess and Biosystems Engineering, 36*(4), 469-487.

Goudar, C., Biener, R., Boisart, C., Heidemann, R., Piret, J., de Graaf, A., & Konstantinov, K. (2010). Metabolic flux analysis of CHO cells inperfusion culture by metabolite balancing and 2D [13C,1H] Cosy NMR spectroscopy. *Metabolic Engineering, 12*(2), 138-149.

Harper, M. E., Antoniou, A., Bevilacqua, L., Bezaire, V., & Monemdjou, S. (2002). Cellular energy expenditure and the importance of uncoupling. *Journal of Animal Science, 80*(E. Suppl. 2), E90-E97.

Hayduk, E. J., Choe, L. H., & Lee, K. H. (2004). A two dimentional electrophoresis map of Chinese hamster ovary cell proteins based on fluorescence staining. *Electrophoresis, 25*(15), 2545–2556.

Hayduk, E. J., & Lee, K. H. (2005). Cytochalasin D can improve heterologous protein productivity in adherent Chinese hamster ovary cells. *Biotechnology and Bioengineering 90*(3), 354–364.

Heyland, J., Blank, L. M., & Schmid, A. (2011a). Quantification of metabolic limitations during recombinant protein production in Escherichia coli. *Journal of Biotechnology, 155*(2), 178-184.

Heyland, J., Fu, J., Blank, L. M., & Schmid, A. (2011b). Carbon metabolism limits recombinant protein production in Pichia pastoris. *Biotechnology and Bioengineering, 108*(8), 1942-1953. doi: 10.1002/bit.23114

Irani, N., Beccaria, A. J., & Wagner, R. (2002). Expression of recombinant cytoplasmic yeast pyruvate carboxylase for the improvement of the production of human erythropoietin by recombinant BHK-21 cells. *Journal of Biotechnology 93*(3), 269-282.

Kim, N. S., Byun, T. H., & Lee, G. M. (2001). Key determinants in the occurrence of clonal variation in humanized antibody expression of CHO cells during dihydrofolate reductase mediated gene amplification. *Biotechnology Progress, 17*(1), 69-75.

Konrad, M. W., Storrie, B., Glaser, D. A., & Thompson, L. H. (1977). Clonal variation in colony morphology and growth of CHO cells cultures on agar. *Cell, 10*(2), 305-312.

Lamboursain, L., St-Onge, F., & Jolicoeur, M. (2002). A lab-respirometer for plant and animal cell culture. *Biotechnology Progress 8*(6), 1377-1386.

Lee, Y. Y., Wong, K. T., Tan, J., Toh, P. C., Mao, Y., Brusic, V., & Yap, M. G. (2009). Overexpression of heat shock proteins (HSPs) in CHO cells for extended culture viability and improved recombinant protein production. *Journal of Biotechnology 143*(1), 34-43.

Lehninger, A. L. (1977). *Biochemistry*. Worth: New York.

Li, F., Vijayasankaran, N., Shen, A., Kiss, R., & Amanullah, A. (2010). Cell culture processes for monoclonal antibody production. *MAbs, 2*(5), 466-477.

Link, T., Bäckström, M., Graham, R., Essers, R., Zörner, K., Gätgens, J., . . . Noll, T. (2004). Bioprocess development for the production of a recombinant MUC1 fusion protein expressed by CHO-K1 cells in protein-free medium. *Journal of Biotechnology,110*(1), 51-62.

Mailier, J., Delmotte, A., Cloutier, M., Jolicoeur, M., & Vande Wouwer, A. (2011). Parametric sensitivity analysis and reduction of a detailed nutritional model of plant cell cultures. *Biotechnology and Bioengineering, 108*(5), 1108-1118.

Martens, D. E. (2007). Metabolic Flux Analysis of Mammalian Cells. In M. Al-Rubeai & M. Fussenegger (Eds.), *Systems Biology* (Vol. 5, pp. 275-299): Springer Netherlands.

Metallo, C. M., Walther, J. L., & Stephanopoulos, G. (2009). Evaluation of 13C isotopic tracers for metabolic flux analysis in mammalian cells. *Journal of Biotechnology, 144*(3), 167-174.

Mo, M. L., Palsson, B. O., & Herrgård, M. J. (2009). Connecting extracellular metabolomic measurements to intracellular flux states in yeast. *BMC Systems Biology, 3*, 37.

Mullick, A., Xu, Y., Warren, R., Koutroumanis, M., Guilbault, C., Broussau, S., . . . Massie, B. (2006). The cumate gene-switch: a system for regulated expression in mammalian cells. *BMC Biotechnology, 6*(43).

Naderi, S., Meshram, M., Wei, C., McConkey, B., Ingalls, B., Budman, H., & Scharer, J. (2011). Development of a mathematical model for evaluating the dynamics of normal and apoptotic Chinese hamster ovary cells. *Biotechnology Progress, 27*(5), 1197-1205.

Niklas, J., Schräder, E., Sandig, V., Noll, T., & Heinzle, E. (2011). Quantitative characterization of metabolism and metabolic shifts during growth of the new

human cell line AGE1.HN using time resolved metabolic flux analysis. *Bioprocess and Biosystems Engineering, 34*(5), 533-545.

Nissom, P. M., Sanny, A., Kok, Y. J., Hiang, Y. T., Chuah, S. H., Shing, T. K., . . . Philp, R. (2006). Transcriptome and proteome profiling to understanding the biology of high productivity CHO cells. *Moleclular Biotechnology 34*(2), 125-140.

Nolan, R. P., & Lee, K. (2010). Dynamic model of CHO cell metabolism. *Metabolic Engineering, 13*(1), 108-124.

Oh, M. K., Scoles, D. R., Haipek, C., Strand, A. D., Gutmann, D. H., Olson, J. M., & Pulst, S. M. (2003). Genetic heterogeneity of stably transfected cell lines revealed by expression profiling with oligonucleotide microarrays. *The Journal of Cellular Biochemistry, 90*(5), 1068–1078.

Pavlou, A. K., & Belsey, M. J. (2005). The therapeutic antibodies market to 2008. *European Journal of Pharmaceutics and Biopharmaceutics, 59*(3), 389-396.

Peterson, J. A. (1976). Clonal variation in albumin messenger RNA activity in hepatoma cells. *Proceedings of the National Academy of Sciences of the United States of America*
6(6), 2056-2060.

Reich, J. G., & Sel'Kov, E. E. (1981). *Energy metabolism of the cell - a theoritical treatise*. London: Academic.

Sengupta, N., Rose, S. T., & Morgan, J. A. (2011). Metabolic Flux Analysis of CHO Cell Metabolism in the Late Non-Growth Phase. *Biotechnology and Bioengineering, 108*(1), 82-92.

Seth, G., Philp, R. J., Lau, A., Jiun, K. Y., Yap, M., & Hu, W. S. (2007). Molecular portrait of high productivity in recombinant NS0 cells. *Biotechnology and Bioengineering 97*(4), 933-951

Sheikholeslami, Z., Jolicoeur, M., & Henry, O. (2013). Probing the metabolism of an inducible mammalian expression system using extracellular isotopomer analysis. *Journal of Biotechnology, 164*(4), 469-478.

Shukla, A. A., Hubbard, B., Tressel, T., Guhan, S., & Low, D. (2007). Downstream processing of monoclonal antibodies—application of platform approaches *Journal of Chromatography B, 848*(1), 28-39.

Smales, C. M., Dinnis, D. M., Stansfield, S. H., Alete, D., Sage, E. A., Birch, J. R., . . . James, D. C. (2004). Comparative proteomic analysis of GS-NS0 murine myeloma cell lines with varying recombinant monoclonal antibody production rate. *Biotechnology and Bioengineering, 88*(4), 474-488.

Templeton, N., Dean, J., Reddy, P., & Young, J. D. (2013). Peak antibody production is associated with increased oxidative metabolism in an industrially relevant fed-batch CHO cell culture. *Biotechnology and Bioengineering, 110*(7), 2013-10204.

Yoon, S. K., Hwang, S. O., & Lee, G. M. (2004). Enhancing Effect of Low Culture Temperature on Specific Antibody Productivity of Recombinant Chinese Hamster Ovary Cells: Clonal Variation. *Biotechnology Progress, 20*(6), 1683-1688.

Zagari, F., Jordan, M., Stettler, M., Broly, H., & Wurm, F. M. (2013). Lactate metabolism shift in CHO cell culture: the role of mitochondrial oxidative activity. *New Biotechnology, 30*(2), 238-245.

Zamorano, F., Vande Wouwer, A., Jungers, R. M., & Bastin, G. (2012). Dynamic metabolic models of CHO cell cultures through minimal sets of elementary flux modes. *Journal of Biotechnology 146*(3), 409-422.

Zdzienicka, M., Cupido, M., & Simons, J. W. (1985). Increase in clonal variation in Chinese hamster ovary cells after treatment with mutagens. *Somatic Cell and Molecular Genetics, 11*(2), 127-134.

Zomorrodi, A. R., Suthers, P. F., Ranganathan, S., & Maranas, C. D. (2012). Mathematical optimization applications in metabolic networks. *Metabolic Engineering, 14*(6), 672-686.

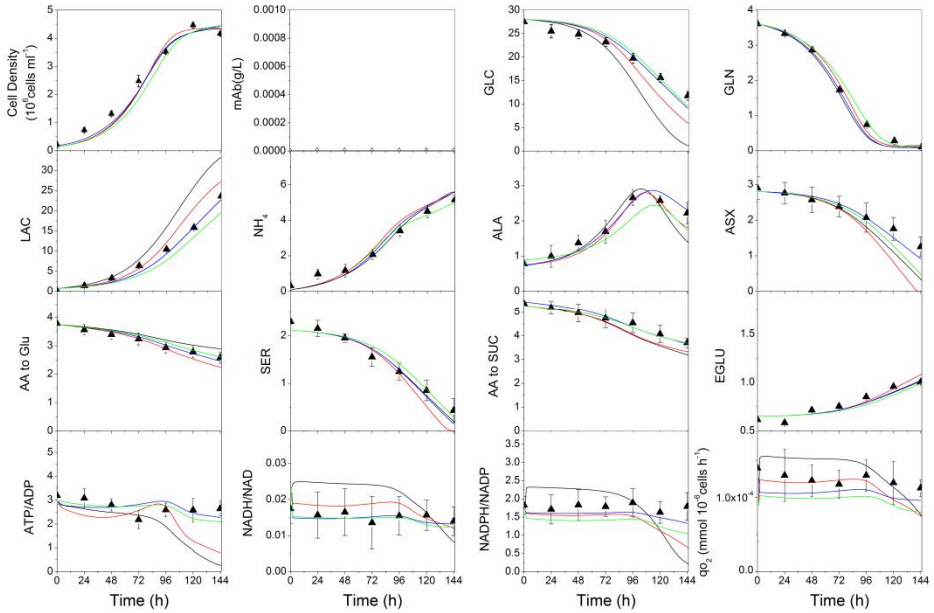

Figure 5.10(Supplementary) Comparison of model simulations with regard to enzymatic regulation for parental culture for extracellular and energetic metabolites.
Same conditions as in figure 5.2 applied.

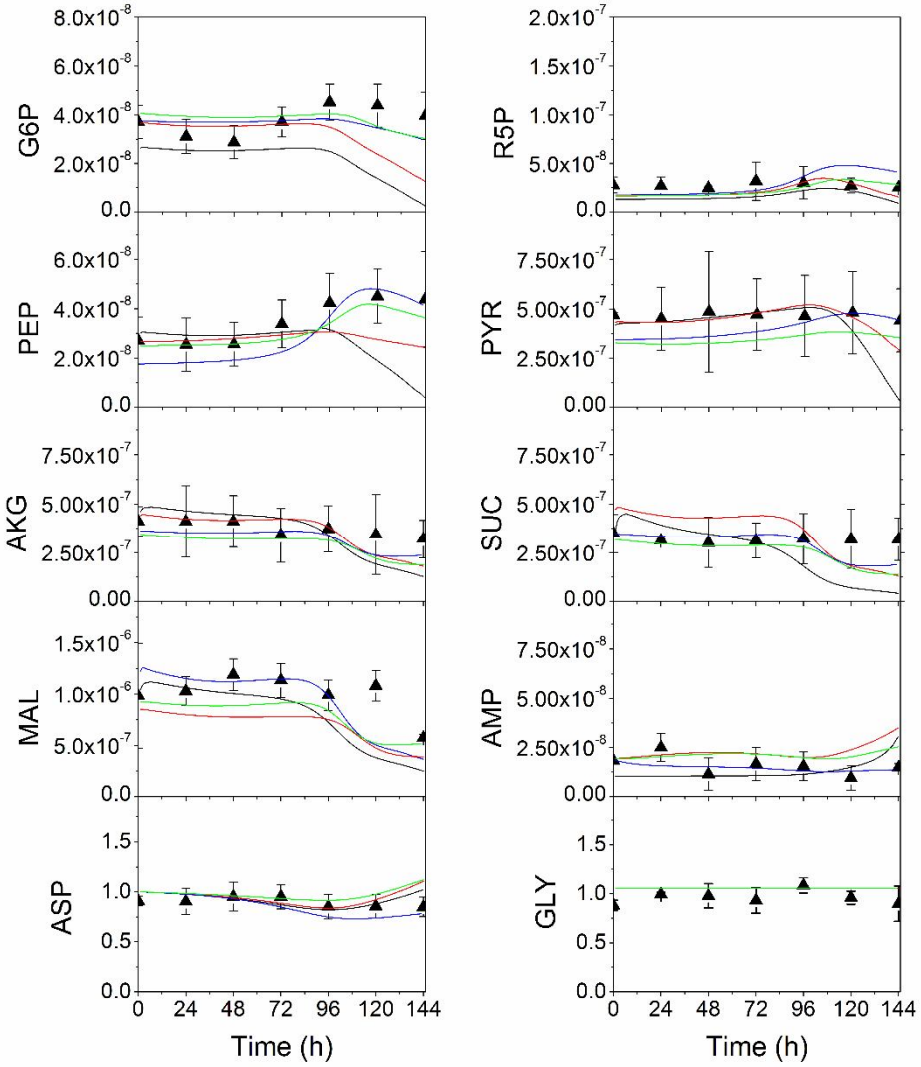

Figure 5.11(Supplementary) Comparison of model simulations with regard to enzymatic regulation for parental culture for intracellular metabolites.
Same conditions as in figure 5.2 applied.

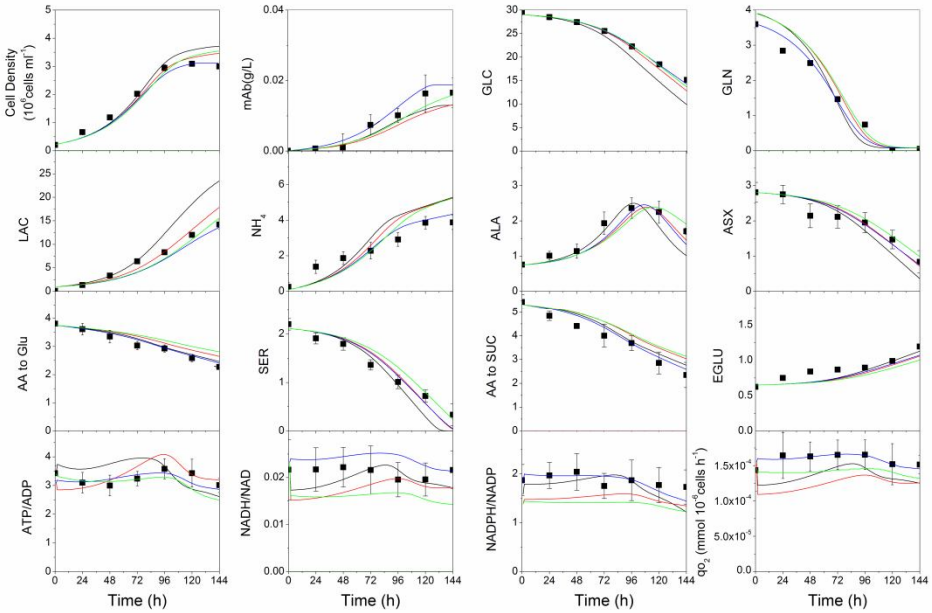

Figure 5.12(Supplementary) Comparison of model simulations with regard to enzymatic regulation for induced low-producing culture for extracellular and energetic metabolites. Same conditions as in figure 5.2 applied.

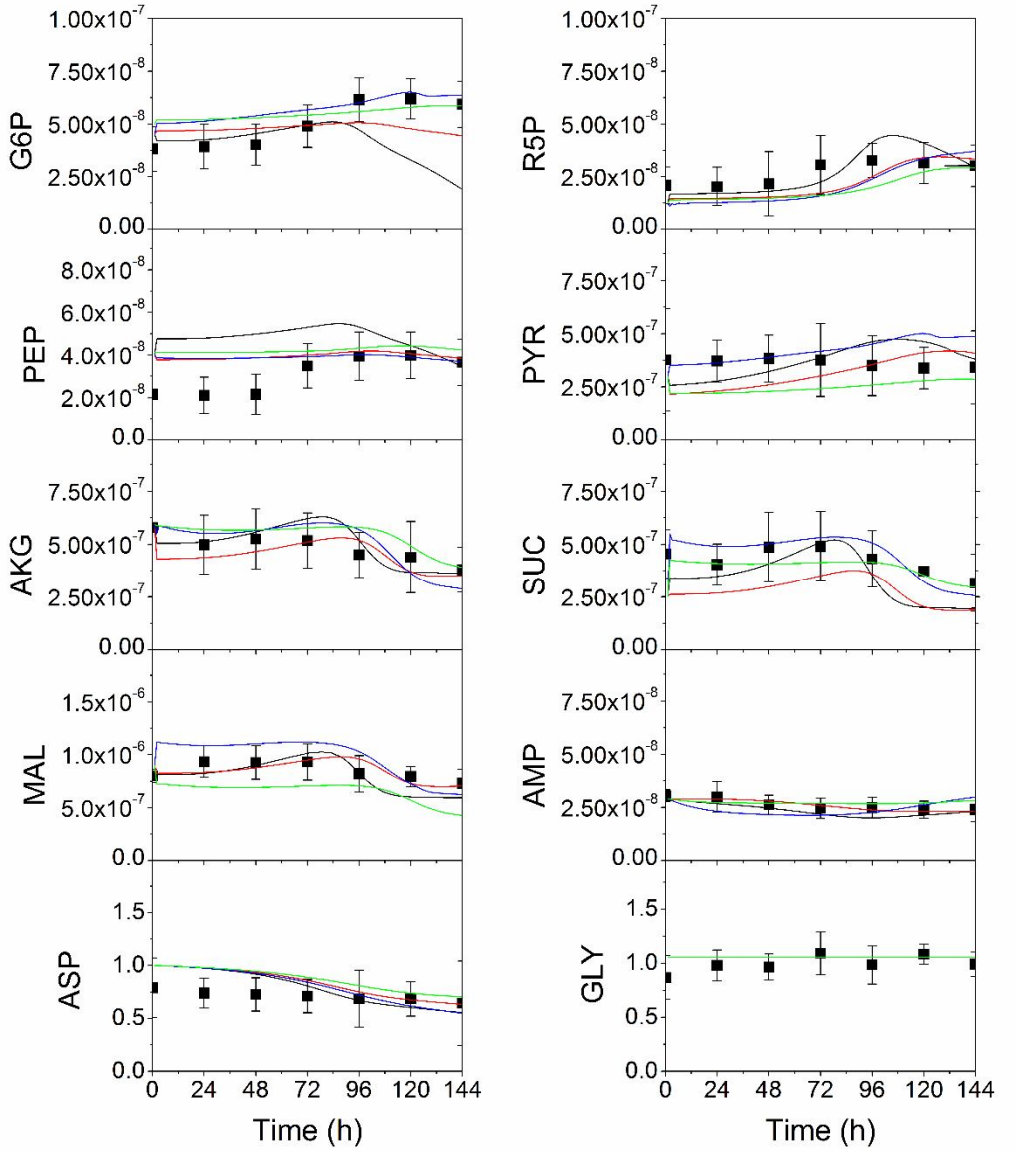

Figure 5.13 (Supplementary) Comparison of model simulations with regard to enzymatic regulation for induced low-producing culture for intracellular variables.
Same conditions as figure 5.2 applied.

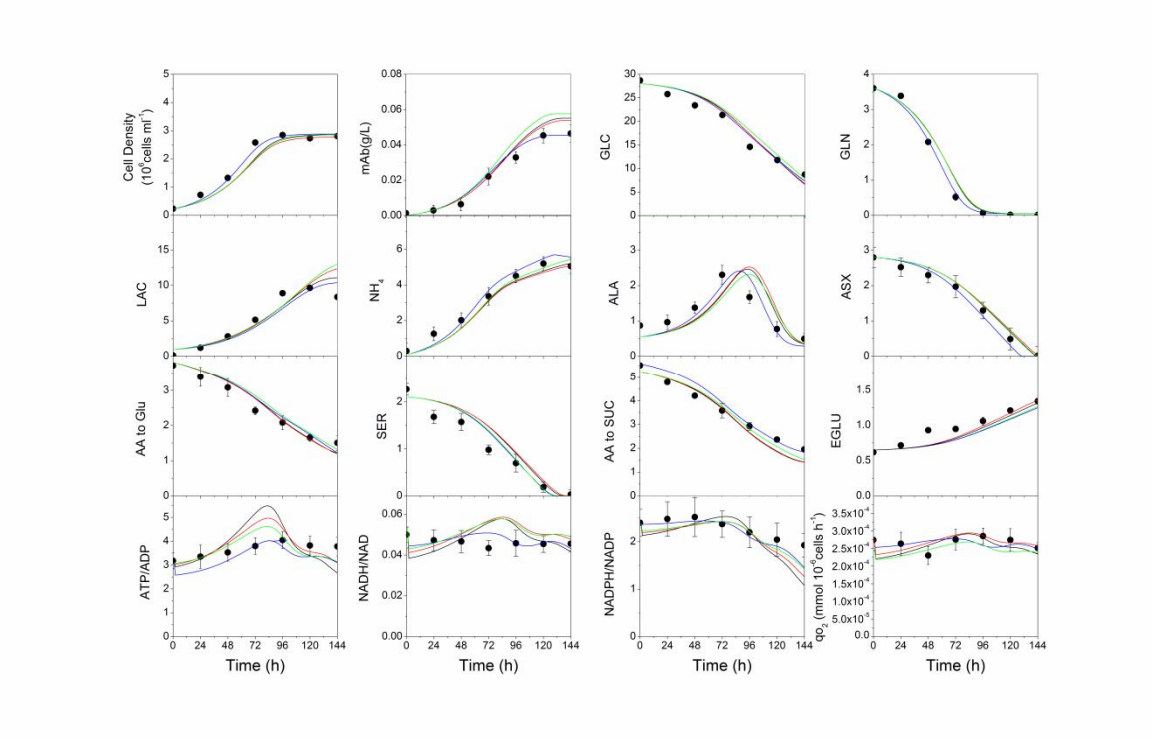

Figure 5.14(Supplementary) Comparison of model simulations with regard to enzymatic regulation for induced high-producing culture for extracellular and energetic metabolites. Same conditions as in figure 5.2 applied.

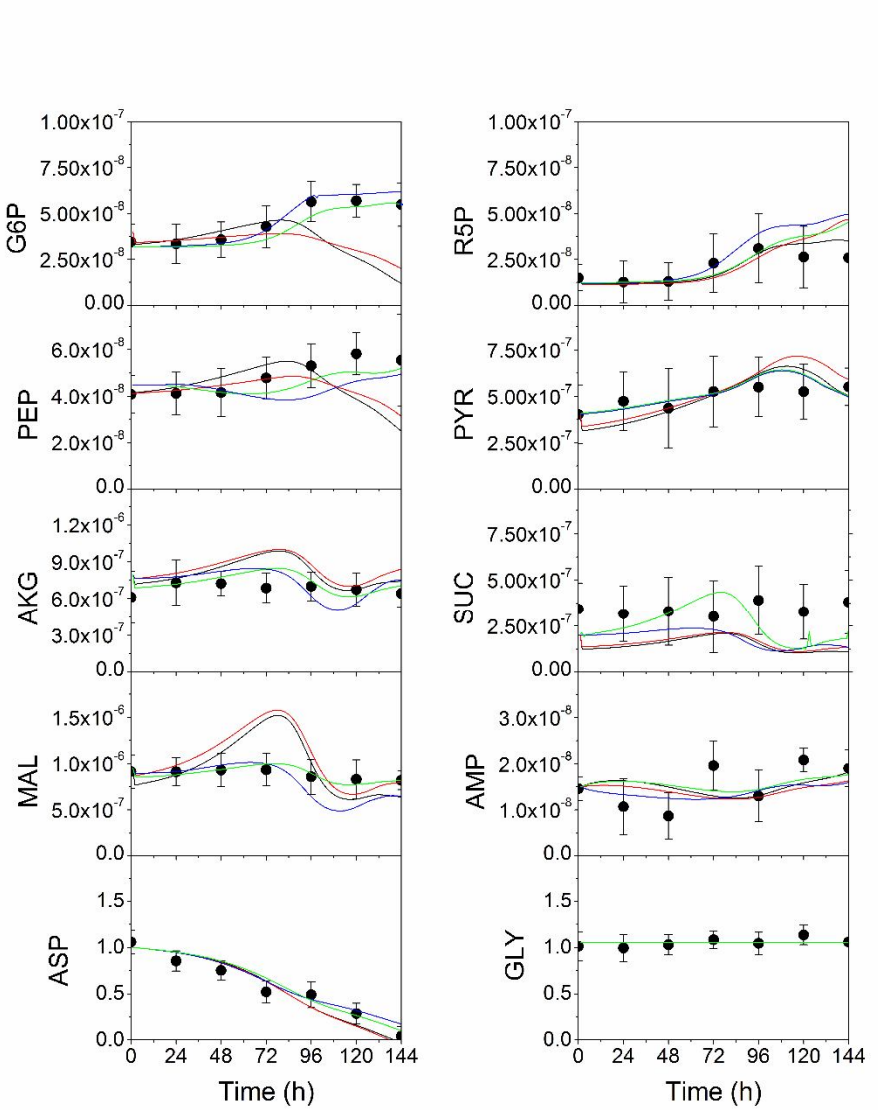

Figure 5.15 **(**Supplementary) Comparison of model simulations with regard to enzymatic regulation for induced high-producing culture for intracellular metabolites.
Same conditions as in figure 5.2 applied.

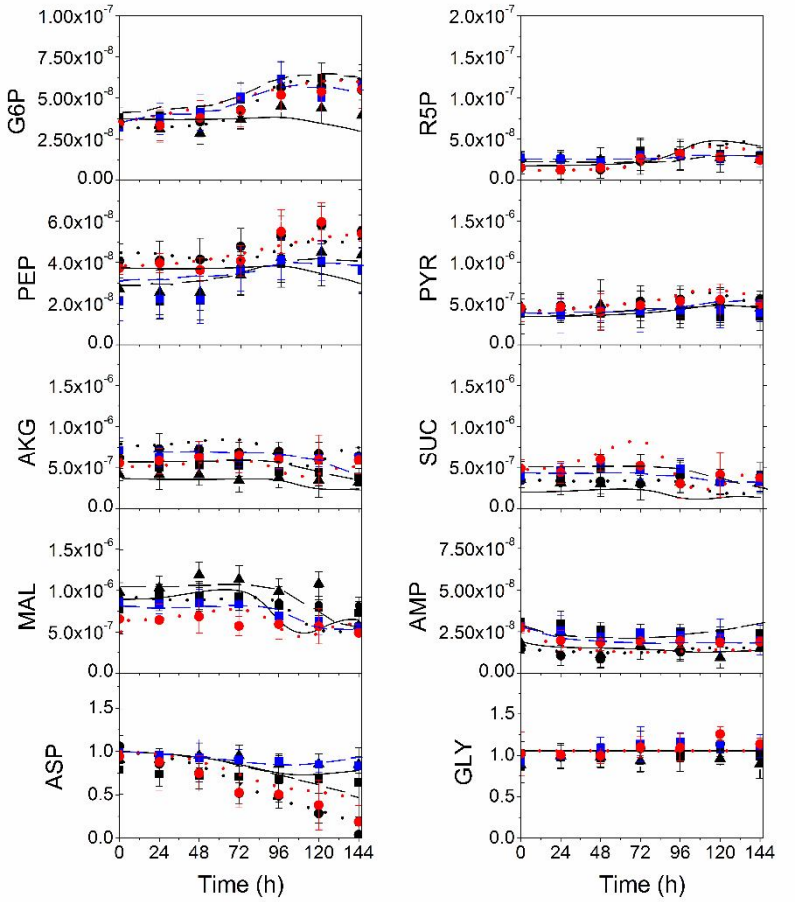

Figure 5.16 (Supplementary) Simulated and experimental data for parental, induced low-producer, non-induced low producer, induced high-producer, and non-induced high-producer.
Parental: experimental data: black triangles, simulated data: solid black line, induced low-producer: experimental data: black squares, simulated data: dashed black line, non-induced low producer: experimental data: blue squares, simulated data: dashed blue line, induced high-producer: experimental data: black circles, simulated data: dotted black line, and non-induced high-producer: experimental data: red circles, simulated data: dotted red line cell lines.

CHAPTER 6 AN IN-SILICO STUDY OF THE REGULATION OF CHO CELLS GLYCOLYSIS

Atefeh Ghorbaniaghdam[1], Olivier Henry[2], Mario Jolicoeur[1,*]

[1]Canada Research Chair in Applied Metabolic Engineering,

[2]Department of Chemical Engineering, École Polytechnique de Montréal,

P.O. box 6079, Centre-ville Station, Montréal, Québec, H3C 3A7, Canada

*Corresponding author: mario.jolicoeur@polymtl.ca

(Submitted to the Journal of Theoretical Biology)

6.1 Presentation of the article

In line with the general purpose of this work to describe CHO cells culture, we here attempted to elucidate the regulatory background of metabolism. This was translated to the question that to what extent our modeling approach can be used to dynamically describe the contribution of regulatory mechanisms involved in the glycolysis pathway. The model is used to design an in silico experiment to impose a sudden change in CHO cell culture with a hypoxic shock. Combining model simulations with available biological knowledge, we were able to comment on the capacity of this modeling framework to describe the regulation of cell metabolism.

6.2 Abstract

In this work, a kinetic metabolic model previously developed for CHO cells is used to study glycolysis regulation. The model is assessed for its biological relevance by analyzing its ability to simulate metabolic events induced following a hypoxic perturbation. Feedback and feedforward regulatory mechanisms known to occur to either inhibit or activate fluxes of glycolysis, are implemented in various combined scenarios and their effects on the metabolic response were analyzed. This study aims at characterizing the role of intermediates of glycolysis and of the cell energetic state, described as the AMP-to-ATP ratio, as inhibitors and activators of glycolysis pathway. In addition to the glycolysis pathway, we here describe the transient metabolic response of pathways that are connected to glycolysis, such as the pentose phosphate pathway, TCA cycle, cell energetic state, glutamine and amino acids metabolisms. Taken individually, each regulatory mechanism leads to an oscillatory behaviour in response to a hypoxic perturbation, while their combination clearly damps oscillations. However, only the addition of the cell energetic state to the regulatory mechanisms results in a non-oscillating response leading to metabolic flux rate rearrangement corresponding to the anaerobic metabolism expected to prevail under hypoxic conditions. We thus demonstrate in this work, from model simulations, that the robustness of a cell energetic metabolism can be described from a combination of feedback and feedforward inhibition and activation regulatory mechanisms of glycolysis fluxes, involving intermediates of glycolysis and the cell energetic state itself.

*Keywords:*metabolic regulation, hypoxic stress, kinetic metabolic model, glycolysis, CHO cells

6.3 Introduction

Phenotypic characteristics of mammalian cells, such as Chinese hamster ovary cells (CHO), consist of an integrated output of regulatory processes occurring at various interconnected functional levels, including the genome, the transcriptome, the proteome and the metabolome (Cascante et al., 2002). This complex system can now be tractable thanks to the use of multi "omics" technologies, which, however, generate an impressive amount of data that are still difficult to be comprehensively understood. Although restricted to the effective expression of the cell system, metabolomic studies have allowed characterizing highly interconnected and regulated cellular metabolic networks (Grimbs , Selbig , Bulik, Holzhutter, & Steuer, 2007), under various culture conditions (Riehl & Segrè, 2008). In this context, metabolic flux analysis (MFA) and metabolic flux balance analysis (MFBA) approaches have been widely used to allow the estimation of metabolic flux distribution. Moreover, metabolic control analysis (MCA) approach allows identifying control points in a metabolic network, based on experimental data obtained after genetically re-engineering a cell metabolic capacity. Significant improvements in the performance of various biosystems have then been realized by applying MFA (Altamirano et al., 2006; Feist & Rosenbloom, 2011; Wilkens, Altamirano, & Gerdtzen, 2011; Zamorano, Wouwer, & Bastin, 2010) , MFBA (Martínez et al., 2013; Savinell & Palsson, 1992) and MCA (Almaas et al., 2004; Wang, Birol, & Hatzimanikatis, 2004) approaches. However, although highly useful to identify flux redistribution (MFA), optimal solution for flux rates (MFBA) and metabolic network control (MCA), these approaches were developed to draw a precise picture of a cell metabolic steady-state at a given time. Indeed, production bioprocesses using a mammalian cell platform normally include defined perturbations from the use of chemical additives (Kumar, Gammell, & Clynes, 2007), inducible promoters (Mullick et al., 2006) or a transient transfection strategy (Durocher, Perret, & Kamen, 2002; Pham, Kamen, & Durocher, 2006). Therefore, since steady-state conditions rarely prevail in biological processes, some modelling approaches now include the description of flux kinetics (Gallazo & Bailey, 1990; Hatzimanikatis, Floudas, & Bailey, 1996; Starbuck & Lauffenburger, 1992). Mathematical modelling approaches are drawing increasing interest, as they offer a complementary tool for characterizing the dynamic properties of

biosystems (D'Alexandri, Scolari, & Ferreira, 2010). Models can also allow to investigate outside the experimental space (Steuer et al., 2006). Indeed, we have developed in previous works a kinetic metabolic model framework that was shown to be adaptable to plant (Cloutier, Perrier, & Jolicoeur, 2007; Valancin et al., 2013) and CHO cells (Ghorbaniaghdam, Henry, & Jolicoeur, 2012), simulating experimental data of transient cell cultures. This model describes central carbon metabolism without accounting, however, for metabolic regulation. In a perspective of enabling a model to predict dynamic behaviours in constantly changing environments, it is thus crucial that it includes regulatory mechanisms governing metabolic homeostasis (Kitano, 2002). Indeed, cells have developed various regulation mechanisms for adapting to sudden changes in their environment, with the major aim of maintaining a capacity to continuously extract energy from available resources. In that context, oxygen has a specific role because it acts, in many cell types, as the final electron acceptor driving ATP turnover along the respiratory chain (Solomon, Berg, & Martin, 2005). Glycolysis is thus a key pathway while being the entry point of the major carbon sources, such as glucose, as well as generating intermediates that are feeding most of the anabolic pathways including TCA, which directly supports respiration. The mechanisms allowing the regulation of a cell energetic metabolism with regard to the availability of oxygen are well described in literature, including the establishment of anaerobic glycolysis following hypoxic conditions (Frezza et al., 2011). Therefore, in this work, we have challenged our model with a hypoxic perturbation and assessed its ability to describe this well documented phenomenon by accounting for most probable feedback and feedforward regulatory mechanisms of glycolysis described in literature (Bali & Thomas, 2001; Chandra, Buzi, & Doyle, 2009; Cloutier & Wellstead, 2010; Connett & Sahlin, 1996; Frezza et al., 2011; Korzeniewski & Liguzinski, 2004).

6.4 Methods

6.4.1 The kinetic metabolic model

As mentioned previously, a kinetic metabolic model describing the primary metabolism of CHO cells recently developed was used as a framework for the analysis presented in (Ghorbaniaghdam, Henry, & Jolicoeur, et al., 2012) and Ghorbaniaghdam et al. (2013) (Chapter 5). The complete description of the model, withmass balances, kinetic equations

and hypotheses is given in (Ghorbaniaghdam, Henry, & Jolicoeur, et al., 2012) and in chapter 5 and illustrated in Figure 6.1. Briefly, the model has 46 differential equations, i.e. mass balances on state variables, which are solved using the Matlab software (The MathWorks Inc., Natick, MA, USA). Each flux (reaction rate) is described by a Michaelis-Menten kinetic formulation. The model response was analyzed qualitatively and quantitatively after a step-wise change of the dissolved oxygen concentration. According to previous studies showing that CHO cells oxygen consumption rate is not affected at oxygen concentrations above ~ 20 µM (Froncisz, Lai, & Hyde, 1985; Lai, Hopwood, Hyde, & Lukiewicz, 1982), a step change from 100% to 10% air saturation resulting in a sudden decrease of the dissolved oxygen concentration to 22 µM, was induced at 48 h post inoculation corresponding to the middle of the exponential growth phase (see supplementary material for details) assuming that the cell growth rate will remain similar in normal and hypoxia conditions (Ghorbaniaghdam, Henry, & Jolicoeur, et al., 2012). Oxygen concentration is used in a monod-type relation to evaluate the oxygen consumption rate. Initial parameter values for the inhibition and activation regulatory mechanisms were taken from literature, as indicated in the caption of Table 6.2, and then optimized (see below) for each of the scenarios of regulatory mechanisms studied, keeping with all the other model parameters as identified in a recent work.

6.4.2 Regulatory mechanisms of glycolysis

The regulatory mechanisms involved in glycolysis are described as follows (Figures 6.1). Regulation of hexokinase, phosphoglucose isomerase, pyruvate kinase, and of backward lactatedehydrogenase were considered based on information derived from the literature as detailed in Figure 6.1. Given the importance for the cell to maintain its energetic status (Hardie & Hawley, 2001), regulatory mechanisms related to the AMP-to-ATP ratio were also studied. Activation and inhibition mechanisms of the enzymatic reactions are expressed through negative and positive feedback and feedforward loops, modifying the Michaelis-Menten rate laws as illustrated in Table 1 (Heinrich & Papoport, 1977).

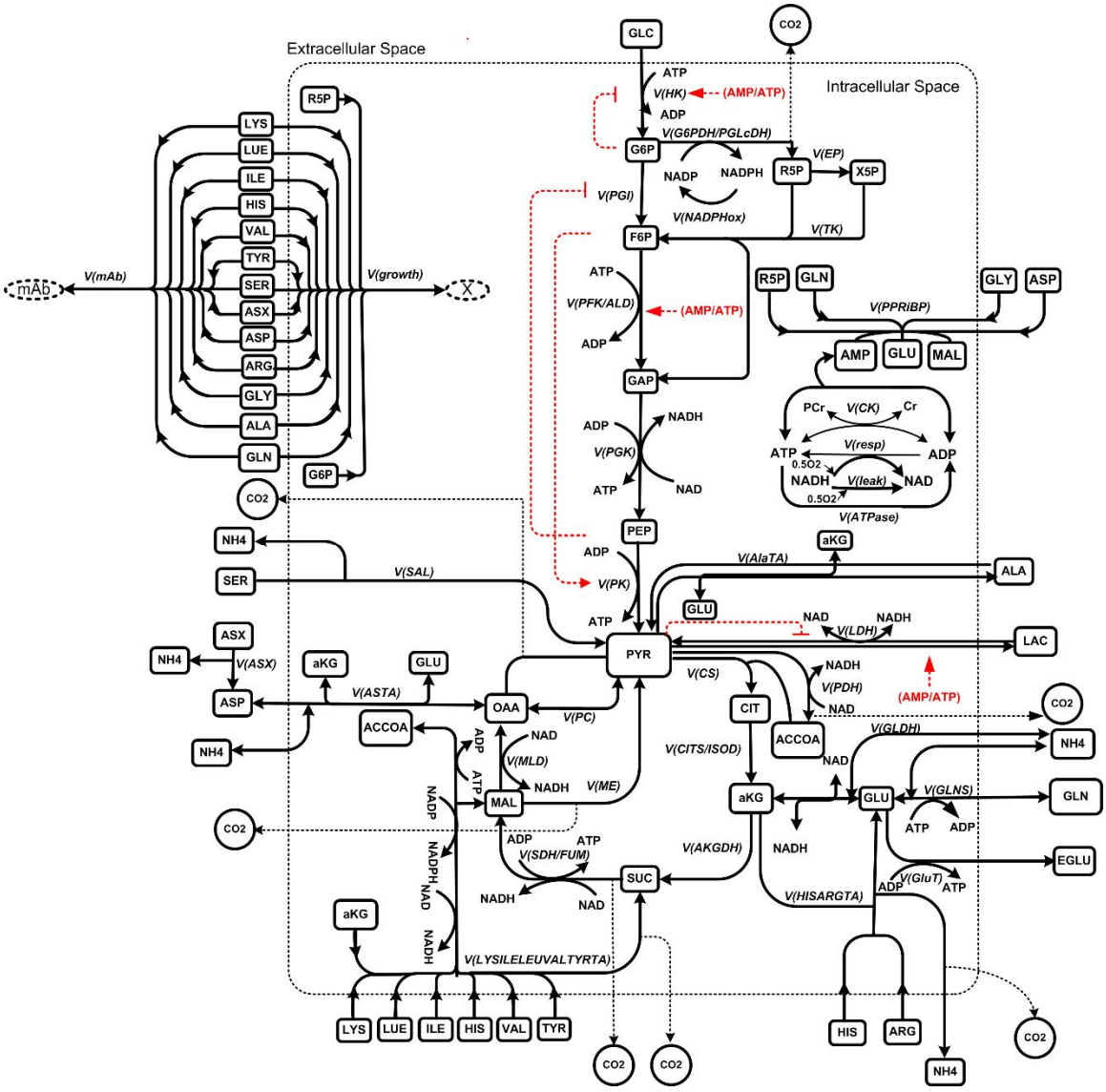

Figure 6.1The metabolic network considered in the model.

Glycolytic enzymes are either activated (↓) or inhibited (⊥) by an effector as indicated.Each regulationmechanism is taken from literature with mechanism (a) in (Berg, Tymoczko, & Stryer, 2002), (b) in (Berg, Tymoczko, & Stryer, 2002), (c) in (Garreau & Buc-Temkine, 1972), (d) in (Wang, 1977), and (e) in (Berg, Tymoczko, & Stryer, 2002; Jing & Ismail-Beigi, 2007).

Table 6.1Kinetic expression for each of the regulatory mechanisms.
All regulatory scenarios, metabolites and fluxes are defined in Figure 6.1.

Regulatory mechanism		Kinetic expression
(a)		$v_{HK} = v_{maxHK} * \frac{GLC}{GLC + Km_{GLC}} * \frac{\frac{ATP}{ADP}}{\frac{ATP}{ADP} + Km_{\frac{ATP}{ADP}}} * \frac{Ki_{G6P}}{G6P + Ki_{G6P}}$
(b)		$v_{PGI} = v_{maxPGI} * \frac{G6P}{G6P + Km_{G6P}} * \frac{Ki_{PEP}}{PEP + Ki_{PEP}}$
(c)		$v_{PK} = v_{maxPK} * \frac{PEP}{PEP + Km_{PEP}(1 + \frac{ka_{F6P}}{F6P})}$
(d)		$v_{rLDH} = v_{maxrLDH} * \frac{LAC}{LAC + Km_{LAC}} * \frac{Ki_{PYR}}{PYR + Ki_{PYR}}$
(e)	(e_1)	$v_{HK} = v_{maxHK} * \frac{GLC}{GLC + Km_{GLC}\left(1 + \frac{ka_{AMP}}{\frac{ATP}{AMP}}\right)}$
	(e_2)	$v_{PFK} = v_{maxPFK} * \frac{F6P}{F6P + Km_{F6P}\left(1 + \frac{ka_{AMP}}{\frac{ATP}{AMP}}\right)}$
	(e_3)	$v_{fLDH} = v_{maxfLDH} * \frac{PYR}{GLC + K_{mPYR}\left(1 + \frac{ka_{AMP}}{\frac{ATP}{AMP}}\right)}$

6.4.3 Characterization of the oscillatory behaviour

Damped oscillatory behaviour can be characterized from a parameter referred as the quality factor (q_f). Generally, the quality factor represents the number of oscillations that are completed before attenuating to a negligible value (< 5 % of initial value). Considering an exponential decay of the signal amplitude with time, damped oscillations are mathematically described as follows:

$$x(t) = a(t) \cos(\omega t - \varphi) \quad (10)$$

With a(t) (amplitude of the oscillation, the unit depends on the nature of the signal), ν (damping constant, h^{-1}), ω (fixed angular frequency, radians h^{-1}), and φ (phase angle, radians). This equation is interpreted as a periodic oscillation whose amplitude decays exponentially in time (Fitzpatrick, 2013) as follows:

$$a(t) = a_0 \exp(-\nu/2\, t) \quad (11)$$

where a_0 is the initial amplitude of the oscillation. The quality factor of an oscillatory system is then obtained as the ω-to-ν ratio. In this work, we have focused our analysis on the different regulatory mechanisms looking at q_f, a_0, ν, and ω values for the oscillatory behaviour of the ATP-to-ADP ratio. Lower values of q_f, a_0, and ω, and higher values of ν, indicate the damping of an oscillatory behaviour.

6.4.4 Calibration of the activation or inhibition parameters

In a first step and for each of the scenarios studied, initial values for the activation and inhibition parameters were found in literature (see references in caption of Table 6.2) and then optimized to maximize the damping of the ATP-to-ADP oscillatory behaviour, while minimizing the simulation error from the ideal smooth response behaviour ($a(t) = a_0 \exp(-\nu/2\ t)$) using the Matlab optimization toolbox (see caption of Supplementary Figure 6.1). This approach was selected because of the lack of experimental data to compare with. Briefly, optimal parameter values were obtained by minimizing the normalized sum-squared errors using a Least-squares minimization function in MATLAB's Optimization Toolbox for non-linear regression. Finally, 95% confidence intervals for regulatory parameters and model simulation behaviour (q_f, a_0, and ω) were calculated using built-in MATLAB functions "nlparci.m" and "nlpredci.m", respectively.

6.5 Results and discussion

This study is limited to the early cell response (< 24 h) following the establishment of hypoxic conditions (10% air saturation), during which cell death by either necrosis or apoptosis is not expected to occur massively, as previously reported in CHO cells (Van der Valk et al., 1998) and in mouse embryonic stem cell cultures (M. H. Kim, Kim, Heo, Kim, & Han, 2008).

6.5.1 Integration of the regulation mechanisms of glycolysis into the model

The calibration step of regulatory parameters (*Ki* and *Ka*) showed that minimization of q_f did not result in unique solutions but in space of solutions within a 95% confidence interval, in all scenarios (Table 6.2), as confirmed by a sensitivity analysis on these model parameters (Supplemental Figure 6.1). Therefore, because of the latter observation as well as for their biological relevance, the optimal parameters values determined for each regulatory mechanism and within each scenario (Table 6.2) were used thereafter.

Table 6.2Characterize of ATP-to-ADP oscillatory behaviour and of regulatory parameters for various regulatory scenarios.
Optimal parameters values are indicated and their 95% confidence interval in [brackets]. Initial values of parameters used for the optimization procedure were taken from literature; K_{iG6P}= 8e-8 (Aragón et al., 1980), K_{iPEP}= 2e-7(Aragón et al., 1980), K_{aF6P}=2e-7(Wang, 1977), K_{iPYR}= 7e-9 (Aragón et al., 1980), $K_{Aamp/atp}$= 0.01 (Hardie & Hawley, 2001). See the Methods section for the definition of qf, a, v and ω parameters as well as for the description of the parameter optimization procedure. All regulatory scenarios are defined in Figure 6.1.

Regulatory scenario	q_f	a	v	ω	**Parameter value**				
					K_{iG6P}	K_{iPEP}	K_{af6p}	K_{iPYR}	$K_{aAMP/ATP}$
Single mechanism									
-	[16,17.5]	[0.8,1.1]	[0.7,1.4]	[11.3,12.5]	-	-	-	-	-
a	[8.8, 10]	[0.7,0.9]	[1.1,1.3]	[11,11.5]	2e-8 [8e-9,8e-7]	-	-	-	-
b	[9.5,10]	[0.6,0.8]	[1.2,1.4]	[12.3,13.3]	-	1e-7 [¨2e-8,6e-7]	-	-	-
c	[9.7,10.2]	[0.7,0.9]	[0.99,1.1]	[11.7,12.6]	-	-	9e-8 [2e-8,5e-7]	-	-
d	[8.3,9.5]	[0.6,0.8]	[1.2,1.3]	[11.6,12]	-	-	-	3e-8 [7e-10,7e-8]	-
e_1	[8.1,13.5]	[0.4,0.6]	[1.1,1.4]	[12.2,12.5]	-	-	-	-	0.01 [0.001,0.1]
e_2	[8.4,13.9]	[0.4,0.6]	[1.1,1.4]	[12.2,12.5]	-	-	-	-	0.01 [0.001,0.1]
e_3	[7.9,13.3]	[0.4,0.6]	[1.1,1.4]	[12.2,12.5]	-	-	-	-	0.01 [0.001,0.1]
Combined mechanisms									
a-b	[3.3,4.0]	[0.5,0.7]	[2.5,2.6]	[8.2,9.2]	1e-8 [8e-9,4e-7]	6e-7 [2e-8,2e-6]	-	-	-
a-c	[1.5,2.1]	[0.4,0.6]	[3.7,4.6]	[7.1,8]	3e-8 [8e-9,6e-7]	1e-6 [2e-8,2e-6]	3e-7 [2e-8,1e-6]	-	-
a-d	critical damping	[0.7,1.2]	[4.7,6.3]	0	5e-8 [8e-9,7e-7]	6e-7 [2e-8,2e-6]	1e-6 [2e-8,2e-6]	5e-9 [7e-10,4e-8]	-
a-e_1	-	-	-	-	3e-8 [8e-9,5e-7]	1e-6 [2e-8,2e-6]	9e-7 [2e-8,2e-6]	9e-9 [7e-10,4e-8]	0.02 [0.001,0.1]
a-e_1,e_2	-	-	-	-	5e-8 [8e-9,6e-7]	8e-7 [2e-8,2e-6]	1e-6 [2e-8,2e-6]	1e-8 [7e-10,8e-8]	0.04 [0.001,0.08]
a-e	-	-	-	-	1e-7 [8e-9,8e-7]	5e-7 [2e-8,1e-6]	5e-7 [2e-8,1e-6]	4e-8 [7e-10,7e-8]	0.01 [0.001,0.1]
e (e_1, e_2 and e_3 combined)	-	-	-	-	-	-	-	-	0.01 [0.001,0.1]

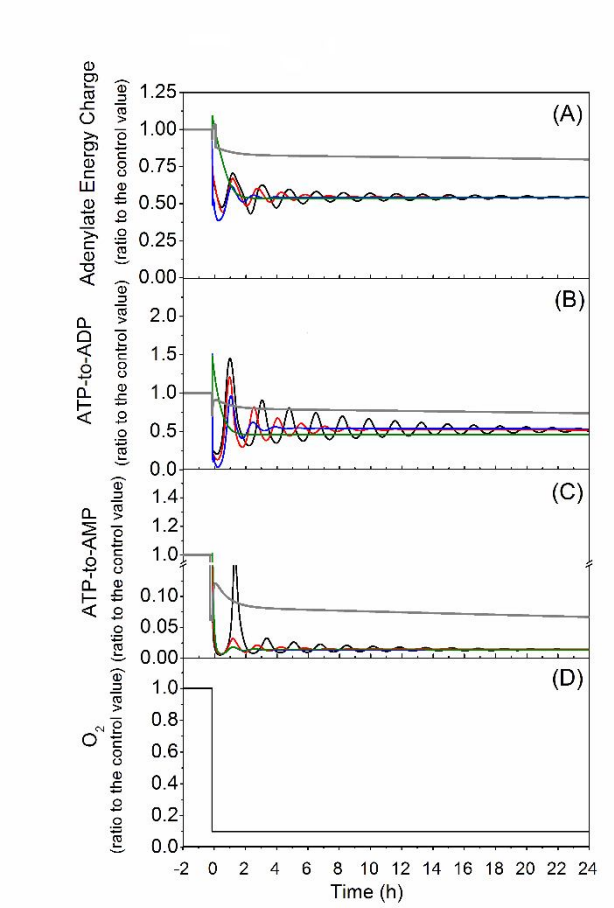

Figure 0.2Model simulations of energetic ratios following a hypoxic perturbation. Adenylate energy charge (ATP+0.5ADP-to-ATP+ADP+AMP ratio)(A), ATP-to-ADP ratio (B), ATP-to-AMP ratio (C), and dissolved O_2concentration (D). No regulation: solid black line, accounting for regulatory scenario a: solid red line, scenario a-b: solid blue line, scenario a-d: solid green line, and scenario a-e: solid gray line. All values are relative to control conditions, i.e. model simulations at air saturation oxygen concentration. All regulatory scenarios are defined in Figure 6.1.

6.5.2 Cell energetic robustness relies on the regulation of glycolysis

The calibrated model was first used, for every scenario, to assess the cells' response to a hypoxic stress, focusing on the cell energetic state. Various energetic markers such as the adenylate energy charge, (ATP+0.5ADP)-to-(ATP+ADP+AMP), ATP-to-ADP and ATP-to-AMP ratios were considered. As expected, the level of regulation of glycolysis strongly affects the cell energetic stability and the final quasi-steady-state level (Figure 6.2). Without any regulation, a stepwise decrease of the dissolved oxygen concentration to a hypoxic level of 10 % of air saturation in the culture medium induces immediate but transient (i.e. damped) oscillations for all cell energetic markers. The responses indicate

that the stress occurrence was sufficient to take the system from initial steady state to a lower ATP-to-ADP ratio. The adenylate energy charge and the ATP-to-ADP ratio both oscillate rapidly at around 50% and 55% of their initial values, respectively, showing a similar quality factor of 16.75±0.75 (Table 6.2). Initial response shows ATP concentrations to reach almost a zero value, while the adenylate energy charge reaches 27% of the initial level. Although the absence of any flux regulation (other than the various substrate concentrations) leads to an oscillatory behaviour of cell energetics, these oscillations were shown to attenuate with time, reaching ~ 5% of their initial amplitude after 18 complete oscillation cycles. Hexokinase feedback inhibition by G6P (Figure 6.1, mechanism a) increases the damping of the oscillatory behaviour, both in time and in amplitude with a q_f of 9.4±0.6, while reaching similar final levels than the case without any regulation. It can be seen that the single regulatory mechanism slowly damp the oscillations by decreasing hexokinase inhibition (Figure 6.3A, red line). Accounting for both phosphoglucose isomerase (Figure 6.1, mechanism b) and hexokinase feedback inhibition mechanisms limits the oscillatory response to ~3 h and a q_f of 3.64±0.35, while still reaching similar steady-state values as when there is no regulation. The respective regulatory mechanisms are shown to accelerate their contributions in damping the oscillations by decreasing both enzymes inhibition (Figure 6.3 A-B, blue lines). The influence of negative feedback mechanisms rapidly increases glycolytic fluxes to compensate for the reduced energy production. However, the high gain in energy production by oxidative phosphorylation is still exacerbating the increase in glycolytic fluxes to remove the destabilizing effect. Then, incorporating pyruvate kinase feedforward activation by F6P (Figure 6.1, mechanism c) to that of hexokinase and phosphoglucose isomerase decreases q_f to 1.8±0.35 and the oscillatory response to ~2 h (data not shown). Furthermore, incorporating the feedforward inhibition regulation mechanism of the reverse lactate dehydrogenase reaction by pyruvate (Figure 6.1, mechanism d) to the latter combined scenario results in a single oscillatory cycle that stabilizes at a similar adenylate energy charge value, but at a ~ 10% lower ATP-to-ADP ratio. From that scenario, each regulatory mechanism shows no oscillation, while decreasing enzymes inhibition and decreasing enzyme activation (Figure 6.3 A-D, green lines). Addition of feedback activation regulatory mechanisms directly involving the

energetic output (Figure 6.1, mechanism e_1) to that of a-d improves the robustness of the predicted cell metabolic response to the hypoxic perturbation (Figure 6.4). Finally, the addition of all feedback activation regulatory mechanisms directly involving the energetic output of the metabolic network system, i.e. the cell energetic level described as the AMP-to-ATP ratio (Figure 6.1, mechanisms e_1,e_2,e_3), further improves the robustness of the predicted cell metabolic response to the hypoxic perturbation. As expected and in agreement with literature, the cell energetic state then shows no oscillation with, indeed, contributions of the regulatory mechanisms, i.e. increasing hexokinase and phosphoglucose isomerase inhibition, increasing pyruvate kinase activation and more pronounced increasing hexokinase, Phosphofructokinase and the forward reaction of lactate dehydrogenase activation (Figure 6.3 A-E, gray lines). Moreover, although the cells' ATP-to-ADP ratio and the adenylate energy charge decrease respectively at ~ 75% and ~ 78% of their initial values, these levels were 25% to 50% higher than when not accounting for energetic regulatory mechanisms. Therefore, simulated CHO cells when accounting for scenario a-e reach new energetic quasi steady states that are closer to the initial ones (prior to the hypoxic perturbation) when the cell energetic state plays an active role in the regulation of enzymes of glycolysis, as clearly shown when comparing responses of the ATP-to-ADP ratio in all non-oscillatory scenarios (Figure 6.4).

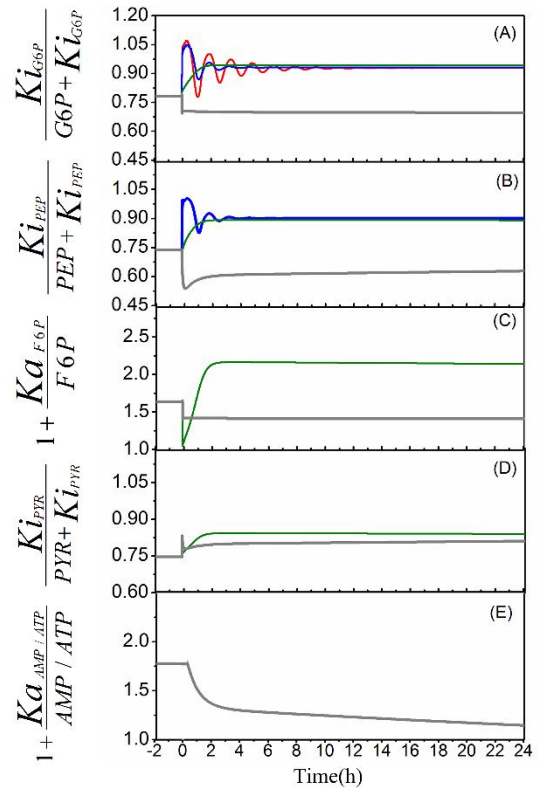

Figure 6.3Specific contribution of the regulatory mechanisms.
The inhibitory term proportional to G6P (mechanism a) (A); red line (scenario a), blue line (scenario a-b), green line (scenario a-d), gray line (scenario a-e) , the inhibitory term proportional to PEP (mechanism b) (B); (blue line (scenario a-b), green line (scenario a-d), gray line (scenario a-e), the activation term corresponding to F6P (mechanism c) (C); green line (scenario a-d), gray line (scenario a-e), the inhibitory term proportional to PYR (mechanism d) (D); green line (scenario a-d), gray line (scenario a-e), the activation term corresponding to AMP-to-ATP ratio (mechanism e) (E); gray line (scenario a-e). All regulatory scenarios are defined in Figure 6.1.

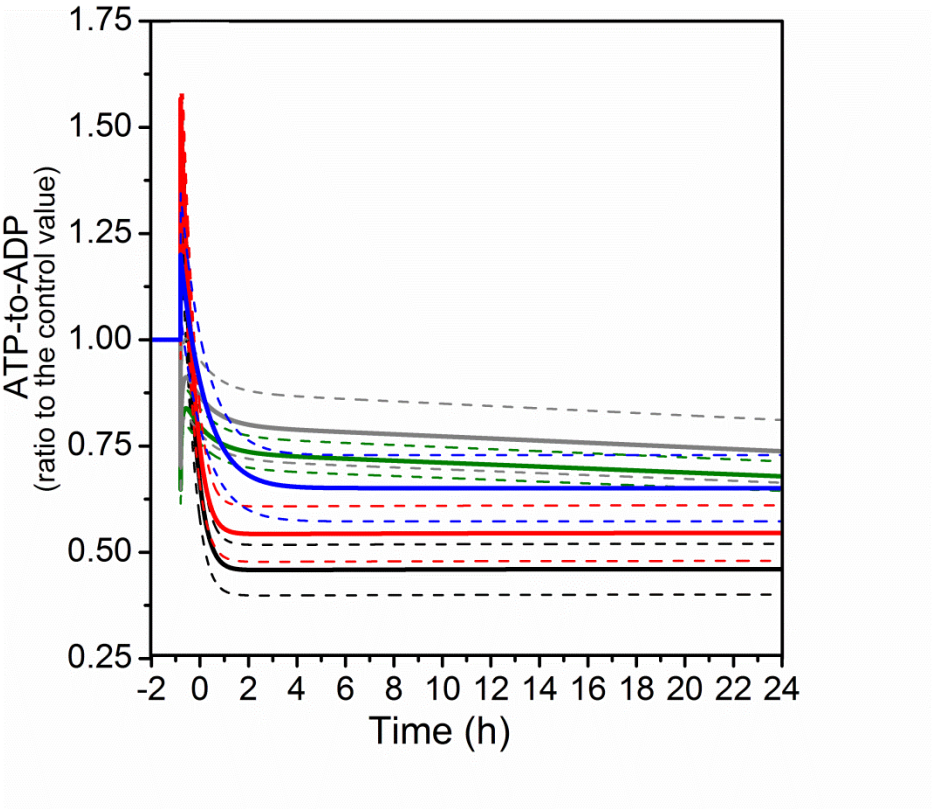

Figure 6.4Model simulations of ATP-to-ADP with 95% confidence intervals for regulatory scenarios avoiding oscillatory responses.
Solid black line: scenario a-d, Solid red line: scenario a-e_1, Solid blue line: scenario a-e_1,e_2, Solid green line: scenario e (e_1,e_2,e_3), Solid gray line: scenario a-e (e_1,e_2,e_3). Dashed lines are 95% confidence intervals for each regulatory scenario with respective colors, all regulatory scenarios are defined in Figure 6.1.

6.5.3 The model simulates biomarkers of anaerobic glycolysis

Simulated metabolic fluxes of glycolysis (*V(HK), V(PK), V(LDH)*) rapidly exhibit a transient oscillatory behaviour following a hypoxic perturbation. Interestingly, all these fluxes reach new steady states that are at ~50% of their respective control values. The complete regulation scenario, i.e. including mechanisms of feedback regulation by the AMP-to-ATP ratio (mechanisms a-e in Figure 6.1), however, results in a distinct behaviour with higher fluxes rates than control values for the hexokinase (~ +75%; including glucose transport as well), pyruvate kinase (~ +75%) and lactate dehydrogenase (~ +200%) enzymes (Figure 6.5 A, B, C). This behaviour agrees with an anaerobic glycolysis, a phenomenon that is observed under oxygen limitation (Frezza et al., 2011).

Elevated level of glycolysis eventually leads to an increased ratio of lactate produced toglucose consumed, at a value ~ 50% higher than respective controls (Figure 6.6A). This suggests that lactate production accounts for the excess glucose consumption in anaerobic glycolysis. When direct activation of glycolysis is not considered, however, this value remains unchanged (Figure 6.6A). Hypoxic condition has been reported to result in the up-regulation of the key glycolytic enzymes studied here (as illustrated in Figure 6.1) (J. W. Kim, Tchernyshyov, Semenza, & Dang, 2006; Wheaton & Chandel, 2011). In all cases where glycolysis is regulated only from intermediates (i.e. mechanisms a-d in Figure 6.1), the main metabolites (i.e. G6P, GAP and PYR) (Figure 6.7 C, D, G) exhibit a decrease in concentration in accordance with glycolytic fluxes. But when feedback regulatory mechanisms involving the cell energetic state are also considered glycolytic intermediates concentrations are instead found to increase. (Figure 6.7 C, D). Indeed, the increase of G6P (~ 50%), GAP (~125% to 60%), and LAC (~ 300 %) (Figure 6.7 B) cope with the decrease of PYR (~ -30%) (Figure 6.7 G); the latter being consistent with the metabolic regulation of lactate dehydrogenase by ATP-to-AMP ratio and a lower value for the pyruvate branch point ratio (Figure 6.6B). These simulation results are in agreement with expected physiological ranges, including extreme intermediates metabolites accumulation, reported for hypoxia condition in human cells (Wheaton & Chandel, 2011). Model simulations show similar final values for the contribution of glycolysis to TCA cycle (Figure 6.6C), suggesting that less carbon skeleton is available to enter TCA cycle, which in turn explains a lower TCA cycle flux (Figure 6.5E). The values for the glucose level when feedback regulatory mechanisms involving the cell energetic state are also considered exhibit a ~ 90% decrease (Figure 6.7A) that can be attributed to the higher simulated glucose uptake rates (Figure 6.5A).

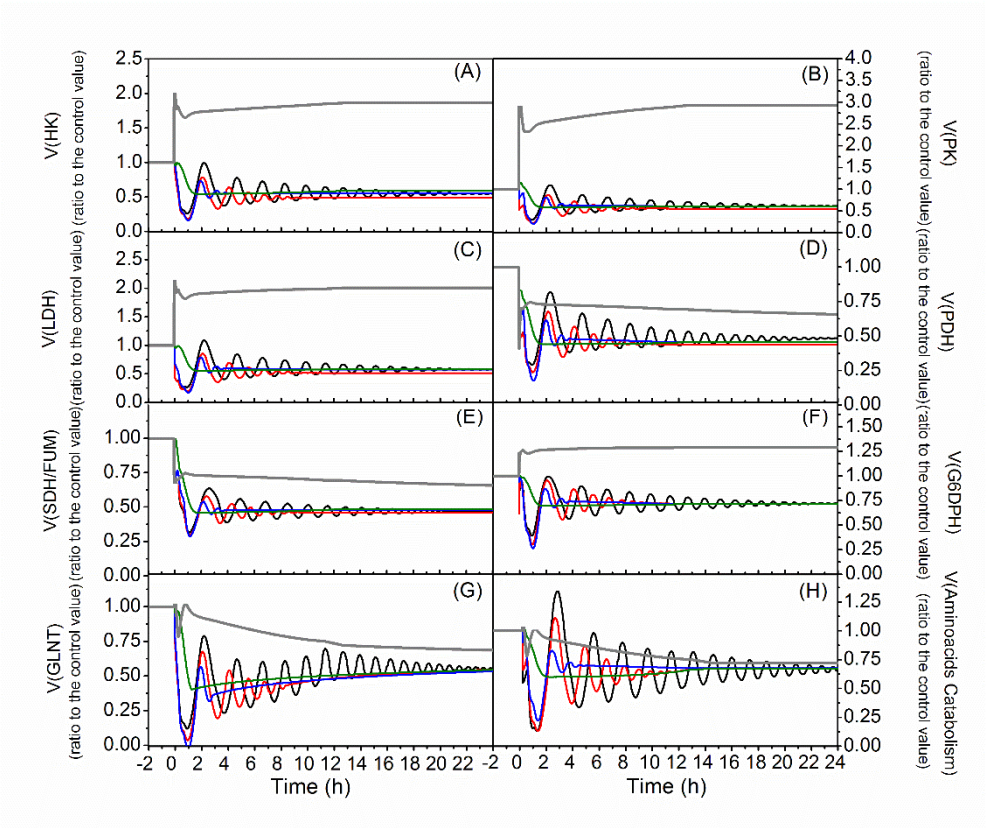

Figure 6.5Model simulations of metabolic fluxes following a hypoxic perturbation. *v(HK)* (A), *v(LDH)* (B), *v(PK)* (C), *v(PDH)* (D), *v(SDH/FUM)* (E), *v(G6DPH)* (F), *v(GLNT)* (G), *v(Amino acids Catabolism)*. *v(Amino acids Catabolism)* as (v(SAL)+v(ASX)+v(HISARGTA)+v(LYSILELEUVALTYRTA)+v(AlaTA)).All captions are the same as in Figure 2. All fluxes are defined in Figure 6.1.

6.5.3.1 Amino acid metabolism

glutamine is typically another important carbon and energy source for mammalian cells and its metabolism is often linked to that of glucose . Glutamine shows a decreased uptake rate (*V(GLNT)*) in all regulation scenarios (Figure 6.5G). This metabolic flux (V(GLNT)) thus followed the behaviour for TCA cycle (*V(SDH/FUM)*) (Figure 6.5E), with a final glutamine uptake rate at ~ 50% of its control value and remained at ~ 75% of its control value when applying all regulatory terms (Figure 6.5G). This simulated observation suggests a decreased demand in glutamine under hypoxic condition, a result that is expected because TCA cycle is also down-regulated. The contribution of glutamine to TCA cycle also decreases with theestablishment of an anaerobic glycolysis (Figure 6.6D). Finally, amino acids catabolic rate, which feeds TCA cycle (*V(amino*

acids catabolism)), reaches similar lower steady state levels (~70%) than for the control following the hypoxic perturbation, irrespectively of the regulation mechanism studied (Figure 6.5H).

6.5.3.2 Pyruvate branch point

The pyruvate branch point ratio shows a ~ 44 % decrease when the metabolism is switching to an anaerobic glycolysis (Figure 6B), which means a reduction (-45%) of the flux from pyruvate to TCA (*V(PDH)*) (Figure 6.5D). The TCA cycle flux (*V(SDH/FUM)*) also show to decrease at ~ 50% of its control value when considering only regulation involving intermediates of glycolysis, while it remained at 75% of its control value when applying all regulatory mechanisms (Figure 6.5E). The reduction of TCA activity has also been described as an adaptive response to hypoxia (Wheaton & Chandel, 2011). The reduction of metabolic intermediates and fluxes in the TCA cycle can also be expected from the decreased levels of pyruvate under anaerobic glycolysis (Figure 6.7G). Finally, the sudden increase of the cell redox state, which is expressed as the NADH-to-NAD ratio in our model, is also simulated by the model (Figure 6.7F); a result that is in agreement with lower values of the pyruvate branch point ratio as well as with literature (Frezza et al., 2011). This result may suggest NADH accumulation as a result of a decreased oxidative phosphorylation (i.e. cell respiration). Lactate dehydrogenase activation, by reducing NADH oxidation through TCA cycle, also contributes to the increase of the NADH-to NAD ratio. The case with feedback activation of glycolysis from cell energetic state shows a moderate increase of NADH-to-NAD level compared to the other cases (Figure 6.7F). Due to the activation of lactate dehydrogenase, pyruvate conversion to lactate (*V(LDH*) proceeds at a higher rate (Figure 6.7B), a reaction fuelled by NADH and thus contributing to the oxidation of NADH to NAD.

6.5.3.3 G6P branch point

Taking its source from G6P, the global flux through the pentose phosphate pathway (*V(G6DPH)*) follows the same trend as glycolysis (Figure 6.5F), although to a lesser extent. While reduced at ~75% of that for the control for scenarios a-d, *V(G6DPH)* only increases by ~ 25% when adding feedback activation mechanisms from cell energetic state (Figure 6.5F). This phenomenon of an increased pentose phosphate pathway has been reported in human cells submitted to hypoxic

conditions (Frezza et al., 2011). A part of the glycolytic flux overflow is thus automatically re-directed to feed pentose phosphate pathway intermediate metabolites such as R5P (Figure 6.7E) with a ~ 25% concentration increase for the scenario incorporating all regulatory mechanisms. Although higher levels of R5P were simulated by the model, induction of anaerobic glycolysis causes a ~ 25% decrease in the percentage of glucose flowing through the pentose phosphate pathway, defined as the ratio of pentose phosphate oxidative flux to glucose uptake rate (Figure 6.6E). Lower values for the percentage of glucose flowing through the pentose phosphate pathway in the case of anaerobic glycolysis suggests, in counterpart, a higher glucose overflow to lactate production. The ratio of the pentose phosphate reflux to glycolysis (non-oxidative) to the pentose phosphate oxidative flux, however, shows stable values (Figure 6.6F). Therefore, since higher flux levels are channeled through pentose phosphate pathway (*V(G6DPH)*), and higher flux levels are chanelled back to glycolysis, one can expect that the establishment of anaerobic glycolysis does not reasonably modify the pentose phosphate pathway fluxes distribution (Figure 6.6F). Moreover, similar dynamic behaviours, characterized by the strength of the oscillations, have been observed for both G6P and R5P.

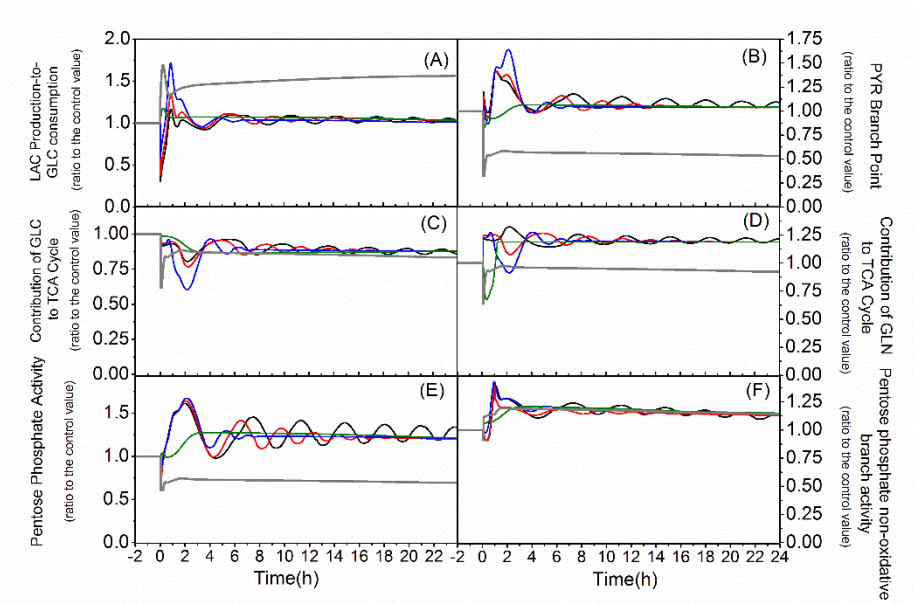

Figure 6.6Model simulations of metabolic flux distribution and metabolic ratios following a hypoxic perturbation.

Lactate production-to-glucose consumption (A), pyruvate branch point (B), contribution of glucose to TCA cycle (C), contribution of glutamine to TCA cycle (D), pentose phosphate activity (E), pentose phosphate non-oxidative branch activity (F)**.**Lactate production-to-glucose consumption ratio as *((vf(LDH)-vr(LDH))/v(HK))*, pyruvate branch point as the ratio of the pyruvate influx through TCA cycle divided by the total flux into pyruvate pool *(v(PDH/(v(PK)+v(SAL)+v(ML-PC)+v(AlaTA))*, when the last two fluxes positively fed pyruvare, Contribution of glucose to TCA cycle as the ratio of pyruvate influx to TCA cycle via *v(PDH)*, considering most of the *v(PDH)* has been originated from v(PK), to the total flux channeled through TCA cycle via its intermediates (*v(PDH)/(v(PDH)+ v(ASTA)+ v(GLDH)+ v(LYSILELEUVALTYRTA)+v(PC))*, Contribution of glutamine to TCA cycle as the ratio of glutamate influx to TCA cycle either via *v(GLDH)* to the total flux channeled through TCA cycle via its intermediates *(v(GLDH) /(v(PDH)+v(ASTA)+v(GLDH)+v(LYSILELEUVALTYRTA)+v(PC)))*, The pentose phosphate activity is defined as the percentage of the glycolytic flux channeled through pentose phosphate pathway, i.e. the ratio of pentose cycle oxidative flux to the glucose uptake *(v(G6PDH/PGLcDH)/v(HK))*. Pentose phosphate non-oxidative branch activity as the ratio of the pentose phosphate reflux to glycolysis to the pentose phosphate oxidative flux *(v(TK/TA)/(v(G6PDH/PGLcDH))* (see Figure 6.1). All captions are the same as in Figure 6.2. All fluxes are defined in Figure 6.1.

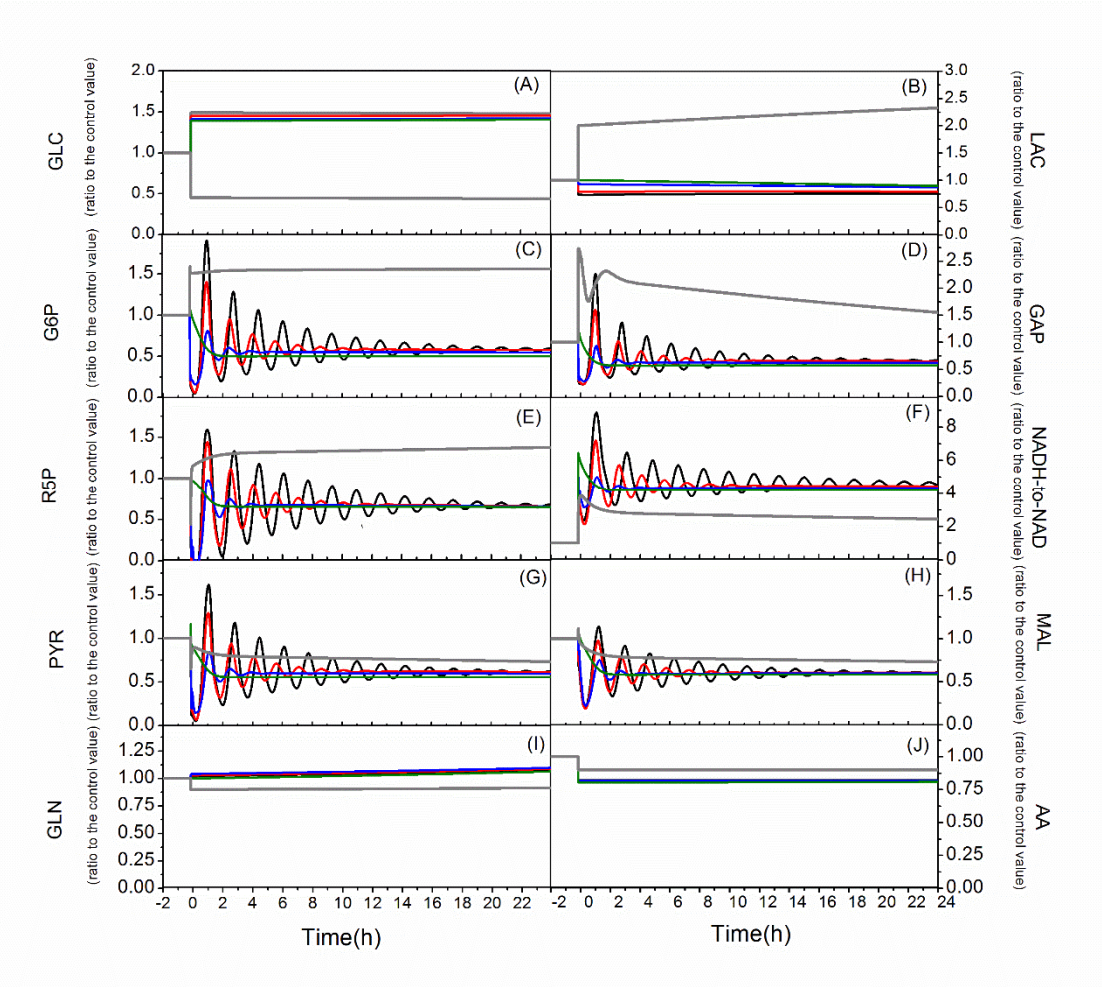

Figure 6.7Model simulations of metabolic concentrations following a hypoxic perturbation.
GLC (A), LAC (B), G6P (C), GAP (D), R5P (E), NADH-to-NAD (F), PYR (G), MAL (H),GLN(I),AA(J).AAas(SER+ASX+HIS+ARG+ALA+LYS+LUE+ILE+HIS+VAL+TYR) (see Figure 6.1). All captions are the same as in Figure 6.2. All metabolites are defined in Figure 6.1.

6.5.4 The model simulates cell alternatives to an efficient energy production

From in silico model simulations, it was shown that applying to glycolysis pathway a limited but crucial set of feedback and feedforward regulation mechanisms that are known to occur in mammalian cells, the model description of metabolism gains in robustness in its response to a strong O2 perturbation. We observed that not only each intracellular metabolic intermediate and metabolic flux gained in stability, but that the expected activation of an anaerobic glycolysis was simulated so as to maintain a high cell energetic state. Interestingly, immediately after the onset of the oxygen stress, the flux

through oxidative phosphorylation (respiration) decreases at 60% of the control (Figure 6.8D), following a transient oscillatory pattern depending on the regulatory mechanisms involved. The total ATP turnover rate reduces to ~ 50% of the control when no feedback related to energy is involved (Figure 6.8E). Of the remaining energy production capacity, the contribution of glycolysis reduces to ~ 48% (Figure 6.8F), while that from oxidative phosphorylation only shows to slightly reduce (Figure 6.8G), both showing highly attenuated oscillatory patterns. The only increase is attributed to a ~ 125% higher contribution from the kinases associated to energetic shuttles such as creatin/phosphocreatin and adenylate kinases (Figure 6.8H), both showing slowly attenuated oscillations. However, the switch to anaerobic glycolysis predominantly favors ATP turnover from glycolysis, as expected. Indeed, although the total ATP turnover rate reduces at ~ 70% of the control (Figure 6.8E), the contribution of glycolysis increases of ~ 100% while that from oxidative phosphorylation reduces by ~ 40% (Figure 6.8 F, G). The contribution of kinases from the management of the energetic shuttles reduces by ~ 50% (Figure 6.8H). Therefore, the complete regulatory scenario leads to simulations suggesting a total ATP turnover rate of only ~ 30% lower than the control, compared to a ~ 50% lower level when cell energetic is not included in the regulation of glycolysis. Thus, under hypoxic condition, the cells compensate the reduced contribution of TCA by increasing the glycolytic activity, a less efficient process but occuring at a higher rate comparing to TCA which is more efficient but the fluxes are much lower (Harper, Antoniou, Bevilacqua, Bezaire, & Monemdjou, 2002).

Finally, given its importance, the cellular bioenergetics system must be properly controlled when facing environmental changes, and the role of energetic shuttles in the ATP homeostasis phenomenon has been widely described (Dzeja & Terzic, 2003). In our model, the respective reversible reactions catalyzed by creatine kinase and adenylate kinase are described (Figure 6.1) as an energy buffering system. Indeed, as shown here (Figure 6.8H), the combined contributions of both kinases in ATP generation rate increase of ~ 125% when considering regulation mechanisms involving intermediates metabolites of glycolysis only. However, and it may seem surprising, the combined kinases contribution decreases when the full regulatory scenario is considered, although

creatine kinase reaction is only slightly being reduced, its relative contribution to the total is more reduced than in the other cases.

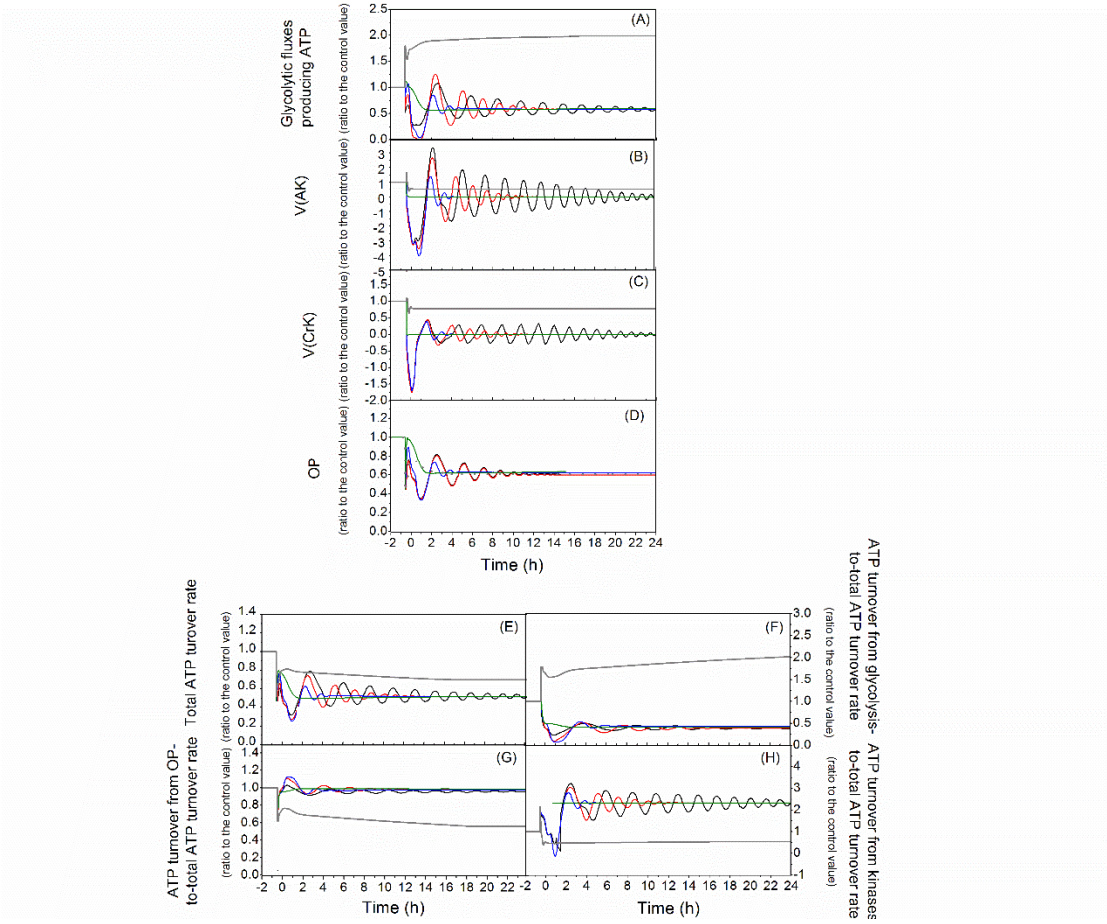

Figure 6.8Model simulations of cell bioenergetics state following a hypoxic perturbation. Glycolytic fluxes producing ATP (A), v(AK) (B), v(CrK) (C), OP (D), total ATP turnover rate (E), ATP turnover from glycolysis-to-total ATP turnover rate (F), ATP turnover from OP-to-total ATP turnover rate (G), ATP turnover from Kinases-to-total ATP turnover rate (H). Glycolytic fluxes as *(v(PGK)+v(PK))*, OP as v(resp), ATP turnover rate as (v(PGK)+v(PK)+v(SCOA)+ vr(GlnT)+ vf(CK)+vr(AK)+2P/O ratio*v(resp)), ATP turnover from OP-to-total ATP turnover rate as the portion of ATP generated from oxidative metabolism divided by total ATP production rate *(2P/O ratio*v(resp)/ (v(PGK)+v(PK)+v(SCOA)+ vr(GlnT)+ vf(CK)+vr(AK)+2P/O ratio*v(resp))*, ATP turnover from glycolysis-to-total ATP turnover rate as the sum of glycolytic fluxes producing ATP over the total ATP production rate *((v(PGK)+v(PK))/(v(PGK)+v(PK)+v(SCOA)+ vr(GlnT)+ vf(CK)+vr(AK)+2P/O ratio*v(resp))*, ATP turnover from Kinases-to-total ATP turnover rate as*(vf(CK)+vr(AK))/(v(PGK)+v(PK)+v(SCOA)+ vr(GlnT)+ vf(CK)+vr(AK)+2P/O ratio*v(resp))*(see Figure 6.1).All captions are the same as in Figure 6.2. All metabolites and fluxes are defined in Figure 6.1.

6.6 Conclusion

In this work, we have demonstrated that a kinetic-metabolic model can be used to simulate the fast response of CHO cells to a hypoxic perturbation. By including a combination of regulatory mechanisms that are known to occur in the glycolysis pathway of mammalian cells, model simulations of the cell metabolic and energetic behaviours were in agreement with responses described in literature. The model was thus able to predict the shifting from an oxidative metabolism to an anaerobic glycolysis. We report here that this metabolic shift can only be properly described by the model when accounting for the cell energetic state as a regulatory mechanism of the glycolysis, in addition to mechanisms involving metabolic intermediates of this pathway. For all other regulatory scenarios, an oscillatory behaviour was simulated. Although glycolytic oscillations have been reported in literature under specifically designed experimental conditions and by using mathematical models, there are no obvious known physiological role that has been identified so far, to the best of our knowledge. Indeed, these simulation results clearly suggest the biologically relevance of the mathematical model structure.

6.7 Acknowledgements

The authors wish to thank the NSERC Canadian Monoclonal Antibody Network (MabNet) for financial support.

6.8 references

Almaas, E., Kovacs, B., Vicsek, T., Oltvai, Z. N., & Barabasi, A. L. (2004). Global organization of metabolic fluxes in the bacterium Escherichia coli. Nature, 427(697), 839–843.

Altamirano, C., Illanes, A., Becerra, S., Cairo, J. J., & Godia, F. (2006). Considerations on the lactate consumption by CHO cells in the presence of galactose. *Journal of Biotechnololgy*, *125*(4), 547-556.

Aragón, J. J., Felíu, J. E., Frenkel, R. A., & Sols, A. (1980). Permeabilization of animal cells for kinetic studies of intracellular enzymes: in situ behavior of the glycolytic enzymes of erythrocytes. *Proceedings of the National Academy of Science, 77*(11), 6324-6328.

Bali, M., & Thomas, S. R. (2001). A modelling study of feed forward activation in human erythrocyte glycolysis. *Comptes Rendus de l'Académie des Sciences - Series III, ,324*(3), 185–199.

Berg, J. M., Tymoczko, J. L., & Stryer, L. (2002). Biochemistry.

Cascante, M., Boros, L. G., Comin-Anduix, B., de Atauri, P., Centelles, J. J., & W-N Lee, P. (2002). Metabolic control analysis in drug discovery and disease. *Nature Biotechnology, 20*(3), 243-249.

Chandra, F. A., Buzi, G., & Doyle, J. C. (2009). Linear control analysis of the autocatalytic glycolysis system. Paper presented at the chez In Proc of the American Control Conf., St Louis, MO.

Cloutier, M., Perrier, M., & Jolicoeur, M. (2007). Dynamic flux cartography of hairy roots primary metabolism. *Phytochemistry, 68*(16-18), 2393-2404.

Cloutier, M., & Wellstead, P. (2010). The control systems structures of energy metabolism *Journal of the Royal Society Interface, 7*(45), 651–665.

Connett, R., & Sahlin, K. (1996). Control of Glycolysis and Glycogen Metabolism *chez Handbook of physiology* (pp. 870–911). New York: Oxford University Press.

D'Alexandri, F. L., Scolari, S., & Ferreira, C. R. (2010). Reproductive biology in the "omics" era: what can be done? *Animal Reproduction Science, 7*(3), 177-186.

Durocher, Y., Perret, S., & Kamen, A. (2002). High-level and high throughput recombinant protein production by transient transfection of suspension-growing human 293-EBNA1 cells. *Nucleic Acids Research, 30*(2), E9.

Dzeja, P. P., & Terzic, A. (2003). Phosphotransfer networks and cellular energetics. *The Journal of Experimental Biology, 206*(Pt 12), 2039-2047.

of Recombinant Protein. *Molecular Biotechnology*, 34(2) 225-237.

Feist, A., & Rosenbloom, J. (2011). Improving mammalian cell line protein production using a metabolic model-based approach. *European Society for Animal Cell Technology, 22*, ESACT meeting.

Fitzpatrick, R. (2013). *Oscillations and Waves: An Introduction* (1 ed.): CRC Press.

Frezza, C., Zheng, L., Papkovsky, D. B., Hedley, B. A., Kalna, G., Watson, D. G., & Gottlieb, E. (2011). Metabolic Profiling of Hypoxic Cells Revealed a Catabolic Signature Required for Cell Survival. *PLOS ONE, 6*(9), e24411.

Froncisz, W., Lai, C. S., & Hyde, J. S. (1985). Spin-label oximetry: kinetic study of cell respiration using a rapid passage T1 sensitive electron spin resonance display. *Proceedings of the National Academy of Sciences, 82*(2), 411-415.

Gallazo, J. L., & Bailey, J. E. (1990). Fermentation pathway kinetics and metabolic flux control in suspended and immobilized Saccharomyces cerevisiae. *Enzyme and Microbial Technology, 12*(3), 162-172.

Garreau, H., & Buc-Temkine, H. (1972). Allosteric activation of human erythrocyte pyruvate kinase by fructose-1,6-diphosphate: Kinetic and equilibrium binding studies. Biochimie, 54(9), 1103–1107.

Ghorbaniaghdam, A., Henry, O., & Jolicoeur, M. (2012). A kinetic-metabolic model based on cell energetic state: study of CHO cell behavior under Na-butyrate stimulation. *Bioprocess and Biosystems Engineering, 36*(4), 469-487.

Grimbs , S., Selbig , J., Bulik, S., Holzhutter, H. G., & Steuer, R. (2007). The stability and robustness of metabolic states: identifying stabilizing sites in metabolic networks. *Molecular Systems Biology, 3* 146.

Hardie, D. G., & Hawley, S. A. (2001). AMP-activated protein kinase: the energy charge hypothesis revisited. *Bioessays, 23*(12), 1112-1119.

Harper, M. E., Antoniou, A., Bevilacqua, L., Bezaire, V., & Monemdjou, S. (2002). Cellular energy expenditure and the importance of uncoupling. *Journal of Animal Science, 80*(E. Suppl. 2), E90-E97.

Hatzimanikatis, V., Floudas, C. A., & Bailey, J. E. (1996). Optimization of regulatory architectures in metabolic. *Biotechnology and Bioengineering, 52*(4), 485–500.

Heinrich, R., & Papoport, S. M. (1977). Metabolic regulation and mathematical models. *Progress in Biophysics and Molecular Biology, 32*, 1-82.

Jing, M., & Ismail-Beigi, F. (2007). Critical role of 5'-AMP-activated protein kinase in the stimulation of glucose transport in response to inhibition of oxidative phosphorylation. American Journal of Physiology, 292(1), C477-487.

Kim, J. W., Tchernyshyov, I., Semenza, G. L., & Dang, C. V. (2006). HIF-1-mediated expression of pyruvate dehydrogenase kinase: a metabolic switch required for cellular adaptation to hypoxia. *Cell Metabolism, 3*(3), 177-185.

Kim, M. H., Kim, M. O., Heo, J. S., Kim, J. S., & Han, H. J. (2008). Acetylcholine inhibits long-term hypoxia-induced apoptosis by suppressing the oxidative stress-mediated MAPKs activation as well as regulation of Bcl-2, c-IAPs, and caspase-3 in mouse embryonic stem cells. *Apoptosis, 13*(2), 295-304.

Kitano, H. (2002). Systems biology: a brief overview.*Science,* 295(5560),1662–1664.

Korzeniewski, B., & Liguzinski, P. (2004). Theoretical studies on the regulation of anaerobic glycolysis and its influence on oxidative phosphorylation in skeletal muscle. *Biophysical Chemistry, 110*(1-2), 147-169.

Kumar, N., Gammell, P., & Clynes, M. (2007). Proliferation control strategies to improve productivity and survival during CHO based production culture. *Cytotechnology, 53*(1-3), 33-46.

Lai, C. S., Hopwood, L. E., Hyde, J. S., & Lukiewicz, S. (1982). ESR studies of O2 uptake by Chinese hamster ovary cells during the cell cycle. Proceedings of the National Academy of Science, 79(4), 1166-1170.

Martínez, V. S., Dietmair, S., Quek, L. E., Hodson, M. P., Gray, P., & Nielsen, L. K. (2013). Flux balance analysis of CHO cells before and after a metabolic switch from lactate production to consumption. *Biotechnology and Bioengineering, 110*(2), 660-666.

Mullick, A., Xu, Y., Warren, R., Koutroumanis, M., Guilbault, C., Broussau, S., . . . Massie, B. (2006). The cumate gene-switch: a system for regulated expression in mammalian cells. *BMC Biotechnology, 6*(43).

Pham, P. L., Kamen, A., & Durocher, Y. (2006). Large-Scale Transfection of Mammalian Cells for the Fast Production of Recombinant Protein. *Molecular Biotechnology, 34*(2), 225-237.

Riehl, W. J., & Segrè, D. (2008). Optimal metabolic regulation using a constraint-based model. *Genome Informatics, 20*, 159-170.

Savinell, J., & Palsson, B. O. (1992). Network analysis of intermediary metabolism using linear optimization. II. Interpretation of hybridoma cell metabolism. *Journal of Theoritical Biology, 73*(4), 154-455.

Solomon, E. P., Berg, L. R., & Martin, D. W. (2005). *Biology* (9th ed.).

Starbuck, C., & Lauffenburger, D. A. (1992). Mathematical model for the effects of epidermal growth-factor receptor trafficking dynamics on fibroblast proliferation responses *Biotechnology Progress, 8*(2), 132-143

Steuer, R., Grossa, T., Selbigb, J., & Blasiusa, B. (2006). Structural Kinetic Modeling of Metabolic Networks. *The Proceedings of the National Academy of Sciences of the United States of America, 103*(32), 11868–11873.

Valancin, A., Srinivasan, B., Rivoal, J., & Jolicoeur, M. (2013). Analyzing the effect of decreasing cytosolic triosephosphate isomerase on Solanum tuberosum hairy root cells using a kinetic-metabolic model. *Biotechnology and Bioengineering, 110*(3), 924-935.

Van der Valk, P., Gille, J. J. P., van der Plas, L. H. W., Jongkind, J. F., Verkerk, A., Konings, A. W. T., & Joenje, H. (1998). Characterization of oxygen-tolerant Chinese hamster ovary cells: II. Energy metabolism and antioxidant status. Free Radical Biology and Medicine, 4(6), 345-356.

Wang, C. S. (1977). Inhibition of human erythrocyte lactate dehydrogenase by high concentrations of pyruvate. Evidence for the competitive substrate inhibition. *european Journal of biochemistry, 78*(2), 569-574.

Wheaton, W. W., & Chandel, N. S. (2011). Hypoxia. 2. Hypoxia regulates cellular metabolism. *American Journal of Physiology, 300*(3), 385-393.

Wilkens, C., Altamirano, C., & Gerdtzen, Z. (2011). Comparative metabolic analysis of lactate for CHO cells in glucose and galactose. *Biotechnology and Bioprocess Engineering, 16*(4), 714-724.

Wilson, D. F., Erecinska, M., Drown, C., & Silver, I. A. (1977). Effect of oxygen tension on cellular energetics. *American Journal of Physiology, 233*(5), 135-140.

Zamorano, F., Wouwer, A. V., & Bastin, G. (2010). A detailed metabolic flux analysis of an underdetermined network of CHO cells. *Journal of Biotechnology, 150*(4), 497-508.

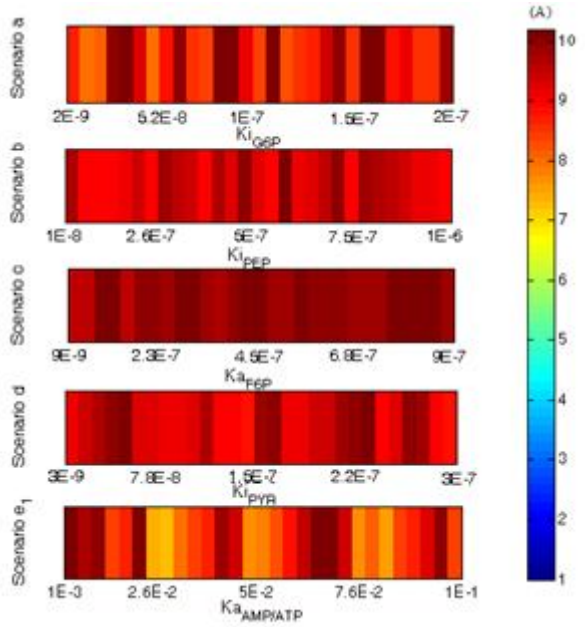

Figure 6.9(Supplementary) Sensitivity analysis on the parameters of regulatory mechanisms for individual mechanisms a, b, c, d, and e_1.
The colormap represents q_f values corresponding to model simulations of ATP-to-ADP ratio when the parameter value of each mechanism is changed between 0.1x to 10x of its optimal value. Colors denote q_f values for each sampling of the parameter space. All regulatory scenarios are defined in Figure 6.1.

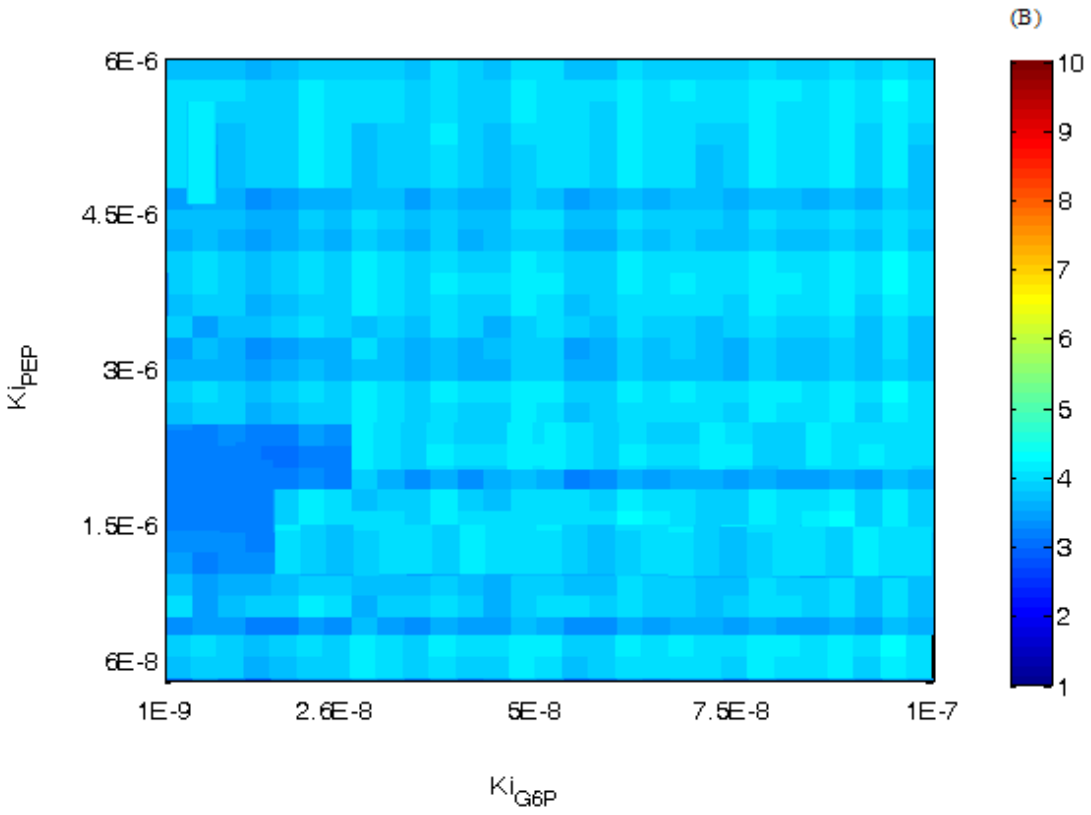

Figure 6.10(Supplementary) Sensitivity analysis on the parameters of regulatory mechanisms for scenario a-b.
The colormap represents q_f values corresponding to model simulations of ATP-to-ADP ratio when the parameter value of mechanisms a and b changed between 0.1x to10x of their respective optimal values. Colors denote q_f values for each sampling of the parameter space. All regulatory scenarios are defined in Figure 6.1.

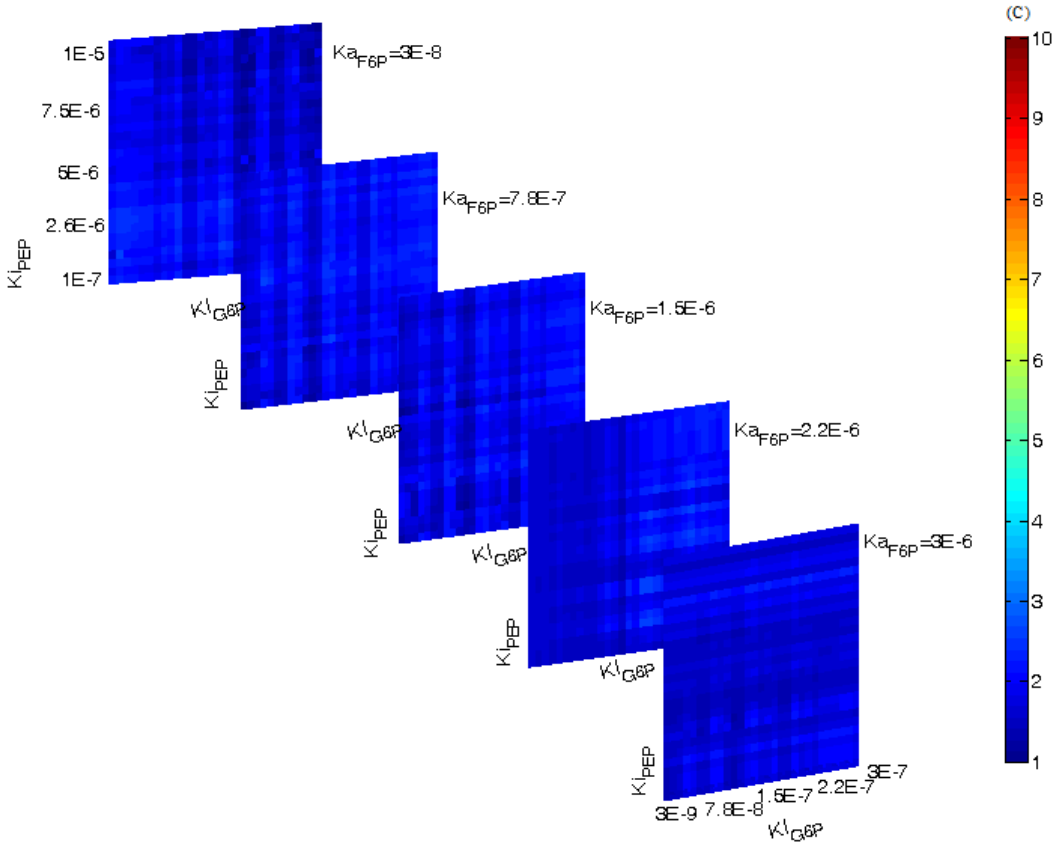

Figure 0.11(Supplementary) Sensitivity analysis on the parameters of regulatory mechanisms for scenario a-c.
The colormap represents q_f values corresponding to model simulations of ATP-to-ADP ratio when the parameter value mechanisms a and b changed between 0.1x to10x of their respective optimal values at different parameter values for mechanism c. Colors denote q_f values for each sampling of the parameter space. All regulatory scenarios are defined in Figure 6.1.

CHAPTER 7 GENERAL DISCUSSION

The main objective of this work was to shed light on the transient metabolic behaviour of CHOcells grown under batch conditions. In particular, we aimed at characterizing CHO cells metabolism, and its regulation, in responseto various perturbations. We have also devoted a large part of the work developing a modelling tool able to capture cell dynamics, namely a fully kinetic-metabolic model. In this regard, a previously described kinetic-metabolic framework that was shown to be successful at describing (Cloutier et al., 2007) as well as for controlling bioreactor cultures of plant cells(Cloutier et al., 2009)provided the initial motivation of the present work. The model was first developed and calibrated on previously published experimental data from our research group on a stable CHO cell line producing a recombinant t-PA, and stimulated by the addition of sodium butyrate, a chemical compound that is widely used to enhance recombinant protein production (McMurray-Beaulieu et al., 2009). In this work, we investigated to what extent our modelling approach could be adapted and calibrated having only a limited amount of experimental data (the concentration of cells, glucose, lactate, glutamine and ammonia, and intracellular concentrations of energetic nucleotides and cell specific oxygen consumption, with time). These data are generally the ones routinely measured in the biopharma industry. Moreover, the model has been challenged to describe the effect of sodium butyrate addition. Indeed, model simulation results clearly show that it can be applied to describe culture behaviour prior and after butyrate stimulation, with only limited model adaptation requirements. The effect of sodium butyrate was described through changing only 4 kinetic parameters (on a total of 72) at the time of sodium butyrate addition. These modifications were related to the fluxes corresponding to lactate production, glutamine uptake rate, energy consumption, and finally cell growth rate, all reported in literature to vary in response to sodium butyrate addition. These results have proven the biological relevance of such modeling framework. Our simulation results of difficult-to-measure metabolic fluxes and ratios agreed and even were complementary to the experimental results of our previous work (McMurray-Beaulieu et al., 2009). Determination of confidence intervals and sensitivity analysis were then performed on model parameters, and relatively narrow confidence intervals were obtained for the most sensitive parameters. Model simulations of

metabolic fluxes suggested a distinct cellular behaviour in response to sodium butyrate addition, i.e. enhanced stability of glucose and glutamine uptake, a lower lactate production-to-glucose consumption rate,as well as a higher oxidative phosphorylation rate, all corresponding to asustained high cell metabolic activity level favouring energy production. The model thus showed its ability to describe the switch to a more efficient metabolism in response to a production enhancer such as sodium butyrate, a phenomenon that is also reported in literature (De Leon et al., 2007; McMurray-Beaulieu et al., 2009; Yee et al., 2008).

This first contribution led to some important clarifications on specific mathematical aspects of this kind of models, and at the same time suggested that one can use such model to explore the behaviour of key physiological markers while drawing biologically relevant conclusions. However, although model simulations tend to agree with literature and with the known biology of CHO cells, given the high number of model parameters, we have focused at minimizing the simulation global error without being able to identify adequately all the parameter values. We then decided to push further the validation of the modelling approach by increasing significantly the size of the experimental dataset in both extra- and intracellular metabolites concentrations. In the second contribution, we studied another CHO cell system by considering two cell clones (a high-producer and a low-producer) and the parental cell line from which they were derived. The producing cell lines have been stably transformed to produce a monoclonal antibody (mAb) under the induction of a cumate gene switch. The model was then challenged in multiple ways, looking (a) to what extent two CHO cell lines metabolomically differ from each other, (b) two sub-clones differ from each other and (c) from their parental cell line, and (d) how far the induction of recombinant protein expression affects the cell metabolism. A major effort has then been accomplished to obtain a series of metabolomics measurements that are highly difficult to obtain, specially from cell extracts for intracellular metabolites concentrations. Then, keeping the same model structure determined in our first contribution (Ghorbaniaghdam, Henry, & Jolicoeur, 2012), the framework was extended to also describe recombinant monoclonal antibody production kinetics usinga larger set of experimental data. In this process, only a limited number of parameters had to be modified for adapting the model to the second CHO parental cell line.

From a total of 92 parameters, only 11 needed being modified from those of our first contribution, in addition to newly introduced parameters, i.e. the ones related to amino acids metabolism. These sensitive parameters were related to glucose uptake and lower part of glycolysis, i.e. pyruvate kinase and lactate dehydrogenase, pentose phosphate pathway, i.e. epimerase, TCA cycle, i.e. citrate synthase, reactions connecting glycolysis to TCA cycle, i.e. malic enzyme, amino acid and glutamine catabolism, i.e. alanine transaminase and glutamate transferase, NADH consuming reactions, i.e. proton leak, and fuelling reactions, i.e. oxidation of NADPH. All of these are known to be involved in the major metabolic pathways and thus, their value is thought to define specific traits of different cell lines grown under different experimental conditions.

Moreover, the low- and high-producer clones only required the adjustment of few parameters, i.e. the ones related to lactate and ATP consumption, TCA cycle, connections of glycolysis and TCA cycle and mAb production, from those of the parental, for enabling the model simulations to cope with experimental data. So, a limited subset of model parameters are driving, in fact, the *in silico* clonal variation in cell behavior**.**While adapting the model structure, we have also inserted a more detailed description of fluxes regulation within the glycolysis pathway, which was shown to enable further improvements of the descriptive and the predictive capacities of the model. Another motivation selecting this second cell line set was to examine clone-to-clone variations using the model, analyzing growth characteristics, as well as mAb productivity and metabolic profiling.Significant metabolic changes between different clones were observed experimentally and also simulated by the model. The differences were more pronounced between the parental cells and the high-producer clone, and to a lesser extent between the low-producer clone and either the parental or the high-producer clone. A more efficient metabolic state was assessed in the high-producer clone, i.e. lower values of lactate production rate-to-glucose consumption at non-limiting glucose conditions, and higher glycolytic fluxes channeled into pyruvate and consequently causing the up regulation of TCA. In addition to more efficient glucose metabolism, model simulations of anaplerotic reactions also showed an higher replenishment of TCA cycle intermediates from these reactions, a result which is also supporting the up regulation of the TCA. However, the two low- and high- producer clones, both exhibited fairly similar behaviour

with or without the induction of recombinant protein (mAb) synthesis. Taken together the experimental results and model simulations showed a more efficient metabolic activity, an enhanced oxidative phosphorylation activity and a higher energy yield from glycolysis in the high-producer clone. We demonstrated the use of a kinetic metabolic model to investigate the key characteristics of recombinant Chinese hamster ovary (CHO) cell clones producing respectively high and low monoclonal antibody titers. In accordance with our first contribution, *in silico* analysis of the different cultures, involving the parental as well as the low- and the high-producer, provided reliable and valuableinsights for theunderstanding of these sub-clones different behaviours, all in agreement with literature or in line with biological relevant hypotheses.

In the first two contributions, we applied the model to study slow dynamics of a metabolic network in the context of a batch culture, which does normally last one to two weeks. In a third and final contribution, however, we focused on challenging the model with a sudden external perturbation that can unfortunately easily occur in cell culture, i.e. a hypoxic stress. In this context, the concept of dynamic stability was introduced as the cellular ability to reach a new steady state after the introduction of a perturbation. The dynamic stability of the parental cell line metabolism (investigated in contribution number two) was thus characterized from its transient simulated response. An emphasis has been placed on evaluating different regulatory mechanisms, alone or in combination, while limiting our focus on the regulation of fluxes of the glycolysis pathway. The transient behaviour of the model was then analyzed looking at specific responses, i.e. fluxes and fluxes ratios, and metabolites concentrations, of central metabolic pathways. Without any regulation, the model simulated an immediate oscillatory response. However, different levels of regulation of glycolysis clearly showed to induce the damping of the oscillatory behaviour.

Accounting for the complete regulation of glycolysis, the combination of regulatory mechanisms led to a smooth non-oscillatory transient response.The model structure was thus readily adaptable to include regulation mechanisms, since no obvious known physiologicalrole of glycolytic oscillations has been identified so far, to the best of our knowledge, for the experimental condition designed *in silico* by our model. *In silico* model simulations of metabolic flux distribution, metabolic ratios and metabolic

concentrations showed higher glycolytic fluxes and concentrations, lower TCA cycle activity and TCA intermediates concentrations, an overflow of glycolytic fluxes to lactate production, and higher contribution of glycolysis to ATP production corresponding clearly to anaerobic glycolysis. This anaerobic glycolysisphenomenon has been widely reported in mammalian cells under hypoxia conditions. The model has thus shown its capacity to predict a switch from respiration to an anaerobic glycolysis metabolism.

Despite all the advantages revealed in this work about having a descriptive mathematical model that is biologically relevant, the approach has some important limitations that need to be discussed. On the one hand, and this is mostly what we were able to do here, we keep a high number of non-identifiable parameters because our focus is on the model biological relevancy level, although simplified. Mathematically speaking, one parameter is considered identifiable if changing its value influences the model output. In the first and second contributions, we followed a classical approach to quantify the influence of a parameter and scanned all model parameters to verify which ones can be identified within the related experimental space, i.e. sensitivity analysis. A high number of non-sensitive parameters were found due to the lack of experimental solicitation. However, parameters that we were able to identify with confidence intervals still in biological range were mostly related to the major reactions of CHO cells primary metabolism, i.e. glucose uptake and glycolytic fluxes, the reaction connecting glycolysis to TCA cycle, glutamine uptake and channeling into TCA cycle, catabolic reactions in amino acid metabolism, and specific growth rate. All other non-identifiable parameters were kept at this stage of model development since they are biologically relevant for describing existing metabolic pathways and kinetics of enzymatic reactions. This approach has also allowed us to interpret model simulations, i.e. metabolic fluxes and ratios, in relation to statistical significance within the experimental space. On the other hand, one can still work at simplifying this model with the aim of ending with a structure having only identifiable parameters. Although mathematically validated, the cost of proceeding this way is definitely a loss of biological relevancy.

CHAPTER 8 CONCLUSION

This PhD thesis proposed a dynamic modeling approach for CHO cell metabolism to make a new step forward in the understanding of mammalian cells metabolism. One of the main contributions of this work lies in the richness and diversity of the metabolomic data collected. Few projects have reported this large number of measurements for the intermediate metabolites of CHO cells and for their monitoring over time. Another significant contribution is the development of a comprehensive dynamic model giving information about the transient behavior of CHO cells. Using the information available on metabolite levels and enzyme kinetics from literature, a kinetic model representing significant parts of central carbon metabolism was constructed. It was therefore built to provide some answers to the question on the effect of changing a cell environmental condition, through the introduction of a stimulus (e.g. the depletion of main nutrients) on the primary metabolism. In a first part, we have constructed a kinetic model describing CHO cell central carbon metabolism following sodium butyrate addition. The model presented in this part was the first complete metabolic model describing the kinetics of primary metabolism for CHO cells. In addition, although having been calibrated to a limited dataset normally see in industry, the model showed a real predictive capacity with simulations of intracellular flux distributions that were in agreement with literature. Then, the kinetic metabolic model was applied to another CHO cell line cultured under different conditions, which enabled further model improvements, including regulation mechanisms of glycolysis pathway. A large set of experimental data also allowed the extension of the model to describe recombinant monoclonal antibody production kinetics. Furthermore, fitting the model to the new cell line and culture conditions, only a limited number of parameters needed to be adjusted, which demonstrated that the model is readily adaptable to other CHO cell lines. The model also showed its ability to describe clonal variation with relatively slight adjustments. This second contribution did enhance our confidence level in the model structure and parameters estimates. Also, it is important to note that parameters values agree with ranges proposed in literature. The model was thus consistent with respect to cell biology. Finally, an *in silico* perturbation experiment, mimicking the sudden introduction of an oxygen limitation into the system, was

performed. Interestingly, the model produced some unexpected oscillatory behaviour, which was identified to originate from the lack of regulatory mechanisms. Implementation of a combination of known regulatory interactions into the model demonstrated that the regulation of central carbon metabolism is crucial in many scenarios including sudden perturbations in the oxygen level, and that a cell strongly looks at the homeostasis of its energetic level. Indeed, we observed through model simulations that the controlling regulatory metabolism may mainly relies on the cell energetic state itself.

CHAPTER 9 RECOMMENDATIONS

We assume that the future of the modelling approach developed in this work should push further its description of regulatory mechanisms for enabling a better understanding of cellular behavior. The following are some suggestion following the current work:

1. Although a large amount of experimental data were made available in this study, there are some important ones that were not measured, such as lipids and sugar nucleotides, and these are needed to increase the confidence on the model structure and parameter estimates.

2. Although some statistical analysis has been performed to assess identifiable parameters a more elaborated and systematic approach in view of estimating the ‘‘quantitative identifiability’’, or estimability of model parameters should be applied. This approach is completely explained in Meshram et al. (2013) (Meshram et al., 2013). The method begins with the determination of the scaled sensitivity of the j^{th} parameter on the i^{th}model output for which experimental data is available at each sampling time$t$ from which a scaled sensitivity matrix can be calculated as follows:

$$M = \begin{bmatrix} \frac{k_1}{y_1}\frac{\partial y_1}{\partial k_1}(t_1) & \cdots & \frac{k_p}{y_1}\frac{\partial y_1}{\partial k_p}(t_1) \\ \vdots & \ddots & \vdots \\ \frac{k_1}{y_r}\frac{\partial y_r}{\partial k_1}(t_1) & \cdots & \frac{k_p}{y_r}\frac{\partial y_r}{\partial k_p}(t_1) \\ \frac{k_1}{y_1}\frac{\partial y_1}{\partial k_1}(t_2) & \cdots & \frac{k_p}{y_1}\frac{\partial y_1}{\partial k_p}(t_2) \\ \vdots & \ddots & \vdots \\ \frac{k_1}{y_r}\frac{\partial y_r}{\partial k_1}(t_m) & \cdots & \frac{k_p}{y_r}\frac{\partial y_r}{\partial k_p}(t_m) \end{bmatrix}$$

Parameters estimability can then be determined by the orthogonalization method as first proposed by Yao et al. (2003) (Yao et al., 2003) . First the magnitude of each column of M (the sum of squares of each column) should be calculated. The first estimable parameter is selected whose column has the largest magnitude. The corresponding column is marked as X_1 and the magnitude of largest sum of squares of the column elements is called estimable score. $\widehat{M}$ as an estimate of the sensitivity matrix using this subset of column is the calculated as : $\widehat{M} = y_1 * (y_1^T y_1)^{-1} y_1^T M$. The residual matrix

$R = M - \widehat{M}$is then calculated to proceed the analysis with respect to the remaining parameters. The sum of squares of the residuals in each column this time for R is calculated and the parameter whose column has the largest magnitude is identified as the second estimable parameter. The original matrix $y_1$is augmented by including the new column and the sequential process continues until all columns of M are taken into account.

3. The last part of the work opened a very interesting avenue about metabolic regulation. Preliminary results presented here suggest that introducing a sudden perturbation to a culture can improve our description of metabolic regulation. It would be interesting to further apply this approach to analyze model behavior under various other stresses such as those related to glucose and glutamine limitations and over-feeding.

4. The model would get its best use if it would enable us to implement a control strategy based on the knowledge it provides. The scope of the strategy would be to include the explicit estimation of the current state of cell culture, which should then be driven toward and maintained at a desired state. The model should be first applied to the cell cultures in the bioreactor and at least one set of data should be obtained to calibrate the model. Afterwards, the model can be used as an on-line monitoring tool to predict culture behaviour with time. It can also be used to establish a control function relating growth and productivity to process variables. Such model-based control that utilizes controllable variables to maintain the desirable metabolic state can then be implemented in a bioreactor culture.

5. Product quality is a major issue which is generally assessed a posteriori via off-line quality control assays. Product quality is mostly affected by the availability of intracellular sugar nucleotides and culture conditions. Although the model can describe growth and productivity, product quality and in particular the production of sugar nucleotides and their contribution to mAb production is not addressed in the current model. It can be interesting to update the current model to also account for mass balances of sugar nucleotides. In parallel, analysis of glycans in mAb should also be performed with liquid chromatography techniques coupled to mass spectroscopy.

BIBLIOGRAPHY

Abu-Absi, S. F., Yang, L., Thompson, P., Jiang, C., Kandula, S., Schilling, B., & Shukla, A. A. (2010). Defining process design space for monoclonal antibody cell culture. *Biotechnology and Bioengineering, 106*(6), 1097-0290.

Aggarwal, K., Jing, F., Maranga, L., & Liu, J. (2011). Bioprocess optimization for cell culture based influenza vaccine production. *Vaccine, 29*(17), 3320-3328.

Ahn, W. S., & Antoniewicz, M. R. (2011). Metabolic flux analysis of CHO cells at growth and non-growth phases using isotopic tracers and mass spectrometry. *Metabolic Engineering, 13*(5), 598-609.

Ailor, E., Takahashi, N., Tsukamoto, Y., Masuda, K., Rahman, B. A., Jarvis, D. L., . . . Betenbaugh, M. J. (2000). N-glycan patterns of human transferrin produced in Trichoplusia ni insect cells: effects of mammalian galactosyltransferase. *Glycobiology, 10*(8), 837-847.

Alberts, B., Johnson, A., Lewis, J., Raff, M., Roberts, K., & Walter, P. (2002). *Molecular Biology of the Cell* (4 ed.). New York: Garland Science (Taylor & Francis Group).

Alete, D. E., Racher, A. J., Birch, J. R., Stansfield, S. H., James, D. C., & Smales, C. M. (2005). Proteomic analysis of enriched microsomal fractions from GS-NS0 murine myeloma cells with varying secreted recombinant monoclonal antibody productivities. *Proteomics 5*(18), 4689-4704.

Almaas, E., Kovacs, B., Vicsek, T., Oltvai, Z. N., & Barabasi, A. L. (2004). Global organization of metabolic fluxes in the bacterium Escherichia

coli. . *Nature, 427*(697), 839–843.

Altamirano, C., Illanes, A., Becerra, S., Cairo, J. J., & Godia, F. (2006). Considerations on the lactate consumption by CHO cells in the presence of galactose. *Journal of Biotechnololgy, 125*(4), 547-556.

Altamirano, C., Illanes, A., Casablancas, A., Gamez, X., Cairo, J. J., & Godia, C. (2001). Analysis of CHO cells metabolic redistribution in a glutamate-based defined medium in continuous culture. *Biotechnology Progress, 17*(6), 1032-1041.

Altamirano, C., Paredes, C., Cairo, J. J., & Godia, F. (2000). Improvement of CHO cell culture medium formulation: simultaneous substitution of glucose and glutamine. *Biotechnology Progress, 16*(1), 69-75.

Altamirano, C., Paredes, C., Illanes, A., Cairo, J. J., & Godia, F. (2004). Strategies for fed-batch cultivation of t-PA producing CHO cells: substitution of glucose and glutamine and rational design of culture medium. *Journal of Biotechnology, 110*(2), 171-179.

Álvarez-Sánchez, B., Priego-Capote, F., & Castro, M. D. L. (2010). Metabolomics analysis II. Preparation of biological samples prior to detection

TrAC Trends in Analytical Chemistry, 29(2), 120-127.

Alves, R., & Savageau, M. A. (2000). Systemic properties of ensembles of metabolic networks: application of graphical and statistical methods to simple unbranched pathways. *Bioinformatics, 16*(6), 534–547.

Andersen, D. C., & Krummen, L. (2002). Recombinant protein expression for therapeutic applications. *Current Opinion in Biotechnology, 13*(2), 117-123.

Anderson, D. C., & Krummen, L. (2002). Recombinant protein expression for therapeutic applications. *Current Opinion in Biotechnology, 13*(2), 117–123.

Antoniewicz, M. R. (2006). *Comprehensive analysis of metabolic pathways through the combined use of multiple isotopic tracers.* PhD, Massachusetts Institute of Technology.

Aragón, J. J., Felíu, J. E., Frenkel, R. A., & Sols, A. (1980). Permeabilization of animal cells for kinetic studies of intracellular enzymes: in situ behavior of the glycolytic enzymes of erythrocytes. *Proceedings of the National Academy of Science, 77*(11), 6324-6328.

Atkinson, D. E. (1968). Energy charge of the adenylate pool as a regulatory parameter. Interaction with feedback modifiers. *Biochemistry, 7*(11), 4030-4034.

Atkinson, D. E. (1977). *Cellular energy metabolism and its regulation*. New York: Academic Press.

Bailey, J. E., & Ollis, D. F. E. (1986). *Biochemical engineering fundamentals* (2nd ed.). New York.: McGraw-Hill.

Bali, M., & Thomas, S. R. (2001). A modelling study of feed forward activation in human erythrocyte glycolysis. *Comptes Rendus de l'Académie des Sciences - Series III 324*(3), 185–199.

Barnes, L. M., Bentley, C. M., & Dickson, A. J. (2000). Advances in animal cell recombinant protein production: GS-NS0 expression system. *Cytotechnology, 32*(2), 109–123.

Bastin, G., & Dochaln, D. (1990). *On-line Estimation and Adaptive Control of Bioreactors*. United Kingdom: Elsevier Science Ltd.

Batt, B. C., & Kompala, D. S. (1989). A structured kinetic modeling framework for the dynamics of hybridoma growth and monoclonal antibody production in continuous suspension cultures. *Biotechnology and Bioengineering 34*(4), 515–531.

Beard, D. A. (2006). Modeling of oxygen transport and cellular energetics explains observations on in vivo cardiac energy metabolism. *PLoS Computational Biology, 2*(9), 1093-1097.

Beauvieux, M. C., Tissier, P., Gin, H., Canioni, P., & Gallis, J. L. (1986). Butyrate impairs energy metabolism in isolated perfused liver of fed rats. *Journal of nutrition, 131*(7), 1986-1992.

Bebbington, C. R., Renner, G., Thomson, S., King, D., Abrams, D., & Yarranton, G. T. (1992). High-level expression of a recombinant antibody from myeloma cells using a glutamine synthetase gene as an amplifiable selectable marker. *Biotechnology (NY), 10*(2), 169-175.

Beck, A., Wagner-Rousset, E., Bussat, M. C., Lokteff, M., Klinguer-Hamour, C., Haeuw, J., . . . corvaia, N. (2008). Trends in glycosylation, glycoanalysis and glycoengineering of therapeutic antibodies and Fc-fusion proteins. *Current Pharmaceutical Biotechnology, 9*(6), 482–501.

Bedair, M., & Sumner, L. W. (2008). Current and emerging mass-spectrometry technologies for metabolomics. *TrAC Trends in Analytical Chemistry, 27*(3), 238-250.

Berg, J. M., Tymoczko, J. L., & Stryer, L. (2002). *Biochemistry*.

Berthiaume, F., MacDonald, A. D., Kang, Y. H., & Yarmush, M. L. (2003). Control analysis of mitochondrial metabolism in intact hepatocytes: effect of interleukin-1β and interleukin-6. *Metabolic Engineering, 5*(2), 108–123.

Bi, J. X., Shuttleworth, J., & Al-Rubeai, M. (2004). Uncoupling of cell growth and proliferation results in enhancement of productivity in p21CIP1-arrested CHO cells. *Biotechnology and Bioengineering 85*(7), 741-749.

Birch, J. R., Mainwaring, D. O., & Racher, A. J. (2005). Use of the glutamine synthetase (GS) expression system for the rapid development of highly productive mammalian cell processes *Modern Biopharmaceuticals:Design, Development and Optimization (ed J. Knäblein)* (pp. 809–832). Weinheim, Germany: Wiley-VCH Verlag GmbH.

Birch, J. R., & Racher, A. J. (2006). Antibody production. *Advanced Drug Delivery Reviews, 58*(5-6), 671–685.

Bode, B. P., & Souba, W. W. (1994). Modulation of cellular proliferation alters glutamine transport and metabolism in human hepatoma cells. *Annals of Surgery 220*(4), 411-424.

Boeger, H., Bushnell, D. A., Davis, R., Griesenbeck, J., Lorch, Y., Strattan, J. S., . . . Kornberg, R. D. (2005). Structural basis of eukaryotic gene transcription. *FEBS Letters, 579*(4), 899–903.

Böer, E., Steinborn, G., Kunze, G., & Gellissen, G. (2007). Yeast expression platforms. *Applied Microbiology and Biotechnology, 3*(3), 513-523.

Bohnensack, R. (1981). Control of energy transformation of mitochondria: Analysis by aquantitative model. *Biochimica et Biophysica Acta (BBA) - Bioenergetics, 634*, 203-218.

Bonarius, H. P., Hatzimanikatis, V., Meesters, K. P., de Gooijer, C. D., Schmid, G., & Tramper, J. (1996). Metabolic flux analysis of hybridoma cells in different culture media using mass balances. *Biotechnology and Bioengineering, 50*(3), 299-318.

Bonarius, H. P., Houtman, J. H., de Gooijer, C. D., Tramper, J., & Schmid, G. (1998). Activity of glutamate dehydrogenase is increased in ammonia-stressed hybridoma cells. *Biotechnology and Bioengineering, 57*(4), 447-453.

Bonarius, H. P., Houtman, J. H. M., Schmid, G., De Gooijer, C. D., & Tramper, J. (2000). Metabolic-flux analysis of hybridoma cells under oxidative and reductive stress using mass balances. *Cytotechnology, 32*, 92-107.

Bonarius, H. P., Schmid, G., & Tramper, J. (1997). Flux analysis of underdetermined metabolic networks: the quest for the missing constraints. *Trends in Biotechnology, 15*, 308-314.

Bonarius, H. P., Timmerarends, B., de Gooijer, C. D., & Tramper, J. (1998). Metabolite-balancing techniques vs. 13C tracer experiments to determine metabolic fluxes in hybridoma cells. *Biotechnology and Bioengineering, 58*(2-3), 258-262.

Boumphrey, F. (2009). Cell_structure. In C. s. p. diagram of cell .pp ,KB 108 .Vol) ,(.Ed) .(structure

Bree, M. A., Dhurjati, P., Geoghegan, R. F., & Robnett, B. (1988). Kinetic modelling of hybridoma cell growth and immunoglobulin production in a large-scale suspension culture. *Biotechnology and Bioengineering, 32*(8), 1067-1072.

Cacciatore, J. J., Chasin, L. A., & Leonard, E. F. (2010). Gene amplification and vector engineering to achieve rapid and high-level therapeutic protein production using the Dhfr-based CHO cell selection system. *Biotechnology Advances 28*(6), 673–681.

Cascante, M., Boros, L. G., Comin-Anduix, B., de Atauri, P., Centelles, J. J., & W-N Lee, P. (2002). Metabolic control analysis in drug discovery and disease. *Nature Biotechnology, 20*(3), 243-249.

Caspi, R., Altman, T., Dale, J. M., Dreher, K., Fulcher, C. A., Gilham, F., . . . Karp, P. D. (2010). The MetaCyc database of metabolic pathways and enzymes and the BioCyc collection of pathway/genome databases. *Nucleic Acids Research 38(Database issue): D473–D479*.

Castilho, L., Moraes, A., Augusto, E., & Butler, M. (2008). Animal Cell Technology: From Biopharmaceuticals to Gene Therapy(pp. 506).

Castro, P. M., Ison, A. P., Hayter, P. M., & Bull, A. T. (1995). The macroheterogeneity of recombinant human interferon-gamma produced by Chinese-hamster ovary cells is affected by the protein and lipid content of the culture medium. *Biotechnology and Applied Biochemistry 21*(Pt 1), 87-100.

Cazzador, L., & Mariani, L. (1993). Growth and production modeling in hybridoma continuous cultures. *Biotechnology and Bioengineering, 42*(11), 1322–1330.

Chandra, F. A., Buzi, G., & Doyle, J. C. (2009). *Linear control analysis of the autocatalytic glycolysis system.* Paper presented at the chez In Proc of the American Control Conf., St Louis, MO.

Chang, A., Scheer, M., Grote, A., Schomburg, I., & Schomburg, D. (2009). BRENDA, AMENDA and FRENDA the enzyme information system: new content and tools in 2009. *Nucleic Acids Research 37(Database issue):D588–D592*.

Chassagnole, C., Noisommit-Rizzi, N., Schmid, J., Mauch, K., & Reuss, M. (2002). Dynamic modeling of the central carbon metabolism of Escherichia coli. *Biotechnology and Bioengineering, 79*(1), 53-73.

chen, P., & Harcum, S. W. (2007). Differential display identifies genes in Chinese Hamster Ovary cells sensitive to elevated ammonium. *Applied Biochemistry and Biotechnology, 141*(2-3), 349–360.

Chin, C.-S., Chubukov, V., Jolly, E. R., DeRisi, J., & Li, H. (2008). Dynamics and design principles of a basic regulatory architecture controlling metabolic pathways. *PLoS Biology, 6*(6), e146.

Chu, L., & Robinson, D. (2001). Industrial choices for protein production by large-scale cell culture. *Current Opinion in Biotechnology, 12*(2), 180–187.

Chusainow, J., Yang, Y. S., Yeo, J. H., Toh, P. C., Asvadi, P., Wong, N. S., & Yap, M. G. (2009). A study of monoclonal antibody-producing CHO cell lines: what makes a stable high producer? . *Biotechnology and Bioengineering, 102*(4), 1182-1196.

Clark, P., P., C., Curtis, A. S., Dow, J. A., & Wilkinson, C. D. (1990). Topographical control of cell behaviour: II. Multiple grooved substrata. *Developement, 108*(4), 635-644.

Clarke, G. D. (1965). Variations in the tumour-forming capacity of a line of rat fibroblasts (16C) following selection in vitro. *British Journal of Cancer 19*(4), 840-854.

Cloutier, M., Bouchard-Marchand, E., Perrier, M., & Jolicoeur, M. (2008). A predictive nutritional model for plant cells and hairy roots. *Biotechnology and Bioengineering, 99*(1), 189-200.

Cloutier, M., Chen, J., De Dobbeleer, C., Perrier, M., & Jolicoeur, M. (2009). A systems approach to plant bioprocess optimization. *Plant Biotechnology Journal, 7*(9), 939-951.

Cloutier, M., Chen, J., Tatge, F., McMurray-Beaulieu, V., Perrier, M., & Jolicoeur, M. (2009). Kinetic metabolic modelling for the control of plant cells cytoplasmic phosphate. *Journal of Theoritical Biology, 259*(1), 118-131.

Cloutier, M., Perrier, M., & Jolicoeur, M. (2007). Dynamic flux cartography of hairy roots primary metabolism. *Phytochemistry, 68*(16-18), 2393-2404.

Cloutier, M., & Wang, E. (2011). Dynamic modeling and analysis of cancer cellular network motifs. *Integrative Biology (Camb), 3*(7), 724-732.

Cloutier, M., & Wellstead, P. (2010). The control systems structures of energy metabolism *Journal of the Royal Society Interface, 7*(45), 651–665.

Coghill, A. M. (2006). *The ACS style guide: effective communication of scientific information* (3rd ed.). Washington, D.C.: American Chemical Society.

.

Connett, R., & Sahlin, K. (1996). Control of Glycolysis and Glycogen Metabolism *chez Handbook of physiology* (pp. 870–911). New York: Oxford University Press.

Cox, K. M., Sterling, J. D., Regan, J. T., Gasdaska, J. R., Frantz, K. K., Peele, C. G., . . . Dickey, L. F. (2006). Glycan optimization of a human monoclonal antibody in the aquatic plant Lemna minor. *Nature Biotechnology, 24*(12), 1591-1597.

D'Alexandri, F. L., Scolari, S., & Ferreira, C. R. (2010). Reproductive biology in the "omics" era: what can be done? *Animal Reproduction Science 7*(3), 177-186.

Dahodwala, H., Nowey, M., Mitina, T., & Sharfstein, S. T. (2012). Effect of clonal variation in growth, metabolism, and productivity in response to trophic factor stimulation: a study of Chinese hamster ovary cells. *Cytotechnology 64*(1), 27-41.

Dalili, M., & Ollis, D. F. (1989). Transient kinetics of hybridoma growth and monoclonal antibody production in serum-limited cultures. *Biotechnology and Bioengineering, 33*(8), 984-990.

Dalili, M., Sayles, G. D., & Ollis, D. F. (1990). Glutamine-limited batch hybridoma growth and antibody production: experiment and model. *Biotechnology and Bioengineering, 36*(1), 74-82.

Dash, R. K., DiBella, J. A., & Cabrera, M. E. (2007). A computational model of skeletal muscle metabolism linking cellular adaptations induced by altered loading states to metabolic responses during exercise. *BioMedical Engineering OnLine, 6*, 14.

Davies, C. G., Gallo, M. L., & Corvalan, J. R. F. (1999). Transgenic mice as a source of fully human antibodies for the treatment of cancer. *Cancer and Metastasis Reviews, 18*(4), 421–425.

Davies, S. L., Lovelady, C. S., Grainger, R. K., Racher, A. J., Young, R. J., & James, D. C. (2012). Functional heterogeneity and heritability in CHO cell populations. *Biotechnology and Bioengineering, 110*(1), 260-274.

De la Fuente, I. M., Cortes, J. M., Pelta, D. A., & Veguillas, J. (2013). Attractor metabolic networks. *PLoS One, 8*(3), e58284.

De Leon, G. M., Wlaschin, K. F., Nissom, P. M., Yap, M., & Hu, W. S. (2007). Comparative transcriptional analysis of mouse hybridoma and recombinant Chinese hamster ovary cells undergoing butyrate treatment. *Journal of Bioscience and Bioengineering, 103*(1), 82–91.

Dean, J., & Reddy, P. (2013). Metabolic analysis of antibody producing CHO cells in fed-batch production. *Biotechnology and Bioengineering, 110*(6), 1735-1747. doi: 10.1002/bit.24826

Dettmer, K., Aronov, P. A., & Hammock, B. D. (2007). Mass spectrometry-based metabolomics. *Mass Spectrometry Reviews, 26*(1), 51-78.

Dhir, S., Morrow, K. J., Rhinehart, R. R., & Wiesner, T. (2000). Dynamic optimization of hybridoma growth in a fed-batch bioreactor. *Biotechnology and Bioengineering, 67*(2), 197-205.

DiMasi, J. A., Hansen, R. W., & Grabowski, H. G. (2003). The Price of Innovation: New estimates of drug development costs. *Journal of Health Economics, 22*(2), 151-185.

Dinnis, D. M., Stansfield, S. H., Schlatter, S., Smales, C. M., Alete, D., Birch, J. R., . . . James, D. C. (2006). Functional proteomic analysis of GS-NS0 murine myeloma cell lines with varying recombinant monoclonal antibody production rate. *Biotechnology and Bioengineering, 94*(5), 830-841.

Dorka, P., Fischer, C., Budman, H., & Scharer, J. M. (2009). Metabolic flux-based modeling of MAb production during batch and fed-batch operations. *Bioprocess and Biosystems Engineering, 32*(2), 183-196.

Durocher, Y., & Butler, M. (2009). Expression systems for therapeutic glycoprotein production. *Current Opinion in Biotechnology, 20*(6), 700–707.

Durocher, Y., Perret, S., & Kamen, A. (2002). High-level and high throughput recombinant protein production by transient transfection of suspension-growing human 293-EBNA1 cells. *Nucleic Acids Research, 30*(2), E9.

Dzeja, P. P., & Terzic, A. (2003). Phosphotransfer networks and cellular energetics. *The Journal of Experimental Biology, 206*(Pt 12), 2039-2047.

Edwards, J. S., Ramakrishna, R., Schilling, C. H., & Palsson, B. Ø. (1999). Metabolic flux balance analysis. *In: LeeSY, PapoutsakisET, editors. Metabolic engineering. New York: Marcel Dekker* 13-57.

El-Mansi, E. M. T., Dawson, G. C., & Bryce, C. F. A. (1994). Steady-state modelling of metabolic flux between the tricarboxylic cycle and the glyoxylate bypass in escherichia coli. *Computer Applications in the Biosciences (now Bioinformatics), 10*(3), 295-299.

Elliott, S., Chang, D., Delorme, E., Dunn, C., Egrie, J., Giffin, J., . . . Hesterberg, L. (2004). Structural requirements for additional N-linked carbohydrate on recombinant human erythropoietin. *Journal of Biological Chemistry, 279*(16), 16854–16862.

Elliott, S., Egrie, J., Browne, J., Lorenzini, T., Busse, L., Rogers, N., & Ponting, I. (2004). Control of rHuEPO biological activity: The role of carbohydrate. *Experimental Hematology 32*(12), 1146–1155.

Elliott, S., Lorenzini, T., Asher, S., Aoki, K., Brankow, D., Buck, L., . . . Egrie, J. (2003). Enhancement of therapeutic protein in vivo activities through glycoengineering. *Nature Biotechnology, 21*(4), 414–421.

Eppink, M. H. M., Schreurs, R., Gusen, A., & Verhoeven, K. (2009). Platform technology for developing purification processes. *Biopharm International, 20*, 44.

Europa, A. F., Gambhir, A., Fu, P. C., & Hu, W. S. (2006). Multiple steady states with distinct cellular metabolism in continuous culture of mammalian cells. *Biotechnology and Bioengineering 67*(1), 25-34.

Feist, A., & Rosenbloom, J. (2011). Improving mammalian cell line protein production using a metabolic model-based approach. *European Society for Animal Cell Technology, 22*, ESACT meeting.

Fell, D. A. (1997). Increasing the Flux in Metabolic Pathways: A Metabolic Control Analysis Perspective. *Biotechnology and Bioengineering, 58*(2-3), 121-124.

Fernande, E. J. (1987). NMR spectroscopy:a non-invasive tool for studying intracellular processes. *Enzyme and Microbial Technology, 9*(5), 259-271.

Figler, R. A., Graber, S. G., Lindorfer, M. A., Yasuda, H., Linden, J., & Garrison, J. C. (2003). Allosteric enhancers of A1 adenosine receptors increase receptor-G protein coupling and counteract Guanine nucleotide effects on agonist binding. *Molecular Pharmacology, 64*(6), 1557–1564

figueroa, B., J, r., Ailor, E., Osborne, D., Hardwick, J. M., Reff, M., & Betenbaugh, M. J. (2007). Enhanced cell culture performance using inducible anti-apoptotic genes E1B-19K and Aven in the production of a monoclonal antibody with Chinese hamster ovary cells. *Biotechnology and Bioengineering, 97*(4), 877-892.

Fitzpatrick, R. (2013). *Oscillations and Waves: An Introduction* (1 ed.): CRC Press.

Fogolín, M. B., Wagner, R., Etcheverrigaray, M., & Kratje, R. (2004). Impact of temperature reduction and expression of yeast pyruvate carboxylase on hGM-CSF-producing CHO cells. *Journal of Biotechnolology, 109*(1-2), 179-191.

Follstand, B. D., Balcarcel, R. R., Stephanopoulos, G., & Wang, D. I. (2000). Metabolic flux analysis of hybridoma continuous culture steady state mutiplicity. *Biotechnology and Bioengineering, 63*(6), 675-683.

Fox, S. (2004). Maximizing outsourced biopharma production. *Contract Pharma*, 72–78.

Frame, K. K., & Hu, W. S. (1991). Kinetic study of hybridoma cell growth in continuous culture. I. A model for non-producing cells. *Biotechnology and Bioengineering, 37*(1), 55-64.

Frezza, C., Zheng, L., Papkovsky, D. B., Hedley, B. A., Kalna, G., Watson, D. G., & Gottlieb, E. (2011). Metabolic Profiling of Hypoxic Cells Revealed a Catabolic Signature Required for Cell Survival. *PLOS ONE 6*(9), e24411.

Froncisz, W., Lai, C. S., & Hyde, J. S. (1985). Spin-label oximetry: kinetic study of cell respiration using a rapid passage T1 sensitive electron spin resonance display. *Proceedings of the National Academy of Sciences, 82*(2), 411-415.

Fussenegger, M., Schlatter, S., Datwyler, D., Mazur, X., & Bailey, J. E. (1998). Controlled proliferation by multigene metabolic engineering enhances the productivity of Chinese hamster ovary cells. *Nature Biotechnology 16*(5), 468–472.

Gagneur, J., Jackson, D. B., & Casari, G. (2003). Hierarchical analysis of dependency in metabolic networks. *Bioinformatics, 19*(8), 1027-1034.

Gaillet, B., Gilbert, R., Broussau, S., Pilotte, A., Malenfant, F., Mullick, A., . . . Massie, B. (2010). High-level recombinant protein production in CHO cells using lentiviral vectors and the cumate gene-switch. *Biotechnology and Bioengineering 106*(2), 203-215.

Galbraith, D. J., Tait, A. S., Racher, A. J., Birch, J. R., & James, D. C. (2006). Control of Culture Environment for Improved Polyethylenimine-Mediated Transient Production of Recombinant Monoclonal Antibodies by CHO Cells. *Biotechnology Progress 22*(3), 753–762.

Gallazo, J. L., & Bailey, J. E. (1990). Fermentation pathway kinetics and metabolic flux control in suspended and immobilized Saccharomyces cerevisiae. *Enzyme and Microbial Technology 12*(3), 162-172.

Gao, J., Gorenflo, V. M., Scharer, J. M., & Budman, H. M. (2007). Dynamic metabolic modeling for a MAB bioprocess. *Biotechnology Progress, 23*(1), 168–181.

Garfinkel, D. (1971a). Simulation of the Krebs cycle and closely related metabolism in perfused rat liver.I.Construction of a model. *Computers and Biomedical Research 4*(1), 1-17.

Garfinkel, D. (1971B). Simulation of the Krebs cycle and closely related metabolism in perfused rat liver. II. Properties of the model. *Computers and Biomedical Research, 4*(1), 18-42.

Garreau, H., & Buc-Temkine, H. (1972). Allosteric activation of human erythrocyte pyruvate kinase by fructose-1,6-diphosphate: Kinetic and equilibrium binding studies. *Biochimie, 54*(9), 1103–1107.

Gellissen, G., Kunze, G., Gaillardin, C., Cregg, J. M., Berardi, E., Veenhuis, M., & van der Klei, I. (2005). New yeast expression platforms based on methylotrophic Hansenula polymorpha and Pichia pastoris and on dimorphic Arxula adeninivorans and Yarrowia lipolytica - a comparison. *FEMS Yeast Research, 5*(11), 1079-1096.

Genzel, Y., Ritter, J. B., König, S., Alt, R., & Reichl, U. (2005). Substitution of Glutamine by Pyruvate To Reduce Ammonia Formation and Growth Inhibition of Mammalian Cells. *Biotechnology Progress, 21*(1), 58-69.

Gerdtzen, Z. P. (2012). Modeling metabolic networks for Mammalian cell systems: general considerations, modeling strategies, and available tools. *Advances in Biochemical Engineering Biotechnology, 127*, 71-108.

Ghaderi, D., Zhang, M., Hurtado-Ziola, N., & Varki, A. (2012). Production platforms for biotherapeutic glycoproteins. Occurrence, impact, and challenges of non-human sialylation. *Biotechnology and Genetic Engineering Reviews, 28*, 147-176.

Ghorbaniaghdam, A., Chen, J., Henry, O., & Jolicoeur, M. (2013). Metabolomics and in-silico analysis of monoclonal antibody-producing CHO cell clones. *Manuscript submitted for publication*.

Ghorbaniaghdam, A., Henry, O., & Jolicoeur, M. (2012). A kinetic-metabolic model based on cell energetic state: study of CHO cell behavior under Na-butyrate stimulation. *Bioprocess and Biosystems Engineering, 36*(4), 469-487.

Gnoth, S., Jenzsch, M., Simutis, R., & Lübbert, A. (2007). Process Analytical Technology (PAT): Batch-to-batch reproducibility of fermentation processes by robust process operational design and control. *Journal of Biotechnolology, 132*(2), 180-186.

Golemboski, D. B., Lomonossoff, G. P., & Zaitlin, m. (1990). Plants transformed with a tobacco mosaic virus nonstructural gene sequence are resistant to the virus. *Proceedings of the National Academy of Sciences of the United States of America, 87*(16), 6311-6315.

Gomord, V., Fitchette, A. C., Menu-Bouaouiche, L., Saint-Jore-Dupas, C., Plasson, C., Michaud, D., & Faye, L. (2010). Plant-specific glycosylation patterns in the context of therapeutic protein production. *Plant Biotechnol Journal, 8*(5), 564-587.

Goudar, C., Biener, R., Boisart, C., Heidemann, R., Piret, J., de Graaf, A., & Konstantinov, K. (2010). Metabolic flux analysis of CHO cells inperfusion culture by metabolite balancing and 2D [13C,1H] Cosy NMR spectroscopy. *Metabolic Engineering, 12*(2), 138-149.

Grillari, J., fortschegger, K., Grabherr, R. M., O. Hohenwarter, Kunert, R., & Katinger, H. (2001). Analysis of alterations in gene expression after amplification of recombinant genes in CHO cells. *Journal of Biotechnology, 87*(1), 59-65.

Grimbs , S., Selbig , J., Bulik, S., Holzhutter, H. G., & Steuer, R. (2007). The stability and robustness of metabolic states: identifying stabilizing sites in metabolic networks. *Molecular Systems Biology, 3* 146.

Grosvenor, S. (2008). The role of media development in process optimization: an historical perspective. In Guide to Protein Production. *Biopharm International, 21*, S28–S36.

Hames, B. D., & Hooper, N. M. (2005). *Instant Notes in Biochemistry* (3rd edition ed.): Taylor & Francis.

Hardie, D. G., & Hawley, S. A. (2001). AMP-activated protein kinase: the energy charge hypothesis revisited. *Bioessays, 23*(12), 1112-1119.

Harper, M. E., Antoniou, A., Bevilacqua, L., Bezaire, V., & Monemdjou, S. (2002). Cellular energy expenditure and the importance of uncoupling. *Journal of Animal Science, 80*(E. Suppl. 2), E90-E97.

Hatzimanikatis, V., & Bailey, J. E. (1997). Effects of spatiotemporal variations on metabolic control: approximate analysis using (log)linear kinetic models. *Biotechnology and Bioengineering, 54*(2), 91–104.

Hatzimanikatis, V., Floudas, C. A., & Bailey, J. E. (1996). Optimization of regulatory architectures in metabolic. *Biotechnology and Bioengineering, 52*(4), 485–500.

Hayduk, E. J., Choe, L. H., & Lee, K. H. (2004). A two dimentional electrophoresis map of Chinese hamster ovary cell proteins based on fluorescence staining. *Electrophoresis, 25*(15), 2545–2556.

Hayduk, E. J., & Lee, K. H. (2005). Cytochalasin D can improve heterologous protein productivity in adherent Chinese hamster ovary cells. *Biotechnology and Bioengineering 90*(3), 354–364.

Heinrich, R., & Papoport, S. M. (1977). Metabolic regulation and mathematical models. *Progress in Biophysics and Molecular Biology 32*, 1-82.

Hendrick, V., Winnepenninckx, P., Abdelkafi, C., Vandeputte, O., Cherlet, M., Marique, T., . . . Werenne, J. (2001). Increased productivity of recombinant tissular plasminogen activator (t-PA) by butyrate and shift of temperature: a cell cycle phases analysis. *Cytotechnology, 36*(1), 71-83.

Henry, O., Perrier, M., & Kamen, A. (2005). Metabolic flux analysis of HEK-293 cells in perfusion cultures for the production of adenoviral vectors *Metabolic Engineering, 7*(5-6), 467-476.

Heyland, J., Blank, L. M., & Schmid, A. (2011a). Quantification of metabolic limitations during recombinant protein production in Escherichia coli. *Journal of Biotechnology, 155*(2), 178-184.

Heyland, J., Fu, J., Blank, L. M., & Schmid, A. (2011b). Carbon metabolism limits recombinant protein production in Pichia pastoris. *Biotechnology and Bioengineering, 108*(8), 1942-1953. doi: 10.1002/bit.23114

Higgins, E. (2009). Carbohydrate analysis throughout the development of a protein therapeutic. *Glycoconjugate Journal, 27*(2), 211-225.

Hiller, J., Franco-Lara, E., Papaioannou, V., & Weuster-Botz, D. (2007). Fast sampling and quenching procedures for microbial metabolic profiling. *Biotechnology Letters, 29*(8), 1161-1167.

Holzhutter, H. G. (2004). The principle of flux minimization and its application to estimate stationary fluxes in metabolic networks. *Europian Journal of Biochemistry, 271*(14), 2905–2922.

Hossler, P., Khattak, S., & Jian Li, Z. (2009). Optimal and consistent protein glycosylation in mammalian cell culture. *Glycobiology, 19*(9), 936–949.

Hsieh, E. T. (1919). new laboratory animal, cricetiduc griseus. *National Medical Journal of China, 5*, 20-24.

Hynne, F., Danø, S., & Sørensen, P. G. (2001). Full-scale model of glycolysis in Saccharomyces cerevisiae *Biophysical Chemistry, 94*(1-2), 121–163.

Irani, N., Beccaria, A. J., & Wagner, R. (2002). Expression of recombinant cytoplasmic yeast pyruvate carboxylase for the improvement of the production of human erythropoietin by recombinant BHK-21 cells. *Journal of Biotechnology 93*(3), 269-282.

Irani, N., Wirth, M., van Den Heuvel, J., & Wagner, R. (1996). Improvement of the primary metabolism of cell cultures by introducing a new cytoplasmic pyruvate carboxylase reaction. *Biotechnology and Bioengineering, 66*(4), 238-246.

Ishaque, A., & Al-Rubeai, M. (2002). Role of vitamins in determining apoptosis and extent of suppression by bcl-2 during hybridoma cell culture. *Apoptosis, 7*(3), 231–239.

Jakubowski, H. (2008). Biochemistry Online: An Approach Based on Chemical Logic

Jana, S., & Deb, J. K. (2005). Strategies for efficient production of heterogenous proteins in Escherichia coli. *Applied Microbiology and Biotechnology, 67*(3), 289–298.

Jayapal, K., Wlaschin, K., Hu, W.-S., & Yap, M. (2007). Recombinant Protein Therapeutics from Cho Cells - 20 Years and Counting. *CHO Consortium: SBE Special Edition*, 40-47.

Jenkins, N. (2007). Modifications of therapeutic proteins: challenges and prospects. *Cytotechnology, 53*(1-3), 121-125.

Jing, M., & Ismail-Beigi, F. (2007). Critical role of 5'-AMP-activated protein kinase in the stimulation of glucose transport in response to inhibition of oxidative phosphorylation. *American Journal of Physiology, 292*(1), C477-487.

Johnson, C., & Prentice-Hall, D. (1998). *Process Control Instrumentation Technology* (7th ed.): Prentice-Hall

Jolicoeur, M., Chavarie, C., Carreau, P. J., & Archambault, J. (1992). Development of a helical-ribbon impeller bioreactor for high-density plant cell suspension culture. *Biotechnology and Bioengineering 39*(5), 511-521.

Jones, D., Kroos, N., Anema, R., van Montfoort, B., Vooys, A., Van der Kraats, S., . . . Bout, A. (2003). High-level expression of recombinant IgG in the human cell line PER.C6. *Biotechnology Progress 19*(1), 163-168.

Kanani, H., Chrysanthopoulos, P. K., & Klapa, M. I. (2008). Standardizing GC–MS metabolomics. *Journal of Chromatography B, 871*(2), 191-201.

Kanehisa, M., Araki, M., Goto, S., Hattori, M., Hirakawa, M., Itoh, M., . . . Yamanishi, Y. (2008). KEGG for linking genomes to life and the environment. *Nucleic Acids Research 36 (Database issue):D480–D444*.

Karp, P. D., Ouzounis, C. A., Moore-Kochlacs, C., Goldovsky, L., Kaipa, P., Ahrén, D., . . . López-Bigas, N. (2005). Expansion of the BioCyc collection of pathway/genome databases to 160 genomes. *Nucleic Acids Research, 33*(19), 6083–6089.

Kather, H., Rivera, M., & Brand, K. (1972). Interrelationship and Control of Glucose-Metabolism and Lipogenesis in Isolated Fat-Cells - Control of Pentose Phosphate Cycle Activity by Cellular Requirement for Reduced Nicotinamide Adenine-Dinucleotide Phosphate. *Biochemical Journal, 128*(5), 1089-1096.

Kauffman, L. G., Pajerowski, J. D., Jamshidi, N., Palsson, B. O., & Edwards, J. S. (2002). Description and Analysis of Metabolic Connectivity and Dynamics in the Human Red Blood Cell. *Biophysical Journal, 83*(2), 646–662.

Kayser, K., Lin, N., Allison, D., Donahue, L., & Caple, M. (2006). Cell line engineering methods for improving productivity. *BioProcess International, 4*, S6–S13.

Khow, O., & Suntrarachun, S. (2012). Strategies for production of active eukaryotic proteins in bacterial expression system. *Asian Pacific journal of tropical biomedicin, 2*(2), 159-162.

Kim, J., Kim, Y., & Lee, G. M. (2012). CHO cells in biotechnology for production of recombinant proteins: current state and further potential. *Applied Microbiology and Biotechnology, 93*(3), 917-930.

Kim, J. W., Tchernyshyov, I., Semenza, G. L., & Dang, C. V. (2006). HIF-1-mediated expression of pyruvate dehydrogenase kinase: a metabolic switch required for cellular adaptation to hypoxia. *Cell Metabolism, 3*(3), 177-185.

Kim, M. H., Kim, M. O., Heo, J. S., Kim, J. S., & Han, H. J. (2008). Acetylcholine inhibits long-term hypoxia-induced apoptosis by suppressing the oxidative stress-mediated MAPKs activation as well as regulation of Bcl-2, c-IAPs, and caspase-3 in mouse embryonic stem cells. *Apoptosis, 13*(2), 295-304.

Kim, N. S., Byun, T. H., & Lee, G. M. (2001). Key determinants in the occurrence of clonal variation in humanized antibody expression of CHO cells during dihydrofolate reductase mediated gene amplification. *Biotechnology Progress, 17*(1), 69-75.

Kim, N. S., & Lee, G. M. (2001). Overexpression of bcl-2 inhibits sodium butyrate-induced apoptosis in Chinese hamster ovary cells resulting in enhanced humanized antibody production. *Biotechnology and Bioengineering, 71*(3), 184–193

Kimball, E. K., & Rabinowitz, J. D. (2006). Identifying Decomposition Products in Extracts of Cellular Metabolites. *Analytical Biochemistry, 358*(2), 273-280.

Kitano, H. (2002). Systems biology: a brief overview. *Science 295*(5560), 1662–1664

Klamt, S., & Schuster, S. (2002). Calculating as Many Fluxes as Possible in Underdetermined Metabolic Networks. *Molecular Biology Reports, 29*(1-2), 243-248.

Knowles, J. R. (1980). Enzyme-catalyzed phosphoryl transfer reactions. *Annual Review of Biochemistry, 49*, 877–919.

Konrad, M. W., Storrie, B., Glaser, D. A., & Thompson, L. H. (1977). Clonal variation in colony morphology and growth of CHO cells cultures on agar. *Cell 10*(2), 305-312.

Kontoravdi, C., Wong, D., Lam, C., Lee, Y. Y., Yap, M. G., Pistikopoulos, E. N., & Mantalaris, A. (2007). Modeling amino acid metabolism in mammalian cells-toward the development of a model library. *Biotechnology Progress, 23*(6), 1261-1269.

Korzeniewski, B. (1991). An extended dynamic model of oxidative phosphorylation. *Biochimica et Biophysica Acta, 1060*(2), 210-223.

Korzeniewski, B., & Liguzinski, P. (2004). Theoretical studies on the regulation of anaerobic glycolysis and its influence on oxidative phosphorylation in skeletal muscle. *Biophysical Chemistry 110*(1-2), 147-169.

Koshland, D. E. (1968). Regulatory control through conformation changes in proteins. *Advances in Enzyme Regulation, 6*, 291-301.

Koutinas, M., Kiparissides, A., Pistikopoulos, E. N., & Mantalaris, A. (2011). Bioprocess systems engineering: transferring traditional process engineering principles to industrial biotechnology. *Computational and Structural Biotechnology Journal, 3*(4).

Kruger, N. J., & von Schaewen, A. (2003). The oxidative pentose phosphate pathway: structure and organisation. *Current Opinion in Plant Biology, 6*(3), 236-246.

Kumar, N., Gammell, P., & Clynes, M. (2007). Proliferation control strategies to improve productivity and survival during CHO based production culture. *Cytotechnology 53*(1-3), 33-46.

Lai, C. S., Hopwood, L. E., Hyde, J. S., & Lukiewicz, S. (1982). ESR studies of O2 uptake by Chinese hamster ovary cells during the cell cycle. *Proceedings of the National Academy of Science, 79*(4), 1166-1170.

Lai, T., Yang, Y., & Ng, S. K. (2013). Advances in Mammalian Cell Line Development Technologies for Recombinant Protein Production. *Pharmaceuticals, 6*(5), 579-603.

Lambeth, M. J., & Kushmerick, M. J. (2002). A computational model for glycogenolysis in skeletal muscle. *Annals of Biomedical Engineering, 30*(6), 808–827.

Lamboursain, L., St-Onge, F., & Jolicoeur, M. (2002). A lab-respirometer for plant and animal cell culture. *Biotechnology Progress 8*(6), 1377-1386.

Le NovŁre, N., Bornstein, B., Broicher, A., Courtot, M., Donizelli, M., Dharuri, H., . . . Hucka, M. (2006). Biomodels database: a free, centralized database of curated, published, quantitative kinetic models of biochemical and cellular systems. *Nucleic Acids Research 34(Database issue):D689–D691*.

Leader, B., Baca, Q. J., & Golan, D. E. (2008). Protein therapeutics: a summary and pharmacological classification. *Nature Reviews Drug Discovery, 7*(1), 21-39.

Leduc, M., Tikhomiroff, C., Cloutier, M., Perrier, M., & Jolicoeur, M. (2006). Development of a kinetic metabolic model: application to Catharanthus roseus hairy root. *Bioprocess and Biosystems Engineering 28*(5), 295-313.

Lee, S. K., & Lee, G. M. (2003). Development of apoptosis resistant dihydrofolate reductase-deficient Chinese hamster ovary cell line. *Biotechnology and Bioengineering 82*(7), 872–876.

Lee, Y. Y., Wong, K. T., Tan, J., Toh, P. C., Mao, Y., Brusic, V., & Yap, M. G. (2009). Overexpression of heat shock proteins (HSPs) in CHO cells for extended culture viability and improved recombinant protein production. *Journal of Biotechnology 143*(1), 34-43.

Lehninger, A. L. (1977). *Biochemistry*. Worth: New York.

Lewontin, R. (2011). The Genotype/Phenotype Distinction. In E. N. Zalta (Ed.), *Stanford Encyclopedia of Philosophy (Summer 2011 Edition)*. Stanford, CA The Metaphysics Research Lab

Li, F., Vijayasankaran, N., Shen, A., Kiss, R., & Amanullah, A. (2010). Cell culture processes for monoclonal antibody production. *MAbs, 2*(5), 466-477.

Li, J. H., Sun, X. M., & Zhang, Y. X. (2006a). Improvement of hepatitis B surface antigen expression by dimethyl sulfoxide in the culture of recombinant Chinese hamster ovary cells. *Process Biochemistry, 41*(2), 317–322.

Libourel, I. G. L., & Shachar-Hill, Y. (2008). Metabolic Flux Analysis in Plants: From Intelligent Design to Rational Engineering *Annual Review of Plant Biology 59*, 625-650.

Link, T., Bäckström, M., Graham, R., Essers, R., Zörner, K., Gätgens, J., . . . Noll, T. (2004). Bioprocess development for the production of a recombinant MUC1 fusion protein expressed by CHO-K1 cells in protein-free medium. *Journal of Biotechnology 110*(1), 51-62.

Lu, S., Sun, X., Shi, H., & Zhang, Y. (2003). Determination of tricarboxylic acid cycle acids and other related substances in cultured mammalian cells by gradient ion-exchange chromatography with suppressed conductivity detection. *Journal of Chromatography A 1012*(2), 161–168.

Lu, S., Sun, X., & Zhang, Y. (2005). Insight into metabolism of CHO cells at low glucose concentration on the basis of the determination of intracellular metabolites. *Process Biochemistry, 40*(5), 1917-1921.

Lunt, S. Y., & Vander Heiden, M. G. (2011). Aerobic glycolysis: meeting the metabolic requirements of cell proliferation. *Annual Review of Cell and Developmental Biology, 27,* 441-464.

Ma'ayan, A., Blitzer, R. D., & Iyengar, R. (2005). Toward predictive models of mammalian cells. *Annual Review of Biophysics and Biomolecular Structure, 34*, 319–349.

Mackenzie, S., & McIntosh, L. (1991). Higher Plant Mitochondria. *The Plant Cell Online, 11*(4), 571-576.

Macmillan, D., Bill, R. M., Sage, K. A., Fern, D., & Flitsch, S. L. (2001). Selective in vitro glycosylation of recombinant proteins: semi-synthesis of novel homogeneous glycoforms of human erythropoietin. *Chemical Biology, 8*(2), 134-145.

Mahadevan, R., & Schilling, C. H. (2003). The effects of alternate optimal solutions in constraint-based genome-scale metabolic models *Metabolic Engineering, 5*(4), 264-276.

Maharjan, R. P., & Ferenci, T. (2003). Global metabolite analysis: the influence of extraction methodology on metabolome profiles of Escherichia coli. *Analytical Biochemistry, 313*(1), 145-154.

Maier, K., Hofmann, U., Reuss, M., & Mauch, K. (2007). Identification of Metabolic Fluxes in Hepatic Cells From Transient 13C-Labeling Experiments: Part II. Flux Estimation. *Biotechnology and Bioengineering 100*(2), 344-354.

Maier, K., Hofmann, U., Reuss, M., & Mauch, K. (2008). Identification of metabolic fluxes in hepatic cells from transient 13C-labeling experiments: Part II. Flux estimation. *Biotechnology and Bioengineering, 100*(2), 355-370.

Mailier, J., Delmotte, A., Cloutier, M., Jolicoeur, M., & Vande Wouwer, A. (2011). Parametric sensitivity analysis and reduction of a detailed nutritional model of plant cell cultures. *Biotechnology and Bioengineering, 108*(5), 1108-1118.

Martens, D. E. (2007). Metabolic Flux Analysis of Mammalian Cells. In M. Al-Rubeai & M. Fussenegger (Eds.), *Systems Biology* (Vol. 5, pp. 275-299): Springer Netherlands.

Martínez, V. S., Dietmair, S., Quek, L. E., Hodson, M. P., Gray, P., & Nielsen, L. K. (2013). Flux balance analysis of CHO cells before and after a metabolic switch from lactate production to consumption. *Biotechnology and Bioengineering, 110*(2), 660-666.

McDermott, R. H., & Butler, M. (1993). Uptake of glutamate, not glutamine synthetase, regulates adaptation of mammalian cells to glutamine-free medium. *Journal of Cell Science, 104*(Pt 1), 51-58.

McMurray-Beaulieu, V., Hisiger, S., Durand, C., Perrier, M., & Jolicoeur, M. (2009). Na-butyrate sustains energetic states of metabolism and t-PA productivity of CHO cells. *Journal of Bioscience and Bioengineering 108*(2), 160-167.

Meng, M., Chen, S., Lao, T., Liang, D., & Sang, N. (2010). Nitrogen anabolism underlies the importance of glutaminolysis in proliferating cells. *Cell Cycle, 9*(19), 3921-3932.

Meshram, M., Naderi, S., McConkey, B., Ingalls, B., Scharer, J., Budman, H.(2013).Modeling the coupled extracellular and intracellular environments in mammalian cell culture. *Metabolic Engineering*, 19C:57-68.Metallo, C. M., Walther, J. L., & Stephanopoulos, G. (2009). Evaluation of 13C isotopic tracers for metabolic flux analysis in mammalian cells. *Journal of Biotechnology*, 144(3), 167-174.

Meyer, H. P., Brass, J., Jungo, C., Klein, J., Wenger, J., & Mommers, R. (2008). An emerging start for therapeutic and catalytic protein production. *BioProcess International*, 6, S10–S21.

Michaelis, L., Menten, M. L., Johnson, K. A., & Goody, R. S. (2011). The original Michaelis constant: translation of the 1913 Michaelis-Menten paper. *Biochemistry 50*(39), 8264-8269.

Mo, M. L., Palsson, B. O., & Herrgård, M. J. (2009). Connecting extracellular metabolomic measurements to intracellular flux states in yeast. *BMC Systems Biology, 3*, 37.

Morandini, P. (2009). Rethinking metabolic control. *Plant Science, 176*(4), 441-451.

Morris, P. G. (1988). NMR spectroscopy in living systems. *Annual Reports on NMR Spectroscopy, 20*, 1-60.

Mullick, A., Xu, Y., Warren, R., Koutroumanis, M., Guilbault, C., Broussau, S., . . . Massie, B. (2006). The cumate gene-switch: a system for regulated expression in mammalian cells. *BMC Biotechnology, 6*(43).

Nadeau, I., Gilbert, P. A., Jacob, D., Perrier, M., & Kamen, A. (2000). 293SF metabolic flux analysis during cell growth and infection with an adenoviral vector. *Biotechnology Progress, 16*(5), 872–884.

Naderi, S., Meshram, M., Wei, C., McConkey, B., Ingalls, B., Budman, H., & Scharer, J. (2011). Development of a mathematical model for evaluating the dynamics of normal and apoptotic Chinese hamster ovary cells. *Biotechnology Progress, 27*(5), 1197-1205.

Niklas, J., Schräder, E., Sandig, V., Noll, T., & Heinzle, E. (2011). Quantitative characterization of metabolism and metabolic shifts during growth of the new human cell line AGE1.HN using time resolved metabolic flux analysis. *Bioprocess and Biosystems Engineering, 34*(5), 533-545.

Nissom, P. M., Sanny, A., Kok, Y. J., Hiang, Y. T., Chuah, S. H., Shing, T. K., . . . Philp, R. (2006). Transcriptome and proteome profiling to understanding the biology of high productivity CHO cells. *Moleclular Biotechnology 34*(2), 125-140.

Nolan, R. P., & Lee, K. (2010). Dynamic model of CHO cell metabolism. *Metabolic Engineering, 13*(1), 108-124.

Nothaft, H., & Szymanski, C. M. (2011). Protein glycosylation in bacteria: sweeter than ever. *Nature Reviews Microbiology, 8*(11), 765-678.

Oh, M. K., Scoles, D. R., Haipek, C., Strand, A. D., Gutmann, D. H., Olson, J. M., & Pulst, S. M. (2003). Genetic heterogeneity of stably transfected cell lines revealed by expression profiling with oligonucleotide microarrays. *The Journal of Cellular Biochemistry, 90*(5), 1068–1078.

Orth, J. D., Thiele, I., & Palsson, B. Ø. (2010). What is flux balance analysis? *Nature Biotechnology, 28*(3), 245–248.

Palermo, D. P., DeGruf, M. E., Marotti, K. R., Rehberg, E., & Post, L. E. (1992). Production of analytical quantities of recombinant proteins in Chinese hamster ovary cells using sodium butyrate to elevate gene expression. *Journal of Biotechnology 19*(1), 35-48.

Palomares, L. A., Estrada-Mondaca, S., & Ramírez, O. T. (2013). Production of Recombinant Proteins: Challenges and Solutions. In P. Balbás & A. Lorence (Eds.), *Methods in Molecular Biology*. Totowa, NJ: Humana Press Inc.

Paul, M., & Ma, J. K. (2010). Plant-made immunogens and effective delivery strategies. *Expert Review of Vaccines, 9*(8), 821-833.

Pavlou, A. K., & Belsey, M. J. (2005). The therapeutic antibodies market to 2008. *European Journal of Pharmaceutics and Biopharmaceutics, 59*(3), 389-396.

Peterson, J. A. (1976). Clonal variation in albumin messenger RNA activity in hepatoma cells. *Proceedings of the National Academy of Sciences of the United States of America*
6(6), 2056-2060.

Pham, P. L., Kamen, A., & Durocher, Y. (2006). Large-Scale Transfection of Mammalian Cells for the Fast Production of Recombinant Protein. *Molecular Biotechnology, 34*(2), 225-237.

Pitti, R. M., Marsters, S. A., Haak-frendscho, M., Osaka, G. C., Mordenti, J., Chamow, S. M., & Ashkenazi, A. (1994). Molecular and biological properties of an interleukin-1 receptor immunoadhesin. *Molecular Immunology 31*(17), 1345–1351.

Portner, R., & Schafer, T. (1996). Modelling hybridoma cell growth and metabolism—a comparison of selected models and data. *Journal of Biotechnology, 49*(1-3), 119–135

Pörtner, R., Schwabe, J. O., & Frahm, B. (2004). Evaluation of selected control strategies for fed-batch cultures of a hybridoma cell line. *Biotechnology and Applied Biochemistry, 40*((Pt 1)), 47-55.

Price, N. D., Reed, J. L., & Palsson, B. O. (2004). Genome-scale models of microbial cells: evaluating the consequences of constraints. *Nature Reviews Microbiology, 2*(11), 886–897.

Provost, A., & Bastin, G. (2004). Dynamic metabolic modelling under the balanced growth condition. *Journal of Process Control 14*, 717-728.

Quek, L. E., Dietmair, S., Kromer, J. O., & Nielsen, J. (2010). Metabolic flux analysis in mammalian cell culture. *Metabolic Engineering, 12*(2), 161-171.

Rathore, A. S., Bhambure, R., & Ghare, V. (2010). Process analytical technology (PAT) for biopharmaceutical products. *Analytical and Bioanalytical Chemistry, 398*(1), 137-154.

Rathore, A. S., & Winkle, H. (2009). Quality by design for biopharmaceuticals. *Nature Biotechnology, 27*, 26-34.

Reich, J. G., & Sel'Kov, E. E. (1981). *Energy metabolism of the cell - a theoritical treatise*. London: Academic.

Riechmann, L., Clark, M., Waldmann, H., & Winter, G. (1988). Reshaping human antibodies for therapy. *Nature, 332*(6162), 323-327.

Riehl, W. J., & Segrè, D. (2008). Optimal metabolic regulation using a constraint-based model. *Genome Informatics, 20*, 159-170.

Rios-Estepa, R., & Lange, B. M. (2007). Experimental and mathematical approaches to modeling plant metabolic networks. *Phytochemistry, 68*(16-18), 16-18.

Ritter, J. B., Wahl, A. S., S., F., Genzel, Y., & Reichl, U. (2010). Metabolic effects of influenza virus infection in cultured animal cells: Intra- and extracellular metabolite profiling. *BMC Systems Biology 4*, 61.

Rizhaupt, A., Ellis, A., Hosie, K. B., & Shirazi-Beechey, S. (1998). The characterization of butyrate transport across pig and human colonic luminal membrane. *Journal of Physiology, 507*(Pt 3), 819-830.

Rojas, I., Golebiewski, M., Kania, R., Krebs, O., Mir, S., Weidemann, A., & Wittig, U. (2007). Storing and annotating of kinetic data. *In Silico Biology, 7(2Suppl):S37–S44*.

Ryll, T., & Wagner, R. (1991). Improved ion-pair high-performance liquid chromatographic method for the quantification of a wide variety of nucleotides and sugar nucleotides in animal cells. *Journal of Chromatography 570*(1), 77–88.

Samuelson, J. C. (2011). Recent developments in difficult protein expression: a guide to E. coli strains, promoters, and relevant host mutations. *Methods of Molecular Biology, 705*, 195–209.

Saunders, B., Stephen, L., Matthew, D., Brenda, R., Chenette, E., & Subramaniam, S. (2008). The molecule pages database. *Nucleic Acids Research 36(Database issue):D700–D706*.

Sauro, H. M. (2011). *Enzyme Kinetics for Systems Biology* (1th ed.): Lexington, KY : Ambrosius Publishing.

Savinell, J., & Palsson, B. O. (1992). Network analysis of intermediary metabolism using linear optimization. II. Interpretation of hybridoma cell metabolism. *Journal of Theoritical Biology, 73*(4), 154-455.

Schulte, G., & Fredholm, B. B. (2003). The G(s)-coupled adenosine A(2B) receptor recruits divergent pathways to regulate ERK1/2 and p38. *Experimental Cell Research 290*(1), 168–176

Schwarz, F., Huang, W., Li, C., Schulz, B. L., Lizak, C., Palumbo, A., . . . Wang, L. X. (2010). A combined method for producing homogeneous glycoproteins with eukaryotic N-glycosylation. *Nature Chemical Biology, 6*(4), 264-266.

Sellick, C. A., Hansen, R., Maqsood, A. R., Dunn, W. B., Stephens, G. M., Goodacre, R., & Dickson, A. J. (2009). effective Quenching Processes for Physiologically Valid Metabolite Profiling of Suspension Cultured Mammalian Cells. *Analytical Chemistry, 81*(1), 174–183.

Sengupta, N., Rose, S. T., & Morgan, J. A. (2011). Metabolic Flux Analysis of CHO Cell Metabolism in the Late Non-Growth Phase. *Biotechnology and Bioengineering, 108*(1), 82-92.

Seth, G., Philp, R. J., Lau, A., Jiun, K. Y., Yap, M., & Hu, W. S. (2007). Molecular portrait of high productivity in recombinant NS0 cells. *Biotechnology and Bioengineering 97*(4), 933-951

Sheikholeslami, Z., Jolicoeur, M., & Henry, O. (2013). Probing the metabolism of an inducible mammalian expression system using extracellular isotopomer analysis. *Journal of Biotechnology, 164*(4), 469-478.

Shukla, A. A., Hubbard, B., Tressel, T., Guhan, S., & Low, D. (2007). Downstream processing of monoclonal antibodies—application of platform approaches *Journal of Chromatography B 848*(1), 28-39.

Sidorenko, Y., Wahl, A., Dauner, M., Genzel, Y., & Reichl, U. (2008). Comparison of Metabolic Flux Distributions for MDCK Cell Growth in Glutamine- and Pyruvate-Containing Media. *Biotechnology Progress, 24*(2), 311-320.

Siedow, J. N., & Umbach, A. L. (1995). Plant Mitochondrial Electron Transfer and Molecular Biology. *The Plant Cell 7*(7), 821-831.

Smales, C. M., Dinnis, D. M., Stansfield, S. H., Alete, D., Sage, E. A., Birch, J. R., . . . James, D. C. (2004). Comparative proteomic analysis of GS-NS0 murine myeloma cell lines with varying recombinant monoclonal antibody production rate. *Biotechnology and Bioengineering 88*(4), 474-488.

Solomon, E. P., Berg, L. R., & Martin, D. W. (2005). *Biology* (9th ed.).

Starbuck, C., & Lauffenburger, D. A. (1992). Mathematical model for the effects of epidermal growth-factor receptor trafficking dynamics on fibroblast proliferation responses *Biotechnology Progress 8*(2), 132-143

Stephanopoulos, G., Aristodou, A., & Nielsen, J. (1998). *Metabolic Engineering. Principles and Methodologies*: Academic Press, San Diego.

Steuer, R., Grossa, T., Selbigb, J., & Blasiusa, B. (2006). Structural Kinetic Modeling of Metabolic Networks. *The Proceedings of the National Academy of Sciences of the United States of America, 103*(32), 11868–11873.

Sumner, L. W., Mendes, P., & Dixon, R. A. (2003). Plant metabolomics: large-scale phytochemistry in the functional genomics era. *Phytochemistry, 62*(6), 817-836.

Sunstrom, N. S., Gay, R. D., Wong, D. C., Kitchen, N. A., Deboer, L., & Gray, P. P. (2000). Insulin-Like Growth Factor-I and Transferrin Mediate Growth and Survival of Chinese Hamster Ovary Cells. *Biotechnology Progress 16*(5), 698-702.

Szklarczyk, D., Franceschini, A., Kuhn, M., Simonovic, M., Roth, A., Minguez, P., . . . von Mering, C. (2011). The STRING database in 2011: functional interaction networks of proteins, globally integrated and scored. *Nucleic Acids Research 39(Database issue):D561–D568*.

Templeton, N., Dean, J., Reddy, P., & Young, J. D. (2013). Peak antibody production is associated with increased oxidative metabolism in an industrially relevant fed-batch CHO cell culture. *Biotechnology and Bioengineering, 110*(7), 2013-10204.

Thomas, S., Mooney, P. J., Burrell, M. M., & Fell, D. A. (1997). Finite change analysis of glycolytic intermediates in tuber tissue of lines of transgenic potato (Solanum tuberosum) overexpressing phosphofructokinase. *Biochemistry Journal, 15*((Pt 1)), 111-117.

Tjio, J. H., & Puck, T. T. (1958). Genetics of somatic mammalian cells. II. Chromosomal constitution of cells in tissue culture. *The Journal of Experimental Medicine, 108*(2), 259-268.

Tremblay, M., Perrier, M., Chavarie, C., & Archambault, J. (1992). Optimization of fed-batch culture of hybridoma cells using dynamic programming: single and multi-feed cases. *Bioprocess Engineering, 7*, 229-234.

Tsuchiya, H. M., Fredrickson, A. G., & Aris, R. (1966). Dynamics of microbial cell population. *Advanced Chemical Engineering, 6*, 125–206.

Tyson, J. J., Chen, K. C., & Novak, B. (2003). Sniffers, buzzers, toggles and blinkers: Dynamics of regulatory and signaling pathways in the cell. *Current Opinion in Cell Biology 15*(2), 221-231.

Valancin, A., Srinivasan, B., Rivoal, J., & Jolicoeur, M. (2013). Analyzing the effect of decreasing cytosolic triosephosphate isomerase on Solanum tuberosum hairy root cells using a kinetic-metabolic model. *Biotechnology and Bioengineering, 110*(3), 924-935.

Van den Berg, C. J., & Garfinkel, D. (1971). A simulation study of brain compartments:Metabolism of glutamate and related substances in mouse brain. *Biochemical Journal, 123*(2), 211-218.

van der Heijden, R., Heijnen, J., Hellinga, C., Romein, B., & Luyben, K. (1994). Linear constraint relations in biochemical reaction systems. I. Classification of the

calculability and the balanceability of conversion rates. *Biotechnologe and Bioengineering, 43*(1), 3-10.

Van der Valk, P., Gille, J. J. P., van der Plas, L. H. W., Jongkind, J. F., Verkerk, A., Konings, A. W. T., & Joenje, H. (1998). Characterization of oxygen-tolerant Chinese hamster ovary cells: II. Energy metabolism and antioxidant status. *Free Radical Biology and Medicine, 4*(6), 345-356.

Vaseghi, S., Baumeister, A., Rizzi, M., & Reuss, M. (1990). In vivo dynamics of the pentose phosphate pathway in Saccharomyces cerevisiae. *Metabolic Engineering, 1*(2), 128-140.

Vastrik, I., D'Eustachio, P., Schmidt, E., JoshiTope, G., Gopinath, G., Croft, D., . . . Stein, L. (2007). Reactome: a knowledge base of biologic pathways and processes. *Genome Biology, 8*, R39.

Vezina, L. P., Couture, M., Paquet, D., Dargis, M., & D'Aoust, M. A. (2013). Canada Patent No. US20130067807 A1. M. INC.

Voet, D., & Voet, J. G. (2011). *Biochemistry*: John Wiley & Sons.

Wahl, A., Sidorenko, Y., Dauner, M., Genzel, Y., & Reichl, U. (2008). Metabolic flux model for an anchorage-dependent MDCK cell line: Characteristic growth phases and minimum substrate consumption flux distribution. *Biotechnology and Bioengineering, 101*(1), 135-152.

Wang, C. S. (1977). Inhibition of human erythrocyte lactate dehydrogenase by high concentrations of pyruvate. Evidence for the competitive substrate inhibition. *european Journal of biochemistry, 78*(2), 569-574.

Wang, L., Birol, I., & Hatzimanikatis, V. (2004). Metabolic control analysis under uncertainty: framework development and case studies. *Biophysical Journal, 87*(6), 3750-3763.

Wheaton, W. W., & Chandel, N. S. (2011). Hypoxia. 2. Hypoxia regulates cellular metabolism. *American Journal of Physiology 300*(3), 385-393.

Whitford, W. G. (2006). Fed-batch mammalian cell culture in bioproduction. *BioProcess International, 4*(3), 30–44.

Wilkens, C., Altamirano, C., & Gerdtzen, Z. (2011). Comparative metabolic analysis of lactate for CHO cells in glucose and galactose. *Biotechnology and Bioprocess Engineering, 16*(4), 714-724.

Wilson, D. F., Erecinska, M., Drown, C., & Silver, I. A. (1977). Effect of oxygen tension on cellular energetics. *American Journal of Physiology 233*(5), 135-140.

Wlaschin, K., & Hu, W.-S. (2006). Fedbatch Culture and Dynamic Nutrient Feeding. In W.-S. Hu (Ed.), *Cell Culture Engineering* (Vol. 101, pp. 43-74): Springer Berlin Heidelberg.

Wolf, J., Passarge, J., Somsen, O. J. G., Snoep, J. L., Heinrich, R., & Westerhoff, H. V. (2000). Transduction of intracellular and intercellular dynamics in yeast glycolytic oscillations. *Biophysical Journal, 78*(3), 1145–1153.

Wright, B. E., Butler, M. H., & Albe., K. R. (1992). Systems analysis of the tricarboxylic acid cycle in dictyostelium discoideum. i. the basis for model construction. *Journal of Biological Chemistry, 267*(5), 3101–3105.

Wu, F., Yang, F., Vinnakota, K. C., & Beard, D. A. (2007). Computer Modeling of Mitochondrial Tricarboxylic Acid Cycle, Oxidative Phosphorylation, Metabolite

Transport, and Electrophysiology. *Journal of Biological Chemistry, 282*(34), 24525–24537.

Wurm, F. M. (2004). Production of recombinant protein therapeutics in cultivated mammalian cells. *Nature Biotechnology 22*(11), 1393-1398.

Wurm, F. M. (2005). *The industry's workhorses-Mammalian expression systems," Modern biopharmaceuticals* (Vol. 3). Weiheim: Wiley-VCH.

Wysocki, V. H., Resing, K. A., Zhang, Q., & Cheng, G. (2005). Mass spectrometry of peptides and proteins. *Methods, 35*(3), 211-222.

Xie, L., & Wang, D. I. (1996). Material balance studies on animal cell metabolism using a stoichiometrically based reaction network. *Biotechnology and Bioengineering, 52*(5), 579-590.

Xie, L., & Wang, D. I. C. (1996). Energy metabolism and ATP balance in animal cell cultivation using a stoichiometrically based reaction network. *Biotechnology and Bioengineering, 52*(5), 591-601.

Xie, L., & Wang, D. I. C. (2006). Fed-batch cultivation of animal cells using different medium design concepts and feeding strategies. *Biotechnology and Bioengineering, 95*(2), 270-284.

Xun, X., Harish, N., Nathan, E. L., Shengkai, P., Zhiming, C., Xin, L., . . . Jun, W. (2011). The genomic sequence of the Chinese hamster ovary (CHO)-K1 cell line. *Nature Biotechnology, 29*(8), 735–741.

Yang, Z., & Xiong, H. R. (2012). Culture Conditions and Types of Growth Media for Mammalian Cells. In L. Ceccherini-Nelli (Ed.), *Biomedical Tissue Culture* (pp. 1-18).Yao, K. Z., Shaw, B. M., Kou, B., McAuley, K. B., Bacon, D. W. (2003). Modeling ethylene/butene copolymerization with multi-site catalysts: parameter estimability and experimental design. Polymer Reaction Engineering, 11(3), 563-588.

Yee, J. C., De Leon, G. M., Philp, R. J., Yap, M., & Hu, W. S. (2008). Genomic and proteome exploration of CHO and hybridoma cells under sodium butyrate treatment. *Biotechnology and Bioengineering 99*(5), 1186-1204.

Yoon, S. K., Hwang, S. O., & Lee, G. M. (2004). Enhancing Effect of Low Culture Temperature on Specific Antibody Productivity of Recombinant Chinese Hamster Ovary Cells: Clonal Variation. *Biotechnology Progress, 20*(6), 1683-1688.

Zagari, F., Jordan, M., Stettler, M., Broly, H., & Wurm, F. M. (2013). Lactate metabolism shift in CHO cell culture: the role of mitochondrial oxidative activity. *New Biotechnology, 30*(2), 238-245.

Zamorano, F., Vande Wouwer, A., Jungers, R. M., & Bastin, G. (2012). Dynamic metabolic models of CHO cell cultures through minimal sets of elementary flux modes. *Journal of Biotechnology 146*(3), 409-422.

Zamorano, F., Wouwer, A. V., & Bastin, G. (2010). A detailed metabolic flux analysis of an underdetermined network of CHO cells. *Journal of Biotechnology, 150*(4), 497-508. doi: 10.1016/j.jbiotec.2010.09.944

Zanghi, J. A., Renner, W. A., Bailey, J. E., & Fussenegger, M. (2000). The growth factor inhibitor suramin reduces apoptosis and cell aggregation in protein-free CHO cell batch cultures. *Biotechnology Progress, 16*(3), 319–325.

Zdzienicka, M., Cupido, M., & Simons, J. W. (1985). Increase in clonal variation in Chinese hamster ovary cells after treatment with mutagens. *Somatic Cell and Molecular Genetics, 11*(2), 127-134.

Zhang, F., Sun, X., Yi, X., & Zhang, Y. (2006). Metabolic characteristics of recombinant Chinese hamster ovary cells expressing glutamine synthetase in presence and absence of glutamine. *Cytotechnology, 51*(1), 21-28.

Zhang, L., Shen, H., & Zhang, Y. (2004). Fed-batch culture of hybridoma cells in serum-free medium using an optimized feeding strategy. *Journal of Chemical Technology and Biotechnology, 79*(2), 171–181.

Zhou, F., Bi, J. X., Zeng, A.-P., & Yuan, J. Q. (2006). A macrokinetic and regulator model for myeloma cell culture based on metabolic balance of pathways. *Process Biochemistry, 41*(10), 2207-2217.

Živadinovic, D., & Nikcevic, M. (2010). Kinetic properties of lactate dehydrogenase from trout muscle *Archives of Biological Science, 62*(2), 297-300.

Zomorrodi, A. R., Suthers, P. F., Ranganathan, S., & Maranas, C. D. (2012). Mathematical optimization applications in metabolic networks. *Metabolic Engineering 14*(6), 672-686.

Zupke, C., & Stephanopoulos, G. (1995). Intracellular flux analysis in hybridomas using mass balances and in vitro (13)C NMR. *Biotechnology and Bioengineering, 45*(4), 292-303.

APPENDICES

APPENDIX 1Protocol to thaw and pass CHO-cum2 cells

I. Pre-Culture condition

Static conditions: 25 cm^2 or 75 cm^2 T-flasks containing respectively 5.0-7.0 mL or 16-20 ml of SFM4CHO medium culture supplemented with glutamine, dextran sulphate and hygromycine B. Starting density: between 0.4-0.5 $*10^6$ cells/ml; maintain cells at a density ranging from 1.5-2$*10^6$ cells/ml before passing them. Cultivate cells at 37°C, 5% CO_2.

Agitated conditions: 125 mL shaker-flasks containing 20 mL of medium culture supplemented with glutamine, dextran sulphate and hygromycine B. Starting density: between 0.15-0.2 $*10^6$ cells/ml; maintain cells at a density ranging from 1.5-2$*10^6$ cells/ml before passing them. Cultivate cells at 37°C, 5% CO_2, 100 rpm.

II. Protocol to thaw and pass cells

Purpose

To ensure a proper thawing of cells

Background information

As the suspension of cells freezes in liquid nitrogen, ice crystals form. These ice crystals can puncture the plasma membrane, leading to cell death. Dimethyl sulfoxide (DMSO) protects the cells by partially solublizing the membrane to mekae it less prone to puncture in a way that the water can flow out of the cells preventing the formation of ice crystals inside the cells, and also interrupting the lattice of the ice, so that fewer crystals form. Freezing media contains DMSO. Since it is also toxic for the cells (it partially solublizes the membrane, after all), when thawing cells it's important to remove DMSO as soon as possible.

Materials:

1. 15 ml Falcon tube
2. 25 cm^2 T-flasks
3. 1.0 mL Glass Pipette, 10.0 mL Glass Pipette
4. previously prepared fresh cold media

Solution preparation

1. Preparation of pre-culture Medium

SFM4CHO medium culture requires supplementation of glutamine (4 mM), dextran sulphate (0.05 mg/ml) and hygromycine B (0.55-0.6 mg/ml).

2. stock solutions of medium

    1. 100X solution of Dextran sulphate (5 mg/ml)

(Dextran sulphate is a powder. So, Prepare a 100X solution and filter through a 0.22 µm filter. Keep the filtered solution in a falcon at 4°C)

    2. 50X solution of glutamine (200 mmol/l)
    3. 100X solution of hygromycin B (50 mg/ml)

Thawing of cells:

1. Check the frozen cell log sheet to verify the place of the cell aliquot cryovial in the tray rack of liquid N_2 tank (example:Rack 8 ,tray 4)

2. Slowly remove appropriate rack from liquid N_2 tank. Remove long safety pin and take out one cryovial from clones and sub-clones tubes in appropriate tray (each vial contains 5 million cells)

3. Put tray back in slot and put safety pin back in place. Return tray rack to liquid N_2 tank and cap tank again.

4. Thaw the cell suspension gently swirling the cryovial into a 37°C water bath until cells are defrosted(less than one minute). To avoid contamination Do not immerge the cap into water

5. Gently wipe cryovial with EtOH and transfer it under the hood.

6. Under the hood, transfer the contents of the cryovial into a 15 ml Falcon tube containing 10 mL of cold fresh culture medium . Pipet contents of vial (~ 1 mL) into the falcon.

7. Centrifuge 5 min at 1000 rpm at 4°C. A compact cell pellet should be visible

8. Carefully remove the supernatant by aspirating with a 10 mL pipette.

9. Re-suspend the cells pellet into 7.5 ml of fresh medium culture by transferring cells to a 25 Cm^2 T-flask containing 7.5 mL of media(previously placed in the incubator and equilibrated at 37°C). Pipet slowly several times to obtain a homogenous cell suspension.

10. Close the flask by screwing the cap.

11. Cultivate cells at 37°C,5% CO_2.

    Note: if the cap does not have a filter, it should be loosely screwed to allow proper ventilation and CO_2 equilibration.)

12. At day3, count manually the number of cells, using a hematocymeter) and check the viability of cells. If they are in a good shape, dilute them to 0.2-0.4 $*10^6$ cells with the final volumn of 7.5 mL.

13. At day five follow the same structure as 9

14. At day seven transfer cells to a shaker-flask to be expanded to the quantity needed to start the experiment.

APPENDIX 2 Protocol to expand CHO-cum2 cells suspension culture

Purpose

To ensure a reproducible expansion of CHO cells by in vitro culture at a desired level with no loss of cell properties.

Notes

The following SOPs have to be red and understood before performing the present Protocol:

1. Protocol to thaw and pass cellS
2. Hemacotymeter cell counting SOP

This protocol has to be performed rapidly without any lag between manipulations: all material and calculations have to be done prior to each step, or be rapidly performed while proceeding with the protocol when needed.

Materials

Static condition

1. 25 cm^2 T-flask with Vent Cap (Corning, 32-90), QTY:1
2. 75 cm^2 T-flask with Vent Cap (Corning, 32-90), QTY:10
3. 5.0 mL sterile glass pipette (VWR 89130-896), QTY:1
4. 10.0 mL sterile glass pipette (VWR 89130-898), QTY:4
5. 25.0 mL sterile Glass Pipette (VWR 89130-900), QTY:5
6. 50 mL sterile Falcon tube(VWR 525-0402),QTY:1
7. prepared sterile fresh media (please check the protocol of how to pass and thaw CHO cells for details), QTY: 160 mL

Agitation condition

1. 25 cm^2 T-flask with Vent Cap (Corning, 32-90), QTY:1
2. 75 cm^2 T-flask with Vent Cap (Corning, 32-90), QTY:1
3. 5.0 mL sterile glass pipette (VWR 89130-896), QTY:1
4. 10.0 mL sterile glass pipette (VWR 89130-898), QTY:4
5. 25.0 mL sterile Glass Pipette (VWR 89130-900), QTY:3
6. 50 mL sterile Falcon tube(VWR 525-0402),QTY:1
7. prepared sterile fresh media (please check the protocol of how to pass and thaw CHO cells for details), QTY: 80 mL
8. 125 ml sterile Erlenmeyer Flask with 2 µm vent cap (Corning,431143),QTY:3

Cell expansion in T-flasks

The following protocol is to fulfill the total amount of $100*10^6$ cells. Expand cells until the number of viable cells needed is reached.

1. Calculate the required amount of cells to inoculate and perform the experiment and write it down in your lab book. Some examples of calculations are given below.

   Imagine that you want to follow the protocol for freezing CHO cell line. Each freezing tube has to be contained $5*10^6$ cells. So, to end up with 10 freezing tubes, the total amount of cells needed is $50*10^6$. In another example, you want to perform an experiment in which you will have 10 batches of 125 ml shaker-flasks each of them contain 25 ml of cell culture with an initial cells density of $0.2*10^6$ cells. So, the total cell amount needed to start that experiment is calculated by multiplying the total volume of cell culture (mL) to initial cell density (cells/ml) which here is:

   10(number of shaker-flasks)* 25(volume of cell culture in each shaker-flask)*$0.2*10^6$ (cell density at each culture) =$50*10^6$ cells.

2. Count manually the number of cells (using a hematocymeter), as described in hemacotymeter cell counting SOP , in the pre-culture 25 cm^2 T-flask (Corning, 32-90) placed in the incubator at 37°C,5% CO_2 and used as inoculum of the cell expansion cultures; verify cell viability (as explained in hemacotymeter cell counting SOP). Only use the cells if their viability is greater than or equal to 95%. Dilute the required volume of cell suspension to obtain 0.2 $*10^6$ cells/mL (example of calculations given below) for a final volume of 6 ml of culture medium at 37°C (prepared as explained in the protocol of pass and thaw CHO cell culture), transfer this 6 mL cell suspension in a 25 cm^2 T-flask used for cell expansion. Cultivate cells at 37°C, 5% CO_2. For example suppose you counted the total cell number of 350 in four large corner squares using a hemocytometer for a pre-culture 25 cm^2 T-flask (as explained in hemacotymeter cell counting SOP) . You have then 1093570 cells/ml in that T-flask. In this case 1 mL of cell suspension should be diluted intoa 5 mL fresh mediumto get a special cell density of0.2 $*10^6$ cells/ml. Using a 1 ml glass pipette, 1 mL of a cell suspention is transferred into a new 25 cm^2 T-flask and using a 5 ml glass pipette 5 mL of fresh media is added.

3. At day 2, count manually the number of cells (using a hematocymeter) and check the viability of cells.The viability must be of 95% or more and cell density should be around $1*10^6$ cells/ml. Using a 10 ml glass pipette, transfer the whole cell culture (around 6 mL) to a 75-cm^2 T-flask (T-flask 1). Using another 10 ml glass pipette, add 9 mL of fresh medium *at 37°C.*

4. At day 4,count manually the number of cells (using a hematocymeter) and check the viability of cells. Cell density should be around $1*10^6$ cell/ml. Transfer 7 mL of the cell suspension in theT-flask 1 to a new 75-cm^2 T-flask (T-flask 2). Add 9mL of fresh medium to T-flasks 1 and 2at 37°C.

5. At day 6, count manually the number of cells (using a hematocymeter) and check the viability of cells in one of the T-flasks in the incubator. Cell density should be around $1*10^6$ cells/ml. transfer 8 new 75 cm^2 T-flasks under the hood (T-flasks identified as 3,4,5,6,7,8,9, and 10). Using a 25 ml glass pipette, pipette 12 mL of the cell suspension in T-flask 1 and transfer 3 mL into each of the T-flasks 3,4,5, and 6. Using another 25 mL glass pipette , add 12ml of fresh medium to each of the T-flasks 1,3,4,5, and 6. Proceed with T-flask 2 and pipette 12 ml of the cell suspension in T-flask 2 and transfer 3ml into each of the T-flasks 7,8,9, and 10 Using a another 20 ml glass pipette , add 12ml of fresh medium to T-flasks 2,7,8,9, and 10. Incubate 10 T-flasks *at 37°C, 5% CO_2* .

6. At day 8, count manually the number of cells (using a hematocymeter) and check the viability of cells in one of the T-flasks in the incubator. Cell density should be around $1*10^6$ cell/ml .Check your calculations in your lab book again to verify the total number of cells needed. Calculate the total volume of cell suspension should be collected considering that cell density in all T-flasks is almost the same. Here is an example of how to proceed with calculation:From the example in step 1, you can calculate that the total amount of 25 $*10^6$ cells is needed if you want to process 5 freezing tubes at a time.Divide this total *c*ell numberby $1*10^6$ cells/ml to calculate how much cell suspension is needed to be collected. It is calculated that 25 mL of cell suspension should be collected for centrifugation. Using a 25 ml glass pipette, transfer 15 mL of culture in T-Flask 1 into a 50 ml Falcon tube. Transfer the remaining 10 mL from T-Flask 2 to the same Falcon tube*.*

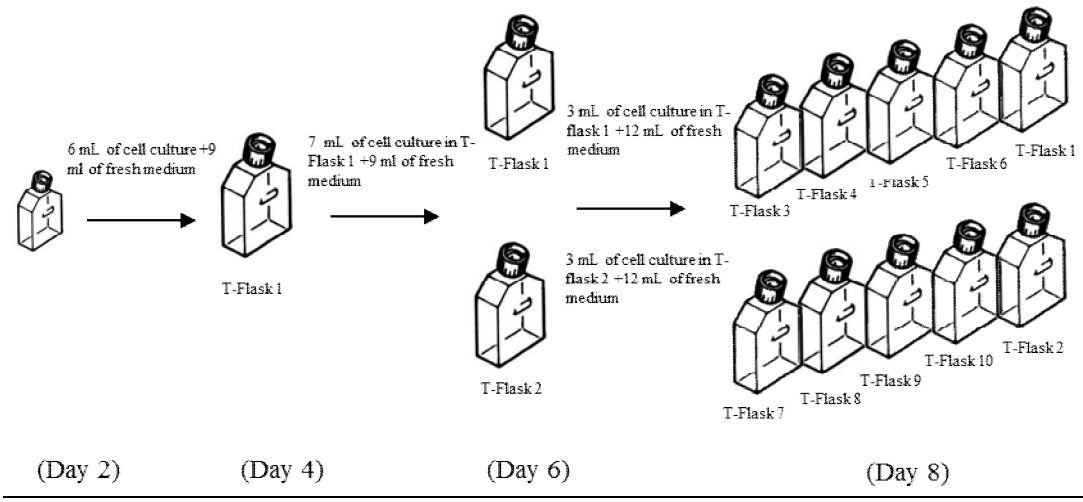

Figure A.0.1 Schematic diagram of cell expansion in T-flasks

7. Harvest the cells in the 50 ml falcon tube by centrifugation(1000 rpm,5 min)

Cell expansion in shake flasks

1. Repeat the expansion process described above (steps 1,2,3).

2. At day 4, count manually the number of cells (using a hematocymeter) and check the viability of cells. The viability must be around 95% or more. Cell density should be around $1*10^6$ cell/ml. Transfer 3 new 125-cm^2 sterile Erlenmeyer Flask with 2 µm vent cap under the hood (Erlenmeyer Flasks identified as 1,2, and3). Using a 25 mL glass pipette, pipette 15 mL of the cell suspension in T-flask 1 and transfer 5 mL into each of the 125 ml Erlenmeyer Flasks (identified as 1,2, and 3). Using another 25 ml glass pipette, add 20mL of fresh medium to each Erlenmeyer Flask. Incubate 3 Erlenmeyer Flasks with a cell density of$0.2 *10^6$ cell/mlat 37°C, 5% CO_2, 100 rpm.

3. At day 6, count manually the number of cells (using a hematocymeter) and check the viability of cells in one of the T-flasks in the incubator. Cell density should be around 1.5-2 $*10^6$ cells/ml. Check your calculations in your lab book again to verify the total number of cells needed. Calculate the total volume of cell suspension should be collected considering that

cell density in all Erlenmeyer Flasksis almost the same. Referring then to the second example in step 1, the total number of 50*10 ^{6} cells is needed. Like the calculations in the last step, divide this total cell number by *2*10^{6} cells*/ml to calculate how much cell suspension is needed to be collected. It is calculated that 50 ml of cell suspension should be collected for centrifugation.

Using a 25 ml glass pipette, transfer 25 mL of culture in Erlenmeyer Flasks1 into a 50 ml Falcon tube.

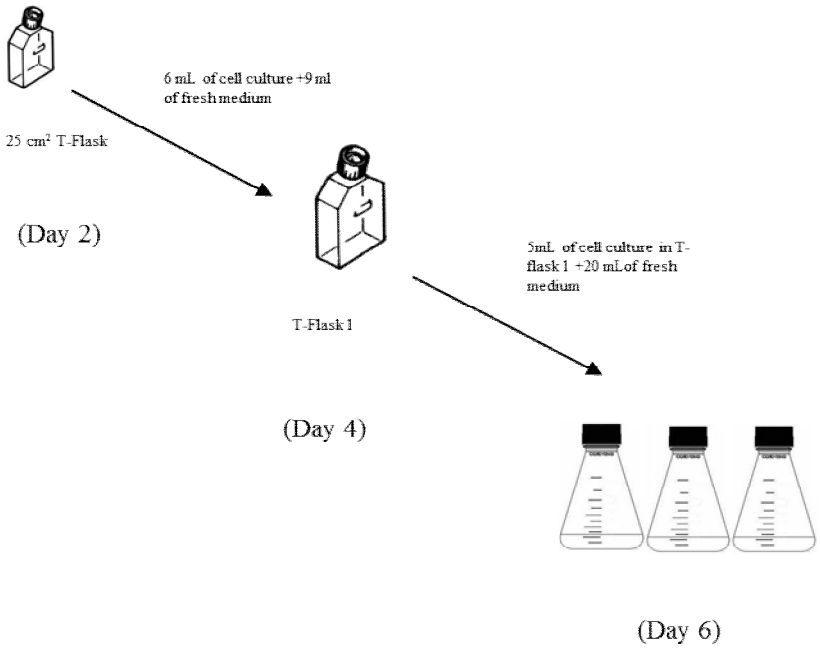

Figure A.0.2 Schematic diagram of cell expansion in shake-flasks

4. Harvest the cells in the 50 ml falcon tube by centrifugation(1000 rpm,5 min)

APPENDIX 3 Protocol for the quantification of CD-20 expressed in CHO-cum2 cells

Materials:

1. Tween 20
2. Casein
3. PBS
4. 1 N hydrochloric acid
5. Sodium carbonate (Fischer Scientific, Burlington, Canada, cat. # S263-1)
6. 3,3,5,5′-Tetramethylbenzidine (TMB) (Sigma, Oakville, Canada, cat. # T0440)
7. Goat anti-human IgG1 (H+L) solution (Jackson ImmunoResearch, PA, USA, cat. # 109-165-003)
8. Peroxidise-conjugated affinipure fragment Goat anti-human IgG (Jackson Immuno Research, PA, USA, cat. # 109-035-003)
9. 96-well plates (Costar) (Fisher Scientific, Burlington, Canada,cat. # 3795)

Solution preparation

Washing solution

1. Add 1 mL of Tween 20 in 1 L o PBS 10 mM (1 pack in 1 L of MilliQ water)

Blockage solution

1. Add 2g of Casein in 200 mL of PBS 10 mM
2. Heat in microwave for 1 min (for larger volumn heat 30 seconds per each 100 Ml)
3. Stir for 3 hours
4. Centrifuge for 5 min at 2000 RPM
5. Gently recuperate the supernatant
6. Incubate overnight at 4ºC

Steps

Adsorbtion of capture antibody on plate

1. Dilute 18 µL of anti-human IgG in 10 mL of sodium Carbonate 50 mM
2. Distribute 50 µL of capture antibody in each well (# 3369)
3. Incubate overnight at 4ºC

Preparation of standard curve

1. Add 0.89 µL of IgG (11.2 mg/mL) to 99.11 µL of blockage solution to prepare 100 µg/mL solution

2. Add 10 µL of standard (100 µL/mL) to 990 µL of blockage solution to prepare 1 µg/mL solution
3. Add 50 µL of standard (1µg/mL) to 1950 µL of blockage solution to prepare 2.5 ng/mL solution

Concentration (ng/mL)	Vol (µL) from STD (25 ng/mL)	Vol (µL) from blockage solution
10	400	600
7	280	720
5	200	800
4	160	840
3	120	880
2	80	920
1	40	960
0	0	1000

Sample loading

1. Wash plate 3 times using 150 µL/well of washing solution
2. Distribute 50 µL/well of sample and standard
3. Incubate 1h at 37 ºC

Secondary antibody

1. Wash plate 3 times using 150 µL/well of washing solution
2. Add 10 µL of peroxidase conjugated goat anti-human IgG in 40 µL of blockage solution
3. Add 6 µL of this solution to 6 mL of blockage solution
4. Distribute 50 µL/well of peroxidase conjugate antibody
5. Incubate1h at 37 ºC

Revelation

1. Wash plate 3 times using 150 µL/well of washing solution
2. Distribute 50 µL/well of substrate TMB
3. Incubate for 5 to 10 min at room temperature in dark
4. Stop reaction by adding 50 µL/well of HCL
5. Read absorbance at 450 nm

APPENDIX 4 Protocol of cold methanol extraction of CHO cells

Objectives

This « procédure d'opération normalisée » (PON) or *standard operating procedure* (SOP) is established to describe the process of mammalian cell extraction in order to perform organic acid analysis by LC-MS

Fields of use and application

This SOP is valuable only for mammalian cell extraction in order to perform organic acid analysis by LC-MS, but one can inspire from it to generate another extraction SOP.

Responsibilities

It is the responsibility of each to respect the SOP directives of all reagents, instruments, or machines used in this SOP.

Security

By following the directives in this SOP and common sense, adequate security will be maintained.

Principle

In order to have as complete understanding as possible of the metabolic activity of cells, it is necessary to study many components of the cellular metabolic network in parallel. So the main challenge in metabolite analysis is the extraction of compounds of interest from biological sample. Several extraction methods have been reported. For example, Maharjan and Fernci (Maharjan & Ferenci, 2003) examined the efficiency of extracting *E.Coli* with boiling ethanol: water, cold methanol: water, and perchloric acid extraction, and they found cold methanol: water (50:50 mixture) to be the best approach. Kimbell et al (Kimball & Rabinowitz, 2006) used cold 80:20 methanol water mixture and found the higher methanol content is preferred.

Based on the reported results (Faijes, Mars, & Smid, 2007; Luo et al., 2007; Faijes et al., 2007) and our own studies, a modified procedure based on cold methanol extraction combined good extraction under mild extraction condition and high enzymatic inactivation and made it very suitable for metabolism studies.

Materials, reagents, and instruments

Material

1. Tips (200 µl-1000 µl and 20-200 µl)
2. Eppendorf (1.5 ml)
3. Dried ice
4. Syringe filter (sigma cat, pore size of 0.2 µm, 13 mm in diameter PTFE)
5. Syringe (BD 0.5 ml Syringe)

Reagents

1. 80% v/v of methanol (HPLC Grade, Fischer Chemical, Cat# A452-4)
2. 50% v/v of methanol (HPLC Grade, Fischer Chemical, Cat# A452-4)
3. SiO_2 sand (A&C ,Cat# S1091)
4. Phosphate buffered saline (PBS), pH ≈ 7-7.4
5. Milli-Q water

Instruments

1. Micro-centrifuge (micromax RF, Thermo IEC)
2. Vortex (mini vortexer, Fischer Scientific)
3. Sonicator (Crest)

Operation method

Sample preparation

1. Count cells to know the cell density;
2. Transfer the appropriate sample of culture to have 5 million cells into extraction vial;
3. Micro-centrifuge at 1050 RPM (200 g) for 5 min at 4°C (need to pre-cool);
4. Discard supernatant;
5. Add 1 ml of cold PBS (pre-cold in ice-water bath);
6. Suspend the cell pellet by pipetting;
7. Centrifuge the cell suspension at 1050 RPM for 5 min at 4°C (repeat washing with PBS twice);
8. Important Note: all the steps before cell extraction should be done in less than 15 mins
9. Discard the supernatant;

Extraction steps

1. Add 0.4 ml of cold 80% methanol (-80°C) and 0.2 g of sand into centrifuge tube;
2. Keep tube on dry ice for 30 min;
3. Vortex suspend cell pellet for 1 min;
4. Cool down in ice-water bath for 1 min (repeat step 8.11 and 8.12 3 times);
5. Sonicate in ice-water bath for 5 min;
   While sonicating keep cell pellets in ice-water
6. Micro-centrifuge at 21 000 g for 7 min, 4°C;
7. Transfer supernatant into new vial (extract vial) → First extract;
8. Add 0.2 ml of cold 50% methanol to the pellet;
9. Suspend the cell pellet with the vortex for 1 min;
10. Cool down in ice-water bath for 1 min ;
11. Sonicate in ice-water bath for 5 min;
    While sonicating keep cell pellets in ice-water

12. Micro-centrifuge at 21 000 g for 5 min, 4°C;
13. Transfer supernatant to the extract vial → Second extract;
14. Add 0.2 ml cold water to the pellet;
15. Micro-centrifuge for 3 min;
16. Transfer supernatant to the extract vial → Third extract;
17. Micro-centrifuge the extract tube at 21 000 g at 4°C for 5 min;
18. Syringe aspirate supernatant;
19. Mount filter and dispense the 0.2 μm extract in a 2 ml screw cap glass vial;
20. Identify vial box and store at -80°C for further LC/MS analysis;

Important note: in all the steps for extraction cell pellets should be kept in ice-water bath.FORMS / REGISTRATIONS

Preparation of standards

All the standard stocks of organic acids have to be prepared in 50% methanol. To prepare standards follow the steps and table:

First part of the table/ how to prepare stock solutions:

1. First weight the mass needed amount and by adding 50% methanol bring it to appropriate total volume (now the concentration would be the same as the first con.(mM))
2. Dilute the standards in order to reach the stock con. (mM)
3. Keep the stock solutions in -20°C for further usage

Second part of the table/ how to prepare standards

4. STD1: Take 100μl of each stock solution and mix them, then dilute it to 10ml
5. STD 2: Take 50μl of each stock solution and mix them, then dilute it to 10ml
6. STD 3: Take 30μl of each stock solution and mix them, then dilute it to 10ml
7. STD 4: Take 15μl of each stock solution and mix them, then dilute it to 10ml
8. STD 5: Take 10μl of each stock solution and mix them, then dilute it to 10ml
9. STD 6: Take 5 μl of each stock solution and mix them, then dilute it to 10ml

From the last part of following table you can find the concentration of each component in the STDs.

APPENDIX 5MATLAB files

% MatLab code of the model © Prof. Mario Jolicoeur's group

****

OVERVIEW

This model describes the dynamics of CHO cells metabolism. The model doesnot discriminate between cellular populations and is thus representative of overall CHO cells metabolism. Moreover, unique cellular compartment is considered in the model. This implementation reproduces the results, as presented in the figures of the associated manuscript.

The model is presented in:
Atefeh Ghorbaniaghdam, Jingkui Chen, Olivier Henry, Mario Jolicoeur
Metabolomics and *in-silico* analysis of monoclonal antibody-producing CHO cell clones.
Computational biology (2013)
Please cite the original article if you use this model.

```
global Allpara Allpara_value
% Paraopt: contains the names of the parameters to be optimized
% Parafixed: contains the names of the parameters to be kept constant
% Get the list of all parameters from Excel
[numexcel,nameexcel]=xlsread('para.xlsx');  %Import parameter names and values from a file
called Paralist.xlsx
% All the name of the parameters
Allpara=nameexcel(2:end,1);
% All their corresponding values (fixed or initial guess)
Allpara_value=numexcel(1:end,1);
% All the name of the parameters to be kept constant
for kk=1:length(Allpara_value)
eval([Allpara(Edwards et al.)'=Allpara_value(kk);']);
end
%Initial values
t=0:1:144;
yinitial=[1.3999999999999999.*10^-7    %ACCOA
1.94000000000000001.*10^-7            %AKG
0.75                %ALA
0.5                 %ASP
1.0900000000000001.*10^-6 %ATP
4.7700000000000001.*10^-7 %ADP
1.99999999999999999e-007  %CIT
1                   %COA
3.89999999999999999e-006   %Cr
3e-007     %F6P
5e-008      %G6P
4e-07       %GAP
7e-4        %GLU
```

```
3.5e-007    %MAL
6.0000000000000002e-005 %OXA
1.9999999999999995e-006  %PCR
0.4e-007       %PEP

1.9999999999999999e-007      %PYR
0.42499999999999995e-007      %R5P
3.9999999999999998e-007     %SCOA
6e-008    %SUC
9.2499999999999999e-008   %X5P
28.010000000000002    %EGLC
3.6       %EGLN
0.75      %LAC
9.00000000000003e-007   %NAD
1.090002000000000001e-008  %NADH
8.999999999999997e-013   %NADP
5.3799999999999999e-012    %NADPH
0.1             %NH4
0.053               %O2
0.0000042999999999999999   %PI
0.18             %X
1e-5           %GLN
1.9e-8      %AMP
0.65          %EGLU
2.80885      %ARG
2.8         %ASX
1           %ASP
0.7         %CYS
1.055029      %GLY
0.940153      %HIS
1.62      %ILE
0.7941       %LEU
1.18003      %LYS
0.45          %MET
0.55029      %PHE
2.918        %PRO
2.11         %SER
0.55029      %THR
0.54491      %TYR
0.8];      %VAL

%% Simulation
[t,y]=ode23s(@eqdiff,t,yinitial,[],Allpara_value);
ACCOA_P=y(:,1);AKG_P=y(:,2)  ;  ALA_P=y(:,3)  ;  ASP_P=y(:,4)  ;ATP_P=y(:,5)  ;
ADP_P=y(:,6)
;COA_P=y(:,8);CIT_P=y(:,7);Cr_P=y(:,9);F6P_P=y(:,10);G6P_P=y(:,11);;GLU_P=y(:,13);MAL
_P=y(:,14);GAP_P=y(:,12);;OXA_P=y(:,15);PCr_P=y(:,16);PEP_P=y(:,17);PYR_P=y(:,18);R5P
_P=y(:,19);SCOA_P=y(:,2);SUC_P=y(:,21);X5P_P=y(:,22);EGLC_P=y(:,23);EGLN_P=y(:,24);
LAC_P=y(:,25);NAD_P=y(:,26);NADH_P=y(:,27);NADP_P=y(:,28);NADPH_P=y(:,29);NH4_P
=y(:,30);O2_P=y(:,31);Pi_P=y(:,32);X_P=y(:,33);GLN_P=y(:,34);AMP_P=y(:,35);EGLU_P=y(:,
36);ARG_P=y(:,37);ASX_P=y(:,38);ASP_P=y(:,39);CYS_P=y(:,40);GLY_P=y(:,41);HIS_P=y(:,
```

```
42);ILE_P=y(:,43);LEU_P=y(:,44);LYS_P=y(:,45);MET_P=y(:,46);PHE_P=y(:,47);PRO_P=y(:,
48);SER_P=y(:,49);THR_P=y(:,50);TYR_P=y(:,51);VAL_P=y(:,52).
%%
%identification of ratios
for i=1:145
B_P(i)=
ADP_P(i)./ATP_P(i);C_P(i)=ATP_P(i)./ADP_P(i);E_P(i)=NADH_P(i)/NAD_P(i);P_P(i)=NADP
_P(i)/NADPH_P(i);PP_P(i)=NADPH_P(i)/NADP_P(i);D_P(i)=NAD_P(i)/NADH_P(i);
End
```

```
function dy=eqdifflastversionparental(t,x,Allpara_value1)
global Allpara
for kk=1:length(Allpara_value1)
   eval([Allpara{kk} '=Allpara_value1(kk);']);
end
ACCOA_P=x(:,1);AKG_P=x(:,2) ; ALA_P=x(:,3) ; ASP_P=x(:,4) ;ATP_P=x(:,5) ;
ADP_P=x(:,6)
;COA_P=x(:,8);CIT_P=x(:,7);Cr_P=x(:,9);F6P_P=x(:,10);G6P_P=x(:,11);;GLU_P=x(:,13);MAL
_P=x(:,14);GAP_P=x(:,12);;OXA_P=x(:,15);PCr_P=x(:,16);PEP_P=x(:,17);PYR_P=x(:,18);R5P
_P=x(:,19);SCOA_P=x(:,2);SUC_P=x(:,21);X5P_P=x(:,22);EGLC_P=x(:,23);EGLN_P=x(:,24);
LAC_P=x(:,25);NAD_P=x(:,26);NADH_P=x(:,27);NADP_P=x(:,28);NADPH_P=x(:,29);NH4_P
=x(:,30);O2_P=x(:,31);Pi_P=x(:,32);X_P=x(:,33);GLN_P=x(:,34);AMP_P=x(:,35);EGLU_P=x(:,
36);ARG_P=x(:,37);ASX_P=x(:,38);ASP_P=x(:,39);CYS_P=x(:,40);GLY_P=x(:,41);HIS_P=x(:,
42);ILE_P=x(:,43);LEU_P=x(:,44);LYS_P=x(:,45);MET_P=x(:,46);PHE_P=x(:,47);PRO_P=x(:,
48);SER_P=x(:,49);THR_P=x(:,50);TYR_P=x(:,51);VAL_P=x(:,52).
B= ADP./ATP;
C=ATP./ADP;
E=NADH/NAD;
D=NAD/NADH;
P=NADP/NADPH;
V_HK = Vmax_HK*mm(EGLC,Km_EGLC,1)*mm(C,Km_C,1)*mm(Kd_G6P,G6P,1);
V_PGI = Vmaxf_PGI*mm(G6P,Km_G6P,1)*mm(Kd_PEP,PEP,1);
V_PFK = Vmax_PFK*mm(F6P,Km_F6P,1)*mm(C,Km_C,1);
V_PGK = Vmax_PGK*mm(GAP,Km_GAP,1)*mm(B,Km_B,1)*mm(D,Km_D,1);
V_PK = Vmax_PK*mm(PEP,Km_PEP,1)*mm(B,Km_B,1);
V_LDH = Vmaxf_LDH*mm(PYR,Km_PYR,1)*mm(E,Km_E,1)-
Vmaxr_LDH*mm(LAC,Km_LAC,1)*mm(D,Km_D,1);
V_G6DPH = Vmax_G6DPH*mm(G6P,Km_G6P,1)*mm(P,Km_P,1);
V_EP = Vmax_EP*mm(R5P,Km_R5P,1);
V_TK =Vmax_TK*mm(R5P,Km_R5P,1)*mm(X5P,Km_X5P,1) ;
V_PDH = Vmax_PDH*mm(PYR,Km_PYR,1)*mm(D,Km_D,1);
V_CS = Vmax_CS*mm(ACCOA,Km_ACCOA,1)*mm(OXA,Km_OXA,1);
V_CITS = Vmax_CITS*mm(CIT,Km_CIT,1)*mm(D,Km_D,1);
V_AKGDH = Vmax_AKGDH*mm(AKG,Km_AKG,1)*mm(D,Km_D,1);
V_SOCAS =0;
V_SDH = Vmax_SDH*mm(SUC,Km_SUC,1)*mm(D,Km_D,1)*mm(B,Km_B,1);
V_MLD = Vmax_MLD*mm(MAL,Km_MAL,1)*mm(D,Km_D,1);
V_ME = Vmax_ME*mm(MAL,Km_MAL,1)*mm(D,Km_D,1);
V_PC = Vmax_PC*mm(PYR,Km_PYR,1);
V_GlnT =Vmaxf_GlnT*mm(EGLN,Km_EGLN,1)*mm(C,Km_C,1)-
Vmaxr_GlnT*mm(GLU,Km_GLU,1)*mm(B,Km_B,1)*mm(NH4,Km_NH4,1);
```

```
V_GLNS=0;
V_GLDH = Vmaxf_GLDH*mm(GLU,Km_GLU,1)*mm(D,Km_D,1)-
Vmaxr_GLDH*mm(AKG,Km_AKG,1)*mm(E,Km_E,1)*mm(NH4,Km_NH4,1);
V_AlaTA = Vmaxf_AlaTA*mm(GLU,Km_GLU,1)*mm(PYR,Km_PYR,1)-
Vmaxr_AlaTA*mm(ALA,Km_ALA,1)*mm(AKG,Km_AKG,1)*(1+KaEGLN/EGLN);
V_GluT=Vmax_GluT*mm(GLU,Km_GLU,1);
V_resp= Vmax_resp*mm(O2,Km_O2,1)*mm(B,Km_B,1)*mm(NADH,Km_NADH,1);
V_ATPase = Vmax_ATPase*mm(ATP,Km_ATP,1);
V_CK =Vmaxf_CK*mm(PCr,Km_PCr,1)*mm(B,Km_B,1)-
Vmaxr_CK*mm(Cr,Km_Cr,1)*mm(C,Km_C,1);
V_AK=Vmaxf_AK*mm(AMP,Km_AMP,1)*mm(ATP,Km_ATP,1)-
Vmaxr_AK*mm(ADP,Km_ADP,1);
V_leak = Vmax_leak*mm(NADH,Km_NADH,1)*mm(O2,Km_O2,1);
V_NADPHox = Vmax_NADPHox*mm(NADPH,Km_NADPH,1);
V_PPRibP=Vmax_PPRibP*mm(R5P,Km_R5P,1)*mm(EGLN,Km_EGLN,1)*mm(ASP,Km_AS
P,1)*mm(GLY,Km_GLY,1);
V_growth =
Vmax_growth*mm(G6P,Km_G6P,1)*mm(EGLN,Km_EGLN,1)*mm(R5P,Km_R5P,1)*mm(LY
S,Km_LYS,1)*mm(ILE,Km_ILE,1)*mm(LEU,Km_LEU,1)*mm(VAL,Km_VAL,1)*mm(TYR,
Km_TYR,1)*mm(ASX,Km_ASX,1)*mm(HIS,Km_HIS,1)*mm(ARG,Km_ARG,1);
V_growth_R5P = 9.11e-
5*Vmax_growth*mm(G6P,Km_G6P,1)*mm(EGLN,Km_EGLN,1)*mm(R5P,Km_R5P,1)*mm(
LYS,Km_LYS,1)*mm(ILE,Km_ILE,1)*mm(LEU,Km_LEU,1)*mm(VAL,Km_VAL,1)*mm(TY
R,Km_TYR,1)*mm(ASX,Km_ASX,1)*mm(HIS,Km_HIS,1)*mm(ARG,Km_ARG,1);
V_growth_G6P =13.65e-
5*Vmax_growth*mm(G6P,Km_G6P,1)*mm(EGLN,Km_EGLN,1)*mm(R5P,Km_R5P,1)*mm(
LYS,Km_LYS,1)*mm(ILE,Km_ILE,1)*mm(LEU,Km_LEU,1)*mm(VAL,Km_VAL,1)*mm(TY
R,Km_TYR,1)*mm(ASX,Km_ASX,1)*mm(HIS,Km_HIS,1)*mm(ARG,Km_ARG,1);
V_growth_CIT =5.25e-
6*Vmax_growth*mm(G6P,Km_G6P,1)*mm(EGLN,Km_EGLN,1)*mm(R5P,Km_R5P,1)*mm(
LYS,Km_LYS,1)*mm(ILE,Km_ILE,1)*mm(LEU,Km_LEU,1)*mm(VAL,Km_VAL,1)*mm(TY
R,Km_TYR,1)*mm(ASX,Km_ASX,1)*mm(HIS,Km_HIS,1)*mm(ARG,Km_ARG,1);
V_growth_GLU=1.86e-
5*Vmax_growth*mm(G6P,Km_G6P,1)*mm(EGLN,Km_EGLN,1)*mm(R5P,Km_R5P,1)*mm(
LYS,Km_LYS,1)*mm(ILE,Km_ILE,1)*mm(LEU,Km_LEU,1)*mm(VAL,Km_VAL,1)*mm(TY
R,Km_TYR,1)*mm(ASX,Km_ASX,1)*mm(HIS,Km_HIS,1)*mm(ARG,Km_ARG,1);
V_growth_GLN= 1.86e-
5*Vmax_growth*mm(G6P,Km_G6P,1)*mm(EGLN,Km_EGLN,1)*mm(R5P,Km_R5P,1)*mm(
LYS,Km_LYS,1)*mm(ILE,Km_ILE,1)*mm(LEU,Km_LEU,1)*mm(VAL,Km_VAL,1)*mm(TY
R,Km_TYR,1)*mm(ASX,Km_ASX,1)*mm(HIS,Km_HIS,1)*mm(ARG,Km_ARG,1);
V_growth_ALA=0.00194*0.013*Vmax_growth*mm(G6P,Km_G6P,1)*mm(EGLN,Km_EGLN,
1)*mm(R5P,Km_R5P,1)*mm(LYS,Km_LYS,1)*mm(ILE,Km_ILE,1)*mm(LEU,Km_LEU,1)*m
m(VAL,Km_VAL,1)*mm(TYR,Km_TYR,1)*mm(ASX,Km_ASX,1)*mm(HIS,Km_HIS,1)*mm
(ARG,Km_ARG,1);
V_growth_ARG=0.00194*0.007*Vmax_growth*mm(G6P,Km_G6P,1)*mm(EGLN,Km_EGLN,
1)*mm(R5P,Km_R5P,1)*mm(LYS,Km_LYS,1)*mm(ILE,Km_ILE,1)*mm(LEU,Km_LEU,1)*m
m(VAL,Km_VAL,1)*mm(TYR,Km_TYR,1)*mm(ASX,Km_ASX,1)*mm(HIS,Km_HIS,1)*mm
(ARG,Km_ARG,1);
V_growth_ASX=0.00194*0.0*Vmax_growth*mm(G6P,Km_G6P,1)*mm(EGLN,Km_EGLN,1)*
mm(R5P,Km_R5P,1)*mm(LYS,Km_LYS,1)*mm(ILE,Km_ILE,1)*mm(LEU,Km_LEU,1)*mm(
```

VAL,Km_VAL,1)*mm(TYR,Km_TYR,1)*mm(ASX,Km_ASX,1)*mm(HIS,Km_HIS,1)*mm(A
RG,Km_ARG,1);
V_growth_ASP=0.00194*0.0261*Vmax_growth*mm(G6P,Km_G6P,1)*mm(EGLN,Km_EGLN,
1)*mm(R5P,Km_R5P,1)*mm(LYS,Km_LYS,1)*mm(ILE,Km_ILE,1)*mm(LEU,Km_LEU,1)*m
m(VAL,Km_VAL,1)*mm(TYR,Km_TYR,1)*mm(ASX,Km_ASX,1)*mm(HIS,Km_HIS,1)*mm
(ARG,Km_ARG,1);
V_growth_GLY=0.00194*0.0165*Vmax_growth*mm(G6P,Km_G6P,1)*mm(GLU,Km_GLU,1)
*mm(GLN,Km_GLN,1)*mm(R5P,Km_R5P,1)*mm(CIT,Km_CIT,1);
V_growth_HIS=0.00194*0.01*Vmax_growth*mm(G6P,Km_G6P,1)*mm(EGLN,Km_EGLN,1)
*mm(R5P,Km_R5P,1)*mm(LYS,Km_LYS,1)*mm(ILE,Km_ILE,1)*mm(LEU,Km_LEU,1)*mm
(VAL,Km_VAL,1)*mm(TYR,Km_TYR,1)*mm(ASX,Km_ASX,1)*mm(HIS,Km_HIS,1)*mm(
ARG,Km_ARG,1);
V_growth_ILE=0.00194*0.01*Vmax_growth*mm(G6P,Km_G6P,1)*mm(EGLN,Km_EGLN,1)
*mm(R5P,Km_R5P,1)*mm(LYS,Km_LYS,1)*mm(ILE,Km_ILE,1)*mm(LEU,Km_LEU,1)*mm
(VAL,Km_VAL,1)*mm(TYR,Km_TYR,1)*mm(ASX,Km_ASX,1)*mm(HIS,Km_HIS,1)*mm(
ARG,Km_ARG,1);
V_growth_LEU=0.00194*0.013*Vmax_growth*mm(G6P,Km_G6P,1)*mm(EGLN,Km_EGLN,
1)*mm(R5P,Km_R5P,1)*mm(LYS,Km_LYS,1)*mm(ILE,Km_ILE,1)*mm(LEU,Km_LEU,1)*m
m(VAL,Km_VAL,1)*mm(TYR,Km_TYR,1)*mm(ASX,Km_ASX,1)*mm(HIS,Km_HIS,1)*mm
(ARG,Km_ARG,1);
V_growth_LYS=0.00194*0.01*Vmax_growth*mm(G6P,Km_G6P,1)*mm(EGLN,Km_EGLN,1)
*mm(R5P,Km_R5P,1)*mm(LYS,Km_LYS,1)*mm(ILE,Km_ILE,1)*mm(LEU,Km_LEU,1)*mm
(VAL,Km_VAL,1)*mm(TYR,Km_TYR,1)*mm(ASX,Km_ASX,1)*mm(HIS,Km_HIS,1)*mm(
ARG,Km_ARG,1);
V_growth_MET=0.00194*0.0033*Vmax_growth*mm(G6P,Km_G6P,1)*mm(EGLN,Km_EGLN
,1)*mm(R5P,Km_R5P,1)*mm(LYS,Km_LYS,1)*mm(ILE,Km_ILE,1)*mm(LEU,Km_LEU,1)*
mm(VAL,Km_VAL,1)*mm(TYR,Km_TYR,1)*mm(ASX,Km_ASX,1)*mm(HIS,Km_HIS,1)*m
m(ARG,Km_ARG,1);
V_growth_PRO=0.00194*0.0081*Vmax_growth*mm(G6P,Km_G6P,1)*mm(EGLN,Km_EGLN
,1)*mm(R5P,Km_R5P,1)*mm(LYS,Km_LYS,1)*mm(ILE,Km_ILE,1)*mm(LEU,Km_LEU,1)*
mm(VAL,Km_VAL,1)*mm(TYR,Km_TYR,1)*mm(ASX,Km_ASX,1)*mm(HIS,Km_HIS,1)*m
m(ARG,Km_ARG,1);
V_growth_SER=0.00194*0.0099*Vmax_growth*mm(G6P,Km_G6P,1)*mm(EGLN,Km_EGLN,
1)*mm(R5P,Km_R5P,1)*mm(LYS,Km_LYS,1)*mm(ILE,Km_ILE,1)*mm(LEU,Km_LEU,1)*m
m(VAL,Km_VAL,1)*mm(TYR,Km_TYR,1)*mm(ASX,Km_ASX,1)*mm(HIS,Km_HIS,1)*mm
(ARG,Km_ARG,1);
V_growth_THR=0;0.00194*0.008*Vmax_growth*mm(G6P,Km_G6P,1)*mm(EGLN,Km_EGL
N,1)*mm(R5P,Km_R5P,1)*mm(LYS,Km_LYS,1)*mm(ILE,Km_ILE,1)*mm(LEU,Km_LEU,1)
*mm(VAL,Km_VAL,1)*mm(TYR,Km_TYR,1)*mm(ASX,Km_ASX,1)*mm(HIS,Km_HIS,1)*
mm(ARG,Km_ARG,1);
V_growth_TYR=0.00194*0.004*Vmax_growth*mm(G6P,Km_G6P,1)*mm(EGLN,Km_EGLN,
1)*mm(R5P,Km_R5P,1)*mm(LYS,Km_LYS,1)*mm(ILE,Km_ILE,1)*mm(LEU,Km_LEU,1)*m
m(VAL,Km_VAL,1)*mm(TYR,Km_TYR,1)*mm(ASX,Km_ASX,1)*mm(HIS,Km_HIS,1)*mm
(ARG,Km_ARG,1);
V_growth_VAL=0.00194*0.0096*Vmax_growth*mm(G6P,Km_G6P,1)*mm(EGLN,Km_EGLN
,1)*mm(R5P,Km_R5P,1)*mm(LYS,Km_LYS,1)*mm(ILE,Km_ILE,1)*mm(LEU,Km_LEU,1)*
mm(VAL,Km_VAL,1)*mm(TYR,Km_TYR,1)*mm(ASX,Km_ASX,1)*mm(HIS,Km_HIS,1)*m
m(ARG,Km_ARG,1);
%%**
V_ASX=Vmax_asx*mm(ASX,Km_ASX,1);

```
V_ASTA= Vmaxf_ASTA*mm(ASP,Km_ASP,1)*mm(AKG,Km_AKG,1)-
Vmaxr_ASTA*mm(GLU,Km_GLU,1)*mm(OXA,Km_OXA,1)*mm(NH4,Km_NH4,1);
V_SDHH=Vmax_SDHH*mm(SER,Km_SER,1);
V_HISARGTA=Vmax_HISARGTA*mm(HIS,Km_HIS,1)*mm(ARG,Km_ARG,1)*mm(AKG,K
m_AKG,1);
V_LYSILELEUVALTYRTA=Vmax_LYSILELEUVALTYRTA*mm(LYS,Km_LYS,1)*mm(IL
E,Km_ILE,1)*mm(LEU,Km_LEU,1)*mm(VAL,Km_VAL,1)*mm(TYR,Km_TYR,1)*mm(AKG
,Km_AKG,1)*mm(D,Km_D,1)*mm(C,Km_C,1)*mm(P,Km_P,1);
V_METSER=Vmax_METSER*mm(MET,Km_MET,1)*mm(SER,Km_SER,1)*mm(D,Km_D,1)
*mm(C,Km_C,1);
V_SHMT=Vmax_SHMT*mm(SER,Km_SER,1);
V_TDH=Vmax_TDH*mm(THR,Km_THR,1)*mm(D,Km_D,1);
V_PRO=Vmax_PRO*mm(PRO,Km_PRO,1)*mm(NADP/NADPH,Km_NADP/NADPH,1);
V_PAH=Vmax_PAH*mm(PHE,Km_PHE,1)*mm(E,Km_E,1);
%%**************************************************************************
V_mAbPro=0;
V_mAb_GLU=0.00794*0.017*V_mAbPro;
V_mAb_GLN= 0.00794*0.0104* V_mAbPro;
V_mAb_ALA=0.00794*0.011*V_mAbPro;
V_mAb_ARG=0.00794*0.005*V_mAbPro;
V_mAb_ASX=0.00794*0.0072*V_mAbPro;
V_mAb_ASP=0.00794*0.0082*V_mAbPro;
V_mAb_CYS=0.00794*0.005*V_mAbPro;
V_mAb_GLY=0.00794*0.0145*V_mAbPro;
V_mAb_HIS=0.00794*0.0035*V_mAbPro;
V_mAb_ILE=0.00794*0.005*V_mAbPro;
V_mAb_LEU=0.00794*0.0142*V_mAbPro;
V_mAb_LYS=0.00794*0.0145*V_mAbPro;
V_mAb_MET=0.00794*0.0028*V_mAbPro;
V_mAb_PHE=0.00794*0.0072*V_mAbPro;
V_mAb_PRO=0.00794*0.0148*V_mAbPro;
V_mAb_SER=0.00794*0.0267*V_mAbPro;
V_mAb_THR=0.00794*0.016*V_mAbPro;
V_mAb_TYR=0.00794*0.0085*V_mAbPro;
V_mAb_VAL=0.00794*0.0189*V_mAbPro;
%%**************************************************************************
V_mAbPro=0;
V_mAb_GLU=0.00794*0.017*V_mAbPro;
V_mAb_GLN= 0.00794*0.0104* V_mAbPro;
V_mAb_ALA=0.00794*0.011*V_mAbPro;
V_mAb_ARG=0.00794*0.005*V_mAbPro;
V_mAb_ASX=0.00794*0.0072*V_mAbPro;
V_mAb_ASP=0.00794*0.0082*V_mAbPro;
V_mAb_CYS=0.00794*0.005*V_mAbPro;
V_mAb_GLY=0.00794*0.0145*V_mAbPro;
V_mAb_HIS=0.00794*0.0035*V_mAbPro;
V_mAb_ILE=0.00794*0.005*V_mAbPro;
V_mAb_LEU=0.00794*0.0142*V_mAbPro;
V_mAb_LYS=0.00794*0.0145*V_mAbPro;
V_mAb_MET=0.00794*0.0028*V_mAbPro;
V_mAb_PHE=0.00794*0.0072*V_mAbPro;
```

```
V_mAb_PRO=0.00794*0.0148*V_mAbPro;
V_mAb_SER=0.00794*0.0267*V_mAbPro;
V_mAb_THR=0.00794*0.016*V_mAbPro;
V_mAb_TYR=0.00794*0.0085*V_mAbPro;
V_mAb_VAL=0.00794*0.0189*V_mAbPro;
%%*************************************************************************
dy(1) = +V_PDH-V_CS+8*V_LYSILELEUVALTYRTA-V_growth*ACCOA;
dy(2) = +V_CITS-V_AKGDH+V_AlaTA+V_GLDH-V_ASTA-
7*V_LYSILELEUVALTYRTA-V_HISARGTA-V_growth*AKG;
dy(3) = +(V_AlaTA)*X*1000;
dy(4) = -2*V_PPRibP+V_ASX-V_growth*ASP;
dy(5) =(-V_HK-V_PFK+V_PGK+V_PK+V_SOCAS+2*Pratio*V_resp-V_ATPase+V_CK-
V_AK-V_METSER);%/(1-d);
dy(6) =-(-V_HK-V_PFK+V_PGK+V_PK+V_SOCAS+2*Pratio*V_resp-V_ATPase+V_CK-
2*V_AK+V_METSER);
dy(7) = +V_CS-V_CITS-V_growth_CIT-V_growth*CIT;
dy(8) = -V_PDH+V_CS-V_AKGDH+V_SOCAS-V_growth*COA;
dy(9) = +V_CK-V_growth*Cr;
dy(10) = +V_PGI-V_PFK+2*V_TK-V_growth*F6P;
dy(11) = +V_HK-V_PGI-V_G6DPH-V_growth_G6P-V_growth*G6P;
dy(12) = 2*V_PFK-V_PGK+V_TK-V_growth*GAP;
dy(13)=V_GLNS+V_GlnT-V_GLDH-V_AlaTA-V_GluT+2*V_PPRibP-
V_growth_GLU+V_ASTA+4*V_LYSILELEUVALTYRTA+4*V_HISARGTA-
V_growth*GLU;
dy(14) = V_SDH-V_MLD-V_ME-2*V_PPRibP+V_LYSILELEUVALTYRTA-
V_growth*MAL;
dy(15) = -V_CS+V_MLD+V_PC+V_ASTA-V_growth*OXA;
dy(16) = -V_CK-V_growth*PCr;
dy(17)= +V_PGK-V_PK-V_growth*PEP;
dy(18) = +V_PK-V_LDH-V_PDH-V_AlaTA+V_ME-V_PC+V_SDHH-V_growth*PYR;
dy(19) = +V_G6DPH-V_EP-V_TK-0.6*V_PPRibP-V_growth_R5P-V_growth*R5P;
dy(20) =0; %+V_AKGDH+3*V_LYSILELEUVALTYRTA+V_METSER-V_growth*SCOA;
dy(21) = +V_AKGDH+3*V_LYSILELEUVALTYRTA+V_METSER-V_SDH-V_growth*SUC;
dy(22) = +V_EP-2*V_TK-V_growth*X5P;
dy(23) = (-V_HK)*X*1000;
dy(24) = (-V_GlnT-V_growth_GLN-2*V_PPRibP)*X*1000;
dy(25) = (V_LDH)*X*1000;
dy(26) = -V_PDH-V_CITS-V_AKGDH-2/3*V_SDH-V_MLD+2*V_resp-
V_PK+V_LDH+2*V_leak-V_GLDH-9*V_LYSILELEUVALTYRTA-
8/3*V_LYSILELEUVALTYRTA-V_METSER;
dy(27) = +V_PDH+V_CITS+V_AKGDH+2/3*V_SDH+V_MLD-2*V_resp+V_PK-V_LDH-
2*V_leak+V_GLDH+9*V_LYSILELEUVALTYRTA+8/3*V_LYSILELEUVALTYRTA+V_M
ETSER;
dy(28) = -V_G6DPH+V_NADPHox-2*V_LYSILELEUVALTYRTA;
dy(29) = V_G6DPH-V_NADPHox+2*V_LYSILELEUVALTYRTA;
dy(30) = (V_GlnT+V_GLNS+V_GLDH+V_ASX)*X*1000;
dy(31)= 0;
dy(32) =0;
dy(33) = V_growth*X;
dy(34) =V_GlnT-V_GLNS-2*V_PPRibP-V_growth*GLN ;
dy(35)=-V_AK+V_PPRibP;
```

```
dy(36)=V_GluT*X*1000;
dy(37)=(-V_HISARGTA-V_growth_ARG-V_mAb_ARG)*X*1000;
dy(38)=(-V_ASX-V_growth_ASX-V_mAb_ASX)*X*1000;
dy(39)=(-V_PPRibP-V_ASTA-V_growth_ASP-V_mAb_ASP)*X*1000;
dy(40)=(V_METSER-V_growth_CYS-V_mAb_CYS)*X*1000;
dy(41)=(-V_PPRibP+V_SHMT+V_TDH-V_growth_GLY-V_mAb_GLY)*1000;
dy(42)=(-V_HISARGTA-V_growth_HIS-V_mAb_HIS)*1000;
dy(43)=(-V_LYSILELEUVALTYRTA-V_growth_ILE-V_mAb_ILE)*X*1000;
dy(44)=(-V_LYSILELEUVALTYRTA-V_growth_LEU-V_mAb_LEU)*X*1000;
dy(45)=(-V_LYSILELEUVALTYRTA-V_growth_LYS-V_mAb_LYS)*X*1000;
dy(46)=(-V_METSER-V_growth_MET-V_mAb_MET)*X*1000;
dy(47)=(-V_PAH-V_growth_PHE-V_mAb_PHE)*X*1000;
dy(48)=(-V_PPRibP-V_PRO-V_growth_PRO-V_mAb_PRO)*X*1000;
dy(49)=(-V_SDHH-V_SHMT-V_growth_SER-V_mAb_SER)*X*1000;
dy(50)=(-V_TDH-V_growth_THR-V_mAb_THR)*X*1000;
dy(51)=(-V_LYSILELEUVALTYRTA+V_PAH-V_growth_TYR-V_mAb_TYR)*X*1000;
dy(52)=(-V_LYSILELEUVALTYRTA-V_growth_VAL-V_mAb_VAL)*X*1000;
dy=dy';
```

```
function K=mm(c,k,n)
K= (c.^n)./(k.^n+c.^n) ;
```

APPENDIX 6 Model analysis

Akaike information criterion

To select a model from a set of models, the chosen model should minimize the distance between the model simulation and experimental data (*WSSRES*). A systematic way is a criterion that seeks a model with a good fit to experimental data considering the number of model parameters.

The Akaike information criterion (AICc) is a measure for model comparison when model formulations with different numbers of parameters are available. It is defined as:

$$AICc = n \ln\left(\frac{WSSRES}{n}\right) + \frac{2np}{n-p-1}$$

where, *WSSRES* is the minimized sum of squared errors, n is the sample size, and $p$is the number of model parameters. Therefore, the value of AICc, in itself, for a given experimental data set has no meaning. It becomes interesting when it is compared to the AICc of a series of model specified *a priori*.The model with the lowest AICc being the best model among all other model formulations specified for the data available. Therefore, we further evaluate different model formulations accounting for different combinations of regulatory mechanisms an check whether the model formulation with the lowest *WSSRES* identified for the parental,induced low- and induced high-producercultures, the model accounts for hexokinase feedback-inhibition by its product (term I), G6P, and phosphoglucose isomerase (term II) by PEP, is also the best among the whole set of candidate models with regards to the AICc values. The results in Table 1 indicate that the model formulation with both hexokinase and phosphoglucose isomerasefeedback-inhibition is the best, i.e. lowest AICc value, given the set of four candidate model formulations in the three cultures.

Table A.1 Akaike information criterion (AICc) of the model formulations with different combinations of regulatory mechanisms of glycolysis

Model Formulation	AICc
no regulation-parental	670.08
with the addition of term I-parental	615.79
with the addition of terms I and II-parental	514.97
the addition of all terms-parental	536.07
no regulation-low-producer	629.47
with the addition of term I- low-producer	585.15
with the addition of terms I and II- low-producer	528.46
the addition of all terms- low-producer	545.41
no regulation- high-producer	599.89
with the addition of term I- high-producer	578.98
with the addition of terms I and II- high-producer	510.25
the addition of all terms- high-producer	554.29

Fisher Information matrix

There is always a desire to compute the probability of obtaining the particular experimental sample, denoted by $x_1,x_2,\ldots,x_n$, for a special model formulation. Considering that the observations in the experimental sample are independent, the generic expression for obtaining this particular sample is as follows:

$$P(X_1 = x_1, X_2 = x_2, \ldots, X_n = x_n) = P(X_1 = x_1)P(X_2 = x_2) \ldots P(X_n = x_n)$$
$$= \prod_{i=1}^{n} P(X_i = x_i)$$

Considering the model formulation, dependent on a set of parameters, i.e. $f(x; \theta_1 \ldots \theta_p)$,the generic probability terms can be replaced by the proposed model.

$$L(\theta_1 \ldots \theta_p, x_1 \ldots x_n) = \prod_{i=1}^{n} P_\Theta(X_i = x_i) = \prod_{i=1}^{n} f(x_i; \theta_1 \ldots \theta_p)$$

Working typically with the log of this expression,the above expression is modified as follows:

$$\log L(\theta_1 \ldots \theta_p, x_1 \ldots x_n) = \sum_{i=1}^{n} \log f(x_i; \theta_1 \ldots \theta_p)$$

The maximum likelihood estimate of parameters are those values with the log-likelihood as large as possible. The analytical protocol is setting the derivatives equal to zero with the derivative of the log-likelihood considered as the score or gradient vector.

The information matrixis an important quantity in likelihood theory which is the matrix of second partial derivatives of the log-likelihood.The matrix of second partial derivatives of the log-likelihood is also called the Hessian matrix. Therefore, the information matrix is just the negative of the Hessian matrix evaluated at the maximum likelihood estimates.

$$Hessian(\theta_1 \dots \theta_p)$$

$$= \begin{bmatrix} \frac{\partial^2}{\partial {\theta_1}^2} \log L(\theta) & \cdots & \frac{\partial^2}{\partial \theta_1 \partial \theta_{P-1}} \log L(\theta) & \frac{\partial^2}{\partial \theta_1 \partial \theta_P} \log L(\theta) \\ \frac{\partial^2}{\partial \theta_2 \partial \theta_1} \log L(\theta) & \frac{\partial^2}{\partial {\theta_2}^2} \log L(\theta) & \cdots & \frac{\partial^2}{\partial \theta_2 \partial \theta_P} \log L(\theta) \\ \vdots & \cdots & \ddots & \vdots \\ \frac{\partial^2}{\partial \theta_P \partial \theta_1} \log L(\theta) & \cdots & \frac{\partial^2}{\partial \theta_P \partial \theta_{P-1}} \log L(\theta) & \frac{\partial^2}{\partial {\theta_P}^2} \log L(\theta) \end{bmatrix}$$

The variance of a parameter estimate and its corresponding element in the fisher information matrix are reciprocals of each other. Therefore, using the relation between the fisher information matrix and the parameter estimate, the variability of the calibrated parameter values can be assessed by estimating associated confidence intervals via the Fisher Information Matrix. The standard error for a parameter estimate can be obtained by taking the square root of the reciprocal of the negative of the its corresponding value in Hessian matrix to construct the confidence intervals for estimate parameters.Considering the value of θ corresponding to the peak of the log-likelihoods and $L(\theta)$ as the elements of fisher information matrix, the following information can be drawn looking at corresponding figure.Low values of the fisher information matrix translates into a high variance of the estimate. Hence confidence intervals for parameter estimate will be wide. High information translates into a low variance of our estimator. Hence confidence intervals for parameter estimate will be narrow.

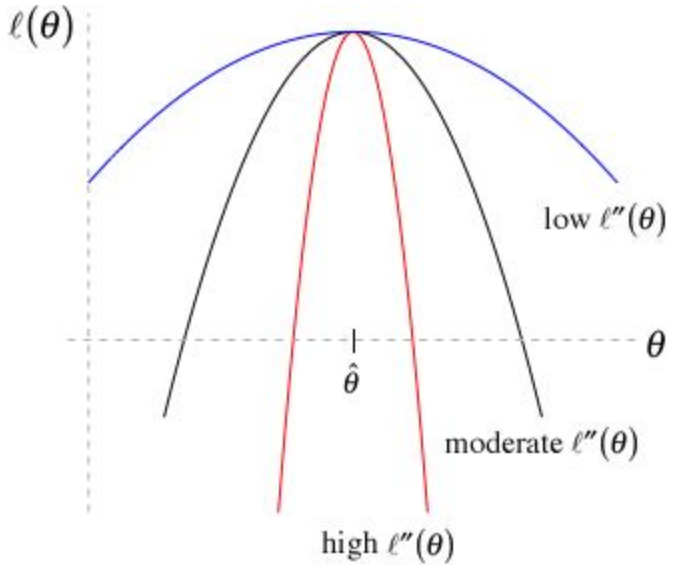

Figure A.3Second partial derivatives of the log-likelihoodand information

Finally, since fisher information matrix presents the inverse of the parameter estimation error covariance, the correlation matrix whose elements can be drawn a follows:

$$R_{kl} = \frac{C_{kl}}{\sqrt{C_{kk}C_{ll}}}$$

Further information on parameter correlations can be extracted from the correlation matrix.

Due to the information the fisher information matrix can provide, the fisher information matrix is calculated for the estimated parameters of the parental culture. Using *Least-squares fit* as an optimization routin, the hessian matrix cannot be calculated as an output. Once the solution using *Least-squares fit* is found, we run one additional iteration of *Fmincon* by calling it directly and starting from the known solution as the initial point. Calling *Fmincon*, with additional arguments let the hessian matrix be achieved as follows.

121	123	84	126	11	12	21	127	0	19	0.001	12	121	123	0.008	123	0.011	1	2	127	0	197	12	26	121	123	0.8
123	125	200	129	11	120	210	129	0.5	190	0.01	121	121	200	0.08	300	0.11	10	20	259	0	19	120	260	12	13	8
8	34	17	0.1	0	1	3	0.2	0.5	20	0.001	6	10	20	0.005	5	0	0	0	10	0	0.23	13	60	0.1	0.05	2
126	127	200	110	0.2	11	360	132	0.4	207	0.8	120	110	86	0.04	204	0.32	10	20	0.1	2	204	81	193	80	450	0.6
0.1	0.11	0	0.002	0	0.03	0.005	0.01	0.006	0.1	0	0	1	0	0	34	0	1	3	0	0.01	0.4	2	10	3	45	0
0.01	0.3	0.2	0.01	0.03	385	171	8	0.1	382	0.03	0.2	20	0.6	24	0	0.1	0	0	34	0.002	0.005	0	35	0.004	3	0
0.002	0.02	0.03	0.03	0.005	700	133	1	0.1	137	0.006	0.1	16	0.03	102	2	0.001	0	0	24	0.004	0.003	0	102	0.001	21	0
127	129	0.0002	132	0.01	8	1	133	0.0005	204	0.001	0.003	141	201	0.002	76	0.009	0.8	8	154	0	100	23	43	10	18	0.3
0	0.06	0.0005	0.004	0.0006	0.19	0.1	0.0005	0.2	1.3	0	0.4	43	10	0	2	0.0002	0	0	201	0	5	0	5	0.001	2	0
19	198	0.02	207	0.11	738	137	20	1.3	223	0.07	2.4	202	150	24	100	0.3	10	4	300	5	198	25	9	100	165	2
0.001	0.01	0.001	0.008	0	0.03	0.006	0.001	0	0.07	0	0	2	0.4	0	4	0.004	1	0.003	5	0	0.2	0.05	1	0.2	3	0.002
0.002	0.1	0.0006	0.02	0.0009	0.2	0.1	0.003	0.4	2	0	0.6	0.4	0.02	0	1	0.02	0	0	2	0	0.04	1	0.5	0.03	0.2	0.0001
20	14	0.002	0.004	0.0003	0.01	0.5	0.002	0.001	1	0	0.08	0.1	0.008	0.0003	1	0.009	0.5	0	0	0	0.1	0.1	0.07	0.2	0.1	0.0003
80	35	0.006	0.01	0.04	0.08	1	0.05	0.01	10	0	0.6	0.9	0.01	0.009	10	0.01	2	0	0.003	0	0.8	0.9	0.1	0.1	0.005	0.001
0.2	0.1	0.01	0.005	0	0.007	0.002	0.05	0.002	0.06	0	0.002	0.5	0	0.0001	20	0.04	0.0001	0	0	0	0.005	1	4	2	70	0.001
10	12	0.001	0.003	0.0002	0.09	0.2	0.001	0.006	10	0	0.03	0.08	0.01	0.0007	6	0.003	0.2	0.001	0.05	0	0.08	0.2	0.03	0.1	0.1	0.0003
0.1	0.3	0.2	0.001	0.05	185	17	80	0.1	282	0.05	0.1	10	0.5	14	0	0.5	0.001	0	44	0.02	0.005	0.001	30	0.04	5	0.01
221	123	94	226	30	12	21	187	0.6	49	0.005	52	120	13	0.008	153	0.01	100	20	227	10	197	92	66	221	123	80
151	121	90	126	40	22	11	87	0.5	39	0.05	32	120	80	0.001	53	0.005	80	10	127	80	97	2	0.6	21	100	40
0.05	8	10	0.05	0.001	0.001	0.006	0.04	0.001	2	0	0.008	10	1	0.001	20	0.04	0.001	0.005	0	0	0.002	1	3	2	60	0.002
0.03	5	10	0.01	0.006	0.007	0.004	0.02	0.0005	20	0.01	0.001	8	5	0.0001	10	0.02	0.002	0.001	0.1	0.001	0.002	4	0.3	20	100	0.02
0.01	0.006	0.0001	0.002	0.0001	05	0.1	0.0005	0.2	1.7	0	0.2	41	15	0	20	0.002	0	0	201	0	4	0	0.1	0.001	1	0.1
0.1	0.002	0.001	0.02	0.001	3	0.5	0.005	0.8	5.7	0.001	0.1	31	12	0.01	10	0.001	0.01	0.1	101	0	3	0	0.2	0.002	10	0.5
0.2	0.09	0.005	0.01	0.005	2	0.2	0.001	0.4	3.7	0.005	0.5	20	15	0.05	20	0.003	0.001	0.2	50	0.01	2	0	0.1	0.001	5	0.2
0.3	0.001	0.002	0.02	0.004	5	0.6	0.004	0.6	3.7	0.003	0.6	51	11	0.04	60	0.001	0.01	0.5	50	0	6	0	0.02	0.02	10	0.5
5	0.06	0.003	0.03	0.002	1	0.1	0.002	0.2	3.5	0.002	0.4	10	19	0.02	20	0.003	0.001	3	40	0.001	2	0	0.1	0.001	10	0.5
181	203	100	186	11	30	50	227	19	100	0.005	15	221	133	0.005	123	0.051	10	20	227	40	297	42	36	221	323	10